Microbial confrontations trigger broad array synthesis of human-toxic secondary metabolites

Dissertation

zur Erlangung des

Doktorgrades der Naturwissenschaften (Dr. rer. nat.)

der

Naturwissenschaftlichen Fakultät III

Agrar- und Ernährungswissenschaften, Geowissenschaften und Informatik

der Martin-Luther-Universität Halle-Wittenberg

vorgelegt von

Herrn Bennet Rohan Devasahayam

Gutachter: Prof. Dr. Holger B. Deising

Prof. Dr. Andreas von Tiedemann

Defense on 13.01.2025

Table of contents

List of abbreviations

A. nidulans	*Aspergillus nidulans*
A. tenuis	*Alternaria tenuis*
ACN	Acetonitrile
AF	Aflatoxin
AFB1	Aflatoxin B1
AGE	Agarose Gel Electrophoresis
AIC	Akaike Information Criterion
ALB	Anthracnose Leaf Blight
antiSMASH	antibiotics & Secondary Metabolite Analysis Shell
approx.	Approximately
ATCC	American Type Culture Collection
B. amyloliquefaciens	*Bacillus amyloliquefaciens*
B. subtilis	*Bacillus subtilis*
B. velezensis	*Bacillus velezensis*
bp	Base pair
BLAST	Basic Local Alignment Search Tool
C. domesticus	*Coprinellus domesticus*
C. graminicola	*Colletotrichum graminicola*
C. higginsianum	*Colletotrichum higginsianum*
C. heterostrophus	*Cochliobolus heterostrophus*
Cladosporium sp.	*Cladosporium* species
CAZymes	Carbohydrate-Active Enzymes
CFW	Calcofluor White
cm	Centimeter
CM	Complete Medium
CSPD	Chemiluminescent Substrate for Phosphate Detection
cv.	Cultivar
CYP	Cytochrome P450
dATP	Deoxyadenosine triphosphate
dCTP	Deoxycytidine triphosphate
DEGs	Differentially Expressed Genes
DEPC	Diethylpyrocarbonate
dGTP	Deoxyguanosine triphosphate
DHN	Dihydroxy Naphthalene
DMSO	Dimethyl Sulfoxide
DMI	Demethylation Inhibitors
DNA	Deoxyribonucleic acid
dNTP	Deoxynucleotide triphosphate
DON	Deoxynivalenol
dpi	days post inoculation
DSMZ	Deutsche Sammlung von Mikroorganismen und Zellkulturen

dTTP	Deoxythymidine triphosphate
dUTP	Deoxyuridine triphosphate
E. coli	*Escherichia coli*
ect.	Ectopic
EDTA	Ethylenediaminetetraacetic acid
ESI	Electrospray Ionization
EU	European Union
et al.	*et alii*, lat.: and others
FCS	Fetal Calf Serum
FM4-64	Lipophilic styryl dye
FRAC	Fungicide Resistance Action Committee
FUM	Fumonisin
g	gram
gDNA	genomic DNA
GNPS	Global Natural Products Social Molecular Networking
GO	Gene Ontology
GYM	Glucose yeast malt medium
h	hours
H_2O	Water
HBSS	Hank's Balanced Salt Solution
HCl	Hydrochloric acid
HCT-116	Human Colorectal carcinoma 116
HDAC	Histone Deacetylase
HEK-293	Human Embryonic Kidney 293
HF	High Fidelity
hpi	hours post inoculation
hph	Hygromycin B phosphotransferase gene
IC_{50}	Inhibitory Concentration 50%
ITS	Internal Transcribed Spacer
kb	Kilobase
KCl	Potassium Chloride
kg	Kilogram
KO	Knock-Out
KOH	Potassium Hydroxide

l	Liter
LB	Lysogeny Broth
LC-MS/MS	Liquid Chromatography - Tandem Mass Spectrometry
LD_{50}	Lethal Dose 50%
M	Molar
mbar	millibar
MBCA	Microbial Biological Control Agent
MCL	Markov Clustering
MCMC	Markov Chain Monte Carlo
MEGA	Molecular Evolutionary Genetics Analysis
MEM	Minimum Essential Medium
MeOH	Methanol
mg	Milligram
mL	Millilitre
mm	Millimeter
MM	Minimal Medium
MoNA	MassBank of North America
mRNA	messenger RNA
µg	Microgram
µL	Microliter
µm	Micrometer
µM	Micromolar
NaCl	Sodium chloride
NaOH	Sodium Hydroxide
NCBI	National Center for Biotechnology Information
ng	Nanogram
NIST 17	National Institute of Standards and Technology 17
nm	Nanometer
NRPS	Non-ribosomal Peptide Synthase
OMA	Oat Meal Agar
OTA	Ochratoxins
PCR	Polymerase Chain Reaction
PBS	Phosphate-Buffered Saline
PDA	Potato Dextrose Agar
PEG	Polyethylene Glycol
PKS	Polyketide Synthase
PLT	Pyoluteorin
PSTF	Pathway Specific Transcription Factor
QoI	Quinol Oxidation Inhibitor
Q-Tof	Quadrupole Time-of-Flight

ReSpect	Repository of Spectral data
RNA	Ribonucleic acid
RNA-Seq	RNA Sequencing
ROS	Reactive Oxygen Species
rpm	Revolutions per minutes
RQN	RNA Quality Number
rRNA	ribosomal RNA
RSLC	Rapid Separation Liquid Chromatography
rt	Retention Time
RT	Room temperature
r.h.	Relative humidity
S. cerevisiae	*Saccharomyces cerevisiae*
SM	Secondary Metabolites
SMBGC	Secondary Metabolite Biosynthetic Gene Clusters
SPE	Solid Phase Extraction
STC	Sterigmatocystin
T. roseum	*Trichothecium roseum*
T. asperellum	*Trichoderma asperellum*
T. harzianum	*Trichoderma harzianum*
TF	Transcription Factor
T_m	Melting Temperature
U	Units
UV	Ultraviolet
V	Volts
WEIZMASS	Weizmann Institute of Science
WT	Wild Type
ZEA	Zearalenone
Ø	Diameter
ºC	Degree Celsius
µE/m2/s	micromoles per square meter per second
%	Percentage
x g	times gravitational acceleration

List of figures

List of supporting figures

List of tables

1 Introduction

1.1 Maize - a global staple facing climate challenges and emerging pathogens

Maize (*Zea mays*) stands as a pivotal crop wielding significant importance in Africa, Central America, and Europe. Revered as the "queen of cereals", its reputation is rooted in unrivaled versatility and adaptability (Karnatam et al., 2023). Beyond serving as a vital food source, maize fulfills roles in fodder production and bioenergy generation (Kashyap et al., 2023). Diverse in its types, including yellow/white grain, sweet corn, waxy corn, high amylase corn, and quality protein maize, this crop plays a central role in global food production (Maqbool et al., 2021). With a domestication history dating back 5000 years to southern Mexico, maize has traversed continents, was introduced to Europe and is now globally dispersed (Jeffreys, 1955; Sluyter & Dominguez, 2006). Worldwide, maize is cultivated across 166 countries on more than 197 million hectares, making it the second most widely grown crop following wheat with an annual global contribution that surpasses 1 billion metric tons (Erenstein et al., 2022). The significance of maize transcends its role as a primary food source; it is a linchpin in various industrial applications (Obadi et al., 2023). Biotechnological advancements have brought market changes, enhancing its productivity and applications (Chavas et al., 2018). In Europe, the demand for maize has surged, with harvested grain reaching 196.9 million metric tons in 2021, up from 192.8 million in 2020, accompanied by higher apparent yields (https://ec.europa.eu/eurostat).

However, the trajectory of maize cultivation faces challenges in the wake of climate change. Europe, experiencing increased dryness and warmth, anticipates elevated abiotic stress conditions, particularly during crucial growth stages like silking and kernel filling (Miedaner & Juroszek, 2021). Simultaneously, the changing climate fosters opportunities and threats, as various plant pathogens and pests adapt to evolving conditions (Meena & Nirupma, 2021). Recent monitoring in European maize fields reveals the emergence of fungal diseases including anthracnose leaf blight (ALB) caused by *Colletotrichum graminicola*, common rust caused by *Puccinia sorghi*, grey leaf spot caused by *Cercospora zeae-maydis*, Kabatiella eyespot caused by *Aureobasidium zeae*, and Northern corn leaf spot caused by *Bipolaris zeicola* (Miedaner & Juroszek, 2021). These diseases present significant challenges for maize producers across Asia, Africa, and Europe (Ekwomadu & Mwanza, 2023; Kumar et al., 2022).

Anthracnose, caused by the hemibiotrophic fungal pathogen *C. graminicola*, poses significant danger to maize impacting various plant tissues with stalk rot and seedling blight being economically damaging (Rogerio et al., 2023). ALB is globally important, causing yield losses up to 40%, with severe cases leading to lodging rates of 80% (University of Delaware; https://www.udel.edu/academics/colleges/canr/cooperative-extension/fact-sheets/anthracnose-leaf-blight-and-stalk-rot-of-corn/). Anthracnose can infect corn throughout the growing season manifesting in phases like leaf blight, top dieback, and stalk rot (Sukno et al., 2008). The "leaf blight" phase, occurring early with moderate temperatures and damp conditions, shows inconspicuous lesions progressing from bottom to upper leaves. Infected leaves wither and die, displaying tan to brown coloration. In fields with significant anthracnose pressure, "top dieback" may occur post-tasseling, where the upper plant section dies prematurely while the lower part remains green. The "stalk rot" phase leads to pith and vascular system decay, reducing water translocation to upper leaves, and causing them to dry down. Disease onset, just before plant maturity results in the entire plant dying with rotted nodes. Shiny black discoloration appears later in the season on the stalk surface, especially on lower internodes accompanied by internal stalk tissue discoloration and softening (Bayer Crop Science; https://www.cropscience.bayer.us/articles/bayer/anthracnose-corn-disease).

1.2 Life cycle, infection process, and genomic insights of *Colletotrichum graminicola*

C. graminicola, belonging to the family of Glomerellaceae in the order of Glomerellales is a facultative pathogen and well adapted to corn-based agrosystems (Cannon et al., 2012). With a short 3- to 4- day life cycle, it prolifically produces asexual spores (conidia), aiding its widespread dissemination in corn fields. The fungus can also thrive on maize residues and overwinters through saprophytic growth on decomposing plant debris. In its reproductive cycle, *C. graminicola* generates sickle-shaped conidia from acervuli enveloped in a water-soluble spore matrix, or mucilage, containing polysaccharides and proteins (Hutchison et al., 2002 ; Mattupalli et al., 2014 ; O'Connell, 1991; Pain et al., 1996). This matrix sustains conidial viability, and dispersal of conidia occurs mainly through water splashing and raindrop impact (Bergstrom & Nicholson, 1999). Following the dispersal of conidia from acervuli and their deposition on a potential host surface, a signal transduction cascade is activated, triggering the expression of genes crucial for

establishing the pathogen-host interaction. This process includes the secretion of glycoproteins essential for spore adhesion and signals for germination (Hutchison et al., 2002). Conidial adhesion, occurring within 30 minutes post-inoculation is a critical step for initiating penetration and invading the host cells (Epstein & Nicholson, 2016).

Around five to six hours later, a germ tube emerges from two-celled septated conidia. In some instances, both halves of the conidia generate germ tubes and appressoria with the infection cell often differentiating directly beside the conidium, resulting in an extremely short germ tube (Bergstrom & Nicholson, 1999). Appressoria facilitates the direct penetration of the host epidermis. This process typically takes around 15-20 hours after conidial adhesion to fully differentiate into a black spherical appressorium approximately 7µm in diameter. The differentiation involves the establishment and maintenance of high turgor pressure into the cell wall of the appressorium and the synthesis of osmolytes like glycerol within the appressorium (Loehrer et al., 2014). The pressure is then directed through an infection pore at its base to the host's epidermal cell wall (Bechinger et al., 1999; Deising et al., 2000). Following the successful penetration of the host's epidermal cell, the fungus undergoes a crucial developmental stage marked by the formation of an infection vesicle and primary hyphae. Operating in a biotrophic mode to this point, the fungus uptakes nutrients from the living host cell and employs diverse strategies to elude plant defense responses, including the concealment of invading hyphae and the active suppression of plant defense mechanisms (Oliveira-Garcia & Deising, 2013; Perfect et al., 1998).

The transition to the necrotrophic mode of nutrition occurs 24 to 36 hours after the initiation of penetration. In this phase, the fungus develops thin-branched secondary hyphae that penetrate host cell walls and membranes. Enzymes responsible for degrading plant cell walls facilitate the invasion of hyphae and utilization of polymeric cell wall compounds as a nutrient source (Howlett, 2006; Perpetua et al., 1996). As the pathogen proliferates within plant tissue, initial symptoms appear as chlorotic spots. With further development, necrotic spots emerge, becoming sites for the fungus to form acervuli and conidia (Bergstrom & Nicholson, 1999).

Comparative genomics of *C. graminicola* revealed extensive sets of genes related to pathogenicity encoding secreted effectors, secondary metabolism enzymes, transporters, and peptidases. The genome-wide transcript profiling uncovered a sequential activation of genes, aligning with critical

phases of pathogenicity. More specifically, the initiation of effectors and secondary metabolism enzymes takes place before and during the biotrophic stage, whereas the increased expression of a majority of hydrolases and transporters occurs at a later stage, coinciding with the transition to necrotrophy (O'Connell et al., 2012). *C. graminicola* is predicted to harbor about 12,000 protein-coding genes. Employing Markov clustering (MCL) to analyze the proteomes revealed a total of 5342 genes and small molecule efflux pumps. *C. graminicola* also possesses a robust repertoire of genes encoding carbohydrate-active enzymes (CAZymes) involved in plant cell wall degradation and fungal cell wall modification. Concerning cell wall related enzymes, a higher percentage of cellulase and hemicellulose-related genes are activated during the necrotrophy phase (de Oliveira Silva et al., 2024). Notably, a higher number of secondary metabolism genes were also identified, organized into 42 distinct clusters. As each of these clusters contributes to the biosynthesis of a specific metabolite, *C. graminicola* is anticipated to produce unusually extensive and conspicuous spectra of secondary metabolites (SMs), possibly including previously unidentified molecules (O'Connell et al., 2012).

1.3 Life cycle, genomics, and chemistries of *Aspergillus nidulans*

The ascomycete *Aspergillus nidulans* is a saprophytic and ubiquitous filamentous fungus with a haploid genome. The life cycle of *Aspergillus nidulans* is a multifaceted adaptable process, showcasing the fungus's reproductive versatility. The single conidiospore germinate giving rise to a network of hyphae and collectively forming a mycelium, thereby facilitating substrate colonization and nutrient acquisition (Lee & Adams, 1994). Under favorable conditions, the fungus engages in asexual reproduction through conidiophore development, generating conidia. These conidia, as resilient propagules, disperse anemochorically and upon encountering a conducive environment, germinate to establish new colonies, perpetuating the vegetative growth phase (Son et al., 2023).

The life cycle also includes sexual reproduction, introducing genetic diversity. This entails cleistothecium formation where ascogenous hyphae undergo gametogenesis, yielding ascospores (Noble & Andrianopoulos, 2013). Notably, this phase involves nuclear fusion and meiosis, resulting in genetically diverse ascospores. Upon cleistothecium rupture, ascospores are released,

germinating to initiate new hyphal colonies. Completing the life cycle, ascospores germinate and give rise to vegetative development (Han, 2009).

The genome of *A. nidulans* strain FGSC A4 was sequenced in 2005, which is ~30 mega base pairs (Mbp) in size contained in eight chromosomes and harbors over 11,000 genes (Pinar et al., 2019). It has received global attention as a prototypical eukaryote and acts as an ideal candidate for genomic approaches (Pontecorvo et al., 1953) to study the regulation of metabolic pathways involving SMs (Chemudupati et al., 2019; Horio et al., 2019; Németh et al., 2019). Some of the notable SMs produced by *A. nidulans* include penicillin (1991), sterigmatocystin (STC) (1996), ferricrocin (2003), emericellamide (2008), orsellinic acid (2009), and asperfuranone (2009). In the last decade, there has been a tremendous increase in the discovery of SMs from this species including xanthone (2011), austinol (2012), aspernidine A (2013), nidulanin A (2013), aspercryptin (2016), diorcinol (2019), and viridicatumtoxin (2020) (Caesar et al., 2020). Comprehending these genetic clusters is imperative for understanding their diverse purposes, including the clarification of the biochemical pathways associated with the synthesis of SMs and the revelation of the functions these metabolites serve in fungal biology. As a pivotal model organism, investigating the secondary metabolite biosynthetic gene clusters (SMBGCs) in *A. nidulans* has not only deepened our understanding of fungal genetics but also significantly advanced genetic and biochemical research, and holds promise for practical applications in domains such as agriculture, and medicine.

1.4 Life cycle, genomics, and applications of *Bacillus* spp.

Bacillus species are a diverse group of rod-shaped, gram-positive bacteria commonly found in soil, water, and air (Schaechter, 2009). Known for their ability to form endospores, they can survive extreme environmental conditions such as high temperatures, radiation, desiccation, and toxic chemicals (Nicholson et al., 2000). The life cycle of *Bacillus* encompasses three distinct phases viz. vegetative growth, sporulation, and germination. Vegetative growth is marked by binary fission under nutrient-abundant conditions, during which chromosomal replication and cell division are tightly coordinated. Sporulation is initiated by multiple environmental signals, including nutrient depletion, high cell density, and specific mineral concentrations, which activate a phosphorelay system leading to the phosphorylation of the master regulator, *Spo0A*. This process

triggers a cascade of gene expression events resulting in the formation of a highly resilient endospore (Sella et al., 2014). Germination is triggered when favorable environmental conditions are detected, such as the presence of specific nutrients or changes in pH and temperature. This process involves the activation of germination receptors (e.g., *GerA*, *GerB*, *GerK*) on the spore's inner membrane, leading to the degradation of the protective cortex and rehydration of the core. Subsequent stages include the resumption of metabolic activity, protein synthesis, and eventual outgrowth into a vegetative cell (Sella et al., 2014).

The genomics of *Bacillus* species revealed significant diversity in genetic content, reflecting their adaptability to various environments and ecological roles. The genome size of *Bacillus* generally ranges from 3 to 6 Mbp, with a high proportion of genes dedicated to metabolic versatility and environmental stress responses (Fritze & Pukall, 2001). Notably, species like *Bacillus subtilis* have a well-annotated genome of approximately 4.2 Mb, containing over 4,100 protein-coding genes (Barbe et al., 2009). This genome is characterized by the presence of genes encoding diverse enzymes, transporters, and regulatory proteins, facilitating rapid adaptation to changing conditions. Moreover, genomic analyses have revealed a considerable number of mobile genetic elements such as plasmids and transposons in many *Bacillus* species, contributing to horizontal gene transfer and the acquisition of antibiotic resistance and virulence factors (Turnbull, 1996). Comparative genomics also highlights significant genomic plasticity, with strain-specific genes often involved in niche adaptation, pathogenesis, and symbiosis (Didelot et al., 2009).

Bacillus species are notable for producing a wide range of SMs that aid in their survival and ecological interactions. These include antibiotics, enzymes, and bioactive compounds like surfactin, fengycin, and iturin, which exhibit broad-spectrum antimicrobial activity (Ongena & Jacques, 2008). Additionally, they also produce polyketides (PKs) such as difficidin and bacillaene with antibacterial and antifungal properties (Stein, 2005). Besides being prolific producers of SMs, *Bacillus* species are renowned contributors as biocontrol agents. For instance, *Bacillus amyloliquefaciens* produces antimicrobial compounds like bacillomycin, bacillibactin, and bacilysin which inhibit the growth of plant pathogens (Arguelles-Arias et al., 2009). Similarly, *Bacillus velezensis* is known for producing bacillomycin D and macrolactin, which have broad-spectrum antifungal and antibacterial activities (Zhu et al., 2020). The application of *Bacillus* species as biocontrol agents through field spraying has shown promising results by inhibiting the

growth of pathogens such as *Fusarium oxysporum* and *Botrytis cinerea*. When sprayed, these bacteria colonize the plant surface, producing antimicrobial lipopeptides and PKs that suppress harmful microbes (Serrão et al., 2024). Thus, *Bacillus* species is assumed to hold considerable promise for sustainable agriculture due to their versatile life style, genomic capacity to produce diverse SMs, and demonstrated effectiveness in biological control.

1.5 Synthetic and eco-friendly chemistries in plant disease management

Plant diseases are caused by various pathogens, including fungi, bacteria, and viruses that adversely affect growth, development, and productivity of plants. Effective management of diseases involves a combination of preventive measures, cultural practices, chemical treatments, and biological control, all aimed at minimizing the impact of disease on crops and ensuring global food security (Singh et al., 2021). Chemical fungicides are designed specifically to eliminate fungal infection in plants and have been used for decades to protect crops (Doble & Kumar, 2005). Since the early use of copper and sulfur (McCallan, 1949), copper hydroxide or copper sulfate have been regarded as contact fungicides, damaging cell membranes and interfering with cellular mechanisms (Tamm et al., 2022). When cells are exposed to copper-based fungicides, copper ions penetrate fungal spores and induce the generation of reactive oxygen species (ROS), leading to oxidative stress and damage to essential cellular components like DNA, proteins, and lipids. Additionally, copper binds to sulfhydryl groups, disrupting protein function and enzyme activity, which compromises several biochemical processes. This mechanism triggers apoptosis-like cell death, as seen in yeast cells where DNA fragmentation occurs. In addition, copper's high affinity for thiol groups reduces antioxidant capacity, further enhancing its cytotoxic effects (Burandt et al., 2024).

Several classes of highly effective fungicides have been developed thereafter, including various lanosterol 14α-demethylation inhibitors (DMIs), which were used as ergosterol biosynthesis blockers in both agriculture and medicine (Tyndall et al., 2016). For the control of maize diseases, several fungicides are commonly used, but they depend on the specific diseases present, local conditions, and the stage of crop growth (Smart, 2003). Classes of Triazoles (DMI fungicides) such as tebuconazole, propiconazole, and metconazole are used against gray leaf spot and northern corn leaf blight due to their ergosterol inhibitory activity (Carpane et al., 2020; Russell, 2005). The

dithiocarbamate fungicide mancozeb in combination with biocontrol agent *Bacillus cereus* C1L has shown efficacy against southern corn leaf blight (Lai et al., 2016). In specific, the primary mechanism of action of mancozeb involves disruption of fungal cell's thiol groups critical for metabolism, respiration, and energy production. This impairment leads to the accumulation of toxic metabolic by-products, ultimately causing cell death (Scariot et al., 2016). Due to its multi-site activity, mancozeb is less prone to resistance development, making it valuable for integrated pest management strategies (Gullino et al., 2010; Soares et al., 2023). On top of that, quinol oxidation inhibitors (QoIs) group of fungicides act by disrupting fungal mitochondrial respiration by binding to the Qo site of cytochrome bc1 complex, leading to a halt in ATP synthesis and energy production (Fernández-Ortuño et al., 2008). Combination of fungicides have also been studied to control plant diseases. For instance, an amalgamation of flutriafol and azoxystrobin applied in two doses (0.5 and 0.6 g/L) employing a CO_2 pressurized sprayer was found to be effective against foliar diseases in corn (Silva et al., 2021).

While chemical fungicides are valuable tools in agriculture, they come with several stumbling blocks. A major concern is its effect on crop growth, physiology, and development (Petit et al., 2012). Of particular relevance is the azole group of fungicides conferring pathogen resistance in *Aspergillus fumigatus* which is thought to have risen from agricultural use. Current literature also states the effect of azole fungicides on humans, including craniofacial malformations, birth defects, and mammalian steroidogenesis (Crofton, 1996), and a considerable number of agricultural azole fungicides target the human liver as the primary organ for toxicity (Marx-Stoelting et al., 2020). They have also been associated with the inhibition of cytochrome P450 monooxygenase *CYP19* which is a crucial enzyme in estrogen biosynthesis (Trösken et al., 2006). These studies underscore the need for careful management and regulation of azole fungicides, considering both their agricultural benefits and associated risks to human health.

Amid growing societal and political concerns, stricter regulatory practices in fungicide legislation are leading to fewer fungicides being registered than banned (Beckerman et al., 2023; Brauer et al., 2019). This shift prompts the urgent exploration of alternative and ecologically compatible plant protection strategies. As antifungals face a decline, the European Union (EU) strives to fulfill the European Green Deal objective, aiming for 25% of agricultural land to be under synthetic chemistry-free organic farming by 2030 (https://commission.europa.eu/strategy-and-policy/

priorities-2019-2024/european-green-deal_en). In place of synthetic chemistries, microorganisms exhibiting hallmark antagonistic properties are thought to warrant control of diseases in crops. Presumably eco-friendly measures such as the application of microbial biological control agents (MBCAs) have achieved global attention due to their notable effectiveness against plant pathogens (Ghorbanpour et al., 2018).

SMs produced by MBCAs are key to their ability to suppress plant diseases. These metabolites are organic compounds that, while not directly involved in the primary growth or reproduction of the organisms, play critical roles in ecological interactions such as competition, defense, and communication. Examples include antibiotics (e.g., penicillin from *Penicillium*), antifungals (e.g., amphotericin B from *Streptomyces*), and immunosuppressants (e.g., cyclosporine from *Tolypocladium inflatum*) (Demain & Sanchez, 2009). These compounds often have complex structures and are biosynthesized via specialized pathways involving multifunctional enzymes such as polyketide synthase (PKS) or non-ribosomal peptide synthetase (NRPS) (Hwang et al., 2020). SMs such as PKs, fatty acids, and some terpenoids, are synthesized through biosynthetic pathways that utilize acetyl-CoA or other acyl-CoA derivatives as building blocks (Hwang et al., 2020). In the polyketide biosynthesis pathway, acetyl-CoA or malonyl-CoA is used as a starter unit, and additional acyl-CoA units are sequentially added by PKSs through Claisen condensation reactions (Shen, 2003). This process involves the formation of a carbon-carbon bond between two acyl groups, resulting in a growing carbon chain that can undergo cyclization, reduction, oxidation, and glycosylation to form structurally diverse and biologically active compounds (Cane et al., 1998). For instance, PKs such as erythromycin are assembled by Type I PKS that contain multiple catalytic domains in a single polypeptide chain. Each domain in the PKS enzyme is responsible for a specific reaction, such as chain initiation, elongation, and modification. This modular organization allows for the assembly of a wide variety of PKs with complex structures and diverse biological activities (Khosla et al., 2007). Similarly, NRPS use acyl-CoA derivatives as substrates to produce non-ribosomal peptides such as antibiotic penicillin and immunosuppressant cyclosporine. The acyl-CoA units are activated and linked together by specific enzymes, leading to the production of linear or cyclic peptide chains (Walsh, 2004).

In general, various fungal and bacterial biocontrol agents are extensively used in suppressing phytopathogens primarily due to the fact that they extensively produce SMs. For instance,

compounds such as surfactin, iturin, and fengycin, produced by *B. subtilis* are critical for their antagonistic interactions against plant pathogens (Ongena & Jacques, 2008). Similarly, *Pseudomonas fluorescens* produces phenazine and pyrrolnitrin, which have been reported to effectively control root diseases caused by *Rhizoctonia solani* and *Pythium ultimum* (Haas & Défago, 2005). In specific, a study conducted on maize showed the role of pyoluteorin (PLT) produced by *Pseudomonas protegens* Pf-5 in suppressing the growth of fungal pathogenic *Pantoea ananatis* causing brown rot on leaves in maize (Gu et al., 2022). In addition, *Trichoderma* species, which are highly interactive in roots and soil environment, also produce SMs such as anthraquinones, daucanes, pyranes, viridiofungins, and 6-pentyl-2H-pyran-2-one (6PP) as agents suited to control other microorganisms (Daoubi et al., 2009; Reino et al., 2008). The recombinant *B. subtilis* 26DCryChS line containing the gene *Btcry1la* from *Bacillus thuringiensis* synthesizes the lipopeptide surfactin and inhibits the growth of the fungal pathogen *Stagonospora nodorum* (Maksimov et al., 2020). These findings highlight the potential of MBCAs and their SMs as effective, eco-friendly strategies for managing a wide range of plant pathogens. This focus on MBCAs underscores the critical role of SMs in ecological interactions, particularly as chemical defenses against other microorganisms.

1.6 Microbial chemical defense - SMs and their regulation

The primary defense strategy employed by fungi and bacteria when confronted by other microorganisms is chemical defense (Kunzler, 2018), which involves the production of SMs. Depending on their ecological niche, microbes produce several structurally and functionally distinct SMs that originate from central metabolic pathways and primary metabolic reservoirs. These compounds are synthesized by SMBGCs under tight transcriptional control. The regulation of SM synthesis involves a complex network of cluster-specific, global, and pathway-specific regulators (Lim et al., 2012). Cluster-specific regulators are proteins encoded within SMBGCs, including pathway-specific transcription factors (PSTFs) such as *AflR*. For example, *AflR* in *Aspergillus* species, encoded by a gene within the aflatoxin (AF) and STC clusters, directly binds to the promoter regions of SMBGCs, activating or repressing the transcription of pathway genes like *aflD*, *aflM*, and *aflP*, which are responsible for AF production (Ehrlich et al., 1999). Additionally, global regulator such as the nuclear methyltransferase-domain protein *LaeA* in

A. nidulans, influence the expression of multiple SMBGCs, coordinating SM production in response to broader environmental cues (Brakhage, 2013). However, a major limitation is that many SMBGCs remain cryptic under lab conditions but are activated only in the presence of microbial predators (Netzker et al., 2015), highlighting the need for further research into their ecological role and regulatory mechanisms.

Over the past four decades, co-culturing methods that are simple and are thought to mimic natural competitions have been increasingly applied to spark cryptic SMBGCs (Netzker et al., 2015). A review study by Bertrand and co-workers emphasized the effectiveness of co-culture experiments in enhancing the diversity of chemical compounds, playing a vital role in SM production (Bertrand et al., 2014). Several examples demonstrate the novel chemistries induced by co-cultivation strategies. For instance, the antibacterial alkaloid aspergicin was obtained from coculture of *Aspergillus* species (Zhu et al., 2011). Similarly, the co-cultivation of *Acremonium* sp. TBP-5 with *Mycogone rosea* DSM 12973 led to the discovery of the lipoaminopeptides, acremostatins A, B, and C (Degenkolb et al., 2002). Another notable example includes a confrontation study between *A. sydowii* and *B. subtilis*, which led to the production of four novel metabolites namely 4´-alkenyl serine sydonate (N6), serine sydonate (N7), hydroxyl serine sydonate (N9), and an isomer of macrolactin U, renamed macrolactin U´ (N20) (Sun et al., 2021). These studies highlight the immense potential of activating SMBGCs through microbial competition and defense, offering a valuable approach for discovering novel SMs with global applications. While these activation strategies hold great promise for understanding novel SMs, it is also important to recognize that the toxic SMs produced under microbial co-cultivations can have unintended detrimental effects in natural environments.

1.7 Toxic chemistries in microbes - health risks and regulatory considerations

As previously mentioned, microbial communities often employ a range of toxic SMs as chemical weapons to outcompete or suppress other microorganisms in their environment. Among these toxic compounds, mycotoxins, primarily synthesized by species of *Aspergillus*, *Fusarium*, and *Penicillium* pose significant threats not only to microbial competitors but also to human and animal health (Madariaga-Mazón et al., 2019). Notable examples include lovastatin from *A. terreus*, which targets the molecule HMG-CoA-reductase, strobilurin from *Oudemansiella mucida*

targeting cytochrome b, and aflatoxin B1 (AFB1) from *A. flavus* which targets DNA (Kunzler, 2018). The most prevalent and toxic mycotoxins with substantial impacts on human and animal health include AF and STC produced by various species of *Aspergillus* (Figure 1).

In addition, mycotoxins such as deoxynivalenol (DON), fumonisin (FUM), and zearalenone (ZEA) produced by *Fusarium* species, as well as patulin and ochratoxins (OTA) produced by *Aspergillus* and *Penicillium* species, are also significant due to their frequent occurrences in various food and feed commodities (Alshannaq & Yu, 2017; Díaz Nieto et al., 2018). These compounds cause a range of toxic effects on human health, including hepatotoxicity, carcinogenicity, immunosuppression, nephrotoxicity, teratogenicity, and disorders affecting the intestines and reproductive system (Benkerroum, 2020b; Heussner & Bingle, 2015; Knutsen et al., 2017; Voss & Riley, 2013). Notably, aflatoxicosis outbreaks have occurred occasionally in Africa and Asia (Benkerroum, 2020a). A major aflatoxicosis outbreak in eastern Kenya in 2004 resulted in 125 deaths of people (Azziz-Baumgartner et al., 2005). Maize samples collected from the affected regions revealed alarmingly high concentrations of AFB1, reaching up to 4400 parts per billion (ppb), which is 220 times greater than the 20 ppb safety limit set by Kenyan authorities for food (Probst et al., 2007). The acute toxicity of other mycotoxins such as ochratoxins, DON, and patulin, as indicated by their LD_{50} values, ranges between 3 - 20 mg/kg, 46 - 78 mg/kg, and 29 - 55 mg/kg, respectively (Alshannaq & Yu, 2017).

While assessing the acute toxicity of mycotoxins, it is also informative to compare these values to those of synthetic fungicides, which are commonly used in agricultural settings. For comparison, the acute oral LD_{50} for triazole group of fungicides in rats ranges between 1453 and >2000 mg/kg of body weight (b.w.) (Rachid, 2010), while the oral LD_{50} of AFB1 in male and female rats is equivalent to 7 and 16 mg/kg b.w., respectively (Butler, 1964). A synthetic insecticide, dichlorodiphenyltrichloroethane (DDT) has been banned in the United States since 1972 due to its adverse environmental and human health effects (Mansouri et al., 2017). The oral LD_{50} of DDT ranges between 113 and 118 mg/kg b.w. in rats and is classified as moderately toxic by the U.S. National Toxicology Program (NTP, https://ntp.niehs.nih.gov/).

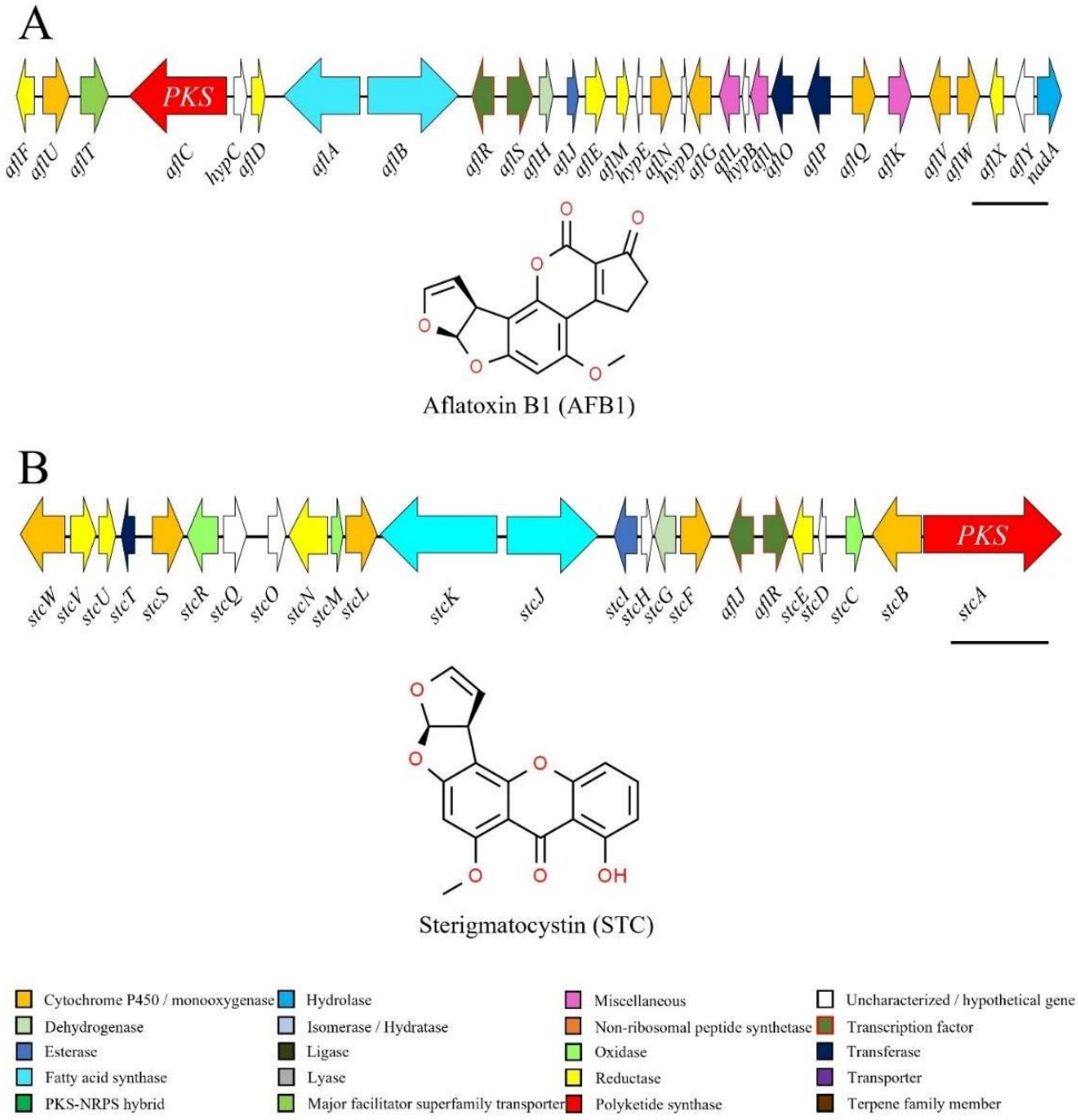

Figure 1. SMBGCs involved in the biosynthesis of the mycotoxins AFB1 and STC.

(A) The AFB1 SMBGC consists of 30 genes, including a core *PKS* gene and two transcription factors (TFs). **(B)** The STC SMBGC comprises 24 genes, also featuring a core *PKS* gene and two TFs. **(A** and **B)** The horizontal arrows represent the SM genes, indicating their transcriptional direction. The color code indicates the putative function of each gene, with corresponding gene names annotated below each gene in the clusters. The chemical structures of AFB1 and STC, obtained from PubChem are shown below their respective SMBGCs, illustrating the molecular products synthesized by these gene clusters. The scale bar, located at the lower right of each cluster, represents 5 kb.

Another mycotoxin, STC, produced by *Aspergillus* species, can induce moderate yet potentially life-threatening effects. Although it is not as widely studied as AFs, the health concerns related to this toxic compound remain poorly addressed. The International Agency for Research on Cancer (IARC) has classified STC as a potential human carcinogen Group 2B (The European Food Safety Authority EFSA) (EFSA, 2013), which has been found to exhibit immunotoxic and immunomodulatory activity (Liu et al., 2014), along with mutagenic effects (Gao et al., 2015). As STC acts as a vital precursor in AF biosynthesis pathway, these mycotoxins exhibit shared toxic effects including genotoxicity and carcinogenicity (Theumer et al., 2018). STC demonstrates an acute oral toxicity with LD_{50} values ranging between 120 and 166 mg/kg b.w., primarily targeting the liver and kidneys (Ráduly et al., 2020), which is higher than most synthetic fungicides. STC is metabolized in the liver and lungs by various CYP enzymes, producing diverse hydroxy metabolites that are subsequently excreted in bile and urine (Díaz Nieto et al., 2018). The CYP enzymes oxidize STC to form highly reactive epoxide intermediates, which can covalently bind to DNA, specifically at the N7 position of guanine, forming STC-N7-guanine adducts that may lead to genetic mutations (Essigmann et al., 1979). Another study describes an alternative mechanism involving the hydroxylation of the aromatic ring to form a catechol 9-hydroxy-STC, capable of reacting with DNA, thereby inducing genotoxic effect (Pfeiffer et al., 2014). Animal experiments have further corroborated the carcinogenic potential of STC, demonstrating its ability to induce liver tumors and other malignancies that align with studies in human-derived cell lines (Díaz Nieto et al., 2018; Tong et al., 2013). Upon oral exposure to STC, there have been reports of premalignant and malignant lesions, including hepatocellular carcinomas and angiosarcomas in brown fat tissues of mice (Enomoto et al., 1982). Additionally, studies on human bronchial epithelial cell lines have shown that STC induces DNA double-strand breaks, which could potentially lead to adenocarcinomas (Cui et al., 2017). Given the complex mechanisms of action and the varying levels of toxicity associated with microbial toxins like AFs and STCs, understanding the interactions and competition among microorganisms becomes crucial. Exploring these interactions helps to elucidate the role of antagonistic microorganisms and their secreted metabolites in natural environments.

1.8 Complexity and specificity of SM dynamics in microbiome

The intricacy of SM formation appears significantly heightened in natural environments, particularly in the phyllosphere. Reports indicate an average of 10^6-10^7 bacteria per cm^2 of leaf surface (Vorholt, 2012), and while fungal propagules on leaves are presumed to be less complex, their significance remains notable (Lindow & Brandl, 2003). Since microbial defense heavily relies on chemistry, the multitude of organisms in the phyllosphere is expected to generate a diverse range of unique SMs. This variety can be amplified through the exchange and enzymatic modification of these compounds. Adding to the complexity of SMs formed and secreted in interactions, a confrontation partner may take up SMs formed by another, modify, and secrete them again, resulting in a highly diverse chemical environment (Figure 2).

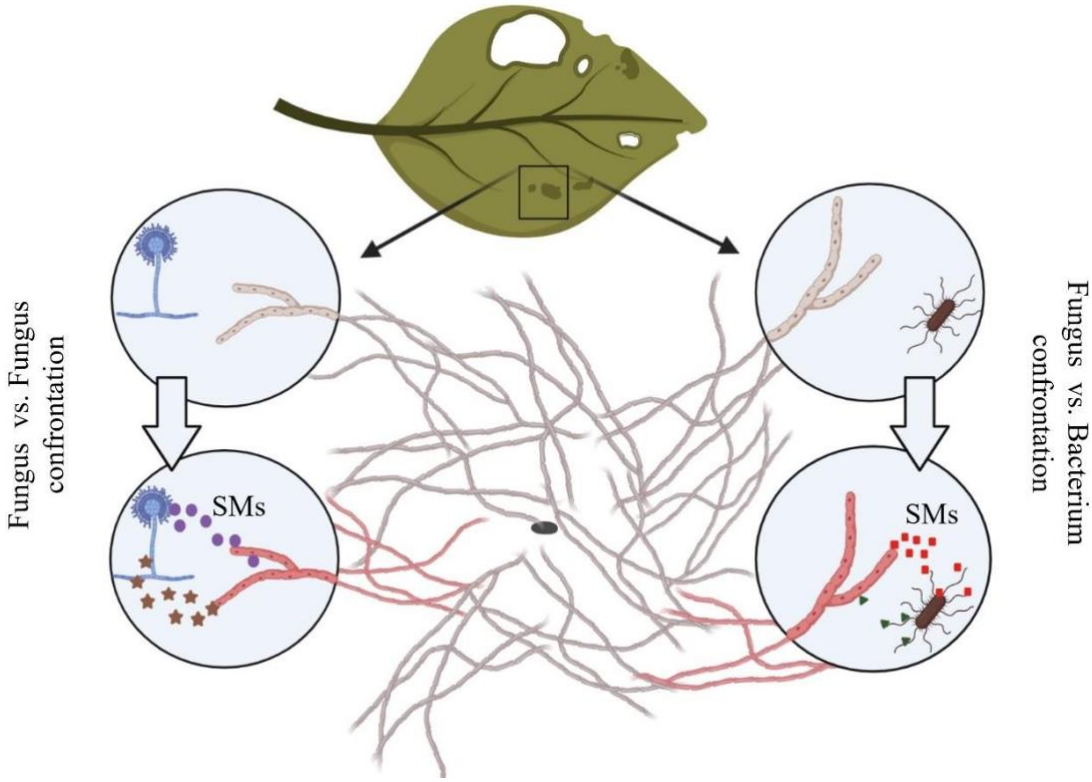

Figure 2. Regulation of chemical defense mechanisms during microbial interactions.

A graphical illustration depicting two types of microbial confrontations: fungus vs. fungus and fungus vs. bacterium. The production and exchange of SMs (represented by purple circles and brown stars for fungal-fungal confrontation, and red squares and green triangles for fungal-bacterial confrontation) are illustrated in response to these rivalries, highlighting their role in chemical defense and competitive strategies. Adapted and modified from (Kunzler, 2018), this figure visually represents the dynamic responses of microbial communities under competitive stress.

Experimental findings involving mutants with defects at different sites/steps of melanin biosynthesis, i.e. the Δ*pks1* mutant of the maize anthracnose fungus *C. graminicola*, lacking *PKS1*, and the *Scd*$^{-}$ mutant of the cucumber anthracnose fungus *C. lagenarium*, lacking the scytalone dehydratase, highlight the exchange of SMs across species (Deising et al., 2017; Kubo et al., 1996). The maize anthracnose fungus was unable to begin dihydroxy naphthalene (DHN) melanin formation due to the disruption of the first gene of the pathways, *PKS1*, encoding a *PKS* (Ludwig et al., 2014). The melanin-deficient scytalone dehydratase mutant 9201Y (*Scd*$^{-}$) of *C. lagenarium* was salmon-colored (Kubo et al., 1996) like the *PKS1* mutant of *C. graminicola*. At the peripheries of these mutants, scytalone produced by the *C. lagenarium* 9201Y strain diffused into the *C. graminicola* melanin-deficient strain with a biosynthetic defect upstream of *SCD1* and was further converted into DHN-melanin, indicating SM exchange across species. In another study, advanced MALDI-TOF and MALDI-FT-ICR imaging mass spectrometry (MALDI-IMS) with MS/MS networking investigated the trans-kingdom interaction between the opportunistic pathogens, *P. aeruginosa* and *A. fumigatus* in the lungs of cystic fibrosis patients. This technique visualized and identified metabolites secreted by these microorganisms. Specifically, the bacterium *P. aeruginosa* produced phenazine metabolites, including pyocyanin and 1-hydroxyphenazine, which inhibited the fungus *A. fumigatus* (Kerr et al., 1999). Notably, *A. fumigatus* transformed bacterial metabolites into phenazine dimers potentially establishing a defense mechanism (Moree et al., 2012). Imaging mass spectrometry revealed intricate trans-kingdom chemical transformations in this microbial interaction. The significance of these findings in assessing the risk associated with SMs produced by antagonistic microorganisms, whether by target or non-target microbes has not been envisioned or experimentally addressed. To investigate the impact of newly introduced bacteria on the bacterial rhizosphere community, Gilbert and co-workers conducted field and growth chamber experiments using soybean seeds coated with the biological control agent *B. cereus.* Analyses of 2651 isolates revealed significant differences in bacterial rhizosphere communities between non-treated and *B. cereus*-coated seed-grown plants in some experiments (Gilbert et al., 1993). This complexity presents a challenge for dissecting the molecular, biochemical and, importantly, chemical tools active in shaping populations.

To create a model microbiome for genetic dissection of community behavior, *B. cereus* as a model rhizosphere bacterium and the "hitchhikers", *Psedudomonas koreensis,* and *Flavobacterium johnsoniae* were employed in trilateral analyses, revealing a hierarchical interstrain-competition

network. Interestingly, *P. koreensis* produced koreenceine, an alkaloid antibiotic inhibiting *F. johnsoniae* growth, and in turn the production of that compound was inhibited by *B. cereus*, thereby stabilizing the consortium (Lozano et al., 2019). Comparative meta-transcriptomics and meta-metabolomics indicated that the transcripts of the SMBGCs differed, suggesting community-dependent secondary metabolism dynamics (Chevrette et al., 2022). These experiments with the defined bacterial community designated as THOR for "the hitchhikers of the rhizosphere" showed that SMs are synthesized in a community-dependent manner. To add to the complexity of intimate microbial interactions, a co-cultivation study from Schroeckh and co-workers involving *A. nidulans* and 58 soil-residing actinomycetes, led to a striking discovery of an intimate physical interaction between the bacterium *Streptomyces hygroscopicus* and the fungus and to identifying a *PKS* gene required for the production of orsellinic acid (Schroeckh et al., 2009). Another research exposes a highly complex tripartite plant-symbiotic-pathogen relationship in rice, where a *Rhizopus* species controls an endosymbiotic bacterium of the genus *Burkholderia*, leading to the production of a mycotoxin, rhizoxin. It was long assumed that rhizoxin was produced by the fungus itself, however, this study led to the surprising finding of a pivotal bacterium as an essential player in interaction between a fungal pathogen and its host plant (Partida-Martinez & Hertweck, 2005).

Given the species complexity of microbial communities (Vorholt, 2012), given the large number of SMBGCs present and putatively activated under micro-organismic confrontations (Baral et al., 2018; Kunzler, 2018; Osbourn, 2010), and given a resulting putative enhancement of compound complexity due to exchange and modification of compounds in different species (Deising et al., 2017; Kubo et al., 1996), one may assume that any disturbance of a consortium by introduction of MBCAs would cause massive changes in SM patterns. These changes could include formation of chemical cocktails of novel compounds with unknown structures and toxicities, and some of these chemistries may even exhibit carcinogenic activity (Deising et al., 2017). Given the potential for MBCAs to alter SM patterns, it is naïve to assume that the formation of putatively toxic microbial SMs poses no risk to consumers or the environment. These compounds, with unknown structures and toxicities, could have unforeseen harmful effects on human health including cytotoxicity and carcinogenicity. Therefore, it is imperative to enforce stricter societal and political regulations to rigorously monitor the toxicological effects of MBCAs and their associated chemical metabolites. This focus on regulation is crucial to safeguard public health and environmental safety.

2 Materials and Methods

2.1 Biological Materials

2.1.1 Fungal material

2.1.1.1 *Colletotrichum graminicola*

The reference wild type (WT) strain CgM2 (syn. M1.001) of *C. graminicola* (Ces.) G.W. Wilson (teleomorph *Glomerella graminicola* D. J. Politis) (Bergstrom & Nicholson, 1999) was gifted by R. L. Nicholson, Purdue University, IN, USA (Nicholson & Moraes, 1980). The WT CgM2 strain, along with the generated ectopic (ect.) and Δ*pks27* strains (see section 2.4.5), were cultivated on oat meal agar (OMA) (Refer appendix 7.2.1) in petri dishes (Ø 5 cm) in an incubator (KB 400, Binder GmbH, Tuttlingen, Germany) at 23 ºC to induce formation of conidia. Conidia from CgM2 WT, ect. and the deletion strains were rinsed with sterile distilled water from OMA plates and preserved in 25% (v/v) glycerol at -80 ºC.

2.1.1.2 *Aspergillus nidulans*

The auxotrophic strain RMS011 of filamentous fungus *Aspergillus nidulans* (teleomorph *Emericella nidulans*) (Stringer et al., 1991) was provided by Dr. Vito Valiante, Hans-Knöll Institute, Jena, Germany. The strain was cultured on potato dextrose agar (PDA) plates (Difco, Becton, Dickinson and company, Maryland, USA) (Refer appendix 7.2.1) for a duration of three weeks at 23 ºC. Post cultivation, the conidia were harvested by rinsing with sterile distilled water and preserved in 25% (v/v) glycerol at -80 ºC.

2.1.1.3 Fungal strains

Unless otherwise stated, the microbial strains were obtained from our lab stocks and grow on PDA. The phytopathogenic fungal strains include *Alternaria tenuis* PP1, *Cochliobolus heterostrophus* C12 (Aliyeva-Schnorr et al., 2023) provided by Dr. Stefan Wirsel (Martin Luther University, Halle (Saale), Germany) and *Colletotrichum higginsianum* KU70 (Ushimaru et al., 2010). The filamentous ascomycetes *Coprinellus domesticus* BRFD1 and a non-defined *Cladosporium* species BRFD2 were isolated from leaves of *Zea mays* cultivar (cv.) ‘Mikado’ grown in the

greenhouse at the Institute of Agricultural and Nutritional Sciences, Halle (Saale), Germany. The isolates were grown on fresh glucose yeast malt (GYM) plates (recommended by DSMZ, Braunschweig, Germany, https://bacmedia.dsmz.de/medium/65; Refer appendix 7.2.1) and incubated at 23 ºC. The fungal biocontrol strains include *Trichoderma asperellum* JKI-BI 7375 and *Trichoderma harzianum* JKI-BI 7374 (Fernando Devasahayam et al., 2024) (both provided by Dr. Ada Linkies, Julius-Kühn Institute, Institute for Biological Control, Dossenheim, Germany) and *Trichothecium roseum* PP2. The killer toxin producing yeast strain *Saccharomyces cerevisiae* T158C (Siddiqui & Bussey, 1981) was provided by Manfred J. Schmitt (Saarland University, Germany). All the cultures were inoculated onto the respective medium and grown under controlled conditions of 23 ºC for one week. All fungal stocks were made with sterile distilled water, preserved in 25% (v/v) glycerol, and stored at -80 ºC for future use.

2.1.2 Bacterial strains

2.1.2.1 Biocontrol strains

The biocontrol bacterial strains used were *Bacillus amyloliquefaciens* JKI-BI 7332/2, *Bacillus subtilis* JKI-BI 7325/1 (Pfeiffer et al., 2021), (both provided by Dr. Ada Linkies, Julius-Kühn Institute, Institute for Biological Control, Dossenheim, Germany). *Bacillus velezensis* NCCB 100737 (Ruiz-García et al., 2005) was obtained from the Westerdijk Fungal Biodiversity Institute, Utrecht, The Netherlands, and another *B. subtilis* strain was isolated from Pflanzenarzt Boden-Fit fertilizer (F. Schacht GmbH & Co, Bültenweg, Braunschweig, Germany). About 2 mL of the fertilizer was subjected to centrifugation in a microcentrifuge tube (Ratiolab, Dreieich, Germany) and the pellet was washed multiple times with sterile distilled water. The obtained pellet was streaked onto a lysogeny broth (LB) medium (Refer appendix 7.2.1) and incubated at 37 ºC in an incubator (C25 classic series, New Brunswick Scientific, NJ, USA) for 16 hours. An individual colony was transferred to and maintained on PDA at 37 ºC and designated as "commercial *Bacillus subtilis*" in this study. All the bacterial stocks were made with 25% (v/v) glycerol and stored at -80 ºC for future use.

2.1.2.2 *Escherichia coli*

Escherichia coli XL1-Blue (*recA1 endA1 gyrA96 thi-1 hsdR17 supE44 relA1 lac* [F´ *proAB lacI*^{q} *Z*Δ*M15* Tn*10* (Tet^{r})] (Stratagene, CA, USA) (Bullock, 1987) was cultivated on LB plates at 37 ºC. To initiate liquid cultures, a colony was inoculated into LB medium and incubated at 37 ºC and 200 rpm. The selection and addition of antibiotics to the media were determined by the specific selection marker employed (See section 7.2.3). A stock culture of *E. coli* was prepared with 7% (v/v) DMSO and stored at -80 ºC.

2.1.3 Plant material

2.1.3.1 *Zea mays*

The maize cv. 'Mikado' was grown in steamed compost in 12 cm diameter pots, with three plants per pot, in a controlled greenhouse at 22 ºC and 60% relative humidity (r.h.). Additional light was provided at a maximum of 15 µE/m^2/s using OSRAM Plantastar 600W (OSRA, Munich, Germany).

Alternatively, maize plants were cultivated in a climate chamber (AR-75L, Percival Scientific, Perry, USA) at 16 hours daylight at 50% r.h. and temperatures of 25 ºC (daytime) or 20 °C (nighttime).

2.2 Chemicals

Chemicals, unless otherwise stated, were from Carl Roth (Karlsruhe, Baden-Württemberg) Germany), Thermo Fisher Scientific (Schwerte, Nordrhein-Westfalen, Germany), VWR Life Science (Darmstadt, Hessen, Germany), or Sigma-Aldrich (Steinheim, Nordrhein-Westfalen, Germany).

2.2.1 Media, buffers, and solutions

Media, buffers, and solutions used in this study are listed in the appendix (Refer appendix 7.2).

2.2.2 Primers

Primers used in this study were obtained from Eurofins Genomics (Ebersberg, Bayern, Germany) and are listed in the appendix (Refer appendix 7.3).

2.3 *In vitro* micro-organismic growth and plant assays

2.3.1 Growth inhibition assays

2.3.1.1 Confrontation assay

The biocontrol bacteria *B. amyloliquefaciens*, and fungus *A. nidulans* were screened for their ability to suppress the mycelial growth of plant pathogenic fungus *C. graminicola* M2 in *in vitro* confrontation assays. A 4 mm agar disc from 14-days-old OMA culture plates of *C. graminicola* was inoculated at the center of a fresh PDA plate (Ø 9 cm) (Greiner Bio-One GmbH, Frickenhausen, Germany). The biocontrol bacteria and *A. nidulans* were inoculated 2.5 cm away from the *Colletotrichum* mycelial disk (Li et al., 2021). As solo cultures, *C. graminicola, B. amyloliquefaciens* and *A. nidulans* were inoculated on fresh PDA plates. All combinations were carried out in triplicates and the plates were incubated at 23 °C. Growth inhibition was evaluated by measuring the distance between microbial colonies and the plates were photographed at 12 days post inoculation (dpi). To evaluate the effect of volatile inhibitors, growth assays were performed on split plates (Tuoxun trade, Zhongshan, China, 2 compartments, Ø 9 cm).

In addition, confrontations were also established between *A. nidulans* and the biocontrol bacteria *B. amyloliquefaciens*, *B. subtilis*, the commercial *B. subtilis* strain, and *B. velezensis*. Moreover, confrontations between *A. nidulans* and fungal strains *A. tenuis*, *C. heterostrophus*, *C. higginsianu*m, *T. roseum*, a strain of an unknown *Cladosporium* species, *C. domesticus*, *T. asperellum* and *T. harzianum*, and yeast *S. cerevisiae* were also investigated. The confrontation assay was carried out as described above with modifications. A mycelial disk of 4 mm^2 size was excised from margins of three-week old cultures of *A. nidulans* and inoculated centrally onto fresh PDA plates for solo and co-cultures. After seven days at 23 ºC, the biocontrol bacteria and fungus, the phytopathogenic fungal strains and yeast were inoculated, and the plates were incubated at 23 ºC for another 7 days. As solo cultures, the confrontation partners were inoculated on individual PDA plates. In the case of *A. nidulans* solo culture, the plates were photographed at 14 dpi, whereas for the solo cultures of confrontational partners, the plates were photographed at 7 dpi. Fungal growth inhibition was evaluated by measuring the growth inhibition distance between microbial colonies at 14 dpi.

Furthermore, confrontation assay was also performed on low-rich minimal medium (MM) plates (Refer appendix 7.2.1) plates. Confrontations were established between *C. graminicola* and biocontrol *B. amyloliquefaciens*, *B. subtilis*, and *B. velezensis* and the experimentation was performed as described above.

2.3.1.2 Fungal growth inhibition by Iturin A and STC

The inhibitory activity of Iturin A (Sigma-Aldrich, Steinheim, Germany) and STC (Sigma-Aldrich, Missouri, USA) were evaluated by the Kirby-Bauer disc diffusion assay (Bauer et al., 1959). PDA plates were centrally inoculated with *C. graminicola* and sterile filter discs with 6 mm diameter were placed at a distance of 2.5 cm from the pathogen. Ten µL containing 50, 100, 300, 500, and 1000 in µg/mL of the respective compounds were impregnated onto the filter discs. Solvents (ethanol for Iturin A and methanol for STC) served as negative controls. The experiment was performed in triplicates and the plates were incubated at 23 ºC for 12 days. Antagonistic activities were evaluated as described (Skidmore & Dickinson, 1976).

2.3.1.3 Co-cultivation of microbes in liquid medium

The co-cultivation study was performed to identify novel class of compounds produced under confrontations. Three mycelial plugs (4 mm diameter) from *C. graminicola* or *A. nidulans* were excised from 2-week-old PDA plates and transferred into sterile potato dextrose broth (PDB). After 4 days of incubation at 28 °C, a single plug (4 mm^2) from a four-day-old PDA plate with *B. amyloliquefaciens* was excised and added to the fungus and incubated for 8 more days. After 12 days, the culture broth was filtered (Ø 0.2 µM pore size, Sartorius Stedim Biotech GmbH, Göttingen, Germany), and the culture filtrates were used for metabolite extraction.

2.3.2 Plant infection

2.3.2.1 Maize inoculation assay

Conidia of *C. graminicola* were harvested from OMA plates at 14 dpi, suspended in 0.02% (v/v) aqueous Tween-20, and adjusted to 10^5 conidia/mL for microscopy and 10^6 conidia/mL for macroscopic symptom assessment. For disease symptom evaluation, third leaves of 14-day-old plants were detached and placed into 12 cm^2 petri dishes (Greiner Bio-One GmbH, Frickenhausen, Germany) containing moist filter paper. Five 10 µL droplets of conidial suspensions prepared from OMA plates were inoculated onto the mid-rib of the adaxial lead surface. The plates were then sealed and placed in a growth chamber (Binder GmbH, Tuttlingen, Germany) and kept at 23 °C in darkness. Mock inoculations were done using 0.02% (v/v) Tween-20. Anthracnose disease symptoms were photographed at 96 hpi.

To assess appressorial penetration rates, leaves were sectioned into small segments at 96 hpi. The abaxial midrib opposite to the inoculation point was removed, and the segments were bleached in ethanol-acetic acid (3:1 (v/v)) for 24 hours. Infection sites were observed by bright field microscopy (Eclipse 600, Nikon, Düsseldorf, Germany).

2.3.2.2 Leaf imprint assay

Zea mays leaves cv. ‘Mikado’ obtained from the experimental station of Martin Luther University (Kühnfeld, Halle (Saale), Germany) were imprinted onto GYM plates. After removal of leaves, plates were incubated at 23 °C for two weeks in darkness and photographed.

2.4 Molecular Biology

2.4.1 Preparation of nucleic acid

2.4.1.1 Genomic DNA isolation from Fungi

The fungal genomic DNA was isolated by a method described by Udo Döbbeling with some modifications (Döbbeling, 2000). Fungal mycelium weighing approx. 500 mg, aged 6 to 8 days in complete medium (CM) (Refer appendix 7.2.1) was dried briefly on absorbent paper towel and then pulverized into a fine powder using a mortar and pestle in liquid nitrogen until homogeneous. To this frozen powder, a mixture of 800 µL of DNA extraction buffer I (Refer appendix 7.2.2) and 800 µL phenol : chloroform : isoamylalcohol (25:24:1) was added and thoroughly blended. The milky mixture was centrifuged in a benchtop centrifuge (Heraeus Fresco 17, Thermo Fisher Scientific, Schwerte, Germany) at 13000 g for 20 minutes at 4 °C. The top phase was transferred to a new microcentrifuge tube and 800 µL of chloroform : isoamylalcohol (24:1) was added, vortexed and homogenized. The resulting phases were separated by centrifugation at 13000 g for 10 minutes at 4 °C. The upper aqueous phase was carefully transferred to a new tube, and DNA was precipitated by the addition of 800 µL of ice-cold isopropanol and incubating at -20 °C overnight. After centrifugation at 6800 g, 15 min, 4 °C, the DNA pellet was dissolved in 700 µL of DNA extraction buffer II (Refer appendix 7.2.2). Subsequent treatment involves digestion with RNase A (10 mg/mL) (Carl Roth, Karlsruhe, Germany) at 37 °C for 30 min, followed by SDS (20%) (Carl Roth, Karlsruhe, Germany) and Proteinase K (20 mg/mL) (Analytik Jena, AJ Innuscreen GmbH, Berlin, Germany) treatment at 60 °C for 60 minutes to remove RNA and remaining proteins. Additional phenol : chloroform : isoamylalcohol and chloroform : isoamylalcohol extractions were performed, followed by isopropanol precipitation as described above. The resulting DNA pellet was washed with 70% ethanol, centrifuged (13000 g for 10 minutes at 4 °C) and air-dried. Finally, the pellet was re-suspended in DEPC-treated H_2O (Refer appendix 7.2.3).

Alternatively, DNA isolation was also carried out using innuPREP Plant DNA kit (Analytik Jena, AJ Innuscreen GmbH, Berlin, Germany) according to the manufacturer's instruction.

2.4.1.2 DNA isolation from Bacteria

Bacterial DNA isolation was carried out by employing a few modifications from the method descried by Wright and co-workers (Wright et al., 2017) involving several sequential steps to ensure efficient isolation. About 1.5 mL of mid-to late-log-phase culture (0.5 to 0.7 OD_{600}) was transferred to a microcentrifuge tube. Subsequently, the cells were pelleted through centrifugation at 12000 g for 2 minutes at 4 ºC, with the supernatant being discarded. Following this, the cell pellet was resuspended in 450 µL of TE buffer (Refer appendix 7.2.2) containing lysozyme (20 mg/mL), along with the addition of 5 µL of RNase A (10 mg/mL). The mixture was thoroughly mixed through inversions and incubated at 37 ºC for 30 minutes in a heat block with shaking to facilitate cell lysis. Following the incubation, 15 µL of 20% SDS and 3 µL of proteinase K (10 mg/mL) were added and the mixture was gently inverted and incubated at 50 ºC for 60 minutes. Subsequently, 550 µL of phenol : chloroform : isoamylalcohol (25:24:1) solution was added, and vortexed thoroughly before centrifugation at 13800 g for 15 minutes at 4 ºC. The upper aqueous phase containing the DNA was carefully transferred to a sterile 1.5 mL microcentrifuge tube, precipitated with 550 µL of ice-cold absolute isopropanol and incubated overnight at -20 ºC. The precipitated DNA was then pelleted by centrifugation at 13800 g for 20 minutes at 4 ºC. The supernatant was discarded, and the pellet was washed with 500 µL of 70% ethanol followed by centrifugation at 13800 g for 5 minutes at 4 ºC. The DNA pellet was then dried under sterile conditions and resuspended in nuclease-free water.

DNA concentrations were measured using DeNovix DS-11 FX+ spectrophotometer / Fluorometer (Biozym Scientific GmbH, Hessisch Oldendorf, Germany) and quality was determined by 0.7% agarose gel (See section 2.4.1.5).

2.4.1.3 Total RNA isolation from Fungi

Total RNA isolation from *C. graminicola* and *A. nidulans* were carried out by employing peqGOLD plant RNA kit (VWR Life Science, Leuven, Belgium) following the manufacturer's instruction. PDA plates were made with 5.5 x 5.5 cm nylon membrane (0.45 µM, Carl Roth, Karlsruhe, Germany) as a substratum for the growth of microbes. The inoculation was carried out as described above (See section 2.3.1.1) and the plates were incubated at 23 °C for 12 days. Total RNA was isolated after the designated time period by using a cell scrapper (13 mm, SPL Life

Sciences, Gyeonggi, Korea). The collected fungal material was transferred to a fresh microcentrifuge tube placed in liquid nitrogen and was grinded with the help of micro pestle (Eppendorf, Thermo Fisher Scientific, Schwerte, Germany). Total RNA was isolated from the powdered sample, purified, and concentrated using the GeneJET RNA cleanup and Concentration Micro kit (Thermo Fisher Scientific, Vilnius, Lithuania). Genomic DNA was removed using the peqGOLD DNase-I-Digest-kit (VWR Life Science, Leuven, Belgium) and the resulting RNA was stored at -80 °C for future use.

2.4.1.4 Total RNA isolation from Bacteria

Total RNA isolation from bacteria was carried out by a method described by Rodiguez and co-workers with several modifications (Villa-Rodríguez et al., 2018). TE buffer-soaked Q-tips were employed to sample bacterial cultures from PDA plates containing nylon membrane. Wet Q-tips were used to swab the confronted bacterial cells, transferred to a microcentrifuge tube with 500 µL of TE buffer, and vortexed thoroughly. Subsequently, centrifugation was carried out at 12000 g for 3 minutes at 4 °C and the resulting pellet was stored at -20 °C for one hour. To further process the samples, homogenization was carried out with the aid of mortar and pestle to create a fine powder. Then, 200 µL of TE buffer containing freshly added lysozyme (20 mg/mL) was added to the powder and vortexed thoroughly. The mixture was then incubated at 37 °C for 30 minutes with occasional shaking. Following this, 1.5mL of TRIzol reagent (Invitrogen, Carlsbad, California, USA) was added, and the solution was vortexed. The mixture was allowed to incubate on ice for 5 minutes before adding 300 µL of chloroform and shaking vigorously. Subsequent centrifugation was performed at 13000 g for 15 minutes at -3 °C. The aqueous phase was carefully transferred to fresh 1.5 mL microcentrifuge tube, and twice the volume of isopropanol was added. After gentle mixing, precipitation was carried out at -80 °C overnight. The precipitate was then centrifuged at 13000 g for 15 minutes at -3 °C. The resulting pellet was washed with 1 mL of 75% ethanol and centrifuged at 13000 g for 5 minutes at -3 °C. The supernatant was discarded, and this washing step was repeated thrice. Finally, the pellet was air-dried in ice under sterile hood and resuspended in 35 µL of nuclease-free water (Ambion, Life Technologies, Texas, USA).

RNA quantity was determined with the help of DeNovix DS-11 FX + spectrophotometer / Fluorometer and quality by 2% agarose gel (See section 2.4.1.5).

2.4.1.5 Agarose Gel Electrophoresis (AGE)

DNA or RNA fragments were separated on agarose gels with concentrations ranging from 0.7% to 2% (w/v) (VWR Life Sciences, Leuven, Belgium). The agarose was dissolved in 1x TAE buffer (prepared from 50x stock; Refer appendix 7.2.2) and prior to loading, 2 µL of DNA/RNA samples were mixed with 1 µL of 6x loading buffer (Refer appendix 7.2.2). Electrophoresis was conducted under constant current conditions ranging between 70 to 95 V in an appropriate electrophoresis chamber. The gels were visualized under UV light at a wavelength of 320 nm and photographic documentation using a UV solo TS2 imaging system (Biometra GmbH, Göttingen, Germany). Size estimation of the resolved fragments was facilitated by including a GeneRuler mix (Refer appendix 7.2.2) (Thermo Fisher Scientific, Vilnius, Lithuania) containing defined sizes of DNA fragments.

2.4.2 Sequencing of nucleic acids

2.4.2.1 DNA sequencing

For DNA sequencing, templates were either PCR products or plasmids. In case of species identification, the genomic DNA extracted from the fungal isolates of maize leaves were subjected to a standard PCR reaction (See section 2.4.4.1) by employing the universal ITS primers ITS1 and ITS4 (Refer appendix 7.3, Table 6). In addition, the fungus *T. roseum* was also subjected to ITS sequencing employing the same primers. Furthermore, *B. amyloliquefaciens* and *B. subtilis* were sequenced by using 16s rRNA primers 27F and 1492R (Refer appendix 7.3, Table 6).

For sequencing of cloned plasmid, positive clones were chosen from colony PCR and was subjected to plasmid DNA isolation by using GeneJet Plasmid Miniprep kit (Thermo Fisher Scientific, Vilnius, Lithuania).

In all cases, 15 µL of the sequence reaction mix was prepared according to the instructions of the manufacturer (Microsynth Seqlab GmbH, Göttingen, Germany) and was sequenced. Sequence evaluation was carried out by employing BLAST searches and MEGA 11 (See section 2.8).

2.4.2.2 RNA sequencing

Total RNA isolated from fungi and bacteria were subjected to RNA-seq according to the manufacturer's instructions (GENEWIZ, Azenta Life Sciences, Leipzig, Germany). 50 µL of purified RNA at a final concentration of 50 ng/µL was provided for sequencing purposes. The integrity and quality of the RNA was determined by Qubit assay. High-quality RNA with a RQN of greater than 6 was used for mRNA library construction. Strand-specific RNA-seq analysis was performed with the Illumina NovaSeq platform with 2 x 150 bp paired-end sequencing. The parameters were applied to achieve a depth of 15 - 20 million reads per sample, ensuring comprehensive coverage of the transcriptome. In fungi, the preferred method for ribosomal RNA (rRNA) removal involved polyA section, which targets and enriches messenger RNA (mRNA) species that have a polyadenylated tail. Conversely, in bacteria where polyadenylation is less common, rRNA removal involved depletion strategies that specifically target rRNA molecules. The raw FASTQ files obtained after sequencing were used to perform RNA-seq analysis by Galaxy (See section 2.4.3.1).

2.4.3 Transcriptomics

2.4.3.1 RNA-seq analysis by Galaxy

The computational profiling of gene expression from RNA-Seq by identifying the Differentially Expressed Genes (DEGs) was accomplished with the help of Galaxy Europe server (https://usegalaxy.eu/) (Batut et al., 2018; Hiltemann et al., 2023). The quality of raw reads was analyzed using FastQC v0.73. Adapters and low-quality reads were trimmed by the Trimmomatic v0.38.1. The obtained clean reads were mapped to the following reference genomes using RNA STAR v2.7.8a as follows:

Colletotrichum graminicola M1.001 (ENSEMBL Fungi, accessed on 20 July 2022, https://fungi.ensembl.org/Colletotrichum_graminicola/Info/Index),

Aspergillus nidulans FGSC A4 (NCBI, accessed on 14 September 2022 and 19 November 2023, https://www.ncbi.nlm.nih.gov/genome/17?genome_assembly_id=299190), and

Bacillus amyloliquefaciens DSM 7 (NCBI, accessed on 12 February 2024, https://www.ncbi.nlm.nih.gov/datasets/genome/GCF_000196735.1/).

The reads per gene were counted by employing FeatureCounts v2.0.1. DEGs were obtained with the help of DESeq2 v2.11.40.7 with a cutoff of $p < 0.05$, Fold Change (FC) > 2 as upregulated, and FC < 0.5 as downregulated. Principal Component Analysis (PCA) and correlation matrix plots were also obtained with the DESeq2 package. A Venn diagram of the DEGs was drawn using BioVenn (https://www.biovenn.nl/index.php) (Hulsen et al., 2008).

2.4.3.2 Functional enrichment studies of DEGs

The three GO ontologies namely molecular function (GO:MF), cellular component (GO:CC), and biological process (GO:BP) for the DEGs from *C. graminicola* and *A. nidulans* were analyzed by gProfiler to perform the functional enrichment analysis (https://b2t.cs.ut.ee/gprofiler/gost) (Raudvere et al., 2019). The respective gene IDs were uploaded into the gProfiler server, and the analyses were performed with the default parameters. In case of *B. amyloliquefaciens,* the gene IDs of DEGs were uploaded into ShinyGO 0.80 tool (http://bioinformatics.sdstate.edu/go/) (Ge et al., 2019) and the gene ontologies were obtained. A gene ontology (GO) bubble plot for the enriched genes was obtained with the help of SRplot (https://www.bioinformatics.com.cn/en) (Tang et al., 2023).

2.4.3.3 SMBGCs analysis by antiSMASH

The antiSMASH (antibiotics & Secondary Metabolite Analysis Shell) tool was employed to identify the SMBGCs of fungal (https://fungismash.secondarymetabolites.org/#!/start), and bacterial genomes (https://antismash.secondarymetabolites.org/#!/start). By incorporating profile Hidden Markov Models (pHMMS) from various databases, antiSMASH accurately predicts specificities of key domains such as PKSs, and NRPSs (Medema et al., 2011). By employing this comprehensive platform, the whole genome file in FASTA format of respective fungi and bacteria were uploaded to the server and was mined for SMBGCs. By using options such as KnownCLusterBlast analysis, SubClusterBlast analysis, and ActiveSiteFinder, the online antiSMASH job was submitted and the calculations for the identification and analysis of the SMBGCs were carried out on the server (Blin et al., 2023). The obtained SMBGCs were studied in detail to get more insights on different chemical compound production. Moreover, the DEGs were manually curated to various SMBGCs, and validation was confirmed using the reference genome of *C. graminicola* (O'Connell et al., 2012). To validate differentially expressed SMBGCs

genes of *A. nidulans*, the published reference genome was used (Inglis et al., 2013; Soukup et al., 2012).

2.4.4 Polymerase chain reaction (PCR)

2.4.4.1 Standard PCR

All PCR reactions were performed in Biometra TAdvanced thermocycler (Analytik Jena, Göttingen, Germany). The buffer and enzyme for standard PCR reactions were obtained from Thermo Fisher Scientific (Vilnius, Lithuania). Typically, a 50 µL reaction mix was set up as follows:

Components	**Volume**
Dream*Taq* Buffer (10x)	12.5 µL
dNTPs (10 mM)	2.5 µL
Forward/Reverse primers (10 µM)	2.5 µL each
Template DNA (50 ng/µL)	2.5 µL
Dream*Taq* DNA polymerase (5 U/µL)	1.25 µL
Nuclease-free H_2O	*ad.* 50 µL

The standard PCR cycles were conducted as follows:

Time	**Temperature**	**Step**	**Cycles**
	98 °C	Hold	
2 min	98 °C	Initial denaturation	
30 s	95 °C	Denaturation	
30 s	T_m + 3-5 °C	Annealing	30 - 40
1 min/Kb	72 °C	Extension	

5 min	72 °C	Final extension	
	4 °C	Hold	

2.4.4.2 PCR with high fidelity (HF) polymerase

All PCRs for amplifying deletion and fusion constructs were performed using Phusion High-Fidelity DNA polymerase. All components were from (Thermo Fisher Scientific, Vilnius, Lithuania). The annealing temperature depends on the T_m of the chosen primers and was calculated using the New England Biolabs (NEB) T_m calculator (https://tmcalculator.neb.com/#!/main). The duration of the extension step depends on the size of the amplified fragment (30 s/Kb). Typically, a 50 µL PCR reaction mix was set up as follows:

Components	**Volume**
Phusion GC Buffer (5x)	10 µL
dNTPs (10 mM)	1 µL
Forward/Reverse primers (10 µM)	2.5 µL each
Template DNA (50 ng/µL)	2.5 µL
Phusion polymerase (2 U/µL)	0.5 µL
Nuclease-free H_2O	*ad.* 50 µL

The standard PCR cycles were conducted as follows:

Time	**Temperature**	**Step**	**Cycles**
	98 °C	Hold	
3 min	98 °C	Initial denaturation	
30 s	98 °C	Denaturation	
30 s	65 °C	Annealing	32

45 s	72 °C	Extension
5 min	72 °C	Final extension
	4 °C	Hold

2.4.4.3 Double-Joint PCR (DJ-PCR)

The creation of deletion cassette, also known as knock-out (KO) for target genes was accomplished using the double joint PCR (DJ-PCR) technique (Yu et al., 2004). Initially, PCR reactions of 50 µL were conducted to produce 5'- and 3'- flanks and fused with the hygromycin B phosphotransferase gene (*hph*) (Punt et al., 1987) by DJ-PCR (Yu et al., 2004). The stoichiometric relation of 5'- flank : resistance marker : 3'- flank is 1:3:1. The product of the first DJ-PCR reaction (DJ1) was used as a template for the second DJ-PCR reaction (DJ2) (See section 2.4.5). Typically, a 50 µL PCR reaction mix was set up as follows:

DJ1	**Components**	**DJ2**
10 µL	Phusion GC Buffer (5x)	10 µL
4 µL	dNTPs (10 mM)	1 µL
-	Forward/Reverse primers (10 µM)	2.5 µL each
1 µL	5' - flank (50 ng/µL)	-
3 µL	Resistance cassette (50 ng/µL)	-
1 µL	3' - flank (50 ng/µL)	-
-	Template (50 ng/µL)	1 µL
0.5 µL	Phusion polymerase (2 U/µL)	0.5 µL
ad. 50 µL	Nuclease-free H_2O	*ad.* 50 µL

The PCR program for the DJ-PCR (DJ1 and DJ2) was performed as follows:

Time (DJ1)	Cycles (DJ1)	Temperature	Time (DJ2)	Cycles (DJ2)	Step
		98 °C			Hold
2 min		98 °C	2 min		Initial denaturation
30 s		98 °C	30 s		Denaturation
30 s	15	66 °C	30 s	30	Annealing
2:15 min		72 °C	2:15 min		Extension
10 min		72 °C	5 min		Final extension
		4 °C			Hold

2.4.4.4 PCR for synthesis of hybridization probes

The PCR for synthesis of southern hybridization probes were performed using Thermopol buffer and *Taq* DNA polymerase obtained from NEB, Frankfurt, Germany. The standard dNTPs were substituted by DIG DNA labeling mix obtained from Roche Diagnostics (Mannheim, Germany) (See section 2.4.6). Typically, a 20 µL reaction mix was set up as follows:

Components	Volume
Thermopol Buffer (10x)	2 µL
DIG labeling mix (10x)	2 µL
Forward/Reverse primers (10 µM)	1 µL each
Template DNA (50 ng/µL)	1 µL
Taq DNA polymerase (5 U/µL)	0.3 µL
Nuclease-free H_2O	*ad.* 20 µL

The PCR cycles were conducted as follows:

Time	Temperature	Step	Cycles
	95 °C	Hold	
30 s	95 °C	Initial denaturation	
30 s	95 °C	Denaturation	
30 s	57 °C	Annealing	32
1 min	68 °C	Extension	
5 min	68 °C	Final extension	
	4 °C	Hold	

2.4.4.5 Analyses of gene transcripts using reverse transcription-polymerase chain reaction (RT-qPCR)

To analyze the transcript abundance of SM genes under confrontations, total RNA was isolated from *C. graminicola*, *A. nidulans,* and *B. amyloliquefaciens* using the peqGOLD plant RNA kit for fungi (See section 2.4.1.3) and a manual method for bacteria (See section 2.4.1.4). RT-qPCR was performed using the iTaq™ Universal SYBR® Green One-Step kit (Bio-Rad laboratories, California, USA) according to the manufacturer's instructions in CFX Connect Real-Time PCR detection system (Bio-Rad, Singapore). A 10 µL reaction mix was set up as follows:

Components	Volume
SYBR Green reaction mix (2x)	5 µL
Forward/Reverse primers (10 µM)	0.2 µL each
iScript reverse transcriptase (125 x)	0.08 µL
Nuclease-free H_2O	2.52 µL
RNA (10 ng/µL)	2 µL

The PCR cycles were conducted as follows:

Time	Temperature	Step	Cycles
30 min	48 °C	Reverse transcription	
10 min	95 °C	Polymerase activation & DNA denaturation	
15 s	95 °C	Denaturation	
1 min	60 °C	Annealing / Extension	39
10 s	95 °C	Pre-melting	
5 s	65 °C	Melt-curve start	
	95 °C	Melt-curve end	

A sigmoidal curve-fitting has been performed for all RT-qPCR analyses (Rutledge, 2004) and relative transcript abundance was quantified by $2^{-\Delta\Delta Ct}$ method (Livak & Schmittgen, 2001). Normalization was carried out using the constitutive housekeeping genes as follows: *α-actin* for *C. graminicola* (Krijger et al., 2008), *actA* for *A. nidulans* (Gao et al., 2011), and *gyrA* for *B. amyloliquefaciens* (Liu et al., 2022). Each reaction was carried out using three independent biological replicates with three technical replicates each. Gene-specific primers used for RT-qPCR are listed in the appendix (Refer appendix 7.3, Tables 1, 2, 3, and 4).

2.4.5 Deletion of Type I *PKS* in *C. graminicola*

Deletion cassette was created through DJ-PCR (See section 2.4.4.3), following the method outlined by Yu and co-workers (Yu et al., 2004). The 5’ - and 3’- flanking regions of the *PKS27* gene (GLRG_10537) were amplified using primer pairs PKSCgF5/PKSCgR5 and PKSCgF3/PKSCgR3 with 50 ng of genomic DNA as the template. The hygromycin phosphotransferase (*hph*) cassette was amplified from plasmid pAN7-1 (Punt et al., 1987) employing primers UniHygTF and UniHygTR. Subsequently, the 5’- and 3’- flanks were fused

with the *hph* cassette in a DJ-PCR, and the entire construct was amplified using primers PKSCgF5 and PKSCgR3. The resulting 4055-bp product was inserted into vector pJET1.2/blunt (Thermo Fisher Scientific, Waltham, USA) according to the manufacturers' instructions. Thermocompetent *E. coli* (XL1-Blue strain) cells were prepared according to (Chung et al., 1989) (Details on LB medium, TSS buffer, and tetracycline selection marker can be found in appendix 7.2). Transformation of thermocompetent *E. coli* strains and subsequent steps were performed according to standard protocol (Details on medium, buffers, and ampicillin selection marker used for transformation can be found in appendix 7.2). The deletion constructs were amplified by PCR, using primers PKSCgF5 and PKSCgR3 and then transformed into conidial protoplast as described by (Werner et al., 2007) (Details on the regeneration medium (RM), yeast extract sucrose medium (YES), Sorbitol Tris Calcium chloride (STC) buffer, and Protoplastization solution used can be found in appendix 7.2). To aid in screening for positive candidate clones containing the KO cassette homologously, genomic DNA was isolated using the DNA isolation method described (See section 2.4.1.1) from fungus grown in CM. Homologous recombination and correct integration of a single copy of the deletion cassette was confirmed by PCR and southern hybridization. For PCR screening, primer pairs PKS10537F and PKS10537R were employed. Southern blot was conducted to confirm the correct integration site of the KO cassette, using the appropriate enzyme, and hybridized with specific probes as following: 411 bp-PKS probe was amplified using PKSCgProbeF and PKSCgProbeR. All primers used in the deletion study are listed in the appendix (Refer appendix 7.3, Table 5).

2.4.6 Southern hybridization

2.4.6.1 Generation of DIG-labeled probes

Hybridization probes were produced using a PCR method with Thermopol buffer, with the modification of substituting the typical dNTP mix with a mixture containing digoxigenin (DIG)-dNTPs (See section 2.4.4.4). This mixture comprised of 1 mM dATP, dCTP, and dGTP, along with 0.65 mM dTTP each, and 0.35 mM DIG-dUTP (DIG DNA labeling mix, Roche diagnostics, Mannheim, Germany). Successful labeling was verified by AGE. Fragments labeled with DIG appeared larger in size than the non-labeled reference fragments attributable to the presence of digoxigenin.

2.4.6.2 Genomic DNA digestion and gel electrophoresis

DNA samples (8 µg) were digested overnight, approx. 16 hours, employing the restriction enzyme BamHI and buffers at 37 ºC in Biometra T-personal 48 thermocycler (Biomedizinische Analytik GmbH, Göttingen, Germany). The resulting DNA fragments were then separated into a 0.7% agarose gel (60 V for 2.5 h) following the addition of 6x loading buffer (Refer appendix 7.2.2).

2.4.6.3 Capillary transfer, hybridization, and detection

Post electrophoresis, the DNA was depurated in 0.25 M HCl for 15 minutes. Subsequently, the gel was subjected to incubation in 0.4 M NaOH lasting for 30 minutes to denature the double-stranded DNA fragments. The fragmented DNA was then transferred to a positively charged nitrocellulose membrane (Hybond-N, GE Healthcare, Amersham, UK) using downward capillary transfer in STC buffer (Refer appendix 7.2.2) for approximately 16 hours.

Following transfer, the DNA fragments on the membrane were cross-linked twice by exposing to UV-light (1200 x 100 µJ/cm^2). Subsequently, the membrane was pre-hybridized in 20 mL of hybridization buffer (Refer appendix 7.2.2) at 65 ºC for 2 hours. The denatured probe (previously heated to 99 ºC for 5 minutes and chilled in ice) was then added to the hybridization buffer and incubated overnight at 65 ºC (HL-2000 HybriLinker, UVP, Upland, CA, USA).

Following hybridization, the membrane was washed stepwise employing wash buffer I and wash buffer M (Refer appendix 7.2.2) as follows: twice with 2x wash buffer I at room temperature (RT) for 5 minutes, once with 0.5x wash buffer I at 68 ºC for 15 minutes, once with 0.25x wash buffer I at 68 ºC for 15 minutes, once with 0.1x wash buffer I at 68 ºC for 15 minutes and finally equilibrated for 1 minute with wash buffer M at RT. Subsequently, the membrane was incubated for 1 hour in blocking buffer (Refer appendix 7.2.2), after which anti-DIG antibody (diluted to 1:10000, anti-DIG AP Fab-Fragment, Roche Diagnostics, Mannheim, Germany) was added to the blocking buffer. Unbound antibodies were removed by three 10-minute washing steps using wash buffer M at RT.

The membrane was briefly immersed in detection buffer (2-minute) (Refer appendix 7.2.2) and placed between two plastic sheets after adding few drops of CSPD solution (0.25mM CSPD ready-to-use, Roche Diagnostics, Mannheim, Germany), followed by a 5-minute incubation in darkness.

The membrane was then sandwiched between two plastic sheets and exposed onto an X-ray film (Hyperfilm ECL, Amersham Pharmacia Biotech, Freiburg, Germany). The exposure time varied depending on the signal strength, ranging from 2 to 4 hours. Finally, the film was developed using a fixing and developing solution (CEA Röntgen, Assamstadt, Germany). The X-ray film was transferred to a fixing solution (CEA Röntgen Tank-Fixierer) and incubated for 3 minutes followed by 1 minute incubation in a developing solution (CEA Röntgen Tank-Entwickler). The film was then transferred to water and incubated for 1 minute and visualized.

2.5 Metabolomics

2.5.1 Solvent extraction of metabolites by Ethyl acetate

The extraction of SMs from PDA plates was done as described (Nickles et al., 2021), with modifications. At 12 dpi, 3 mm stripes of the edges of solo cultures (25 petri dishes) or of cultures at the confrontation sites (100 petri dishes) were excised and transferred into an Erlenmeyer flask. In addition, PDA from the confrontation zone without microbial cells were excised. Non-colonized PDA served as control. Samples were macerated using an Ultra-Turrax homogenizer (T8.01, IKA Labortechnik, Staufen, Germany), suspensions were kept in a shaker (Unitron, Infors AG, Bottmingen, Switzerland) for 3 hours at 200 rpm and filtered (Whatman cellulose round filters, ø125 mm, Carl Roth, Karlsruhe, Germany). Extracts were dried in a rotary evaporator at 45 ºC and 240 mbar (Laborota 4000, Heidolph Instruments GmbH, Schwabach, Germany). The resultant crude extracts were transferred to a pre-weighed glass vial, and dry weights of the crude extracts were measured, and samples were adjusted to a concentration of 1 mg / mL methanol.

2.5.2 Solid phase extraction (SPE) by C18 column

The culture filtrates obtained from co-cultivation experiment in PDB was enriched using solid phase chromatography extraction (SPE) on a Chromabond C18 column (Machery-Nagel, Düren, Germany). The column was conditioned with 1 mL of methanol (MeOH), followed by 1 mL of 2% (v/v) formic acid. The culture filtrate was loaded onto the column, the column was washed twice with 1 mL of water and eluted twice with 1 mL of MeOH containing 2% (v/v) formic acid. The eluates were dried under vacuum (Concentrator Plus, Eppendorf AG, Hamburg, Germany) for

6 h at 40 ºC and subsequently dissolved in 70% (v/v) MeOH in an ultrasonic bath (Elmasonic S 100KH, SK Sonic, Mörfelden-Walldorf, Germany) for 30 min. The eluates were then centrifuged at 13000 g for 10 min at 20 °C.

2.5.3 Liquid Chromatography - Tandem mass spectrometry (LC-MS/MS)

Untargeted metabolome analyses using LC-MS/MS was conducted by Dr. Henriette Uthe at the German Centre for Integrative Biodiversity Research (iDiv) and the Leibniz Institute for Plant Biochemistry (IPB). LC-ESI-Q-ToF-MS measurements were based on (Böttcher et al., 2009) with several modifications. Chromatographic separations were performed at 40 °C on an UltiMate™ 3000 Standard Ultra-High-Pressure Liquid Chromatography system (Thermo Fisher Scientific, Vilnus, Lithuania) equipped with an Acclaim Rapid Separation Liquid Chromatography (RSLC) 120 column (150 x 2.1 mm, particle size 2.2 µm, Thermo Fisher Scientific, Vilnus, Lithuania). The following gradient was used at a flow rate of 0.4 mL/min: 0 - 1 min, isocratic 95% A [water/formic acid 99.95/0.05 (v/v %)], 5% B [acetonitrile/formic acid 99.95/0.05 (v/v %)]; 1 - 2 min, linear gradient from 5 to 20% B; 3 - 8 min, linear gradient from 20 to 25% B; 8 - 16 min, linear gradient from 25 to 95% B; 16 - 18 min, isocratic 95% B; 18 - 18.01 min, linear from 95 to 5% B; 18.01 - 20 min, isocratic 5% B. The injection volume was 3 µL (full loop injection). Eluted compounds were detected from m/z 90 to 1600 at a spectra rate of 5 Hz using an ESI-UHR-Q-ToF-MS (maXis impact, Bruker Daltonics, Bremen, Germany) equipped with an Apollo 2 electrospray ion source in positive ion mode. The instrument settings for positive ion mode : nebulizer gas, nitrogen, 2.5 bar; dry gas, nitrogen, 11 L min - 1, 220 °C; capillary voltage, 4500 V; end plate offset, 500 V; funnel 1 radio frequency (RF), 200 Volts peak-to-peak (Vpp); funnel 2 RF, 220 Vpp; in-source collision-induced dissociation (CID) energy, 0.0 eV; hexapole RF, 120 Vpp; quadrupole ion energy, 4 eV; quadrupole low mass, 100m/z; collision gas, nitrogen; collision energy, 10 eV; prepulse storage, 7 µs. Stepping: on; basic mode; collision cell RF, from 400 Vpp to 1000 Vpp; transfer time, from 30 µs to 70 µs, timing; 50 % / 50 %, collision energy for MSMS, 80 %, timing 50% / 50%. Calibration of the m/z scale was performed for individual raw data files on sodium formate cluster ions obtained by automatic infusion of 1.66 µL/min of 10 mM sodium format solution of NaOH in 50/50 (v/v %) isopropanol/water containing 0.2% (v/v) formic acid at the end of the gradient (HPC mode). For the acquisition of CID (collision induced dissociation) mass spectra, the same settings as above were used with additional settings for data dependent

acquisition (AutoMSMS): Mode: CID, intensity threshold 600, number of precursors, 3; precursor background subtraction on, active exclusion on after 2 spectra, release after 0.5 min, smart exclusion, on, 5x; isolation and fragmentation settings, size and charge dependent, width 3-15 m/z, collision energy 20-30 eV, charge states included: 1z, 2z, 3z.

2.5.4 Data processing and annotation

Pre-processing of data from LC-MS/MS was conducted by Dr. Henriette Uthe. LC-MS and MS/MS data were processed with MetaboScape 5.0 (Bruker Daltonics, Bremen, Germany), using Bruker's T-ReX 3D algorithm with the following settings: intensity threshold 1000 counts, minimum peak length 7 spectra, feature signal = intensity, and mass recalibration auto-detect. Recursive feature extraction: minimum peak length (recursive) 5 spectra, a minimum number of features for recursive extraction 6 of 213. Bucket filter: Presence of features in a minimum number of analyses 6 of 213.

Annotation of compounds was based on 1) an in-house library of analytical standards and known plant metabolites according to mass, retention time (rt) and spectrum, 2), the KNApSAcK family (Afendi et al., 2012) considering mass and spectral similarity to compound class, and 3) via spectral similarity to the databases NIST17, WEIZMASS (Shahaf et al., 2016), Sumner Spectral library (Bruker Daltonics, Bremen, Germany), MoNA (https://mona.fiehnlab.ucdavis.edu/), GNPS (https://gnps.ucsd.edu/), ReSpect (Sawada et al., 2012) and an in-house database via the spectral library search function of MetaboScape.

2.5.5 Post data-processing

Post-data processing of the metabolome using bioinformatic tools was conducted by Dr. Yvonne Poeschl at iDiv and the Institute of Biometrics and Agricultural Informatics, Martin Luther University, Halle (Saale), Germany. Features obtained from preprocessing of metabolome data were uniquely characterized by a pair of mz and rt values. Features can be seen as putative compounds. The feature or compound table resulting from MetaboScape data processing contained samples derived from the assay but also quality control samples like ACN samples and a PDA sample. These are used to account for technical contamination during the MS analysis on

instrument and for unwanted background compounds from the medium (PDA). Hence, only compounds that were not detected in ACN or PDA samples and are additionally marked with "include" by MetaboScape are retained. Other compounds were removed from the compound table and excluded further analyses. Also, corresponding ACN and PDA samples were removed. To account for unreliable measurements, uncertain intensities below 1500 were set to 0. The threshold of 1500 corresponds to the same value used in MetaboScape.

2.5.6 Data analyses

With respect to the *C. graminicola* confrontation study, compounds were considered present in the confrontations if found in at least one sample. To streamline analysis, three samples were merged into one artificial sample representing the confrontation. Overlapping compounds with two control samples were then computed and visualized using Venn diagrams. Two subsets were generated for each confrontation assay: one containing all compounds produced and another containing exclusively produced compounds not found in corresponding control assays. The final compound tables include the three confrontation assay samples and the described subsets of compounds.

2.5.7 Plots generation for metabolome dataset

The confrontation assays employing tripartite system (based on three sample positions - Supporting Figures S4A, *C. graminicola* vs *B. amyloliquefaciens* and S4B, *C. graminicola* vs. *A. nidulans*) in petri dishes were used to create seven distinct prototype profiles representing different combinations of compound presence or absence. These profiles range from "present _ present _ present" to "not-present _ not-present _ present". These profiles were utilized in the Profile-Interaction-Finder (PIF) algorithm, developed by (Poeschl et al., 2014; Trenner et al., 2016), to categorize compounds into sets based on their similarity to these prototype profiles. Each set is defined by the shape of the corresponding profile. Compounds are assigned to the profile they most closely resemble based on their intensity, allowing for a systemic analysis of compound distribution across the sample positions in the petri dish.

Sunburst plots were employed to visually represent hierarchical data. Such as annotation information, in a structured manner from the most general to the most specific levels. These plots

consist of circular rings, each representing a different level of hierarchy from the innermost to the outermost ring. The fractions displayed within the rings denote specific proportions of the data. In the context of metabolome, annotation information typically includes compound classes ranging from superclass to most specific subclass. The fractions depicted in the rings can be calculated either based on the frequency of compound classes or by aggregating the measured intensities of compounds within each class.

In *C. graminicola* project involving two confrontations (*C. graminicola* vs. *B. amyloliquefaciens* and *C. graminicola* vs. *A. nidulans*), a composite compound table from assay-specific tables was created based on sorting by RT. Subsequently, compounds with matching pairs of mz and rt values were identified across both tables, allowing for slight deviation of 0.001 in mz values and up to 10 seconds in rt. This process yielded the composite compound table, facilitating comparative analyses and visualization using alluvial plots.

The analysis of compound table was conducted using R software (RCoreTeam, 2022) (https://www.R-project.org/) along with specific packages: ggplot2 (Wickham, 2016) for generating violin plots, line plots, and bar plots; plotly (Sievert, 2020) for creating sunburst plots; ggalluvial (Brunson & Read, 2019) for constructing alluvial plots; and eulerr (Larsson, 2018) for generating Venn diagrams. These tools facilitated the exploration and visualization of the compound data, enabling comprehensive insights into the metabolome profiles derived from the assays.

2.5.8 Computational toxicity by ProTox 3.0

To evaluate the toxicity of various compound classes, ProTox 3.0 webserver was employed (https://tox.charite.de/protox3/index.php?site=compound_input) (Banerjee et al., 2024). This in silico tool predicts the acute toxicity of chemical compounds by estimating the median lethal dose (LD_{50}). Each compound was individually analyzed, which categorizes toxicity into six classes namely class 1 ($LD_{50} \leq 5$), class 2 ($5 < LD_{50} \leq 50$), class 3($50 < LD_{50} \leq 300$), class 4 ($300 < LD_{50} \leq 2000$), class 5 ($2000 < LD_{50} \leq 5000$) and Class 6 ($LD_{50} > 5000$). The compounds were subsequently color-coded according to their respective toxicity classes for clear visualization and comparative analysis.

2.5.9 Molecular networking and compound classification

LC-MS/MS data obtained for the co-cultivation experiment in PDB medium was analyzed by Global Natural Products Social Molecular Networking (GNPS v1.3.16) using the mzML format for positive mode ionization (Wang et al., 2016). GNPS was performed by Diana Astrid Barrera Adame from the Institute of Pharmacy, Martin Luther University, Halle (Saale), Germany. A molecular network was created with a cosine score above 0.7, and the minimum number of matched fragments ions was adjusted to 6. Further edges between two nodes were kept in the network only if each of the nodes appeared in each other's respective top 10 most similar nodes. Additionally, before networking, the filter "Spectra from G6" was set as "Blank". The MS/MS spectra were searched against GNPS' spectral libraries, using a minimum of 6 matched fragments for spectral matching. Cytoscape v3.9.0 was employed for molecular network visualization. Manual classification of compound clusters was achieved by submitting the mzML output files from MSConvertGUI (v3.0.19330, ProteoWizard, USA) to Sirius 5.7.2 + CSI: FingerID + Canopus for prediction of the elemental composition (C,H,N,O,S,P) (Dührkop et al., 2019; Dührkop et al., 2021; Dührkop et al., 2015; Shen et al., 2014) and molecular structure database search with *m/z* tolerance set to 5 ppm.

2.6 Microscopical examination

Differential interference contrast (DIC) and fluorescence microscopy were performed with a Nikon Eclipse 600 microscope (Nikon, Düsseldorf, Germany). Digital images were taken with a Nikon microscope camera DS-Ri2, and the image processing was performed with NIS-Elements imaging software (Nikon).

2.6.1 Calcofluor white staining

A Calcofluor white stain (CFW) (Refer appendix 7.2.3) dissolved in 10% KOH (1:1) was used to stain fungal cell walls (Monheit et al., 1984). Antagonists-induced distortions of hyphae were examined by excising thin squared slices of mycelia at the confrontation interface with a sterile blade and placed on a clean glass slide. About 20 µL of CFW was applied to the sample and was covered with a sterilized coverslip. The specimen was sealed with foil and incubated for 10 minutes

at RT before being visualized by fluorescent microscopy. A 40X plan Fluor leans at an excitation wavelength of 350 nm and a laser light transmission of 25% was used for imaging.

2.6.2 FM lipophilic styryl dye staining

FM dyes are lipophilic styryl compounds used in studies concerning plasma membrane and vesiculation. A commercially available FM4-64 dye (Thermo Fisher Scientific, Schwerte, Germany) (Refer appendix 7.2.3) was used in this study to stain the fungal mycelia (Vida & Emr, 1995). 5µL (1 µg/mL) of the red lipophilic dye was used on the specimen, sealed with a foil, and incubated for 20 minutes on ice. Mycelia was then washed with HBSS (Thermo Fisher Scientific, Illinois, USA), and the specimen was visualized by fluorescent microscopy. A 40X Plan Fluor lens at an excitation wavelength of 633 nm and an emission wavelength ranging between 580 to 660 nm (650LP detection channel) was employed.

2.6.3 Schaeffer-Fulton staining

Bacterial endospores were visualized by employing the Schaeffer-Fulton staining technique with the use of malachite green and safranin (Schaeffer & Fulton, 1933). The staining process involves heat-fixing a bacterial smear on a slide and flooding it with malachite green, which penetrates the endospores. After cooling, excess stain is removed from vegetative cells with water. Counterstaining with safranin highlights vegetative cells pink, while endospores retain their green color.

2.7 Cytotoxicity assay

Cell viability studies and post data processing were carried out by Dr. Robert Rennert at IPB. In this study, the impact of metabolic extracts from confrontation cultures of *A. nidulans* against *B. amyloliquefaciens, B. subtilis,* and *T. roseum* were assessed. The viability and proliferation of human cells were evaluated using *in vitro* cell viability assays with HEK-293 (human embryonic kidney) and HCT-116 (colorectal carcinoma) cell lines. Both cell lines were obtained from ATCC (Manassas, VA, USA) and DSMZ (Braunschweig, Germany), respectively. For cell culture, MEM

(high glucose) and McCoy's 5A basal media, fatal calf serum (FCS), L-glutamine (200 mM), phosphate buffered saline (PBS), and 0.05% trypsin-EDTA were purchased from Capricorn Scientific GmbH (Ebsdorfergrund, Germany). Trypan blue was procured from Invitrogen (Waltham, MA, USA), resazurin and digitonin were from Sigma Aldrich (Taufkirchen, Germany), and DMSO was from Duchefa Biochemie (Haarlem, The Netherlands). Cell culture plastics were supplied by TPP (Trasadingen, Switzerland), Greiner Bio-One (Frickenhausen, Germany), and Sarstedt (Nümbrecht, Germany). The HEK-293 and HCT-116 cells were maintained in their respective growth media: MEM (high glucose) for HEK-293 and McCoy's 5A for HCT-116, each supplemented with 10% heat-inactivated FCS and 2 mM L-glutamine. Cells were cultured in T-75 flasks in a humidified atmosphere with 5% CO_2 at 37 ºC until they reached 70 -80% sub confluency before being sub-cultured or used in assays. Cells were rinsed with PBS and detached using 0.05% trypsin-EDTA in PBS for passaging and seeding.

The effects of the extracts on cell viability and proliferation were evaluated using fluorometric resazurin-based cell viability assays, following a protocol established by (Kufka et al., 2019; Lam et al., 2023). HEK-293 cells were seeded at 6,000 cells/well and HCT-116 cells at 10,000 cells/well in 96-well plates, achieving an initial confluency of 10-20%. Cells were allowed to adhere overnight and then treated for 48 hours with metabolic extracts from confronted *A. nidulans*, as well as reference extracts from PDA and non-confronted *A. nidulans*, in a concentration range of 0.98-250 µg/mL. Controls included 0.5% DMSO (negative control, set to 100% cell viability). After the 48 hours treatment, media were discarded, and cells were rinsed with PBS. Fresh resazurin solution in basal medium was added to a final concentration of 50 µM and cells were incubated under standard conditions for 2 hours. The conversion of resazurin to resorufin by viable cells was measured fluorometrically (λexc. 540 nm / λem. 590 nm) using a SpectraMax iD5 multiwell plate reader (Molecular Devices, San Jose, USA). Data were collected from at least four biological replicates with technical triplicates. IC_{50} (half-maximal inhibitory concentration) curves and values were determined using a four-parameter function and GraphPad Prism v10.1 software (San Diego, CA, USA).

2.8 Bioinformatic tools

In silico sequence analyses, gene deletion, gene fusion, and primer construction were made using Clone Manager 9 professional (Sci-Ed, Cary, NC, USA)

Phylogenetic analyses was conducted using MEGA11 software (Tamura et al., 2021) and MrBayes (Huelsenbeck & Ronquist, 2001). The query sequence was blasted with the available highly similar sequences in the GenBank database by using the BLAST algorithm (https://blast.ncbi.nlm.nih.gov/Blast.cgi) (Altschul et al., 1997) and thereafter aligned with our query sequence using the MUSCLE algorithm in MEGA 11. The sequences for alignment were chosen based on sequence homology and various literature searches. The aligned sequences were used to determine the optimal evolutionary model based on Akaike's Information Criterion (AIC) (Luo et al., 2010). Further, the conversion to NEXUS file via MEGA11 was performed and imported into MrBayes v3.2.7a for the construction of phylogenetic tree (Huelsenbeck & Ronquist, 2001). MrBayes relies on the Markov chain Monte Carlo (MCMC) numerical method to estimate the posterior probability distribution of model parameters. The acquired data was visualized using FigTree v1.4.4 (Rambaut, 2010) (http://tree.bio.ed.ac.uk/software/figtree/) to generate a phylogenetic tree based on branch probabilities.

Statistical differences between groups were performed using a single-factor ANOVA test, followed by Tukey-HSD with an alpha degree of $p < 0.05$. The data were assessed with the help of Microsoft Excel and R (RCoreTeam, 2022).

2.9 Photography

All photographs of petri dishes, conical flasks, and plants were shot in Sony Cyber-shot DSC-HX100V camera (Minato, Tokyo, Japan).

3 Results

3.1 Metabolic re-programming in confrontations of *C. graminicola* and *A. nidulans* with *Bacillus* biocontrol agents

3.1.1 Confrontations between *C. graminicola* and different *Bacillus* species on MM cause formation of hyphal conglobations

On MM, *C. graminicola* exhibits radial growth and develops filamentous hyphae, as shown by DIC and fluorescence microscopy after CFW staining (Figure 3A). Under UV-light, fungal colonies show only background auto-fluorescence (Figure 3A). In contrast, all *Bacillus* species tested exhibited massive fluorescence under UV-light (Figure 3B, green arrow). The fact that fluorescence surrounded the entire bacterial colony suggested that fluorescing compounds are constitutively produced and secreted into the medium, and that *C. graminicola* encounters these and other compounds at confrontation sites.

The effects of these *Bacillus* SMs on *C. graminicola* are notable. Indeed, microscopy of fungal hyphae confronting colonies of *B. amyloliquefaciens*, *B. subtilis*, or *B. velezensis* exhibited severe swellings, similar as those induced by cyclic lipopeptides such as iturin A or plipastatin A (Gong et al., 2015) produced by *Bacillus* species (Figures 3C - 3E, arrowheads). Fluorescence around *Bacillus* colonies and occurrence of hyphal conglobations at confrontation sites revealed that SMs are present in the inhibition zone. Intriguingly, in interactions with *B. amyloliquefaciens* and *B. velezensis*, but not in the interaction with *B. subtilis*, a red pigment was formed (Figures 3C and 3E, red arrows), suggesting differential secretion of SM(s) at specific confrontations.

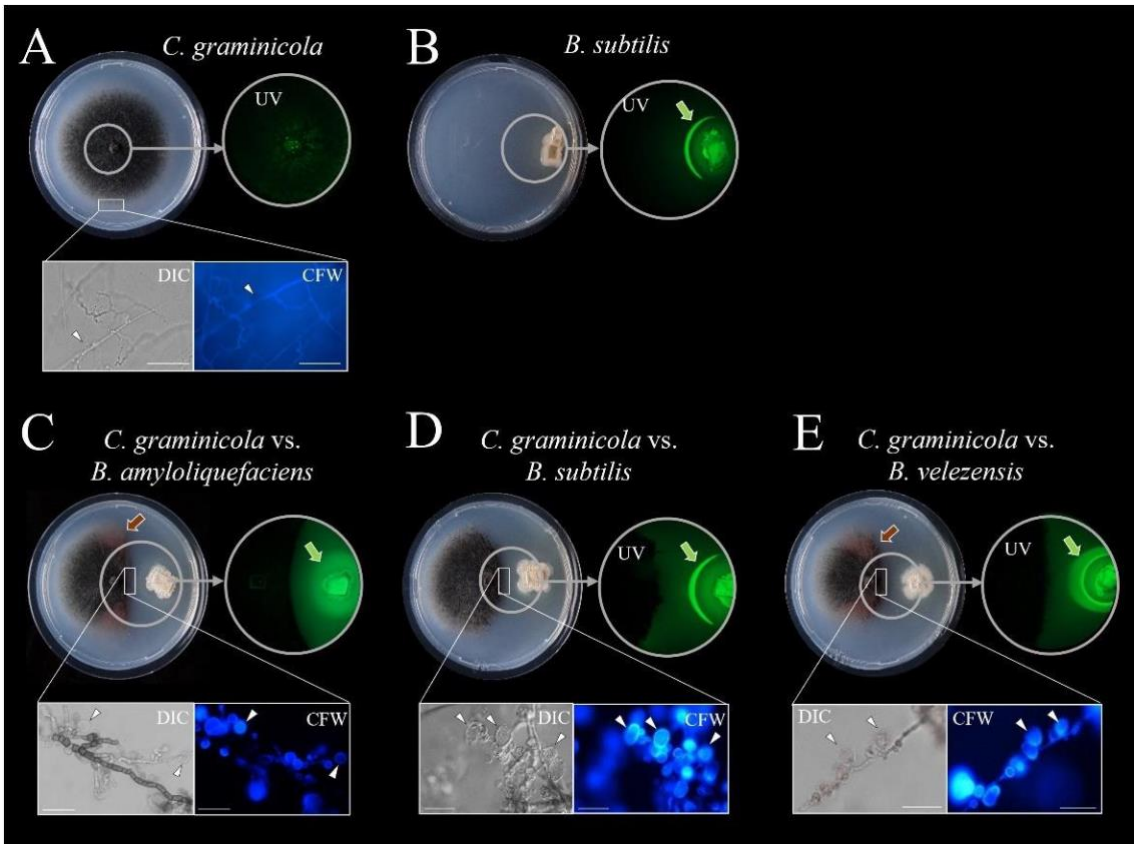

Figure 3. *In vitro* microbial confrontations of the maize pathogen *C. graminicola* and biocontrol *Bacillus* spp. on MM agar at 12 days post inoculation (dpi).

(A, B) show solo cultures of *C. graminicola* and *B. subtilis*. **(C - E)** Confrontations between *C. graminicola* and *B. amyloliquefaciens*, *B. subtilis*, and *B. velezensis*. Circled areas of the plates show UV light excitation; DIC and fluorescence microscopy images after CFW staining of hyphae (highlighted in rectangles) are displayed below the petri dishes. Arrowheads in **(A)** point to smooth hyphae of the fungus, while arrowheads in **(C - E)** indicate hyphal protrusions in response to biocontrol bacteria. Green arrows denote fluorescing chemistries secreted by *Bacillus* strains, and red arrows indicate red discoloration of fungal mycelia. Scale bars represent 20 µm. CFW, Calcofluor White; DIC, Differential Interference Contrast; UV, Ultraviolet.

Not only on solid substrata, but also in liquid medium, confronting interactions between *C. graminicola* and *A. nidulans* with the biocontrol bacterium *B. amyloliquefaciens* were observed (Figure 4). In co-cultures both fungi formed smaller ball-like colonies, in comparison to large-diameter colonies formed in solo cultures (Figure 4, compare mono- and co-cultures, left panel, white boxes). Moreover, like on solid substrata, hyphae of the maize anthracnose fungus *C. graminicola* exhibited large protrusions in co-cultures in liquid PDB, rather than hyphal

filaments, as revealed by DIC and fluorescence microscopy after CFW-staining (Figure 4, *C. graminicola* + *B. amyloliquefaciens*, blue arrowheads; compare with Figure 3, *C. graminicola* vs *B. amyloliquefaciens*, DIC and CFW, white arrowheads). Intriguingly, by contrast, the hyphal morphology of *A. nidulans* appeared to be not affected by the biocontrol bacterium (Figure 4, *A. nidulans* + *B. amyloliquefaciens*, DIC and CFW). These findings highlight the complexity and differential interactions between fungus and bacteria, where *Bacillus*-derived SMs significantly affect fungal growth and morphology, potentially offering insights into toxic biocontrol mechanisms.

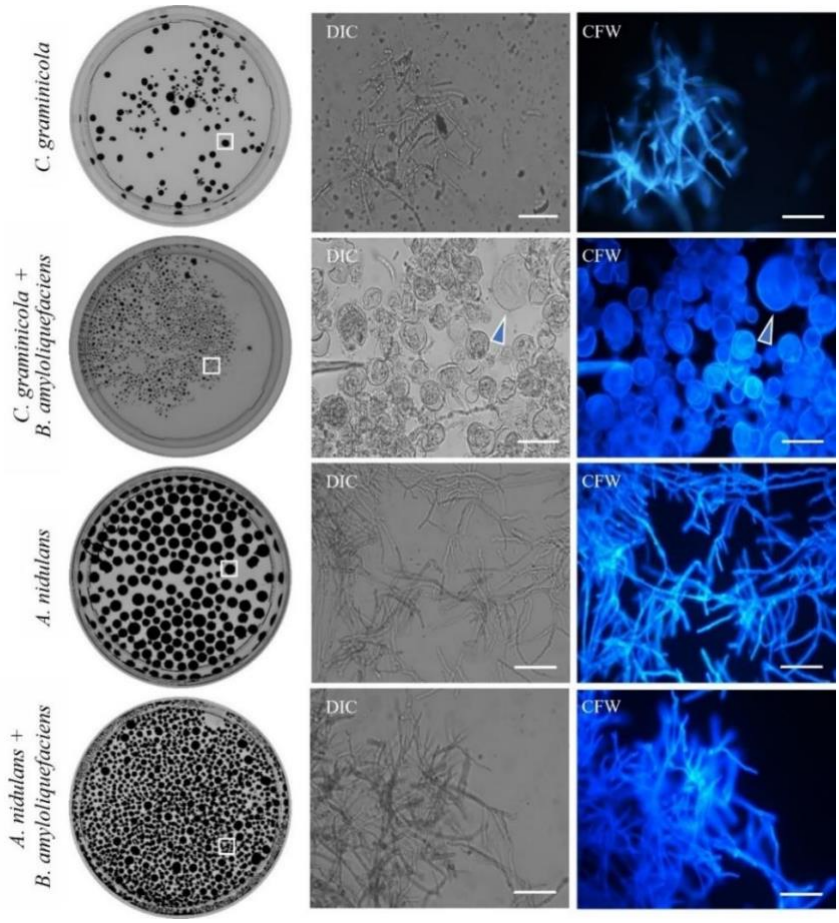

Figure 4. Phenotypical and microscopical observation of micro-organismic interaction between *C. graminicola* and *A. nidulans* with *B. amyloliquefaciens* in PDB.

Photographs were taken at 12 dpi. The left panel shows mycelial balls from control and confrontation samples (indicated by white squares). The right panel presents microscopy images of fungal hyphae obtained by DIC and fluorescence microscopy after CFW staining. The arrowhead indicates regions of large hyphal swelling. Size bars represent 20 µm. CFW, Calcofluor White; DIC, Differential Interference Contrast.

3.1.2 Confrontational metabolome of liquid co-cultures of *C. graminicola* and *B. amyloliquefaciens* indicated major metabolic re-programming

Changes in pigmentation, presumably indicative of altered secondary metabolism were clearly seen in culture filtrates obtained from the confrontations, but not or to lesser extent in those of solo cultures (Figure 5A).

In order to detect metabolic differences of mono-cultures of *C. graminicola* and co-cultures of this fungus with *B. amyloliquefaciens*, the culture filtrates were analyzed by LC-MS/MS, and the data were compared using the GNPS platform (Allard et al., 2016). The resulting molecular networking of the co-cultivated *C. graminicola* + *B. amyloliquefaciens* samples consisted of 417 nodes representing compound ions, as compared with 310 and 315 ions detected in the mono-cultures of *C. graminicola* and *B. amyloliquefaciens*, respectively (Figure 5B). The global molecular networking-based Venn diagram displays the ion distribution obtained from culture filtrates of mono- and co-cultures (Figure 5C). Importantly, 96 ions, many of which belong to the fatty amines according to prediction with the software SIRIUS (https://bio.informatik.uni-jena.de/software/sirius/), were only present in the co-culture. Several ions indicative of highly unsaturated compounds as well as α-amino acids and their derivatives were formed by *B. amyloliquefaciens* monocultures (Figures 5B and 5C).

Collectively, LC-MS/MS analyses showed an enormous plasticity of metabolic responses in this microbial confrontation. The assumption that microbial confrontations would modify SM production led to the discovery that SM formation can easily be visualized in liquid media. The method described here would be applicable to two- or multi-membered consortia and may allow preliminary evaluation of consumers' risks imposed by biological control agents at early stages of legislation.

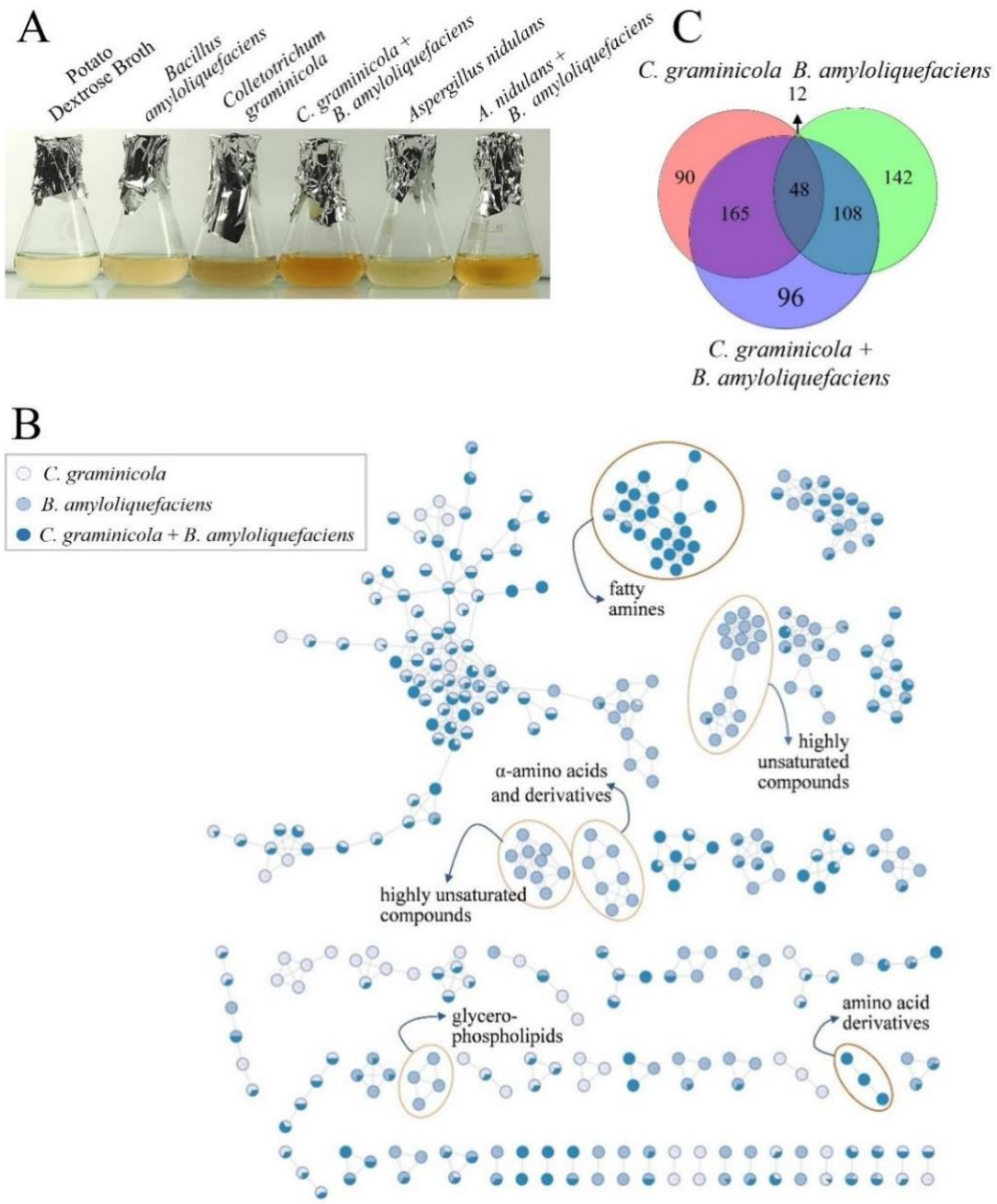

Figure 5. Metabolome re-programming in liquid cultures under confrontations at 12 dpi.

(A) Induction of SM formation in *C. graminicola* and *A. nidulans* co-cultivated with *B. amyloliquefaciens*, compared to their respective solo cultures. **(B)** Global molecular network of the co-culture between *C. graminicola* and *B. amyloliquefaciens*. Nodes represent detected ions: White nodes for ions from *C. graminicola* solo cultures, light-blue nodes for ions from *B. amyloliquefaciens* solo cultures, and dark-blue nodes for ions from co-cultures. Clusters unique to co-cultivation include fatty amines and amino acid derivatives, indicating specific metabolome reprogramming during microbial. **(C)** Venn diagram based on the molecular network, showing unique and shared ions among the cultures. Red indicates ions obtained from fungal solo culture, green from bacterial solo culture, and purple from co-cultures, with 96 unique ions identified in the co-culture.

3.2 Microorganismic confrontations elicit a wide spectrum of SMs with potential human toxicity

3.2.1 Confrontations of the maize pathogen *C. graminicola* with the biocontrol bacterium *B. amyloliquefaciens* or the saprophytic model fungus *A. nidulans*

The biocontrol bacterium *B. amyloliquefaciens* effectively inhibits anthracnose disease symptom expression caused by the pathogen *C. graminicola* (Fig 6A). To characterize microbial interactions, confrontations of the maize anthracnose fungus *C. graminicola* with *B. amyloliquefaciens* and with the non-pathogenic model fungus *A. nidulans* were established *in vitro* (Fig 6B). In both interactions, distance inhibition (Bertrand et al., 2014) occurred at the confrontation sites, suggesting secretion of inhibitory chemistries (Figures 6B and 6C). The fact that growth inhibition did not occur opposite of the confrontation partner nor on split petri dishes argues that inhibitory chemistries were not volatile (Figure 6B and Supporting Figure S1). Fluorescence microscopy of Calcofluor White-stained hyphae of *C. graminicola* confronting *B. amyloliquefaciens* and DIC microscopy revealed massive conglobations (Figure 6D, arrowheads) and vacuolation, as indicated by FM4-64 staining (Figure 6D, DIC, arrows in insert). Conglobations and vacuolation are known to be induced in fungal hyphae by bacterial cyclic lipopeptides such as iturin A and/or plipastatin A, respectively (Gong et al., 2015). In fact, large swellings were also observed in *C. graminicola* hyphae growing in the vicinity of filter disks soaked with commercially available iturin A (Supporting Figures S2A, Iturin A and S2B). Hyphae of *C. graminicola* from control plates (Figure 6D, *C. graminicola*) and from confrontations with *A. nidulans* (Figure 6D, *C. graminicola* vs. *A. nidulans*) were normal filaments, with regularly spaced septae (Figure 6D, Calcofluor White, arrows). Importantly, environmental communities of microorganisms isolated from maize leaf surfaces by imprinting onto a petri dish only rarely exhibit inhibition zones (Figure 6E).

Collectively, these data suggest that growth of both confrontation partners of the *C. graminicola* vs. *B. amyloliquefaciens* and of the *C. graminicola* vs. *A. nidulans* interaction are strongly inhibited at the confrontation zone, resulting in distance inhibition. Moreover, these data highlight that non-volatile secreted inhibitory compounds, either newly formed or modified in the confrontation, represent molecular determinants of the outcome of the interactions between the maize anthracnose fungus and either a biocontrol bacterium or a ubiquitous fungus.

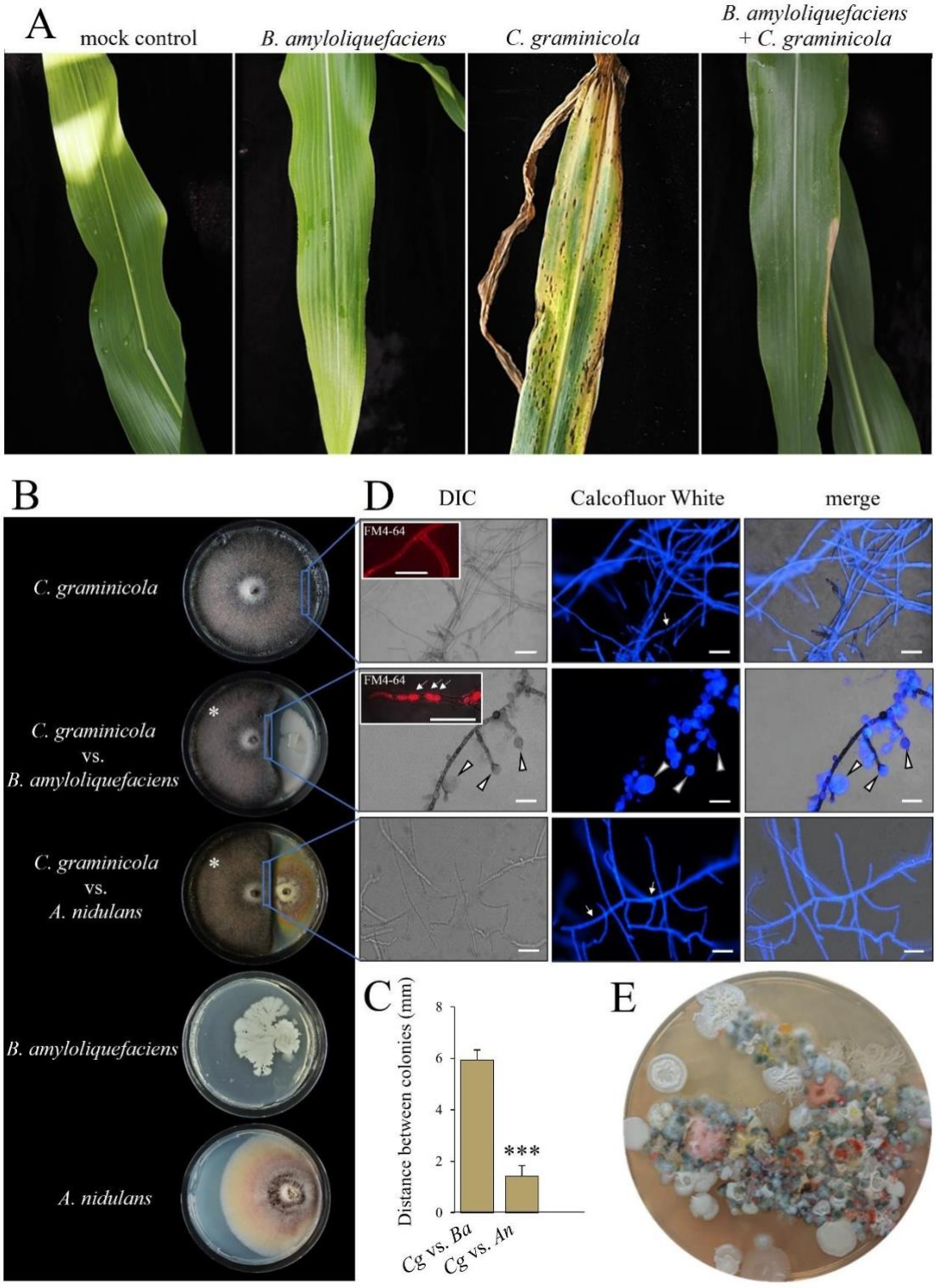

Figure 6. *In vitro* confrontation assay with the maize pathogen *C. graminicola* versus. the biocontrol bacterium *B. amyloliquefaciens* or the ubiquitous fungus *A. nidulans*.

(A) Maize leaves inoculated with *C. graminicola* showed severe anthracnose disease symptoms, but leaves pre-treated with *B. amyloliquefaciens* did not. Leaves only treated with *B. amyloliquefaciens* and mock-inoculated leaves showed no disease symptoms. Photos were taken at 7 dpi. **(B)** Confrontation assay between *C. graminicola* and *B. amyloliquefaciens* or *A. nidulans* on PDA indicate distance inhibition. White asterisks indicate *C. graminicola*. Photos were taken at 12 dpi. **(C)** Distance between microbial colonies indicated distance growth inhibition at 12 dpi. Error bars represent + SDs and asterisk indicate significant differences between the samples (*** $p < 0.001$). **(D)** Microscopy revealed that hyphae of *C. graminicola* formed swellings in confrontation with *B. amyloliquefaciens*, but not with *A. nidulans* or in solo cultures. The cell wall dye Calcofluor white visualized hyphal swellings in confrontation with *B. amyloliquefaciens* (Calcofluor White; arrowheads) and thin hyphae with regularly spaced septae (Calcofluor White; small arrows). The membrane dye FM4-64 (DIC, inserts) highlighted vacuolization in confrontation with *B. amyloliquefaciens* (FM4-64, arrows). Photos were taken at 12 dpi. The merged image displays the overlay of DIC and CFW channels. Scale bar represents 50 µm. **(E)** A maize leave imprint on GYM medium showing diverse microbial colonies contacting each other without inhibition zones. Experiments were performed in triplicates. DIC, Differential Interference Contrast; *Cg* vs. *Ba*, *C. graminicola* vs. *B. amyloliquefaciens*; *Cg* vs. *An*, *C. graminicola* vs *A. nidulans*.

3.2.2 The confrontational transcriptome

To identify genes de-regulated in confrontations of *C. graminicola* with *B. amyloliquefaciens* or *A. nidulans*, mRNA was isolated from the peripheral 5 mm of three individual colonies of each partner facing the confrontation zone. RNA extracted from margins of three independent solo cultures of *C. graminicola*, *B. amyloliquefaciens* and *A. nidulans* growing on control plates without a confrontation partner served as controls. The three independent libraries of *C. graminicola*, *B. amyloliquefaciens* and *A. nidulans* solo cultures yielded a total of 23.9, 32.2, and 32.7 million clean reads, respectively. From the confrontation with *B. amyloliquefaciens* and *A. nidulans*, 43.2 and 33.5 million clean reads were obtained for *C. graminicola*, and 40.2 and 34.6 million clean reads were obtained for *B. amyloliquefaciens*, and *A. nidulans*. The obtained clean reads were mapped to the 12,399 genes of the *C. graminicola* reference genome and to the 4,147 and 10,518 genes of the *B. amyloliquefaciens* and *A. nidulans* reference genomes (See section 2.4.3.1), respectively. DEGs in individual microbes in distinct confrontations were identified by DESeq2, with a -fold change (FC) of > 2 defined as upregulated, and a FC of < 0.5 as downregulated**.**

PCA showed clear separation of three independent biological repeats of pure cultures of *C. graminicola* (*Cg*), *B. amyloliquefaciens* (*Ba*) and *A. nidulans* (*An*) and the confrontations between *C. graminicola* and *B. amyloliquefaciens* (*Cg* vs. *Ba*) or *C. graminicola* and *A. nidulans* (*Cg* vs. *An*) (Figures 7A - 7C). The dissimilarities between the groups were supported by the heatmaps of

the correlation matrices, with sample clustering based on the normalized transcript counts (Figures 7D - 7F). In all confrontations, more genes showed decreased than increased transcript abundances in all partners. In *C. graminicola,* confrontations with *B. amyloliquefaciens* or *A. nidulans* resulted in a total of 1,606 and 2,389 DEGs, respectively, with 570 showing increased and 1036 decreased transcript abundances in the confrontation with the bacterium, and 892 showing increased and 1497 decreased transcript abundances in the confrontation with *A. nidulans* (Figure 7G, *Cg* vs. *Ba* and *Cg* vs. *An*). Nine-hundred-and-thirty-five DEGs were specific for the *C. graminicola* vs. *B. amyloliquefaciens* confrontation, and 1718 distinct DEGs were identified in the *C. graminicola* vs. *A. nidulans* confrontation. Highlighting the specificity of responses in the fungus vs. bacterium and fungus vs. fungus interaction, only 671 DEGs were shared in both confrontations (Figure 7H). Intriguingly, 82 of all DEGs of *Colletotrichum* in the confrontation with *B. amyloliquefaciens* and 116 in the confrontation with *A. nidulans* belonged to the category of secondary metabolism genes. Thus, more than 50% of the 300 *C. graminicola* genes categorized as SM genes (O'Connell et al., 2012) were de-regulated in the microbial confrontations studied, with 12% of the SMBGC genes de-regulated in both confrontations (Figure 7I). While more SM genes showed increased transcript abundances in the confrontation partners, more SM genes showed decreased transcript concentrations in *C. graminicola* in confrontations (Figure 7J).

Due to the establishment of distance inhibition in the confrontations of *C. graminicola* with the bacterial and with the fungal partner (Figure 6B), and due to the prominent response of SM genes (Figure 7I), I decided to study genes organized into SMBGCs in more detail.

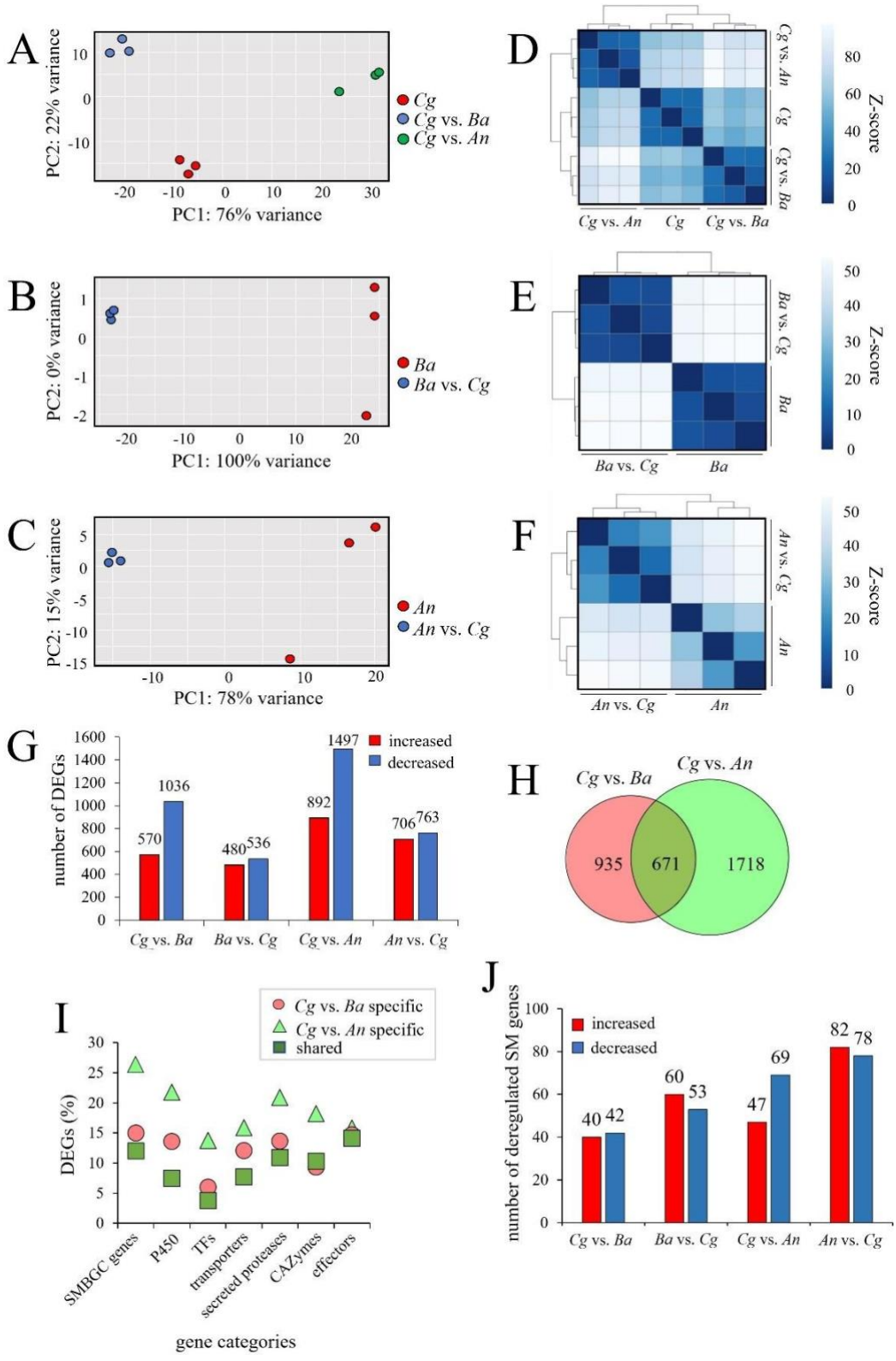

Figure 7. Transcriptome analysis of DEGs under confrontations.

(A) Principal component analyses (PCA) show clear cluster separation of *C. graminicola* (*Cg*) solo cultures and hyphae confronting *B. amyloliquefaciens* (*Cg* vs. *Ba*) or *A. nidulans* (*Cg* vs. *An*). **(B)** PCA plot showing distinctness of *B. amyloliquefaciens* (*Ba*) solo cultures and cultures confronting *C. graminicola* (*Ba* vs. *Cg*). **(C)** PCA plot showing distinctness of solo cultures of *A. nidulans* (*An*) and mycelia confronting *C. graminicola* (*An* vs. *Cg*). Sample groups are indicated by different color codes. Each replicate is plotted as an individual data point. **(D)** Heatmap of the sample-to-sample distance matrix obtained from solo cultures of *C. graminicola* and confrontations with *B. amyloliquefaciens* and *A. nidulans*. **(E)** Heatmap of the sample-to-sample distance matrix of *B. amyloliquefaciens* solo cultures and cultures confronting *C. graminicola*. **(F)** Heatmap of the sample-to-sample distance matrix of *A. nidulans* solo cultures and cultures confronting *C.* graminicola. The color codes in figures **(D - F)** indicate the distance between the samples, as based on the Z-score. Dark blue denotes shorter distance i.e., replicates are grouped closer in distance. **(G)** DEGs identified in different confrontations and confrontation partners. Red and blue bars indicate increased (FC > 2) and decreased (FC < 0.5) transcript abundances with adjusted $p < 0.05$. **(H)** Venn diagram representing the distribution of the DEGs of *C. graminicola* confronting *B. amyloliquefaciens* (*Cg* vs. *Ba*) or *A. nidulans* (*Cg* vs. *An*). The number in the overlap denotes the mutual DEGs between distinct confrontations. **(I)** Scatter plot showing confrontation-specific and shared DEGs of *C. graminicola*. Genes are grouped according to functional categories. **(J)** Bar graph showing the number of SM genes deregulated in different confrontation partners in distinct confrontations. Red and blue bars indicate increased and decreased transcript abundances of differentially expressed SM genes. Experiments were performed in triplicates. *Cg*, *C. graminicola*; *Ba*, *B. amyloliquefaciens*; *An*, *A. nidulans*; *Cg* vs. *Ba*, *C. graminicola* vs. *B. amyloliquefaciens*; *Cg* vs. *An*, *C. graminicola* vs *A. nidulans*; *Ba* vs. *Cg*, *B. amyloliquefaciens* vs. *C. graminicola*; *An* vs. *Cg*, *A. nidulans* vs. *C. graminicola*; DEGs, Differentially Expressed Genes; SMBGC, Secondary Metabolite Biosynthetic Gene Cluster; PC, Principal Component; TFs, Transcription Factors; CAZymes, Carbohydrate-Active Enzymes; Z-score, Standard normal distribution.

In *C. graminicola*, 300 genes belong to 42 SMBGCs (O'Connell et al., 2012). Twenty-nine and 36 of these clusters harbor at least one transcriptionally de-regulated gene in the confrontation with *B. amyloliquefaciens* or *A. nidulans*, respectively (Figures 8A and 9A).

In the confrontation with *B. amyloliquefaciens*, 40 SM genes present in 29 SMBGCs of *C. graminicola* showed increased and 42 showed reduced transcript abundances (Figures 8A and 7J, *Cg* vs. *Ba*). The de-regulated genes included 12 *PKS*, 2 *NRPS*, and 1 *PKS-NRPS* hybrid gene. Interestingly, in SMBGC 27, harboring a core PKS gene called *PKS27* (GLRG_10537), 17 out of 18 SM genes showed increased transcript concentrations (Figure 8A, SMBGC 27).

In the confrontation with *A. nidulans*, 47 and 69 SM genes of *C. graminicola*, organized into 36 SMBGCs, showed increased and decreased transcript abundances, respectively (Figures 9A and 7J, *Cg* vs. *An*). Genes de-regulated in this fungus vs. fungus confrontation included 17 *PKS*, 3

NRPS, and 4 *PKS-NRPS* hybrid genes. Again, highlighting the specificity of the SM response, 45 and 79 SM genes of *C. graminicola* were de-regulated in the confrontation with *B. amyloliquefaciens* or *A. nidulans*, respectively, and only 37 were de-regulated in both confrontations (Figures 8A and 9A). RT-qPCR experiments confirmed de-regulation of genes of SMBGCs 27 and 35 under confrontations with *B. amyloliquefaciens* and *A. nidulans* and supported RNA-Seq data (Supporting Figures S3A and S3C).

In *B. amyloliquefaciens* confronting *C. graminicola* (*Ba* vs. *Cg*), a total of 1016 significantly DEGs, with 480 showing increased and 536 decreased transcript abundances was recorded (Figure 7G, *Ba* vs. *Cg*). Of these 1016 DEGs, 113 SM genes were organized into 11 SMBGCs of *B. amyloliquefaciens*, with 60 genes showing increased and 53 decreased transcript abundances (Figures 8B and 7J, *Ba* vs. *Cg*). The de-regulated genes included 8 *NRPS* in 11 clusters. SMBGCs 6 and 11 responsible for the production of iturin and bacilysin had 18 and 25 deregulated genes, respectively, across the entire clusters. To validate the authenticity of the RNA-Seq data, two iturin genes (*ituB* and *ituC*) and three bacilysin genes (*bacA*, *bacC,* and *bacE*) were subjected to RT-qPCR analyses, thereby confirming increased mRNA abundance of these genes (Supporting Figure S3B).

Of the 1,469 DEGs of *A. nidulans* confronting *C. graminicola* (*An* vs. *Cg*), 706 and 763 showed increased or reduced transcript abundances (Figure 7G, *An* vs. *Cg*). In *A. nidulans*, 160 SM genes in 50 SMBGCs were deregulated, 82 of which showed increased and 78 reduced transcript abundances, respectively (Figures 9B and 7J, *An* vs. *Cg*). The DEGs included 14 *PKS*, 14 *NRPS*, 1 *PKS-NRPS* hybrid, and 2 terpene synthase genes. Importantly, most genes of SMBGC 21 responsible for production of the carcinogenic polyketide STC showed increased transcript abundances in both RNA-Seq and RT-qPCR analyses (Figure 9B, SMBGC 21; Supporting Figure S3D). Interestingly, commercial STC caused only minor inhibition of vegetative hyphal growth of *C. graminicola* (Supporting Figure S2A, Sterigmatocystin).

Taken together, although both the bacterial and fungal confrontation of *C. graminicola* resulted in distance inhibition, comparisons of genome-wide transcriptional responses indicated specific recognition of different confrontation partners and translation into specific transcriptional SM responses.

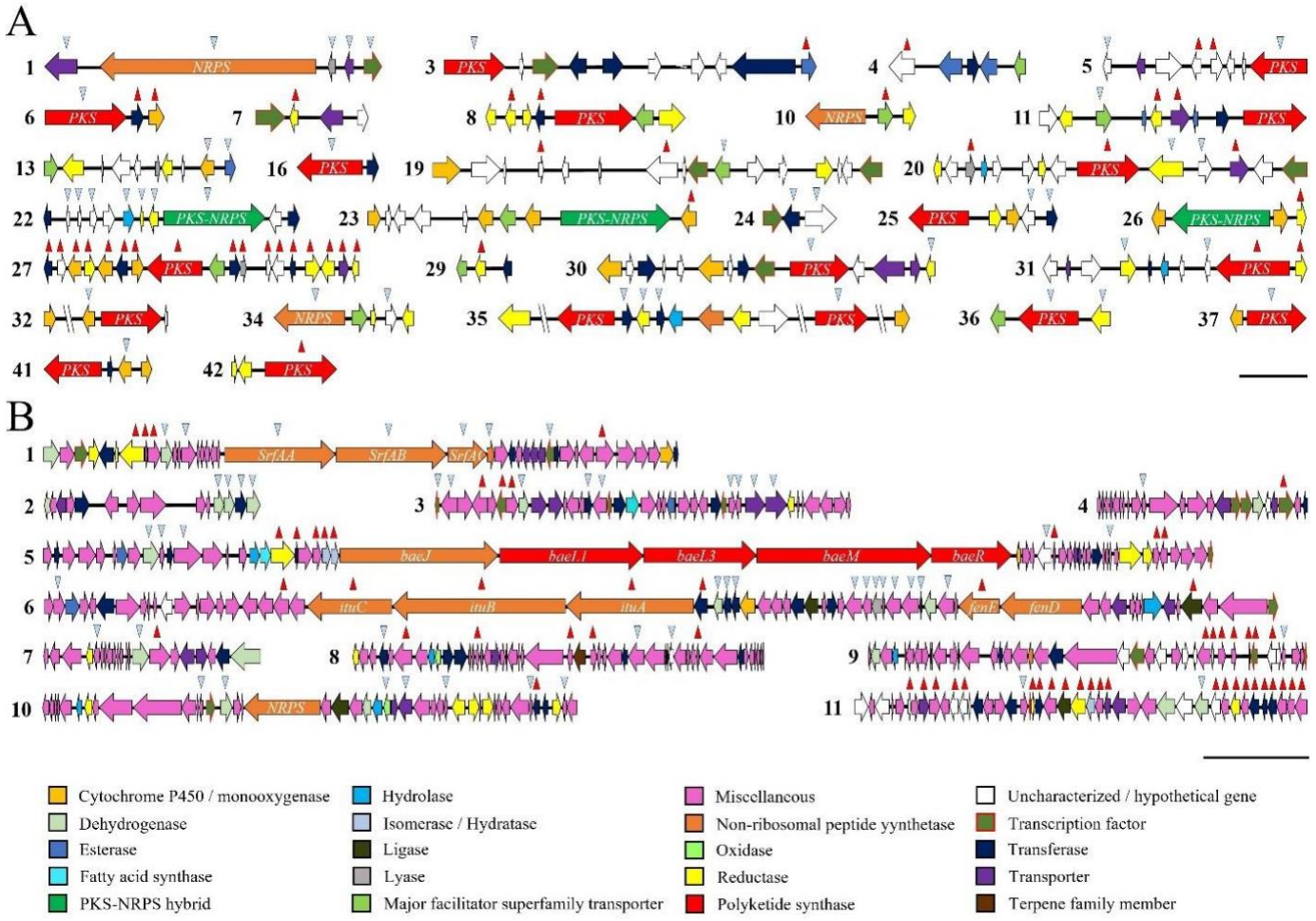

Figure 8. Physical map of deregulated SMBGCs in the *C. graminicola* vs. *B. amyloliquefaciens* confrontation.

(A) In *C. graminicola*, 29 out of 42 SMBGCs harbor deregulated genes in confrontation with *B. amyloliquefaciens*. **(B)** In *B. amyloliquefaciens* confronting *C. graminicola*, all 11 SMBGCs harbor de-regulated genes. **(A** and **B)** Horizontal arrows represent SM genes and their transcriptional direction. The putative function is indicated by the color code. Red and blue arrowheads denote increased or decreased transcript abundances in the confrontation. Scale bar represents 10 kb. *PKS*, Polyketide Synthase; *NRPS*, Non-ribosomal Peptide Synthetase.

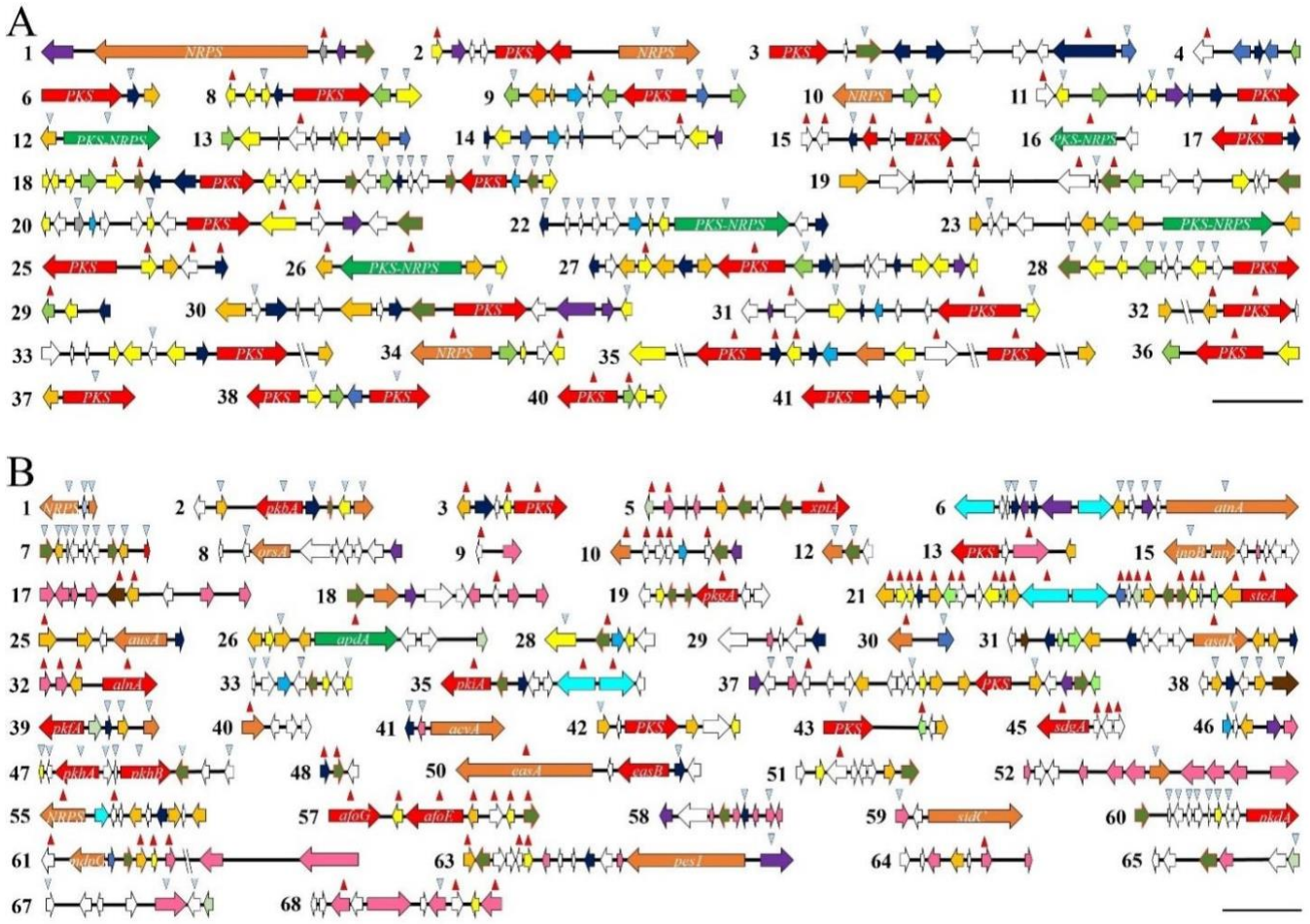

Figure 9. Physical map of deregulated SMBGCs in the *C. graminicola* vs. *A. nidulans* confrontation.

(A) In *C. graminicola*, 36 out of 42 SM SMBGCs harbor deregulated genes in confrontation with *A. nidulans*. **(B)** In *A. nidulans* confronting *C. graminicola*, 50 out of the total of 68 SM clusters are transcriptionally de-regulated. **(A** and **B)** The horizontal arrows represent SM genes and their transcriptional direction. Putative function as indicated by the color code is as in Figure 8. Red and blue arrowheads denote increased or decreased transcript abundances in the confrontation. Scale bar represents 10 kb. *PKS*, Polyketide Synthase; *NRPS*, Non-ribosomal Peptide Synthetase.

3.2.3 The confrontational metabolome

Alterations in transcript abundances of genes present in SMBGC do not necessarily reflect alterations in SM concentrations. Therefore, to generate high-resolution compound partitioning data via LC-MS/MS analyses, metabolites were extracted from the edge of colonies of confrontation partners, as well as from the inhibition zone lacking fungal or bacterial cells but containing secreted chemistries (Figures 10A and 11A, red sections; Supporting Figures S4A and S4B, red sections). Metabolites extracted from the edges of the mycelia of solo cultures of each confrontation partner served as controls (Supporting Figure S4A, blue and yellow sections; Supporting Figure S4B, blue and brown sections). Importantly, 1,738 and 1,466 novel features were detected in the confrontations of *C. graminicola* with the biocontrol bacterium *B. amyloliquefaciens* and with the ubiquitous fungus *A. nidulans*, respectively (Supporting Figures S4C and S4D). Violin plots show the intensities and distribution of all features within individual samples, and of seven patterns of non-overlapping feature distributions between the confrontation partners, referred to as profiles P1 to P7 (Figures 10B and 11B, top panel, all zones and P1 - P7).

The profiles reflect various intensities of features detected in different contexts: those produced by *B. amyloliquefaciens* and *A. nidulans* (Figures 10B and 11B, P1), or *C. graminicola* alone (Figures 10B and 11B, P2); features secreted into the medium by a confrontation partner and *C. graminicola* (Figures 10B and 11B, P3 and P4); features unique to the confrontation zone (Figures 10B and 11B, P5); features common to both *C. graminicola* and its confrontation partner (Figures 10B and 11B, P6); and features present in both organisms as well as the inhibition zone (Figures 10B and 11B, P7). Correspondingly, line plots indicate compound-specific intensities, with intensities corresponding to one compound across samples linked by a black line (Figures 10B and 11B, bottom panel, all zones and P1 - P7). Importantly, patterns P3 - P5, harboring secreted chemistries, add up to 312 features in the *C. graminicola* vs. *B. amyloliquefaciens*, and to 224 features in the *C. graminicola* vs. *A. nidulans* confrontation (Figures 10B and 11B, P3 - P5). In addition, profile P7 shows very different numbers of features, i.e. 316 in the fungus vs. bacterium and 66 in the fungus vs. fungus confrontation (Figures 10B and 11B, P7). In both the confrontations, only a minor fraction of features was annotated (Figures 10C and 11C, top panel).

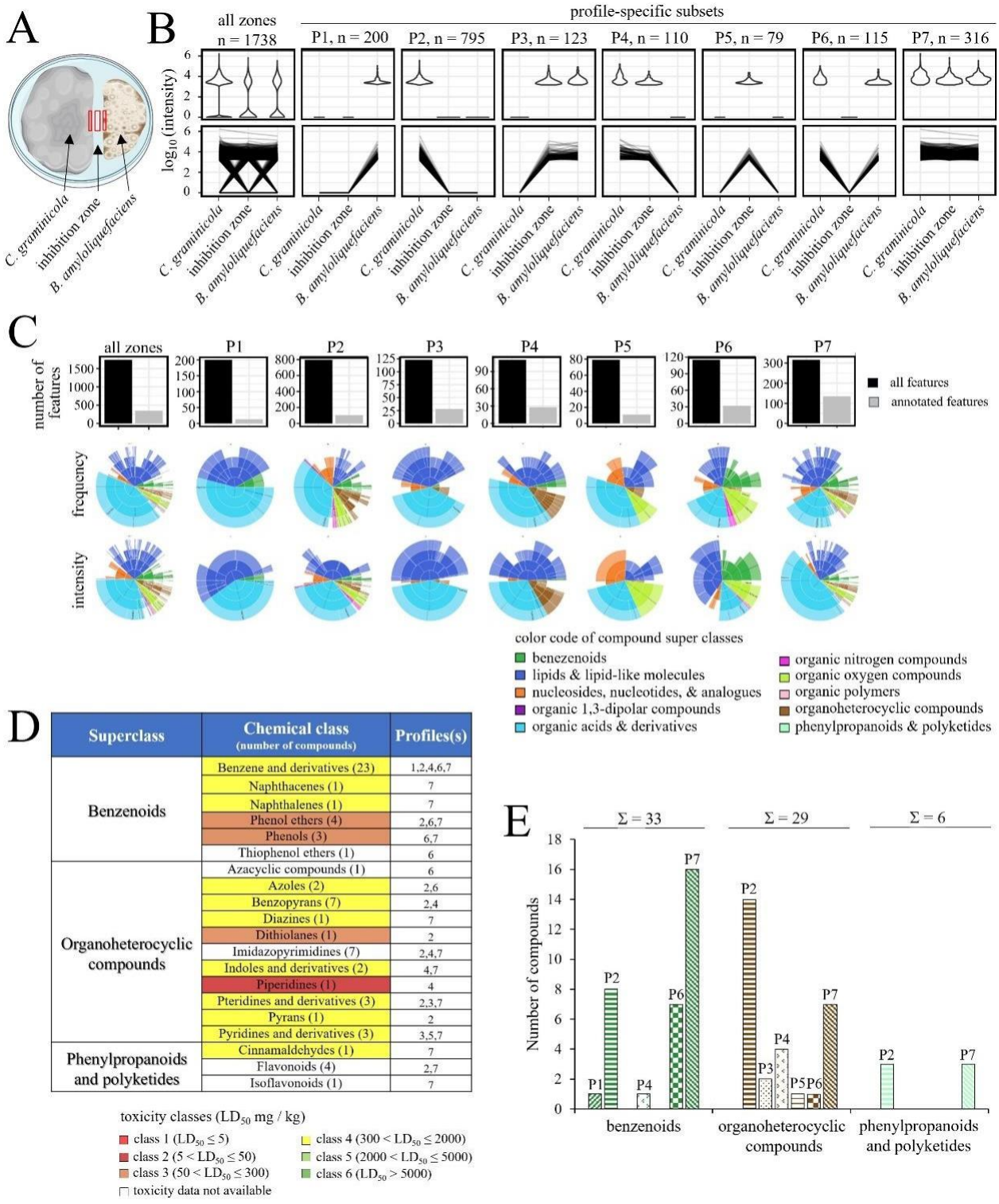

Figure 10. Metabolome analysis of features detected under *C. graminicola* vs. *B. amyloliquefaciens* confrontation.

(A) Diagram of a petri dish depicting the fungal vs. bacterium confrontation. Red rectangles show metabolite sampling sites from *C. graminicola* and *B. amyloliquefaciens* colonies and from the inhibition zone. **(B)** The set of all detected features in all zones is separated into seven profile specific subsets (P1 - P7). The upper panel shows violin plots revealing the distribution of measured compound intensities within individual samples. The lower panel represents line plots displaying the measured intensities per compound, where a black line links intensities corresponding to one feature over all samples. **(C)** Bar plots showing the number of total and annotated features (upper panel) and sunburst plots (lower panel) showing frequencies and intensities of annotated compound classes per set and sample. Four levels of compound annotation ranging from superclass, class, sub class, and most specific class (inside to outside) are given. The color code indicates compound super classes. Fractions in the upper sunburst plots are based on the frequency (number of occurrence) and in the lower on the sum of measured intensities. **(D)** Acute toxicity of features belonging to benzenoids, organoheterocyclic features, and phenylpropanoids and polyketides. Features are color-coded according to their toxicity classes, as indicated by their LD_{50} values. **(E)** Number and occurrence of features belonging to the three major super classes benzenoids, organoheterocyclic features, and phenylpropanoids and polyketides in profiles P1 - P7. P1 - P7, Profiles 1 - 7; LD_{50}, Lethal dose 50%; n, Total number of features; $\sum$, Summation.

Applying the software tool Canopus (https://bio.informatik.uni-jena.de/software/canopus/) and the chemical ontology system ClassyFire (Djoumbou Feunang et al., 2016) allowed annotating SM features to chemical super classes and classes. The fractions of annotated compound classes per set and sample have been used to generate sunburst plots, which show four compound specificity levels, i.e.: super classes, classes, sub classes, and most specific classes (Figures 10C and 11C, bottom panel, inside to outside), with color-coded annotated compound super classes. Fractions in the upper and lower sunburst plot panels are based on number of occurrences (frequency) or the sum of measured intensities (intensity), respectively. In the *C. graminicola* vs. *B. amyloliquefaciens* confrontation, of a total of 68 compounds, 33 fell into 6 classes of the super class of benzenoids, 29 belonged to 11 classes of organoheterocyclic compounds, and 6 belonged to three classes of phenylpropanoids and polyketides (Figure 10D), with distinct compounds attributed to different profiles (Figure 10E). In the *C. graminicola* vs. *A. nidulans* confrontation, the numbers of chemistries and classes they belong to were more complex, with a total of 94 newly synthesized compounds identified. Six, 16 and 6 classes were members of the super classes of benzenoids, organoheterocyclic compounds, and phenylpropanoids and polyketides, respectively (Figure 11D), and, as in the *C. graminicola* vs. *B. amyloliquefaciens* confrontation, were present in distinct profiles (Figure 11E).

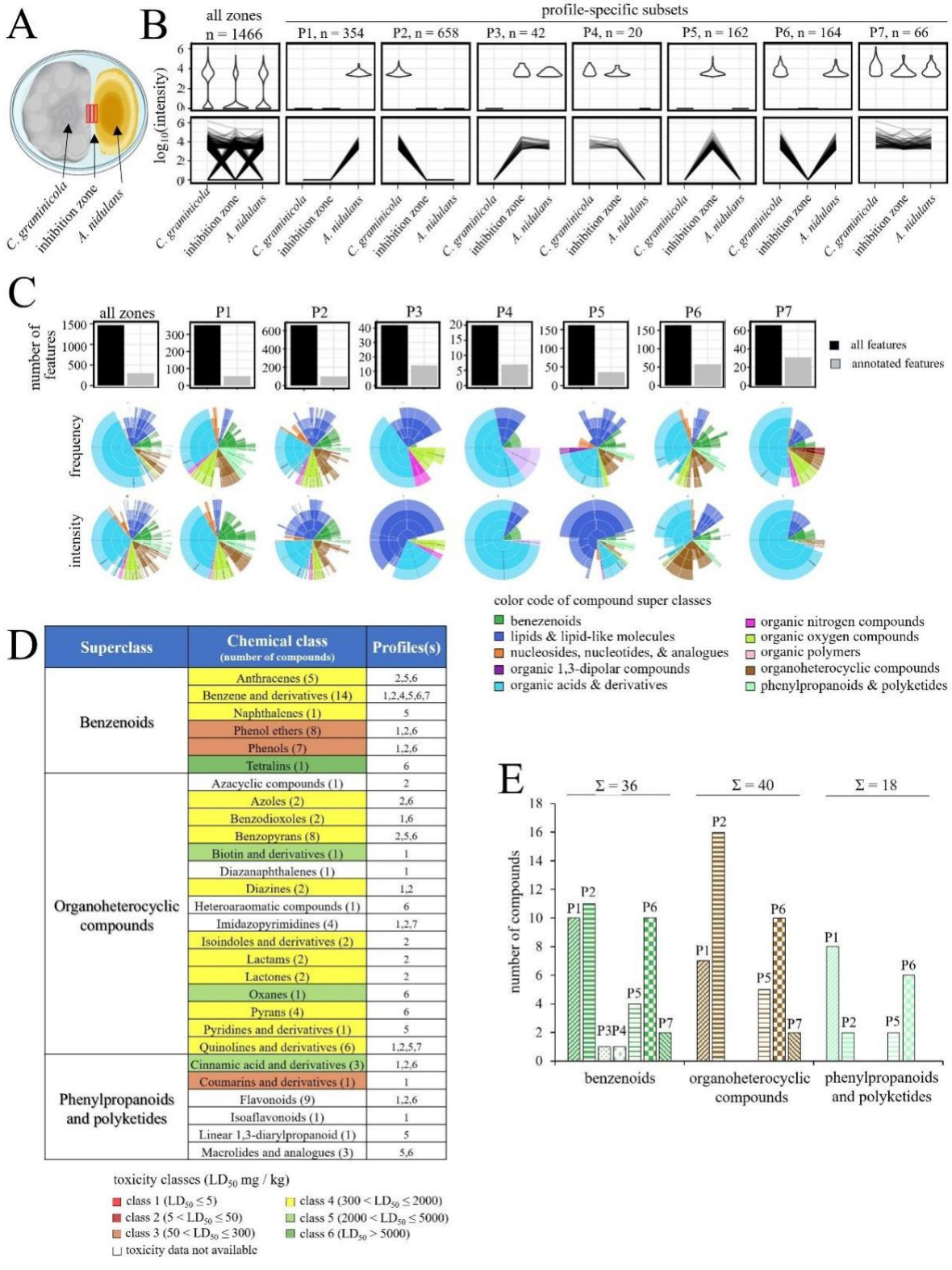

Superclass	Chemical class (number of compounds)	Profiles(s)
Benzenoids	Anthracenes (5)	2,5,6
	Benzene and derivatives (14)	1,2,4,5,6,7
	Naphthalenes (1)	5
	Phenol ethers (8)	1,2,6
	Phenols (7)	1,2,6
	Tetralins (1)	6
Organoheterocyclic compounds	Azacyclic compounds (1)	2
	Azoles (2)	2,6
	Benzodioxoles (2)	1,6
	Benzopyrans (8)	2,5,6
	Biotin and derivatives (1)	1
	Diazanaphthalenes (1)	1
	Diazines (2)	1,2
	Heteroaraomatic compounds (1)	6
	Imidazopyrimidines (4)	1,2,7
	Isoindoles and derivatives (2)	2
	Lactams (2)	2
	Lactones (2)	2
	Oxanes (1)	6
	Pyrans (4)	6
	Pyridines and derivatives (1)	5
	Quinolines and derivatives (6)	1,2,5,7
Phenylpropanoids and polyketides	Cinnamic acid and derivatives (3)	1,2,6
	Coumarins and derivatives (1)	1
	Flavonoids (9)	1,2,6
	Isoaflavonoids (1)	1
	Linear 1,3-diarylpropanoid (1)	5
	Macrolides and analogues (3)	5,6

Figure 11. Metabolome analysis of features detected under *C. graminicola* vs. *A. nidulans* confrontation.

(A) Diagram of a petri dish depicting the fungal vs. fungal confrontation. Red rectangles show metabolite sampling sites from *C. graminicola* and *A. nidulans* colonies and from the inhibition zone. **(B)** The set of all detected features in all zones is separated into seven profile specific subsets (P1 - P7). The upper panel shows violin plots revealing the distribution of measured compound intensities within individual samples. The lower panel represents line plots displaying the measured intensities per compound, where a black line links intensities corresponding to one compound over all samples. **(C)** Bar plots showing the number of total and annotated features (upper panel) and sunburst plots (lower panel) showing frequencies and intensities of annotated compound classes per set and sample. Four levels of compound annotation ranging from superclass, class, sub class, and most specific class (inside to outside) are given. The color code indicates compound super classes. Fractions in the upper sunburst plots are based on the frequency (number of occurrence) and in the lower on the sum of measured intensities. **(D)** Acute toxicity of features belonging to benzenoids, organoheterocyclic features, and phenylpropanoids and polyketides. Features are color-coded according to their toxicity classes, as indicated by their LD_{50} values. **(E)** Number and occurrence of features belonging to the three major super classes benzenoids, organoheterocyclic features, and phenylpropanoids and polyketides in profiles P1 - P7. P1 - P7, Profiles 1 - 7; LD_{50}, Lethal dose 50%; n, Total number of features; ∑, Summation.

Interestingly, compound classes such as piperidines and cinnamaldehydes were found newly synthesized in the *C. graminicola* vs. *B. amyloliquefaciens* confrontation, whereas azoles were discovered in both confrontations. In fact, these three classes of chemistries represent lead structures of synthetic fungicides, possibly explaining the establishment of inhibition zones to some degree. As an approximation of the toxicological potential of chemistry classes to mammals, toxicities of their lead structures were subjected to computational toxicity estimations, using ProTox 3.0 (https://tox.charite.de/protox3/index.php?site=home, (Banerjee et al., 2024). These algorithms employ a comprehensive database of approximately 40,000 compounds with known LD_{50} values from rodent experiments (Banerjee et al., 2024). Intriguingly, MS/MS analyses of chemistries produced in the *C. graminicola* vs. *A. nidulans* confrontation (Figures 11B, profile P1 and 11D, isoflavonoid) yielded feature_562_363.19s_426.13106Da, with a rt of 363.19 seconds and an m/z value of 427.14. Four fragments with m/z means of 247.09, 381.13, 391.11, and 409.12 were identified. Annotation using the MetFrag software (Wolf et al., 2010) suggests that this compound is an isoflavonoid, i.e. the toxic rotenoid villosinol (Figure 12). Though a toxicity class prediction is not provided for the chemical class of isoflavonoids, ProTox 3.0 estimates an acute toxicity of 4 mg/kg body weight for villosinol. This significant toxicity is plausible, as rotenoids act as mitochondrial respiration inhibitors interfering with the transfer of electrons from iron-sulfur centers of complex I to ubiquinone (https://pubchem.ncbi.nlm.nih.gov/ compound/Rotenone).

However, it is important to emphasize that predicted acute toxicities of chemistries produced in confrontations, as deduced from lead structures, may differ significantly from actual toxicities of specific compounds produced in confrontations.

Feature_562_363.19s_426.13106Da

MetFrag Output		
Name	**Molecular Formular**	**Score**
Villosinol	C23H22O8	1.0
#Frag	**Raw Data Value**	**IntCov [%]**
4	27907498.029	58.246

Ion Formular	m/z meas	Delta m/z [mDa]	Intens.	IntCov. [%]
[C14H13O4+H]+H+	247.093	[-2H] 4.2	141.000	7.4
[C22H20O6]+H+	381.131	[-1H] 2.4	80.000	4.2
[C23H18O6]+H+	391.118	[-1H] -0.1	308.000	16.1
[C23H20O7]+H+	409.127	[-1H] 1.4	587.000	30.6

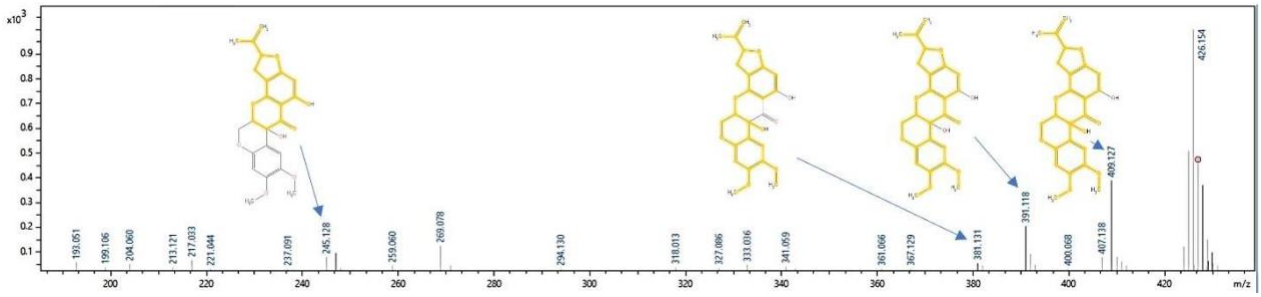

Figure 12. Annotation of compound feature 562 from the *C. graminicola* vs. *B. amyloliquefaciens* confrontation using MetFrag software.

The compound feature 562, identified in the confrontation assay between *C. graminicola* and *B. amyloliquefaciens*, was annotated as villosinol. The MS/MS spectra, with a rt of 363.19 seconds and an m/z value of 427.14, revealed four characteristic fragments with m/z values of 247.09, 381.13, 391.11, and 409.12. These fragments correspond to the stepwise loss of specific groups from the villosinol molecule, supporting its identification. The structures of these fragments are illustrated alongside the MS/MS spectrum, confirming the compound's annotation. m/z, mass-to-charge ratio; Delta m/z, Difference in mass-to-charge ratio; Intens, Intensity; IntCov, Intensity Coverage; rt, Retention time.

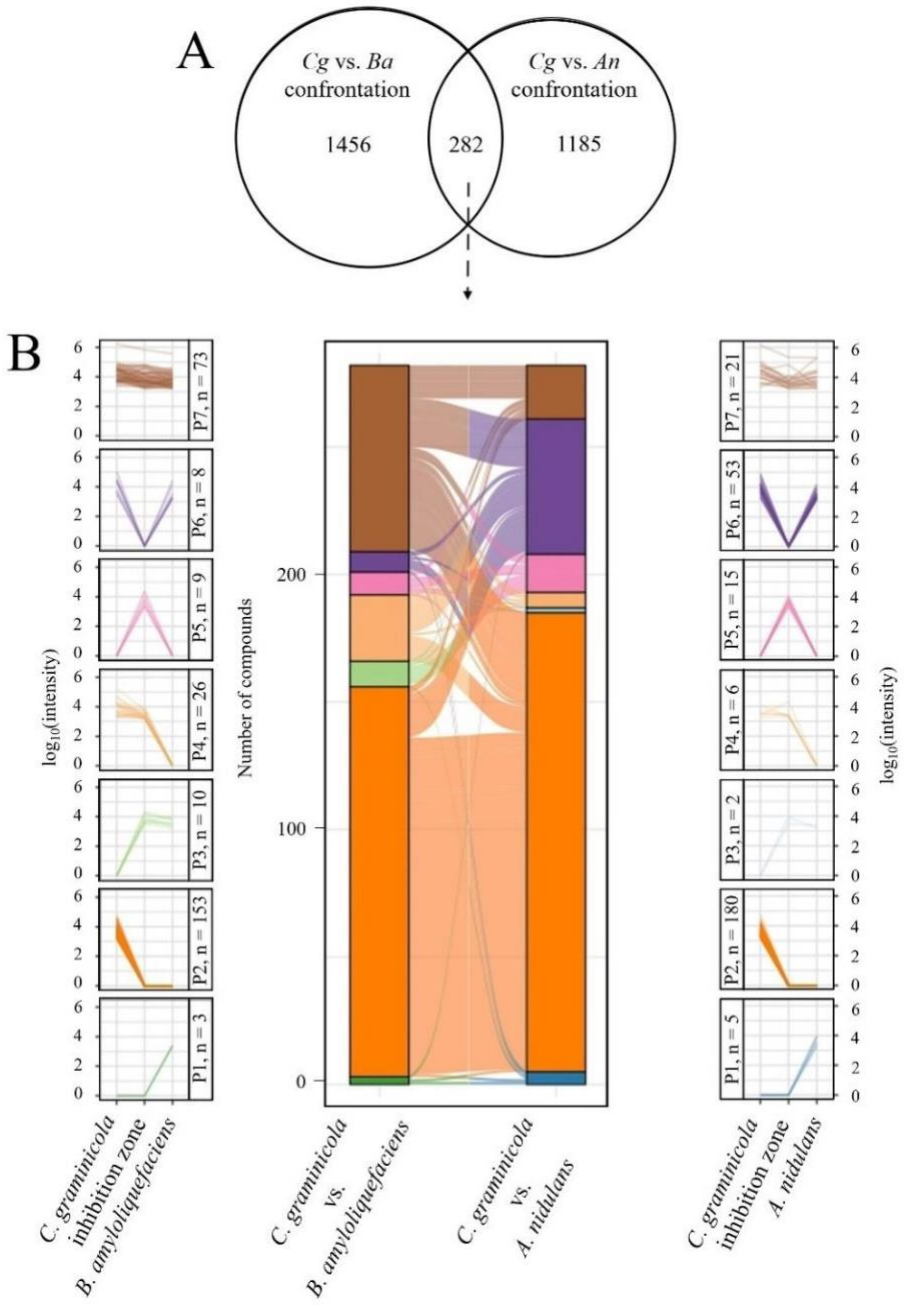

Figure 13. Confrontation- and profile- specificity of features synthesized in the confrontations of *C. graminicola* with *B. amyloliquefaciens* or *A. nidulans*.

(A) Venn diagram indicating that of the 1,738 and 1,466 features synthesized in the fungus vs. bacterium and in the fungus vs. fungus confrontation, with only 282 common to both interactions. **(B)** Alluvial plot showing comparison of the shared 282 features between both confrontations. **(A** and **B)** Profiles P1 - P7 are as in Figures 10 and 11. Stacked bar plots for each of the confrontations show the number of features per subset, with colors corresponding to profile plots. Lines connect the same individual features. *Cg* vs. *Ba*, *C. graminicola* vs. *B. amyloliquefaciens*; *Cg* vs. *An*, *C. graminicola* vs *A. nidulans*; n, Total number of features; P1 - P7, Profiles 1 - 7

The Venn diagram shown in Figure 13A indicates that only 282 newly formed features were common to both, the *C. graminicola* vs. *B. amyloliquefaciens* and the *C. graminicola* vs. *A. nidulans* confrontation. Indicating the specificity of the metabolic response in distinct confrontations, 1,456 and 1,185 novel features were detected either in the fungus vs. bacterium or in the fungus vs. fungus confrontation. Alluvial plots of the 282 common features indicated that some of these occur in different profiles, depending on the confrontations, and underline the plasticity of confrontation-specific metabolic responses (Figure 13B). For example, of the 153 features newly formed in the mycelium of *C. graminicola* confronting *B. amyloliquefaciens* (Figure 13B, *C. graminicola* vs. *B. amyloliquefaciens*, profile P2), 132 were also present in the mycelium of this fungus confronting *A. nidulans* (Figure 13B, *C. graminicola* vs. *A. nidulans*, profile P2). Only a small fraction of the 153 features of *C. graminicola* discovered in the bacterial confrontation was secreted (Figure 13B, *C. graminicola* vs. *A. nidulans*, profile P5) or present in both confrontation partners in the *C. graminicola* vs. *A. nidulans* confrontation (Figure 13B, *C. graminicola* vs. *A. nidulans*, profile P6). This confrontation-specific production of SMs suggests that microbes strategically adjust their metabolite output depending on the microbial competitor. This dynamic modulation of metabolite synthesis in response to the confronting partner underscores the microbe's metabolic plasticity and its evolutionary adaptation to diverse ecological challenges.

Collectively, the data presented here show that activation of SMBGCs and synthesis of chemistries is primarily governed by the species establishing a confrontation. Untargeted high-resolution LC-MS/MS analyses and feature annotation based on the current state of the data bases used suggest that several of the features identified in the confrontations may exhibit significant acute and unknown chronic toxicity to mammals, questioning the health benefit expected from increasing biological control strategies in plant protection.

3.3 A type I *PKS* orchestrates the metabolome of *C. graminicola* under confrontation

3.3.1 Targeted mutagenesis of a *PKS27* gene in *C. graminicola*

A type 1 *PKS* (T1PKS) gene of *C. graminicola,* located in SMBGC 27 was selected for a targeted deletion study due to its central role in synthesis of product of the cluster and due to its notable transcriptional upregulation in response to confrontation with *B. amyloliquefaciens* (Figure 8A, SMBGC 27). The previous transcriptional analysis revealed that SMBGC 27, comprising 18 genes, exhibited dramatic upregulation, with 17 genes showing increased expression under confrontation with bacteria. Among these, the core biosynthetic *PKS* gene, designated as *PKS27* (GLRG_10537), was also significantly activated, suggesting its potential importance in the secondary metabolism response of the fungus, making it a prime candidate for further investigation through gene deletion by homologous recombination (Supporting Figure S5A). Transformants grown on hygromycin were tested by PCR using gene-specific primers PKS10537F and PKS10537R, which amplify a 7.5 Kb fragment of *PKS27* (Supporting Figure S5B, PCR). Primers PKSCgProbeF and PKSCgProbeF were used to generate *PKS27*-specific probe for southern blot analyses. Southern hybridization experiments confirmed that a single copy of the deletion cassette had integrated homologously in two independent Δ*pks27* strains that lacked the 7.5 Kb *PKS27* fragment but contained the 2 Kb *hph* fragment in BamHI-digested genomic DNA. The ectopic (ect.) strain displayed the WT *PKS27* band along with a single, randomly integrated copy of the *hph* cassette (Supporting Figure S5B, Southern). Further characterization involved the WT strain, ect. and two independent deletion mutants denoted as Δ*pks27*. The deletion studies were performed to functionally characterize *PKS27* with respect to its role in response to confronting microbes and to gain insights into reprogramming fungal secondary metabolism in micro-organismic interactions.

3.3.2 Δ*pks27* of *C. graminicola* leads to unaltered phenotype and growth effects

After a cultivation period of 14 days on OMA, the WT, ect. and Δ*pks27* mutant strains of *C. graminicola* exhibited no distinguishable phenotypic differences (Figure 14A). All strains demonstrated similar growth rates (Figure 14B), and detailed microscopic examination and CFW staining of conidia derived from these strains revealed no changes (Figure 14D), a finding further supported by consistent counts of colony formation across all strains (Figure 14C). Quantification

of colonies evolving from these conidia also confirmed unaltered conidial viability in Δ*pks27* strains. However, there was a mild statistical difference in conidial length between the WT, ect. and Δ*pks27* strains, with mean lengths of 36.9 µm for the WT, 36.3 µm for the ect. and 35.2 µm for deletion strains (Figure 14E). In infection assays conducted on non-wounded maize leaf segments of the cv. 'Mikado', no noticeable changes in infection patterns were observed macroscopically at 96 hpi (Figure 14F). Quantitative assessment of appressorial penetration rates and formation of biotrophic hyphae showed mild significant differences, with penetration rates of 81% for WT, 78% for ect. and 90% for Δ*pks27* strains (Figure 14G). This was further corroborated by microscopic analysis, which revealed similar appressorial penetration and formation of biotrophic hyphae among the WT, ect. and deletion strains (Figure 14H).

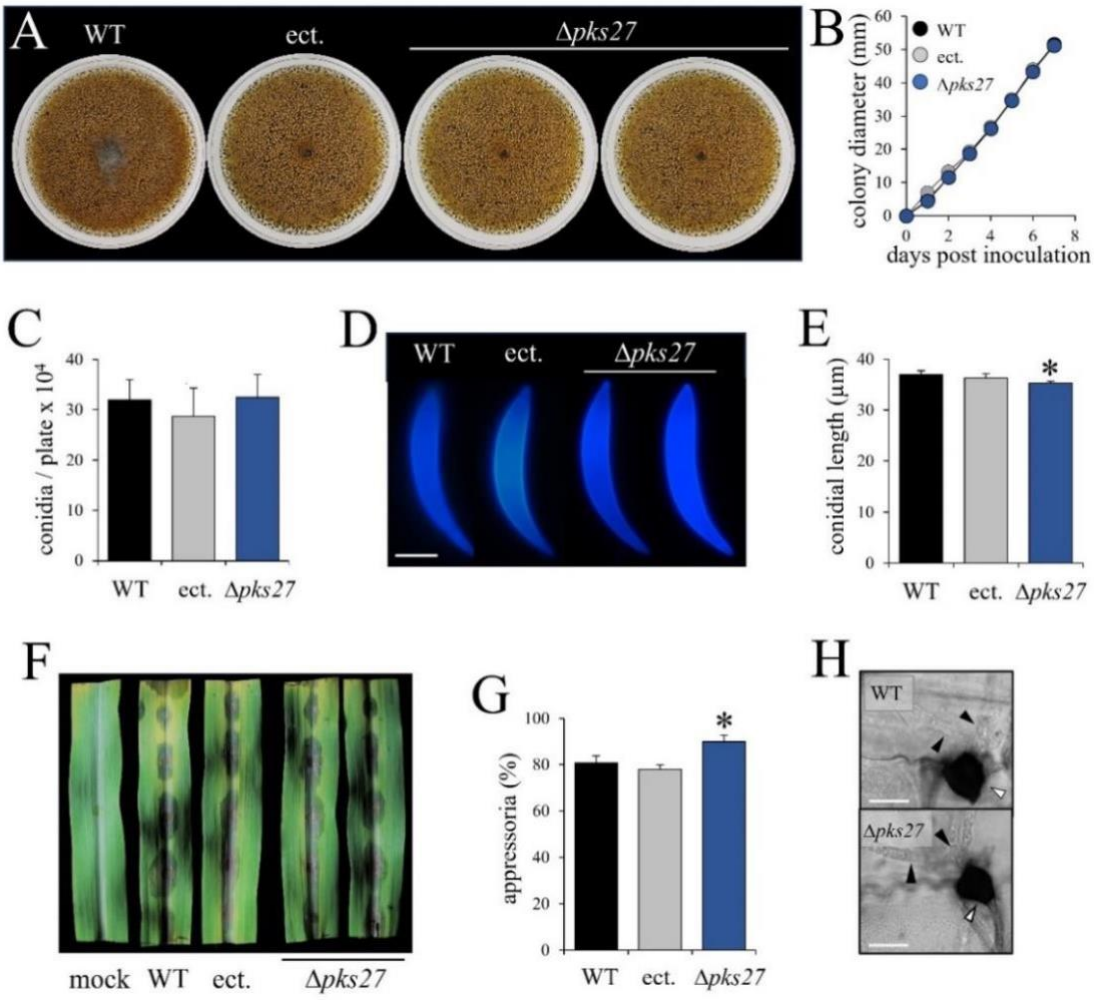

Figure 14. *PKS27* of *C. graminicola* is not required for vegetative growth, conidiation and virulence.

(A) The colony phenotypes of WT, ect. and Δ*pks27* strains grown on PDA, showing no discernible difference. Photographs were taken at 14 dpi. **(B)** Radial growth rates of WT, ect. and Δ*pks27* strains measured daily, indicating no significant differences. **(C)** Comparable number of conidia formed by WT, ect. and Δ*pks27* strains on PDA at 14 dpi. **(D)** The shape of conidia was not altered by deletion of *PKS27*, and length of conidia of Δ*pks27* strains **(E)** was marginally reduced. **(F)** WT, ect. and Δ*pks27* strains elicited comparable disease symptoms in maize (cv. 'Mikado') leaves 96 hpi. Percentage of appressoria differentiated from falcate conidia on maize leaf surfaces were slightly but statistically significantly higher in Δ*pks27* strains **(G)**, but appressoria (white arrowheads) of both WT and Δ*pks27* strains invaded the host epidermal cells and formed normal biotrophic hyphae (black arrows) **(H)**. Scale bar in **(D** and **H)** represents 10 µm. Experiments were performed in triplicates. Error bars represent + SDs. Asterisks in **(E** and **G)** represents mild statistical significance (* $p < 0.05$). WT, Wild type; ect., Ectopic; Δ*pks27*, Deletion mutants.

Altogether, these macroscopic and microscopic evaluations, along with quantitative measurements and infection assays, indicate that deletion of *PKS27* in *C. graminicola* does not lead to any discernible morphological alterations. These data suggest that *PKS27* is not required for fungal development and pathogenicity.

3.3.3 Targeted deletion does not modify confrontation pattern

In order to investigate whether the product of SMBGC 27 affects the competitiveness of *C. graminicola*, confrontation assays of the deletion mutants against *B. amyloliquefaciens* were established. Consistent with the previous findings (Figure 6B, *C. graminicola* vs. *B. amyloliquefaciens*), the confrontation between the fungus and bacteria resulted in inhibition at 12 dpi, indicative of persisting secretion of SMs effectively inhibiting the confrontation partners by the mutant (Figure 15A, petri dishes with confrontations). Microscopic examination by CFW and FM4-64 revealed hyphal protrusions and vacuolations proximal to *B. amyloliquefaciens* in both WT and deletion strains (Figure 15A, Calcofluor White, arrowheads and FM4-64, arrows in insert). In addition, measurements of inhibition zone revealed comparable distances between WT and Δ*pks27* with *B. amyloliquefaciens* (Figure 15B). Quantifying hyphal protrusions at different distances from the border of the *C. graminicola* colony revealed that cell wall-challenging lipopeptides and likely other chemistries migrated ~1 cm into colonies of confrontation partners at 12 dpi (Figures 15C and 15D). These findings collectively show that SMBGC 27 did not affect confrontation with *B. amyloliquefaciens*, indicating that the product of this cluster does not completely contribute to fungal competitiveness with the biocontrol bacterium.

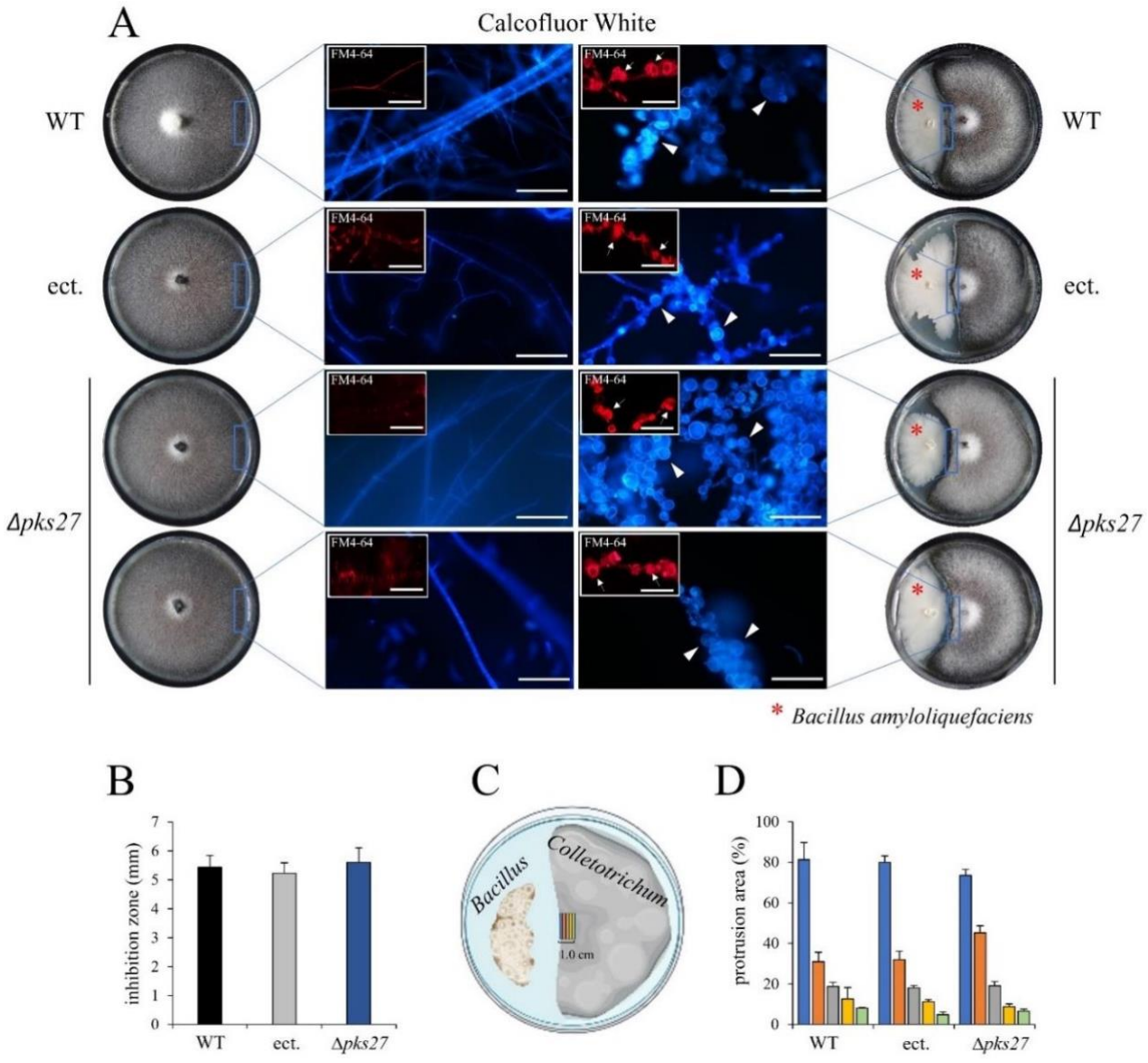

Figure 15. Confrontation assay of *C. graminicola* WT, ect. and Δ*pks27* mutant strains with *B. amyloliquefaciens* on PDA.

(A) Petri dish images of fungal vs. bacterial confrontations at 12 dpi, showing distance inhibition. Microscopic observations reveal hyphal protrusions stained with Calcofluor White (arrowheads) and vacuolization within fungal cells stained with FM4-64 (arrows) in the vicinity of bacteria. Scale bar represents 50 µm. **(B)** Measurement of inhibition zones indicating similar inhibitory effects exerted by *B. amyloliquefaciens* on WT, ect. and Δ*pks27* mutant strains. **(C)** Schematic of the petri dish depicting the sample occupied zones of *C. graminicola* for protrusion quantification. **(D)** Quantification of hyphal protrusion areas during confrontation, demonstrating consistent responses across all strains despite genotypic differences. Experiments were performed in triplicates. Error bars represent + SDs. WT, Wild type; ect., Ectopic; Δ*pks27*, Deletion mutants.

3.3.4 *C. graminicola* WT and Δ*pks27* show different metabolome responses in confrontations with *B. amyloliquefaciens*

To investigate the differences in secondary metabolism between WT and Δ*pks27* deletion strains under non-confronting and confronting conditions, high-resolution compound partitioning LC-MS/MS analyses of metabolites were carried out. PCA revealed clear separation and clustering of WT and ect. strains and of the two Δ*pks27* deletion strains in non-confronting samples. In contrast, in confrontations, WT, ect. and Δ*pks27* strains clustered closely together, suggesting a convergence in metabolite profiles upon bacterial confrontation (Figure 16A). Surprisingly, while PCA revealed massive distinctness of WT and ect. strains from Δ*pks27* strains in solo cultures, all strains were very similar in confrontations with *B. amyloliquefaciens* (Figure 16A).

Moreover, in solo-cultures LC-MS/MS analyses indicated some 3,000 features in WT and the ectopic strain, but more than 5,100 features in the Δ*pks27* mutants (Figure 16B), suggesting that the product(s) of SMBGC 27 may indirectly or directly repress compound formation. In solo-cultures, 2,401 common features were detected in both the WT and the Δ*pks27* strains, and more than 2,700 features were exclusively detected in the Δ*pks27* mutant (Figure 16D). In the *C. graminicola* vs. *B. amyloliquefaciens* confrontation, however, feature numbers derived from LC-MS/MS studies were strongly increased in WT and ectopic strains but remained largely unaltered in the Δ*pks27* strains (Figure 16C). Unexpectedly, the shift in shared features from 2,401 in solo-cultures of WT and Δ*pks27* to 3,919 in confrontations, along with the concomitant reduction of Δ*pks27*-specific feature numbers from 2,726 to 810 (Figure 16E), does not support the hypothesis that SMBGC 27 product(s) contribute to repression of gene expression. In line with feature numbers, annotated SMs such as benzenoids, organoheterocyclic compounds and phenylpropanoids/polyketides, were increased in solo-cultures of the Δ*pks27* strains, when compared with the solo-cultures of WT and the ectopic strain. Again, very similar numbers of these compounds were detected in confrontations of WT, the ectopic and the Δ*pks27* strains with the biocontrol bacterium (Figure 16F). Apparently, despite the deletion in *PKS27* causing a de-repression in feature-synthesis in solo-cultures, this effect was lost during confrontations. Currently, we have no explanation for this effect, but the data strongly suggest a new level of transcriptional control of the genes whose products are responsible for the synthesis of these compounds.

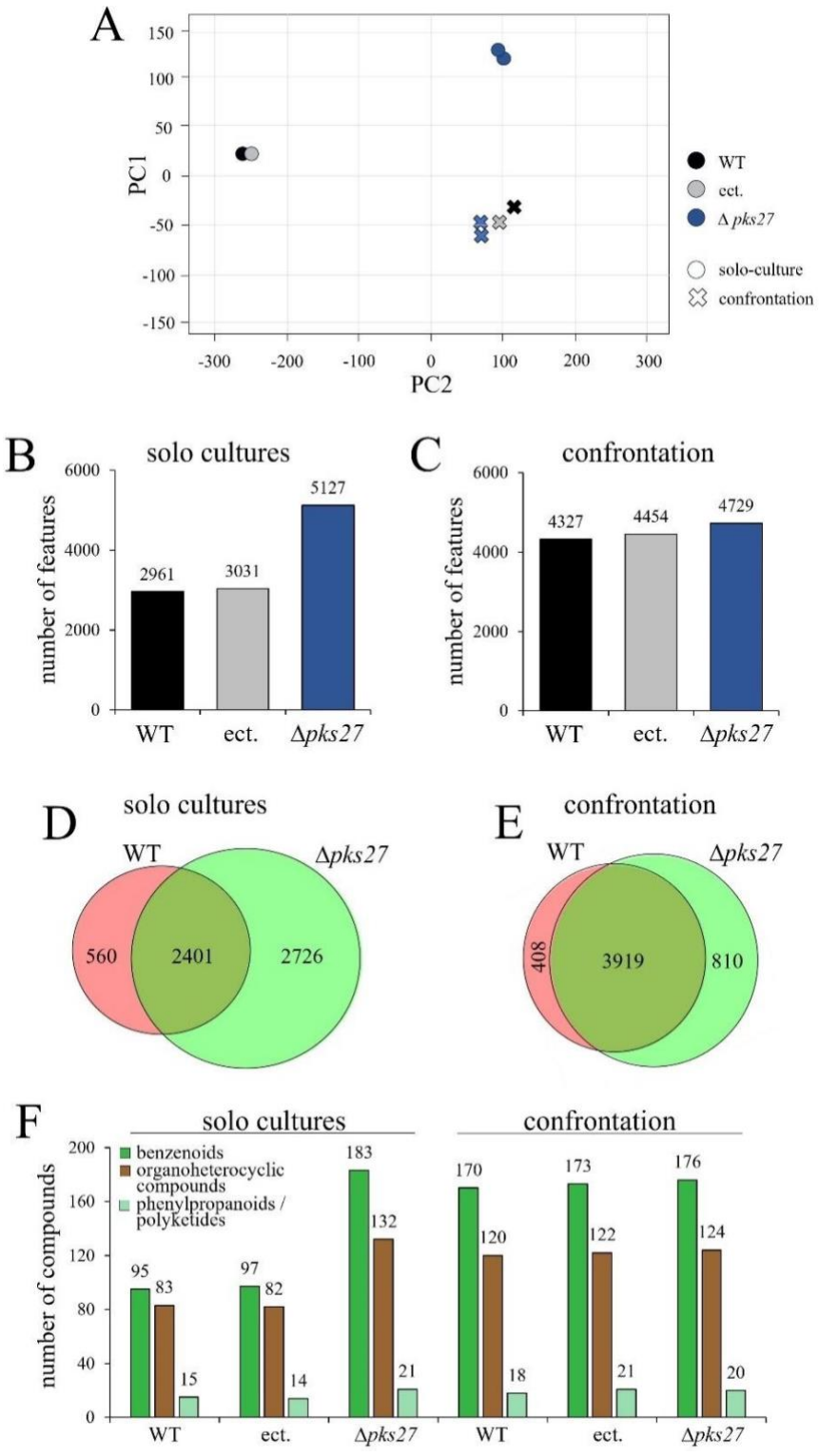

Figure 16. Differential secondary metabolism between WT and Δ*pks27* mutant strains of *C. graminicola* under solo and confrontation conditions.

(A) PCA plot showing the separation of WT, ect. and Δ*pks27* strains under non-confrontation conditions, while close clustering of WT and deletion strains during confrontation with *B. amyloliquefaciens*, indicating convergence of metabolite profiles. **(B)** Quantitative comparison of the number of detected features under solo conditions, with the Δ*pks27* strain displaying significantly more features compared to the WT strain. **(C)** Feature comparison during bacterial confrontation, showing similar numbers of features produced by both WT and Δ*pks27* strains. **(D)** Venn diagram illustrating unique and shared features between WT and Δ*pks27* under solo conditions, highlighting an increase in unique features in the mutant strain. **(E)** Venn diagram showing unique and shared features during confrontation, demonstrating a significant overlap in features between WT and deletion strains. **(F)** Quantitative comparison of the number of benzenoids, organoheterocyclic compounds, phenylpropanoids, and polyketides produced by WT, ect. and Δ*pks27* strains under solo conditions, with Δ*pks27* showing an increase in all compound classes. Under confrontation, all genotypes showed similarities in the number of compounds produced. WT, Wild type; ect., Ectopic; Δ*pks27*, Deletion mutants; PC, Principal Component;

3.4 The ubiquitous fungus *A. nidulans* exhibits differential secondary metabolism responses in confrontations with distinct biocontrol bacteria, yeast, and filamentous fungi

Microbial consortia exhibit complex forms of interactions, which may, for example, be neutralistic, mutualistic, commensalistic, or antagonistic. Antagonistic interactions have been categorized as distance, zone line and contact inhibitions, and overgrowth (Bertrand et al., 2014; Bertrand et al., 2013). Distance inhibition occurs without direct contact, where a microbe releases diffusible compounds that inhibit the growth of the other from a distance. In zone line inhibition, a visible line or barrier forms between two microbial colonies, often marked by pigmentation, indicating mutual inhibition where neither overgrows the other. Under contact inhibition, growth of both microbial partners is halted precisely at the point of contact, indicating a mutually inhibitory effect. In case of overgrowth, one microorganism grows over and completely covers the other, ensuring dominance and outcompeting it for space and resources. Confrontation exhibiting distance or zone line inhibition are likely due to production and secretion of toxic chemistries, with the size of the inhibition zone depending on the toxicity and diffusion constant of the inhibitory compound(s).

I have used the omnipresent ascomycete *A. nidulans* to study microbial interactions with four biocontrol *Bacillus* species, i.e. *B. amyloliquefaciens*, *B. subtilis*, commercial *B. subtilis*, and *B. velezensis*, and with the biocontrol fungi *T. harzianum* and *T. asperellum*, the plant pathogenic fungi *A. tenuis* (syn. *A. alternata*, *A. mali*, *A. rugosa*, *Macrosporium fasciculatum* and *Torula alternata*), *C. heterostrophus*, *C. higginsianum*, and *T. roseum*.

To test the interaction with species naturally occurring on leaf surfaces, we used two fungi isolated from a leaf of *Zea mays* cv. ‘Mikado’. ITS fragments of approx. 600 and 500 bp were obtained by PCR amplification, and the isolates were identified based on nucleotide BLAST (BLASTN) comparisons. The ITS sequences of one isolate were highly similar to ITS sequence of *Cladosporium allicinum* and *Cladosporium floccosum*. As it was not possible to clearly assign the ITS sequence to either of these fungi, this isolate will further on be referred to as *Cladosporium* sp. (Supporting Figure S6A). The second isolate was identified as agaricomycete *Coprinellus domesticus* (Supporting Figure S6B). In addition, *S. cerevisiae* encompassing a killer toxin (Siddiqui & Bussey, 1981) that binds to ß-1,6-glucan was also used in confrontation with *A. nidulans*.

3.4.1 The model ascomycete *A. nidulans* displays distinct interaction patterns with bacteria and fungi exhibiting discrete lifestyles

The confrontations between *A. nidulans* RMS011 and the established biocontrol agents *B. amyloliquefaciens*, *B. subtilis,* and *B. velezensis* showed clear inhibition zones of up to 2 mm between the colonies, indicative of distance inhibition (Figures 17A and 17B, *A. nidulans* vs. *B. amyloliquefaciens*, *B. subtilis,* commercial *B. subtilis* and *B. velezensis,* red arrows). Importantly, not only growth of the *A. nidulans* mycelium, but also of the *Bacillus* strains were strongly restricted (Figure 17A, *B. amyloliquefaciens*, *B. subtilis,* commercial *B. subtilis* and *B. velezensis*). Distance inhibition and growth restriction of both partners suggest secretion of toxic chemistries by the bacterial strains and by *A. nidulans*. The *Bacillus* species used in this study have been known to produce non-ribosomal cyclic lipopeptides known as iturins, which cause cell wall defects (Wang et al., 2020). Accordingly, as observed with *C. graminicola* (Figure 6D, arrowheads), fluorescence microscopy of Calcofluor-stained hyphae of *A. nidulans* confronting *B. amyloliquefaciens*, *B. subtilis,* and *B. velezensis* revealed large swellings indicative of severe cell wall defects (Figure 18A, *A. nidulans* vs. *B. amyloliquefaciens*, *B. subtilis*, commercial *B. subtilis* and *B. velezensis*, arrowheads). Other types of inhibition were also observed during microbial confrontations, including zone line and contact inhibition.

In confrontations showing zone line and contact inhibition, i.e. in confrontations with fungi such as *A. tenuis*, *C. higginsianum*, *T. roseum*, and the *Cladosporium* sp., hyphae of *A. nidulans* also exhibited protrusions (Figure 17A, *A. nidulans* vs. *A. tenuis*, *C. higginsianum*, *T. roseum*, *Cladosporium* sp., orange asterisk). These protrusions were clearly distinct from those caused by *Bacillus* species. In these fungal vs. fungal confrontations, hyphal defects were frequently observed as protrusions and hyperbranching (Figure 18A, *A. nidulans* vs. *A. tenuis*, *C. higginsianum*, *T. roseum*, *Cladosporium* sp., arrowheads and arrows). As these confrontations were categorized as zone line inhibition, one may hypothesize that the close distance between the species may allow diffusion of either chemistries interfering with cell wall function or of cell wall-degrading enzymes that weaken cell walls and cause these lateral protrusions.

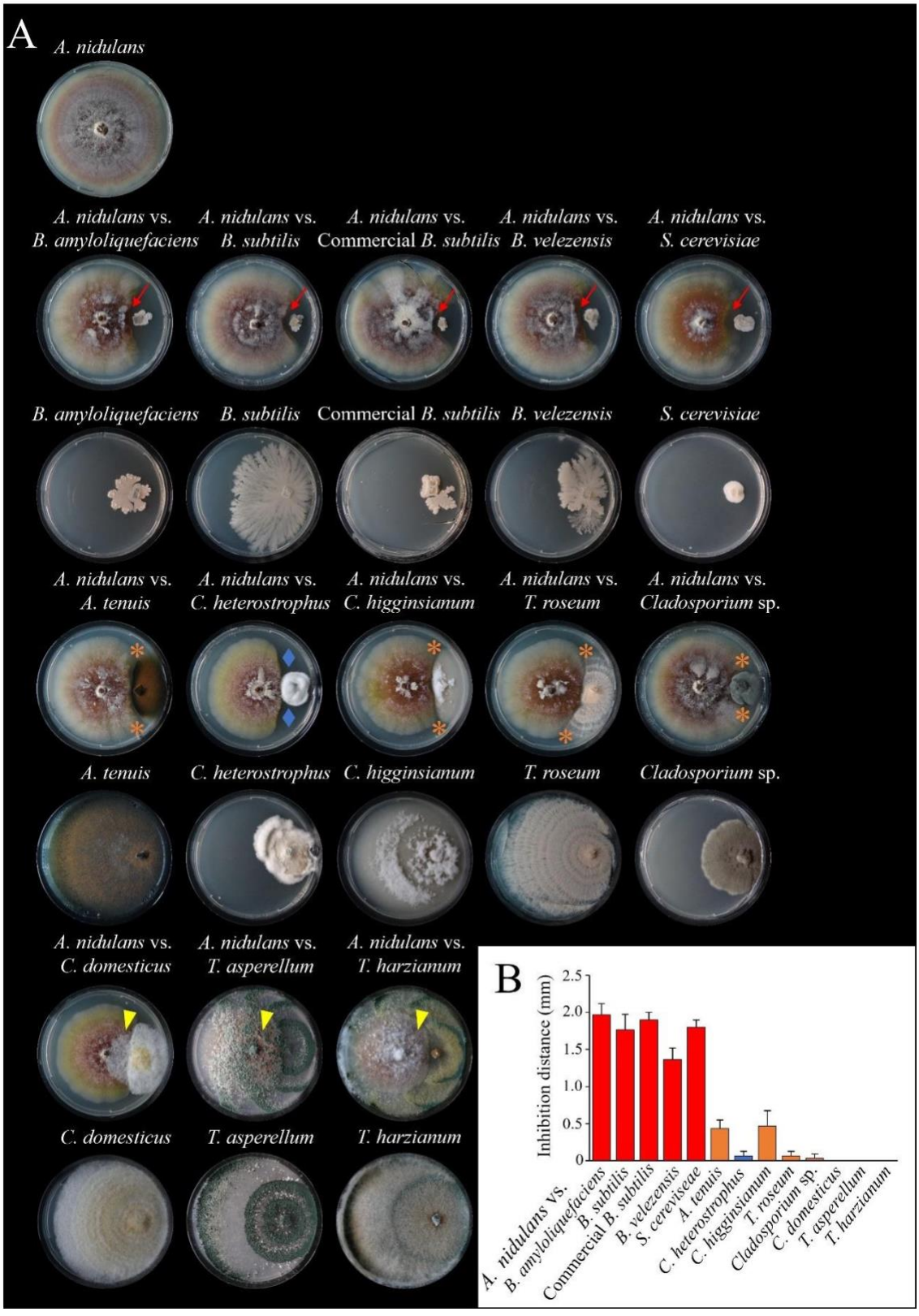

Figure 17. Confrontation assays between *A. nidulans* and various biocontrol bacteria and phytopathogens revealing distinct inhibition patterns in PDA.

(A) Petri dish images showing clear inhibition zones (red arrows) in confrontations with *Bacillus amyloliquefaciens*, *B. subtilis*, Commercial *B. subtilis*, *B. velezensis* and *S. cerevisiae* indicating distance inhibition. Zone-line inhibition (orange asterisk) was observed in confrontations with *A. tenuis*, *C. higginsianum*, *T. roseum*, and *Cladosporium* sp. Contact inhibition (blue diamond) was observed in the confrontation between *A. nidulans* and *C. heterostrophus.* In the confrontations with *C. domesticus*, *T. asperellum*, and *T. harzianum*, overgrowth (yellow arrowheads) was observed, where the antagonistic fungal hyphae have overgrown *A. nidulans.* The solo cultures of *A. nidulans* is placed at the top, while that of the confrontation partners are placed below the respective confrontation setups. Plates were photographed 14 dpi. **(B)** Inhibition distance between microbial colonies measured 14 dpi. Experiment was performed in triplicates. Error bars represent + SDs.

A peculiar case of interaction was observed between *A. nidulans* and the maize pathogen *C. heterostrophus*. In addition to zone line, contact inhibition occurs, where a clear restriction of *A. nidulans* development was observed on both sides of the contact zone (Figure 17A, *A. nidulans* vs. *C. heterostrophus*, blue diamonds). This observation suggests that inhibitory compounds were produced and diffused into the substratum at later stages of the interaction, as indicated by the simultaneous occurrence of both contact and distance inhibition. At confrontation sites, microscopy revealed stunted hyphae and high hyphal densities at colony margins (Figure 18A, *A. nidulans* vs. *C. heterostrophus*, white arrows). Likewise, growth of *C. domesticus* was restricted at immediate contact with the *A. nidulans* colony, but growth inhibition was incomplete, and *C. domesticus* partially overgrew the *A. nidulans* mycelium (Figure 17A, *A. nidulans* vs. *C. domesticus*, yellow arrowheads). Both *Trichoderma* species overgrew the *Aspergillus* colonies almost completely, intensively formed aerial mycelium, and thus represented clear examples of competitive overgrowth (Figure 17A, *A. nidulans* vs. *T. asperellum* and *T. harzianum*, yellow arrowheads). In these overgrowth confrontations, stunted hyphal growth were also observed (Figure 18A, *A. nidulans* vs. *C. domesticus* and *T. asperellum*, white arrows).

Intriguingly, the confrontation between *A. nidulans* and *S. cerevisiae* also resulted in distance inhibition, likely due to the production of a yeast toxin that inhibited the growth of the fungus from a distance. In addition, hyphae spread underneath the yeast colony without visible inhibition, but pigmentation of the *Aspergillus* mycelium was reduced at contact areas (Figure 17A, *A. nidulans* vs. *S. cerevisiae*, red arrow). Surprisingly, this confrontation also led to changes in the shape of the hyphal cells of *A. nidulans* (Figure 18A, *A. nidulans* vs. *S. cerevisiae*, indicated by arrowheads and arrows), suggesting an impact on the fungal cell wall, particularly affecting the β-1,6-glucan

component because of the presence of yeast toxin. Control plates with and undisturbed hyphae of solo cultures of *A. nidulans* are shown above confrontation plates (Figures 17A and 18A).

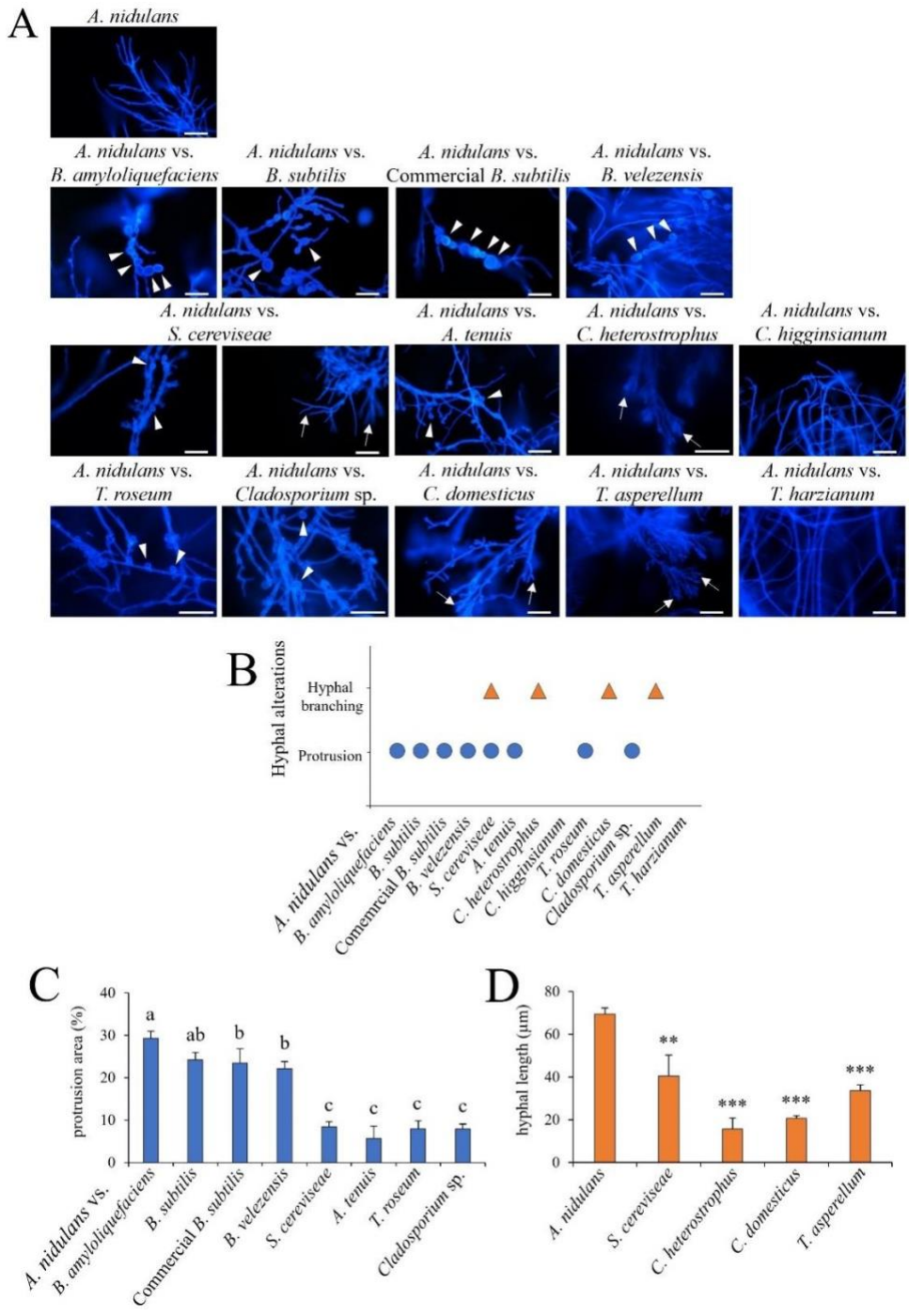

Figure 18. Microscopy and quantitative analysis of hyphal modifications in *A. nidulans* under confrontations documented 12 dpi.

(A) Fluorescence microscopy images of Calcofluor white stained *A. nidulans* hyphae exhibiting large swellings in confrontations with *Bacillus spp*. (white arrowheads), and distinct protrusions (white arrowheads) and branchings (white arrows) under fungal confrontations. Scale bar represents 50 µm. **(B)** Quantification of hyphal alterations of *A. nidulans* under confrontations. The blue circle represents protrusions and orange triangles represents hyphal branchings. **(C)** Comparative analysis of protrusion areas (%), demonstrating a significant increase in protrusions of *A. nidulans* under *Bacillus* confrontations in compared to fungal confrontations. Alphabets indicate statistically significant differences between the mean of confrontations (Tukey HSD, $p < 0.05$). **(D)** Measurement of hyphal branching, demonstrating a significant reduction in length in deformed hyphae during confrontations. Experiments were performed in triplicates. Error bars in **(C)** and **(D)** represent + SDs. Asterisk indicate significant differences between the confrontations (** $p < 0.01$, *** $p < 0.001$).

The hyphal protrusions and branchings in *A. nidulans* observed under various confrontations were quantified via ImageJ (Figure 18B). The protrusions were assessed by calculating the percentage mycelial area, revealing major differences between fungus vs. bacterium and fungus vs. fungus confrontation. Specifically, up to 30% of the area was covered by protrusions as a result of confrontation with biocontrol *Bacillus* species, whereas only 10% of the area was covered by protrusions in fungus vs. fungus confrontations, indicating statistically significant differences (Tukey HSD, $p < 0.05$) (Figure 18C). Additionally, hyphal branching was evaluated by comparing the average hyphal lengths, with deformed hyphae observed in confrontations of *A. nidulans* with *S. cerevisiae*, *C. heterostrophus*, *C. domesticus*, and *T. asperellum* showing an average reduction of vegetative hyphal cell length to 30 - 50 µm ($p < 0.01$ and $p < 0.001$) (Figure 18D). Collectively, these data suggested that distinct interactions result in distinct responses and, in turn, suggest that bilateral recognition of the interaction partners triggers specific responses at the transcriptional level.

3.4.2 Specificity of the transcriptional response of *A. nidulans* to distinct confrontation partners

In order to investigate the specificity of the transcriptional response of *A. nidulans* to distinct related confrontation partners, mRNA was isolated from the mycelial edge challenged by the biocontrol species *B. amyloliquefaciens* and *B. subtilis*, both of which exhibit distance inhibition and both of which cause severe swellings of *Aspergillus* hyphae. In addition, *T. roseum*, a fungus

with dual, i.e. pathogenic and biocontrol abilities (Huang et al., 2000; Zhu et al., 2022), was also chosen to study the transcriptional response of *A. nidulans*. Confirmation of the antagonistic biocontrol bacteria *B. amyloliquefaciens*, *B. subtilis*, and the fungus *T. roseum* was achieved through 16S rRNA and ITS sequencing, as reflected in the phylogenetic trees (Supporting Figures S7A, S7B and S7C). Transcript abundances present in hyphae of the *A. nidulans* strain either confronting biocontrol bacteria or the fungus *T. roseum* were compared to transcript abundances present in hyphae from non-confronting mycelial borders growing in solo cultures. The three independent biological repeats of the *A. nidulans* solo culture, of cultures confronting the two biocontrol bacteria and the culture confronting *T. roseum* yielded 12 libraries, the sequencing of which generated a total of 384.36 million raw reads with 373.6 million clean reads obtained after trimming and quality control. More than 97% of the clean reads were successfully mapped to the reference genome of *A. nidulans* FGSC A4 (See section 2.4.3.1) and corresponded to a total of 10,771 expressed genes. DEGs were identified, based on a cutoff value of $p < 0.05$ and showed increased ($FC > 2$) or reduced ($FC < 0.5$) transcript abundances.

The PCA plot showed that the samples of each treatment clustered closely, indicating uniformity and dependability of the independent replicates of each sample group (Figure 19A). The dissimilarities between the groups were supported by the heatmaps of the correlation matrices, with sample clustering based on the normalized transcript counts (Figure 19B). A total of 591, 1,126 and 1,839 DEGs were obtained for *A. nidulans* confronting *B. amyloliquefaciens*, *B. subtilis*, and *T. roseum*, respectively. Surprisingly, *B. subtilis* caused deregulation of almost twice as many genes as the closely related bacterium *B. amyloliquefaciens*. Of the 591 and 1,126 DEGs in the bacterial confrontations, 439 and 799 genes showed increased, and 152 and 327 genes exhibited reduced transcript abundances in *A. nidulans* confronting *B. amyloliquefaciens* or *B. subtilis*, respectively. In the interaction between *A. nidulans* and *T. roseum*, an even larger number of DEGs was identified, with 978 genes showing increased and 862 decreased transcript abundances (Figure 19C). Intriguingly, the Venn diagram (Figure 19D) revealed 266, 353, and 1037 unique DEG in the interactions of *A. nidulans* with *B. amyloliquefaciens*, *B. subtilis*, and *T. roseum*, and a total of only 91 commonly de-regulated in all three confrontations. Collectively, these data strongly suggest that *A. nidulans* is able to discriminate between and to specifically respond to individual bacterial and fungal challengers.

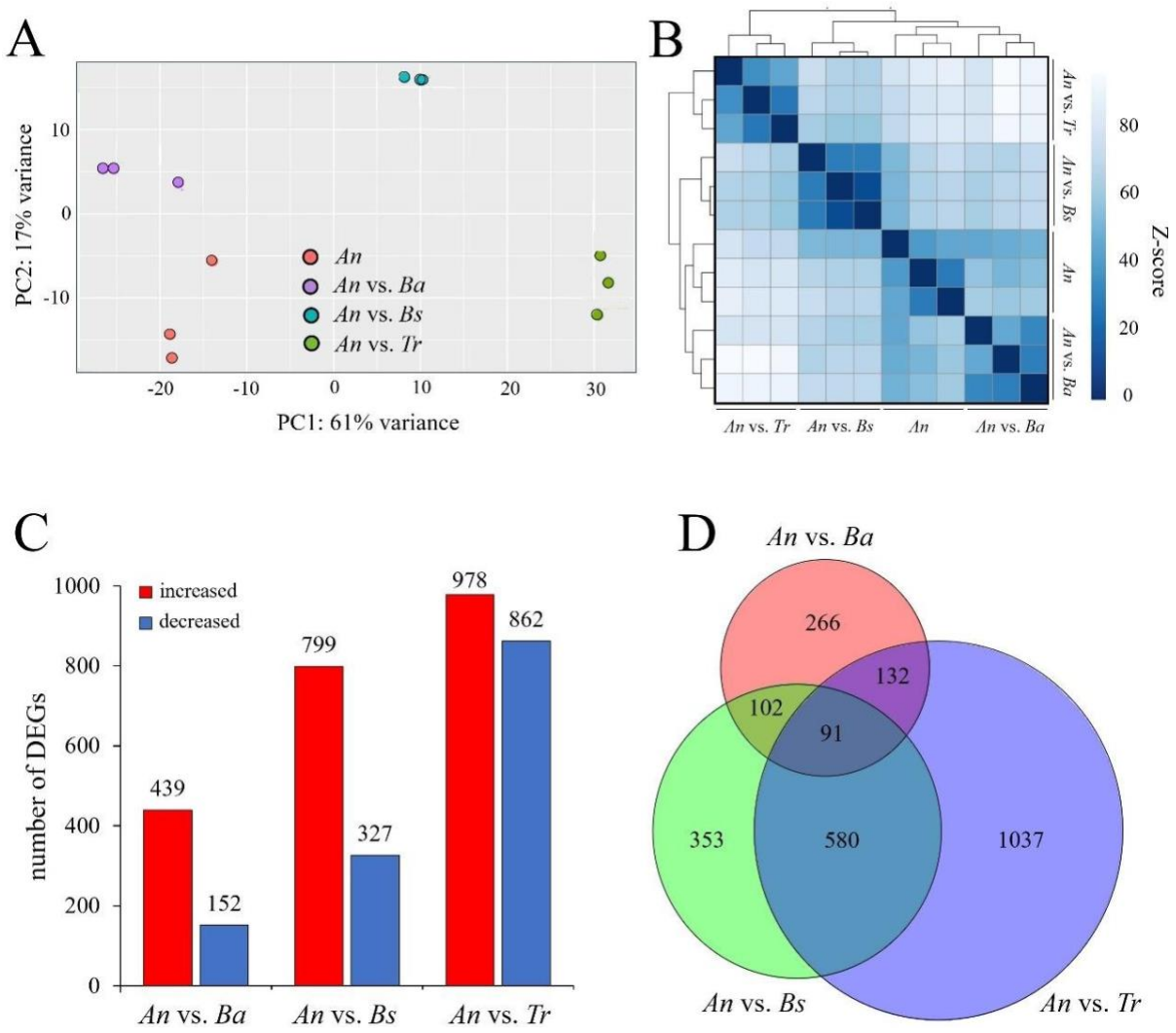

Figure 19. Transcriptome analysis of DEGs of *A. nidulans* under confrontations.

(A) PCA show clear cluster separation of *A. nidulans* (*An*) solo cultures and hyphae confronting *B. amyloliquefaciens* (*An* vs. *Ba*), *B. subtilis* (*An* vs. *Bs*), and *T. roseum* (*An* vs. *Tr*). Sample groups are indicated by different color codes. Each replicate is plotted as an individual data point. **(B)** Heatmap of the sample-to-sample distance matrix obtained from monoculture of *A. nidulans* and confrontations with *B. amyloliquefaciens*, *B. subtilis*, and *T. roseum*. The color codes indicate the distance between the samples, based on the Z-score. Dark blue denotes shorter distance i.e., replicates are grouped closer in distance. **(C)** DEGs identified in different confrontations and confrontation partners. Red and blue bars indicate increased (FC > 2) and decreased (FC < 0.5) transcript abundances with adjusted $p < 0.05$. **(D)** Venn diagram representing the distribution of the DEGs of *A. nidulans* confronting *B. amyloliquefaciens* (*An* vs. *Ba*), *B. subtilis* (*An* vs. *Bs*), and *T. roseum* (*An* vs. *Tr*). The number in the overlap denotes the mutual DEGs between distinct confrontations. Experiments were performed in triplicates. *An*, *A. nidulans*; *An* vs. *Ba*, *A. nidulans* vs. *B. amyloliquefaciens*; *An* vs. *Bs*, *A. nidulans* vs. *B. subtilis*; *An* vs. *Tr*, *A. nidulans* vs. *T. roseum*; DEGs, Differentially Expressed Genes; PC, Principal Component; Z-score, Standard normal distribution.

The functional enrichment of DEGs was carried out by GO analyses, with classification terms involving biological processes (GO:BP) (Figure 20), molecular functions (GO:MF) (Supporting Figure S8), and cellular components (GO:CC) (Supporting Figure S9). In the confrontation with *B. amyloliquefaciens*, 270 genes involved in 19 biological processes were de-regulated in *A. nidulans*. Notably, 209 of these are functionally involved in formation and processing of ribosomal RNA, as well as in ribosome biogenesis, indicative of major translational re-programming in *A. nidulans* in this confrontation (Figure 20, *A. nidulans* vs. *B. amyloliquefaciens*). Re-arrangements in ribosome formation are clearly reflected also in GO:CC (Supporting Figure S9, *A. nidulans* vs. *B. amyloliquefaciens*). In addition to ribosome biogenesis in a broad sense, secondary metabolism is prominently altered at the transcriptional level, as indicated by the GO:BP terms asperfuranone biosynthesis and metabolism (Chiang et al., 2009) and polyketide metabolism (Figure 20, *A. nidulans* vs. *B. amyloliquefaciens*). Supporting the finding of altered secondary metabolism, tertiary alcohol biosynthesis and metabolism are also de-regulated. Tertiary alcohols play a key role in metabolism of sesquiterpenoid toxins, e.g. in the plant pathogen *Botrytis cinerea* (Collado et al., 2007). Intriguingly, in the *A. nidulans* vs. *B. amyloliquefaciens* confrontation, all genes with roles in asperfuranone biosynthetic and metabolic processes, in tertiary alcohol biosynthetic and metabolic processes, and six out of nine genes involved in polyketide metabolism were de-regulated, as indicated by gene ratios of 1.00 for the former and 0.67 for polyketide metabolism genes. These data indicates that reprogramming of the ribosomal protein biosynthesis machinery and formation of SMs are major traits in *A. nidulans* hyphae confronting *B. amyloliquefaciens*.

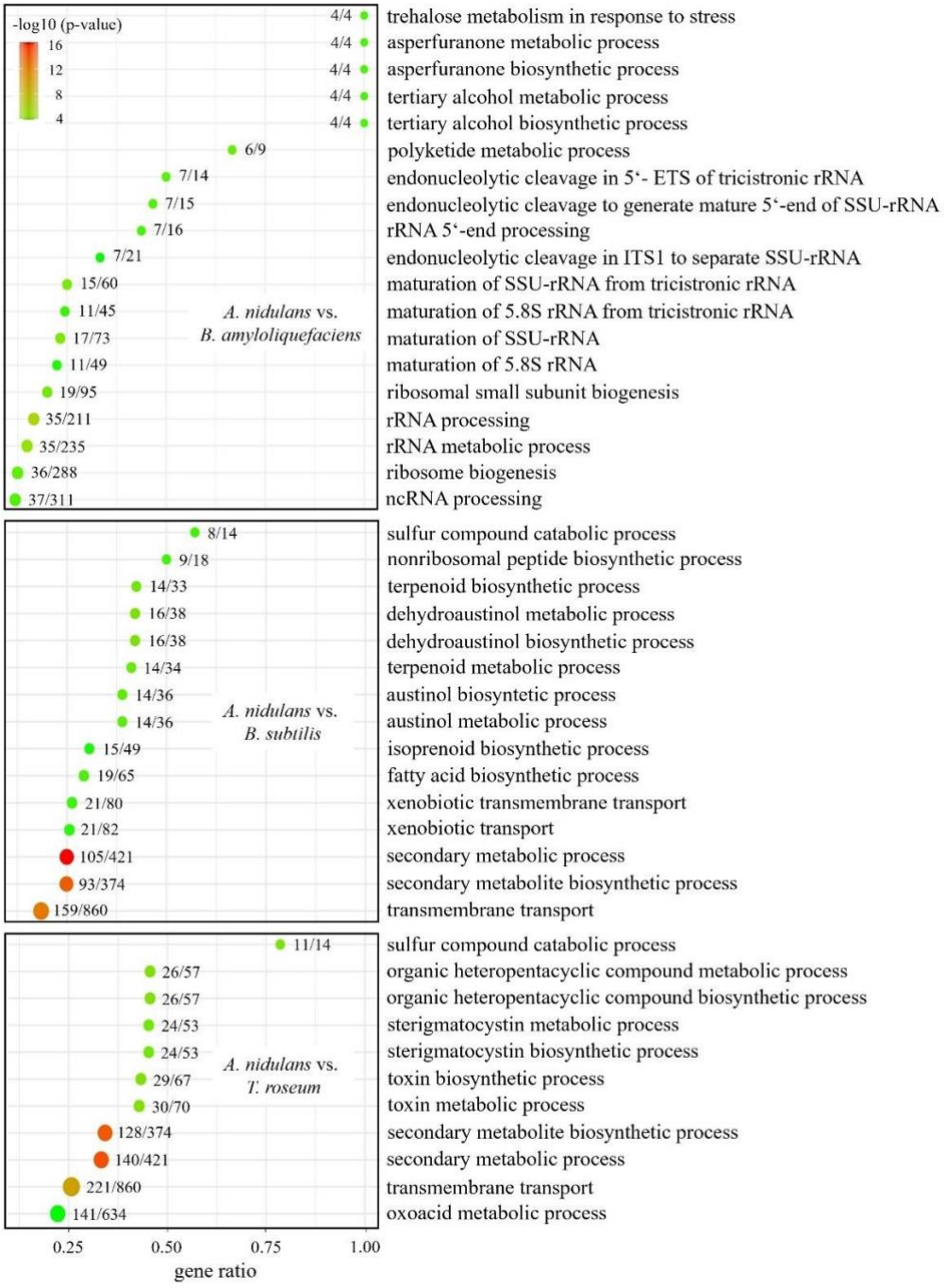

Figure 20. Functional enrichment analysis by GO of DEGs in *A. nidulans* against *B. amyloliquefaciens*, *B. subtilis*, and *T. roseum*.

Bubble plot depicting the GO terms for biological process (BP) ranked by color codes based on the fold enrichment (adjusted $p < 0.05$). The X-axis indicates the gene ratio i.e. the ratio of DEGs to the total number of genes associated with a specific term. The size of each bubble indicates the number of DEGs corresponding to each GO term, while the color gradient reflects the significant level (-log 10 of the adjusted p-value). GO, Gene Ontology.

Also, in the confrontation of *A. nidulans* with the close relative of *B. amyloliquefaciens*, namely the biocontrol bacterium *B. subtilis*, GO:BP terms indicated massive transcriptional de-regulation of secondary metabolism (Figure 20, *A. nidulans* vs. *B. subtilis*). However, striking differences between the interactions of *A. nidulans* with the two bacteria occurred with respect to the classes of chemistries and compounds putatively formed. In this latter confrontation, non-ribosomal peptide biosynthesis, isoprenoid and, consequently, terpenoid biosynthesis and metabolism were affected. In detail, austinol/dehydroaustinol biosynthetic and metabolic processes as well as membrane transport are highlighted in the GO:BP categories (Figure 20, *A. nidulans* vs. *B. subtilis*).

Intriguingly, also in *A. nidulans* hyphae confronting the biocontrol fungus *T. roseum* (Figure 20, *A. nidulans* vs. *T. roseum*), secondary metabolism is dramatically de-regulated, as indicated by GO:BP categories such as heteropentacyclic compound, toxin, secondary metabolite and, importantly, STC biosynthesis and metabolism. STC is a polyketide closely related to AFs and are, like AFs, known as a carcinogen (Brown et al., 1996; EFSA, 2013). The GO:BP category transmembrane transport highlights secretion of putatively formed toxic SMs by *A. nidulans* in this fungal confrontation.

Collectively, transcriptome and functional enrichment studies revealed dramatic differences in the metabolic response of *A. nidulans* to different biocontrol partners. Each microbial interaction triggers distinct changes in SM biosynthesis and associated process, reflecting the unique adaptive and defensive strategies of *A. nidulans* to different microbial challenges. These findings underscore the dynamic and context-dependent nature of microbial confrontations in shaping secondary metabolism.

3.4.3 Distinct confrontation partners cause distinct patterns of SM cluster deregulation in *A. nidulans*

GO analyses highlighted fundamental differences in the transcriptional response of *A. nidulans* to the bacterial as well as to the fungal antagonists in confrontation scenarios. While in confrontation with *B. amyloliquefaciens* prominent effects were seen in ribosome biogenesis in a broad sense, alteration in secondary metabolism was present but less prominent (Figure 20, *A. nidulans* vs.

B. amyloliquefaciens). Confrontation with *B. subtilis*, in comparison (Figure 20, *A. nidulans* vs. *B. subtilis*), primarily evokes transcriptional reprogramming of secondary metabolism, and a comparably prominent SM response was observed in *A. nidulans* confronting the fungal biocontrol agent *T. roseum* (Figure 20, *A. nidulans* vs. *T. roseum*). Therefore, I asked how many and which of the 502 genes of *A. nidulans* harbored in 68 SMBGCs coordinating synthesis of PKs, non-ribosomal peptides (NRPs), hybrid PK-NRPs, indoles, and terpenes (Inglis et al., 2013; Soukup et al., 2012) were de-regulated in the confrontations investigated. Interestingly, even if an SM cluster is considered deregulated if it contains only one deregulated gene, only 21 SMBGCs were affected in *A. nidulans* hyphae confronting *B. amyloliquefaciens*. The only uniformly responding SMBGC was the asperfuranone cluster, in which all seven genes showed increased transcript abundances (Figure 21A, SMBGC 57; compare with Figure 20, *A. nidulans* vs. *B. amyloliquefaciens*).

By sharp contrast, in confrontations with *B. subtilis*, *A. nidulans* exhibited 40 deregulated SM clusters, with only 10 showing alterations in transcript abundance of only a single gene (Figure 21B). Intriguingly, the *NRPS* fellutamide B SMBGC 15 containing the genes *inpB* and *inpA*, the *PKS* asperlin SMBGC 32 containing the gene *alnA*, the *NRPS* microperfuranone SMBGC 34 containing the gene *micA*, and the *PKS* asperfuranone SMBGC 57 harboring the two genes *afoG* and *afoE*, were transcriptionally increased in the presence of *B. subtilis*. In specific, 14 of the 24 genes of the STC SMBGC 21, harboring the *PKS stcA* also exhibited transcriptionally upregulated genes (Figure 21B, SMBGC 21). Interestingly, 7 of the 8 genes of SMBGC 47 required for synthesis of 2,4-dihydroxy-6-[(3E,5E,7E)-2-oxonona-3,5,7-trienyl]benzaldehyde was transcriptionally decreased (Figure 21B, SMBGC 47). Several clusters exhibited transcriptional deregulation of only some genes, and several cases existed in which neither a *PKS* nor a *NRPS*, but several other genes were affected. However, the massive deregulation of a total of 124 SM genes and, moreover, the possibility that enzymes encoded by genes of one SM cluster may contribute to modifying SMs synthesized by another, suggests complex remodeling of SM biosynthesis in this confrontation.

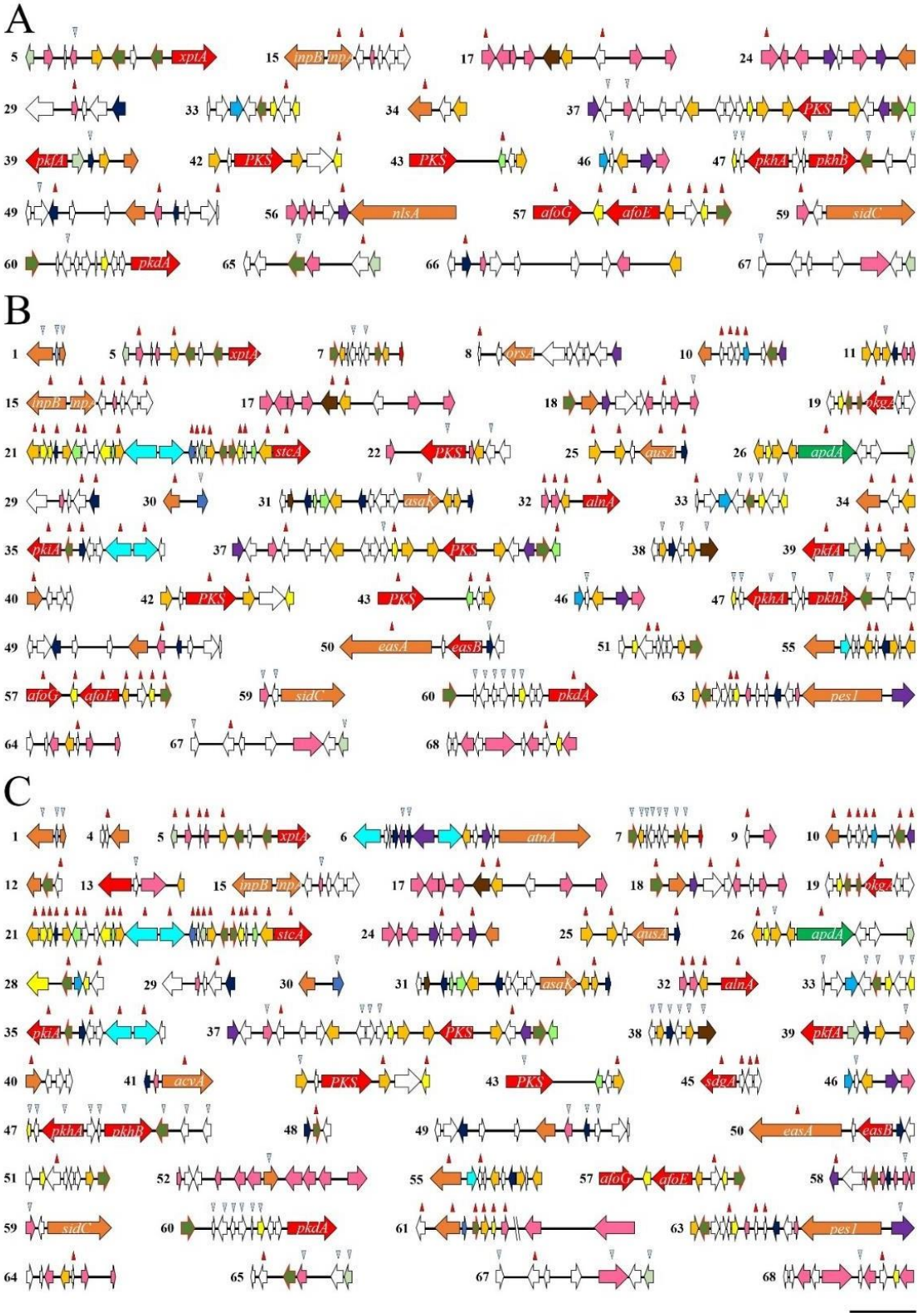

Figure 21. Physical map of deregulated SMBGCs in *A. nidulans* under confrontations.

(A) In *A. nidulans*, 21 out of 68 SM SMBGCs harbor deregulated genes in confrontation with *B. amyloliquefaciens*. **(B)** In *A. nidulans* confronting *B. subtilis*, 40 out of the total of 68 SM clusters are transcriptionally de-regulated. **(C)** In confrontation with *T. roseum*, *A. nidulans* has 50 of the 68 SM clusters de-regulated. **(A, B** and **C)** The horizontal arrows represent SM genes and their transcriptional direction. Putative function as indicated by the color code is as in Figure 8. Red and blue arrowheads denote increased or decreased transcript abundances in the confrontation. Scale bar represents 10 kb. *PKS*, Polyketide Synthase; *NRPS*, Non-ribosomal Peptide Synthetase.

In addition, in hyphae confronting the biocontrol fungus *T. roseum*, RNA-Seq analyses showed massive SM responses in *A. nidulans*, as suggested by bubble plot depiction (Figure 20, *A. nidulans* vs. *T. roseum*). In this confrontation, of 68 SMBGCs, 50 clusters were transcriptionally deregulated. Intriguingly, 15 out of the 50 SMBGCs harbored more than 50% of transcriptionally deregulated genes (Figure 21C). In detail, in SMBGCs 10, 32, and 45, the vast majority of genes showed increased transcript abundances. In the *PKS* SMBGC 21, responsible for synthesis of the carcinogen STC, 22 out of 24 genes were upregulated. In contrast, SMBGCs 1, 7, 38, 47, and 60 contained strongly downregulated DEGs.

The specific response of *A. nidulans* to *B. amyloliquefaciens*, *B. subtilis* and *T. roseum* can be attributed to the distinct metabolic interactions triggered by each microbial partner. This specificity arises from the unique chemical environments and molecular interactions induced by different microbes, leading to differential regulation of SMBGCs. *B. subtilis*, for example, has been known to produce lipopeptides like iturin, fengycin, and plipastatin (Gong et al., 2015; Wang et al., 2020; D. Zhang et al., 2022), which affect specific regulatory pathways in *A. nidulans*. In contrast, in the fungus vs. fungus confrontation, such as with *T. roseum*, may involve mycotoxins or fungal-specific effectors that activate distinct stress and response pathways. These interactions result in varied patterns of SM production, reflecting adaptive and defensive strategies against diverse microbial competitors (Brakhage, 2013; Netzker et al., 2015). Collectively, the data shown here indicates that microbial confrontations, regardless of taxonomic relatedness, elicit distinct transcriptional responses of SMBGCs in hyphae of *A. nidulans*.

3.4.4 RT-qPCR analyses confirmed distinct transcriptional responses of *stcA* to distinct confrontation partners

In order to address the effect of distinct bacterial and fungal confrontation partners on the activation of the STC cluster (SMBGC 21), transcript abundances of the core *PKS* gene *stcA* (ANIA_07825) of *A. nidulans* was quantified by RT-qPCR analyses (Figure 22). RNA isolated from *A. nidulans* growing in solo cultures and from hyphae confronted by bacterial and fungal partners were subjected to RT-qPCR analyses.

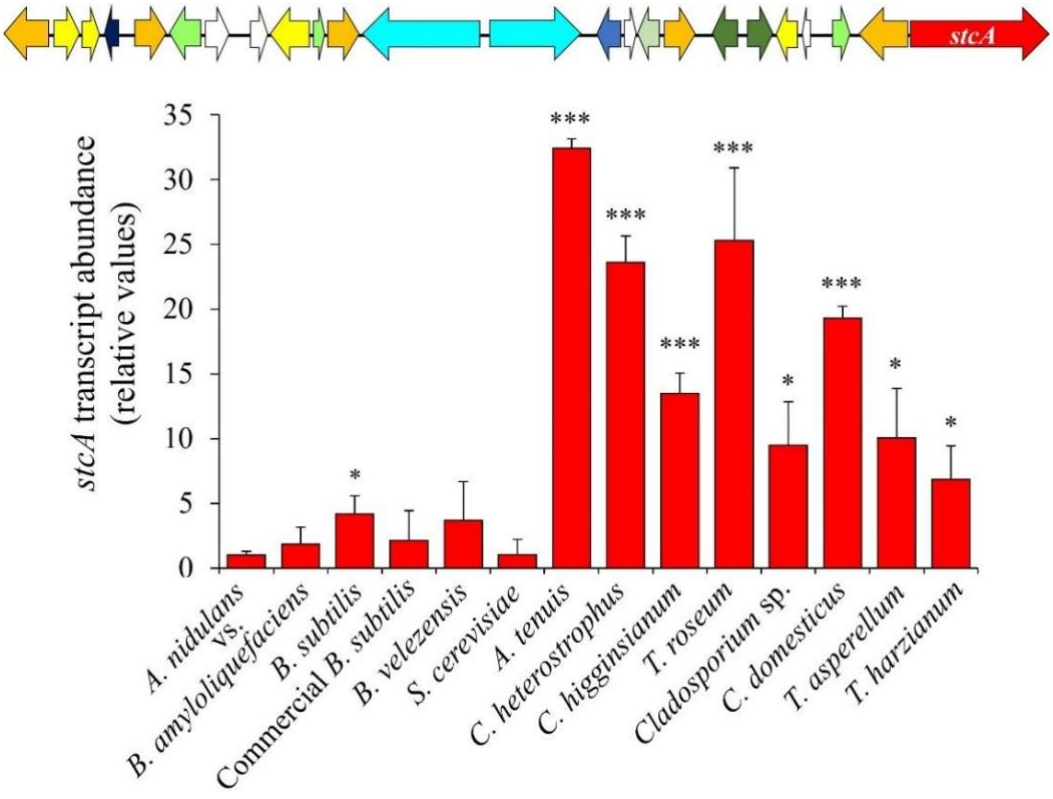

Figure 22. RT-qPCR analysis of *stcA* gene in *A. nidulans* under confrontation with various biocontrol bacterial and phytopathogens.

The core biosynthetic *stcA* gene of the carcinogenic STC SMBGC 21 in *A. nidulans* was subjected to RT-qPCR analysis. The relative transcript levels indicate gene expression of *stcA* under confrontations. The physical map of SMBGC21 is given above the respective bar plot and the bar color indicates the color of the core gene *stcA*. The constitutively expressed actin biosynthesis gene of *A. nidulans* served as standard. Data shown is means of three independent biological replicates and three technical replicates. Error bars are + SDs. The statistical significance is indicated by asterisk (* $p < 0.05$, ** $p < 0.01$, *** $p < 0.001$). *stcA*, sterigmatocystinA.

Of all *Bacillus* confrontation partners, only *B. subtilis* elicited a minor but statistically significant ($p < 0.05$) increase in *stcA* transcript abundance. *Aspergillus* hyphae confronting yeast did not show any increase in *stcA* transcripts. In striking contrast, all filamentous fungi elicited significantly increased *stcA* transcript abundances, with those elicited by *A. tenuis*, *C. heterostrophus*, *C. higginsianum*, *T. roseum*, and *C. domesticus* identified as highly significant ($p < 0.001$). Importantly, in confrontation with *T. roseum* and *A. tenuis*, *stcA* transcript abundances increased 25- and 33-fold over the abundance in *A. nidulans* growing in solo culture. Also, in the presence of the biocontrol fungus *T. harzianum*, *stcA* transcript abundances are 10-fold increased as compared with transcript concentrations in the solo culture. These data strongly argue that the establishment of biocontrol strains in the environment may cause severe shifts in biosynthesis of SMs in confronted microorganisms such as the ubiquitous fungus *A. nidulans*. This scenario argues that implementation of MBCAs may potentially affect consumers' safety.

3.4.5 Distinct biocontrol microorganisms cause severe and differential secondary metabolome re-programming in *A. nidulans*

Massive and distinct patterns of deregulation of SMBGC genes of *A. nidulans* confronting bacterial and fungal antagonists ask for complementary analyses of the secondary metabolome. Non-targeted LC-MS/MS analyses indeed revealed an enormous number of newly synthesized chemistries in vegetative hyphae of *A. nidulans* confronting different biocontrol and plant pathogenic species. To obtain insights into the specific features produced under confrontations, venn diagrams were used to visualize features obtained from solo cultures and confrontations (Supporting Figure S10A). In the confrontation assays between *A. nidulans* and the fungi *C. domesticus*, *T. asperellum*, and *T. harzianum*, instances of fungal overgrowth made it challenging to isolate only the hyphae of *Aspergillus* for metabolome analysis. To address this, the samples were collected from the overgrown regions where the hyphae of *A. nidulans* was mixed with the other fungal hyphae, as well as solo cultures of the respective overgrown fungi. By performing metabolome analyses on both the mixed samples and the corresponding solo cultures, it was possible to differentiate and exclude the metabolites produced by the overgrowing fungi, thus enabling the isolation and identification of metabolites specific to *A. nidulans* (Supporting Figure S10A, bottom panel, *An* vs. *Cd*, *An* vs. *Ta*, *An* vs. *Th*).

In confrontations with *B. amyloliquefaciens*, *B. subtilis*, commercial *B. subtilis*, and *B. velezensis*, 568, 579, 545 and 593 novel features were identified and in confrontations with the fungal pathogens *A. tenuis, C. heterostrophus, C. higginsianum*, 557, 712 and 567 unique features were found. Remarkably, in confrontation with the biocontrol agent *T. roseum*, 808 newly formed features that had not been identified in solo culture were recorded. In addition, under confrontations with the biocontrol fungi *T. asperellum* and *T. harzianum*, 246 and 128 specific features were uncovered. Furthermore, in confrontation with the isolates *Cladosporium* sp., and *C. domesticus*, 535 and 792 confrontation specific features were detected. The confrontation between the fungus and yeast *S. cerevisiae* revealed a total of 495 exclusive features (Supporting Figure S10A). These specific features indicate that distinct micro-organismic confrontations result in differential SM production in *A. nidulans*. Intriguingly, the majority of these chemistries were not annotated (Supporting Figure S10B), with over 50% of the compounds in each confrontations remaining unidentified. This suggests that most of the secreted SMs are potentially novel.

The annotated features specifically produced by *A. nidulans* under confrontations were then used to create sunburst plots to visualize the different classes of compounds present under specific confrontations. These plot illustrate four levels of compound specificity, namely super classes, classes, sub classes, and most specific classes (Supporting Figure S11). Importantly, the compound classes vary specifically, depending on the confrontations. Organic acids and derivatives were the most prevalent in all confrontations, followed by lipids and lipid-like molecules and organoheterocyclic compounds. Notably, confrontations with *Trichoderma* spp. led to a specific increase in the production of organic nitrogen compounds (Supporting Figure S11, *A. nidulans* vs. *T. asperellum* and *A. nidulans* vs. *T. harzianum*). This is corroborated by the bar plots, which effectively illustrate the variation in compound super classes under different confrontations (Figure 23A, bar plots). The intensities of individual compounds corresponding to those in the bar plot were further visualized by violin plots (Figure 23A, violin plots). The distribution and density of compound intensities vary significantly between different confrontations. Each super class exhibits distinct intensity patterns, highlighting the variation in SM production by *A. nidulans* under confrontations.

The research question on how specific these confrontations are is well answered by the upset plot (Figure 23B). The upset plots reveal a substantial amount of unique compounds specific to

individual confrontations, particularly in fungus vs. fungus interactions, indicating a high degree of specificity in SM production (Figure 23B, upper and middle panel). Although the fungus vs. bacterial interactions results in a specific metabolic response, ranging between 13 to 18 discrete compounds, there is also a general SM production involving about 50 compounds. This suggests that *A. nidulans* secretes a set of general SMs against the genus *Bacillus* in addition to the unique compounds. Notably, 225 unique compounds were identified in the confrontation between *A. nidulans* and the biocontrol fungus, *T.* roseum. Intriguingly, 214 compounds were found in the overgrowth confrontations between *A. nidulans* and *T. harzianum.* Confrontations with *C. heterostrophus, C. domesticus* and *T. asperellum* yielded 125, 126 and 121 unique compounds, respectively (Figure 23B, upper panel).

These findings indicate that *A. nidulans* produces a greater number of unique compounds in confrontations with fungal partners than with bacterial partners. The general response against the *Bacillus* biocontrol agents underscores the adaptive metabolic strategies employed by the ubiquitous fungus to encounter diverse microbial threats. The number of specific and general compounds belonging to various super classes include organic acids and derivatives, lipids, organoheterocyclic compounds, and benzenoids. In addition, numerous compounds identified in these confrontations also remain unannotated (Figure 23B, lower panel). These integrated analyses provide compelling evidence that *A. nidulans* exhibits highly specific SM production profiles, depending on the confrontation partner.

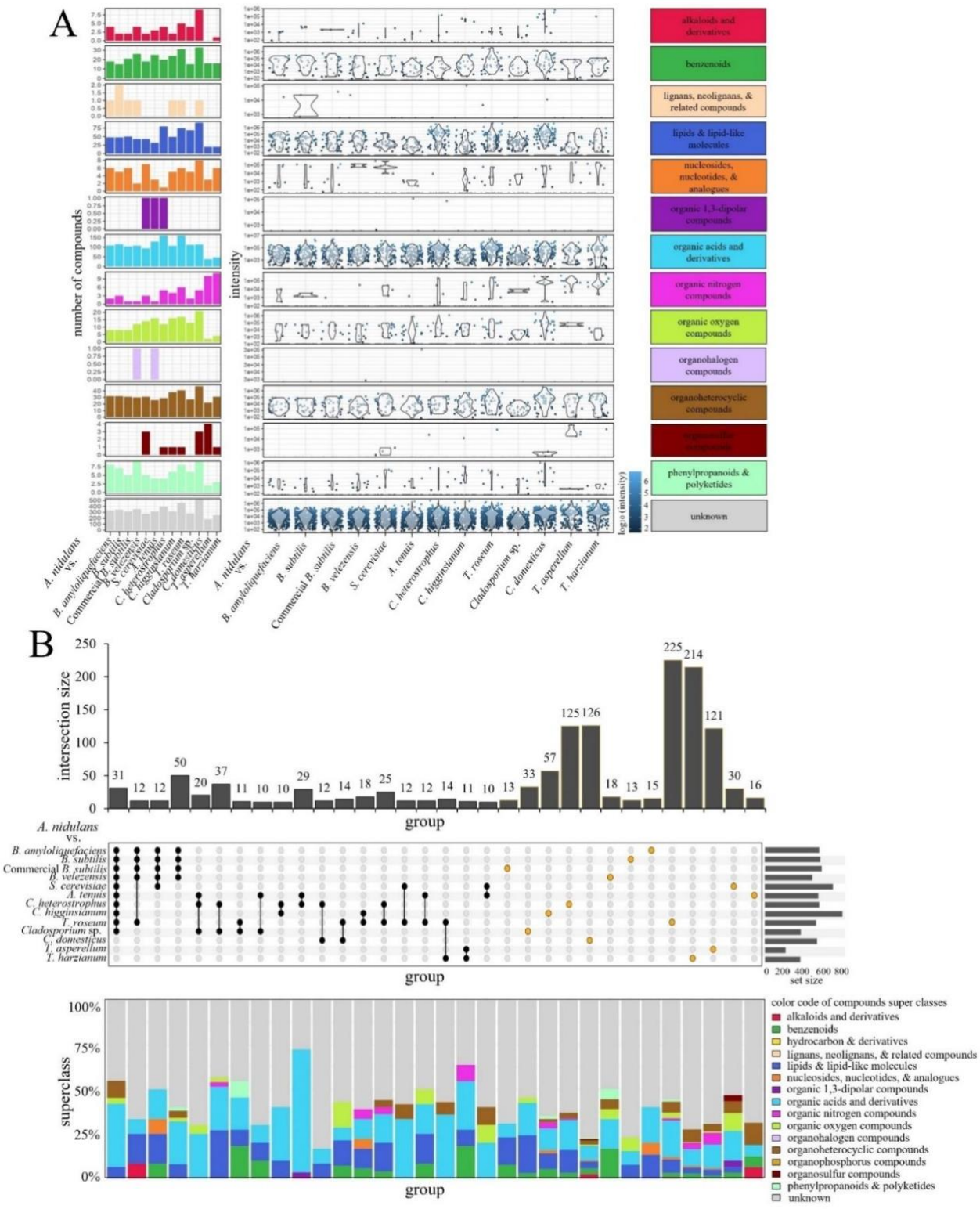

Figure 23. Visualization of unique and shared SMs produced in *A. nidulans* under confrontations.

(A) Bar plots and violin plots illustrating the variation in compound super classes during various confrontations. The bar plots display the number of compounds with specific superclass annotations for each confrontation setup. The violin plots show the distribution and intensity of individual compounds, with each dot representing a compound. **(B)** Upset plot demonstrating the specificity of SM production across different confrontations. **Upper panel**: Bar plot indicating the size of the intersection set, corresponding to the number of compounds. **Middle panel**: Matrix plot features the sets contributing to a specific intersection by black or orange dots. Black dots represent sets contributing to a general SM response, and orange dots indicate unique SMs specific to confrontations. The right bar plot shows the number of compounds within each set/confrontation assay. **Lower panel**: Bar plot illustrates the factions of superclass annotation within the displayed intersection sets. Only sets with a minimum size of 10 compounds are shown.

Interestingly, toxic compound classes such as piperidines, phenol ethers, diazines, furans, pyrrolidines, and coumarins were identified under confrontations. The computational toxicity (LD_{50}) of these compound classes was estimated by ProTox 3.0 (Figure 24). Notably, some compound classes such as azoles, furans, pyridines, and quinolines, recognized as key components in synthetic fungicides were present in confrontations, suggesting that *A. nidulans* may produce SMs with structural similarities to these fungicides, potentially explaining their inhibitory activity and acute toxicity against microbial competitors.

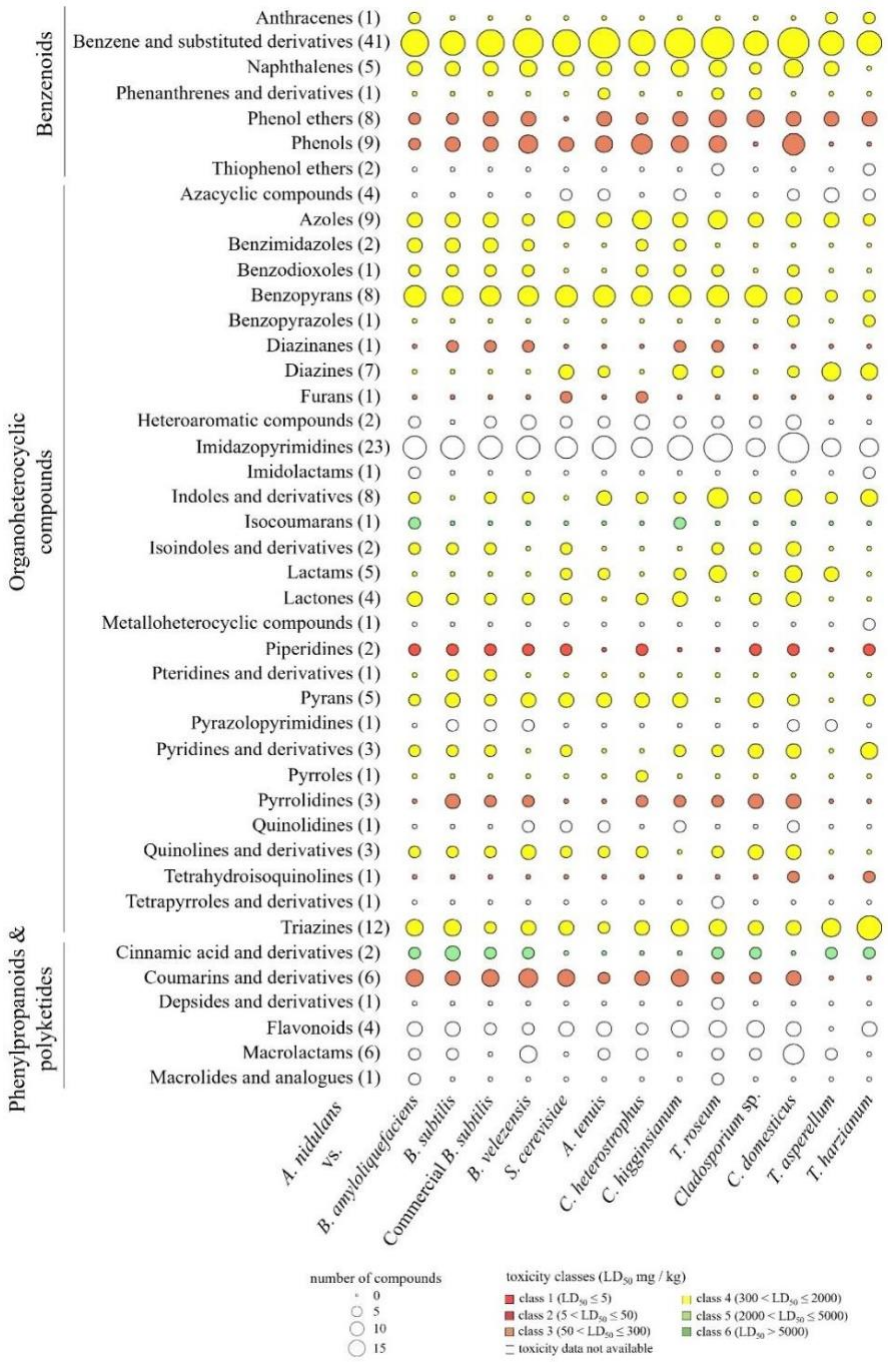

Figure 24. Balloon plot depicting the toxicity of various compound classes in *A. nidulans* under confrontations.

The plot depicts the compound classes that are present under three major super classes viz. benzenoids, organoheterocyclic compounds, and phenylpropanoids and polyketides. The numbers in parentheses following each compound class indicate the total number of individual compounds present. The acute toxicity of these compounds is color-coded according to their toxicity classes, as indicated by their LD_{50} values. The balloon size indicates the number of compounds present under each confrontation. LD_{50}, Lethal dose 50%.

3.4.6 Cytotoxicity assays reveal potential human health risks associated with SMs produced under confrontations

Given that *A. nidulans* produces large numbers of SMs under confrontations with biocontrol agents, it may be considered naïve to assume that biological disease control might not have the potential to harm consumers and/or the environment. Hence, we sought to investigate the potential toxicity of these compounds to humans by cytotoxicity assays. This approach aims to assess whether the compounds produced in response to biocontrol agents exhibit any cytotoxic effects on human cells. SMs obtained from *A. nidulans* under solo culture and in confrontations with the biocontrol bacteria, *B. amyloliquefaciens* and *B. subtilis*, and biocontrol fungus, *T. roseum* were subjected to toxicity assay. The cytotoxic effects of the compounds were assessed using resazurin-based cell viability assays on healthy human HEK-293 and colorectal carcinoma HCT-116 cells. Cells were treated with a concentration range of 0.98 - 250 µg/mL for 48 hours, and cell viability was quantified fluorometrically. IC_{50} values were calculated to determine the inhibitory effects of the extracts on cell proliferation.

The results of the cell toxicity assays demonstrated that metabolites produced by *A. nidulans* under confrontations with biocontrol agents exhibit significantly higher toxicity to both healthy and cancerous human cells compared to controls, i.e. compounds extracted from PDA and *A. nidulans* grown in solo culture (Figure 25). Notably, metabolites from confrontation with *B. subtilis* and *T. roseum* led to cell viabilities of less than 5% in HEK-293 cells, indicating a drastic reduction in cell survival. In contrast, SMs from *A. nidulans* confronted *B. amyloliquefaciens* showed a toxicity profile in HEK-293 cells similar to that of solely grown *A. nidulans*, which reduced cell viability up to 25% (Figure 25A). This similar toxicity profile could be attributed to the possibility that *B. amyloliquefaciens* does not induce the production of additional toxic SMs in *A. nidulans* beyond its baseline level. The diverse array of toxic compounds produced by SMBGCs in *A. nidulans* may already be sufficient to exert substantial cytotoxic effects. The confrontation with *B. amyloliquefaciens* may not stimulate a significant alteration or enhancement in the expression of these clusters, resulting in toxicity levels comparable to those of *A. nidulans* in solo culture. The IC_{50} values further illustrate the toxicity levels of the compounds produced, with values of 135 µg/mL and 52 µg/mL for *A. nidulans* against *B. subtilis* and *T. roseum*, respectively. In contrast, the IC_{50} for the interaction between *A. nidulans* and *B. amyloliquefaciens* exceeds 250 µg/mL.

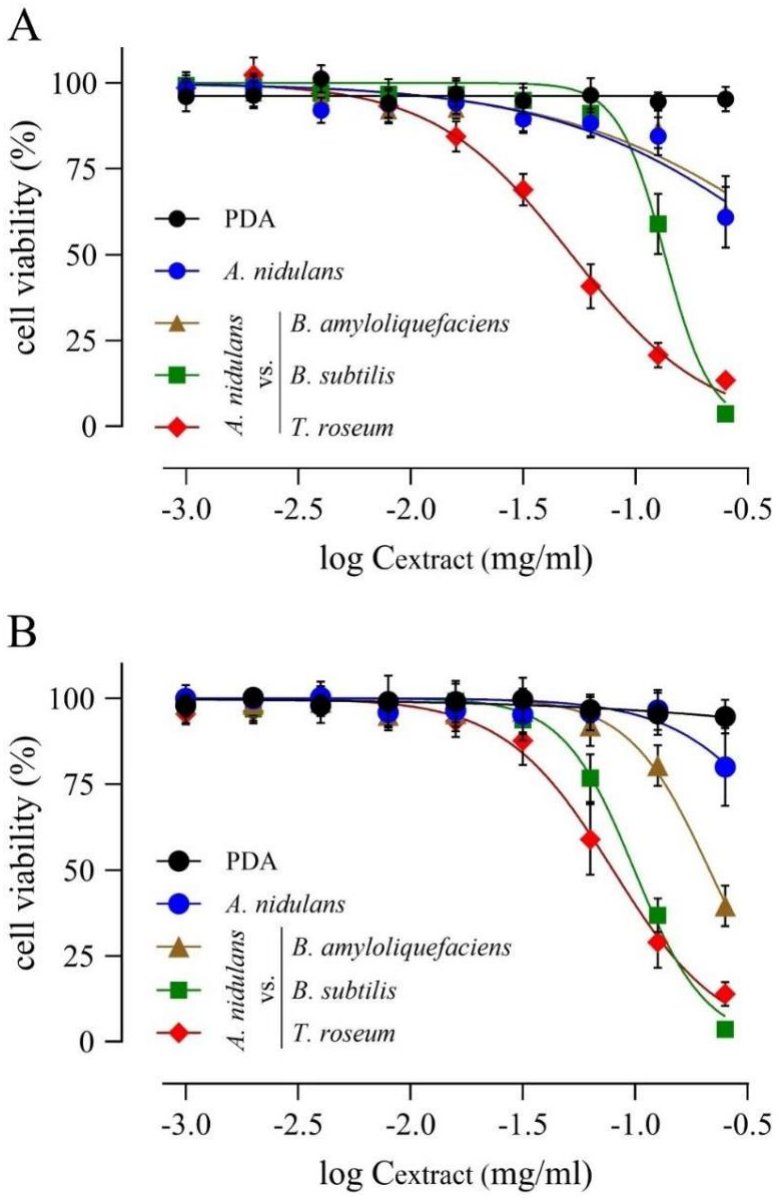

Figure 25. Cytotoxic effects of SMs produced by *A. nidulans* under confrontations with biocontrol bacteria and fungus on HEK-293 and HCT-116 cell lines.

(A) Scatter plot showing the viability of healthy human embryonic kidney cells (HEK-293) exposed to chemistries produced by *A. nidulans* when grown alone (blue circles), and in confrontation with *B.amyloliquefaciens* (brown triangles), *B. subtilis* (green squares), and *T. roseum* (red diamonds). **(B)** Cell viability on human colorectal carcinoma cells (HCT-116) under the same depiction as in scatter plot **(A)**, showing drastic reductions in cell viability. **(A** and **B)** Cell viability (%) is plotted against the logarithm of the SM concentration ($C_{extract}$, mg/mL), showing dose-dependent cytotoxic effects. Data were collected from at least four biological replicates, each with technical triplicates. Error bars represent ± SDs. PDA, Potato Dextrose Agar; $C_{extract}$, Concentration of extract (metabolites).

In case of HCT-116 cells, the chemistries obtained from *A. nidulans* in confrontation with *B. subtilis* and *T. roseum* lead to cell viabilities of less than 5% similar to the ones observed in HEK-293 cells. In addition, metabolites from *A. nidulans* vs. *B. amyloliquefaciens* also exhibited moderate toxicity, with cell viability around 50%. The IC_{50} values further highlight the potency of these toxic compounds, with 214 µg/mL for *A. nidulans* vs. *B. amyloliquefaciens,* 99 µg/mL for *A. nidulans* vs. *B. subtilis,* and 80 µg/mL for *A. nidulans* vs. *T. roseum* (Figure 25B). Also in this case, compounds from non-confronted *A. nidulans* showed mild toxicity, which could be plausible because of the huge repertoire of toxic and carcinogenic metabolites the fungus harbors.

In both the healthy and cancerous cell lines, there is a differential response of SMs produced by *A. nidulans* when confronted by *B. amyloliquefaciens*. This variation in response may be attributed to the unique metabolic or signaling pathways activated in *A. nidulans* during its interaction with *B. amyloliquefaciens*. In healthy cells, these pathways lead to a basal level of toxicity, while in cancer cells, they result in a more moderate toxicity profile. Collectively, these data underscore the potential health risks posed by toxic SMs produced by *A. nidulans* when confronted by MBCAs.

4 Discussion

4.1 Historical and modern context of fungal SMs and their toxicity

The detrimental toxicity of fungal SMs has harmed humanity for centuries. In humans, disease symptoms caused by the ergot alkaloid-producing pathogen of grasses, *Claviceps purpurea*, have been described since 600 BC (Haarmann et al., 2009; Lee, 2009). Moreover, in England approx. 100,000 turkey poults died from groundnut meal contaminated with AFs produced by *A. flavus*. Food contaminated with AF poses a global health threat due its high acute toxicity and, even more, due to its enormous carcinogenic activity (Pickova et al., 2021; Wu, 2014). As a matter of fact, more than 300 mycotoxins, including AF and STC, are of serious concern to human health and livestock (Brown et al., 2021; Sun et al., 2023; Xu et al., 2022; Zingales et al., 2022). Collectively, fungi may produce more than 15,000 distinct SMs (Zhgun, 2023) and only in some cases the signal triggering activation of SMBGCs and their products are known (Brakhage & Schroeckh, 2011; Keller, 2019; König et al., 2013; Schroeckh et al., 2009), with few exceptions. For example, arginine-derived PKs of *Streptomyces* species have been shown to trigger fungal SM production in a cross-kingdom fashion and may thus shape structure and function of complex microbial communities in soil environments (Krespach et al., 2023). Indeed, several putatively toxic SMs and their targets in microbial confrontation partners have been described, and the fact that successful defense against competing microbes is primarily chemistry-based is widely accepted (Brakhage, 2013; Kunzler, 2018; Macheleidt et al., 2016). In spite of this acceptance, questions regarding the complexity, plasticity, and specificity of microbial chemical defense remain largely unanswered. The complexity and diversity of fungal SMs present significant challenges, particularly in understanding their toxic effects within natural environments. As focus shifts from individual SMs to their roles in microbial interactions, it becomes evident that evaluating SM production in real-world microbial confrontations is far more complex than under controlled conditions, due to the context-dependent activation of SMBGCs.

4.2 Challenges in evaluating microbial antagonism in confrontations

While testing consumer and environmental toxicity of defined chemistries such as synthetic chemistries is easily accomplishable, evaluation of antagonistic microorganisms is difficult, as it is unclear which SMBGCs are activated under confrontations with numerous distinct partners. The

difficulty is particularly evident in multi-membered confrontations e.g., on densely inhabited plant surfaces (Lindow & Brandl, 2003; Vorholt, 2012). The exchange and further modification of SMs has been demonstrated with melanin biosynthesis mutants of two different *Colletotrichum* species exhibiting distinct melanin biosynthesis defects (Deising et al., 2017). In a multi-membered consortium, however, one may expect an enormous increase in SM complexity, as compared with co-cultures consisting of two members only. Indeed, in a microcosm experiment employing three rhizosphere bacteria, i.e., *B. cereus*, *F. johnsoniae,* and *P. koreensis,* Handelsman and co-workers showed that the dynamics of secondary metabolism depends on community species composition and inter-species interactions, indicating that microbiome interactions may shape the SM composition in nature (Chevrette et al., 2022). These experiments also suggest that introducing biocontrol agents into a pre-shaped complex microbiome would significantly impact SM formation.

The hypothetical complexity of the reservoirs of distinct fungal and bacterial compounds has been highlighted by comparative genomics and cheminformatics analyses, employing 1,037 genomes from species across the fungal kingdom and a set of 5,453 bacterial genomes (Robey et al., 2021). Remarkably, more than 36,000 fungal SMBGCs were organized into gene cluster families, with more than 2,000 SMBGCs providing predicted metabolite scaffolds. In total, more than 15,000 fungal and over 9,000 bacterial compounds revealed a landscape of largely species-specific compound reservoirs (Robey et al., 2021), highlighting the enormous complexity of novel compounds to be expected in microbial confrontations driven by SMBGCs.

4.3 Complex regulatory networks governing SM production in microbial confrontations

The activation of SMBGCs and the resulting production of toxic SMs are often cryptic in solo cultures growing under laboratory conditions due to stringent transcriptional regulation, which ensures these compounds are synthesized only when necessary (Collemare & Seidl, 2019). To study the functionality of SM clusters, an “orthodox” approach involves inactivating the core biosynthetic gene of the SMBGC through targeted mutagenesis (Brakhage & Schroeckh, 2011). Deleting *PKS* and *NRPS* genes in fungi significantly impacts their secondary metabolism, altering the production of key bioactive compounds. For instance, in *A. fumigatus*, deletion of the *NRPS* gene *encD*, encoding a putative 2-oxoglutarate-Fe(II) type oxidoreductase, increased the

production of the anthraquinone compound endocrocin (Lim et al., 2012). Similarly, deleting the *PKS* gene *easB* in *A. nidulans* led to the identification of the emericellamide biosynthetic pathway (Chiang et al., 2008). Additionally, overexpressing transcriptional regulators of SMBGCs has also facilitated the identification of numerous SMs and their responsible genes. An overexpression of the global transcriptional regulator *laeA* in *A. nidulans* enabled the identification of a bisindole alkaloid, terrequinone A (Bouhired et al., 2007). The production of SMs in fungi is governed by a sophisticated regulatory network that includes pathway-specific, global and epigenetic regulations (Brakhage, 2013; Macheleidt et al., 2016; Yin & Keller, 2011). Pathway-specific regulation is often controlled by PSTFs within SMBGCs that bind to promoters of other genes within the same cluster. Among known ones, *A. nidulans* has 12 SMBGCs containing 16 PSTFs, while *A. fumigatus* has 10 BGCs with 12 PSTFs. Notable PSTFs include *AflR*, which controls AF and STC synthesis in *A. flavus* and *A. nidulans*, respectively, and *GliZ*, which regulates gliotoxin synthesis in *A. fumigatus* (Caceres et al., 2020; Yin et al., 2012). Global regulation involves broad-spectrum regulators that respond to environmental signals and affect multiple SMBGCs and SMs production. For instance, the nitrogen regulator AreA controls gibberellin biosynthesis in *F. fujikuroi* (Schönig et al., 2008), the carbon regulator CreA regulates patulin biosynthesis in *Penicillium expansum* (Tannous et al., 2018), and the pH regulator PacC influences STC biosynthesis in *A. nidulans* (Ke et al., 2013). Furthermore, epigenetic regulation also modifies the chromosomal architecture to influence the transcriptional availability of SMBGCs. This regulation is mediated by proteins such as histone deacetylases (HDACs) and methyltransferases which can activate or repress the expression of cryptic fungal SMBGCs (Cichewicz, 2010; Collemare & Seidl, 2019; Karahoda et al., 2022). Fungal SM regulation is not strictly hierarchical; instead, it involves interactions between multiple regulatory levels. The global regulator *laeA* exemplifies this integration by regulating approximately 50% of SMBGCs and forming a heterotrimeric velvet complex with VelB and VeA to coordinate secondary metabolism and development in response to light signals (Bayram et al., 2008). Additionally, the S-adenosyl methionine binding site in *laeA* indicates its role in influencing chromatin accessibility, further linking epigenetic and global regulatory mechanisms to control the expression of SMBGCs.

4.4 Toxic and carcinogenic SMs in microbial confrontations

Given the large number of toxic SMs putatively synthesized in a microbial community it is surprising that distance inhibition (Bertrand et al., 2014) did not occur on maize leaf imprint on agar, as indicated by the lack of inhibition zones between the numerous colonies that had formed. In this context, it is likewise surprising that a screen of more than 700 environmental isolates from apple trees and fruits of strains identified only four bacterial and three fungal isolates able to reduce lesion development caused by the fruit rot pathogens *Pezicula malicorticis* and *Nectria galligena* (Schiewe & Mendgen, 1992). It is not surprising, however, that in our study, the commercially available antagonist *B. amyloliquefaciens* and one of the best studied SM producers, i.e. *A. nidulans*, displayed distance inhibition in confrontations with *C. graminicola*. Importantly, combined transcriptome and metabolome data revealed an enormous plasticity and specificity in synthesis of complex arrays of novel SMs, i.e. 33 and 36 benzenoids, 29 and 40 organoheterocyclic features, and six and 18 phenylpropanoids / polyketides synthesized in the confrontations of *C. graminicola* with *B. amyloliquefaciens* and *A. nidulans*, respectively. Intriguingly, several compound classes identified in one or both confrontations, e.g. azoles or piperidines, exhibit structural similarities with fungicidal lead structures (FRAC codes 3 and 5). Moreover, the rotenoid villosinol identified in the *C. graminicola* vs. *A. nidulans* confrontation acts as a mitochondrial complex I inhibitor (IRAC code 21) categorized into toxicity class I. Furthermore, cinnamaldehydes are multi-mode-of-action biologicals targeting cell wall biogenesis by inhibiting synthesis of the structural core cell wall polymers chitin and β-1,3-glucan, and are also thought to interfere with membrane function (FRAC code BM03). Thus, interestingly, biochemistries synthesized in microbial confrontations resemble commercially available synthetic chemistries and possibly address the same targets.

The biggest concern, however, relates to the carcinogenic activity of microbial SMs. The polyketide-mycotoxins AF and STC are oxidized by cytochrome P450 enzymes, yielding C-8,9-epoxides, which form covalent bonds between C8 of the toxin and N7 of guanine bases in DNA. Replication of DNA containing these adducts has been shown to cause G → T-mutations. High frequencies of this mutation at codon 249 in the tumor suppressor gene p53 were indeed reported in hepatocellular carcinoma from populations exposed to high levels of AF-contaminated food in South Africa and China (Wang et al., 1999). Hepatocellular carcinomas were also observed in rats exposed to tetralin or anthracene (National Toxicology Program, 2011; Takeda et al., 2023).

Features belonging to these chemistry classes were formed in the *C. graminicola* vs. *A. nidulans* confrontation studied here. Moreover, the insecticidal mitochondrial complex I inhibitor rotenone induced neoplastic, paraneoplastic, and preneoplastic lesions in rats and is considered an environmental carcinogen (Gosálvez, 1983). In the light of the enormous feature numbers observed in the fungus vs. bacterium and in the fungus vs. fungus interaction studied in our research, synergistic activities of toxic compounds in carcinogenesis may be highly relevant. Highlighting this aspect, studies employing mouse models have shown that toxins produced by *Bacterioides fragilis* and *pks+ E. coli* promote colon cancer in a synergistic fashion and that mice colonized by *Bacterioides fragilis* and *pks+ E. coli* had strongly reduced survival rates, as compared with those colonized by either bacterium alone (Dejea et al., 2018).

Our study has clearly shown that a large array of novel and highly diverse chemistries is synthesized in the confrontations between the maize pathogen *C. graminicola* with the biocontrol bacterium *B. amyloliquefaciens* and the ubiquitous model fungus *A.* nidulans. Furthermore, our research study has uncovered a large array of acute toxic and putatively carcinogenic features formed in a confrontation-specific fashion. The confrontation-specificity of the arsenal of chemical weapons employed may not be surprising, given the longtime of chemical evolution during progression in fungus vs. bacterium and fungus vs. fungus interactions, respectively. Interestingly, several forms of mycoparasitism have been uncovered in the excellently preserved 400-million-year-old mycoflora samples of the Lower Devonian Rhynie chert ecosystem (Hass et al., 1994). Given this enormous time span in microbial development, it is not surprising that 1,738 and 1,466 newly synthesized features were specific to the *C. graminicola* vs. *B. amyloliquefaciens* and *C. graminicola* vs. *A. nidulans* confrontation studied here, with a total of 68 and 94 benzenoids, organoheterocyclic features and phenylpropanoids and polyketides synthesized in the two interactions, respectively. These findings underscore the complexity of microbial interactions and the potential for the synthesis of toxic and carcinogenic SMs in such confrontations. The discovery of a diverse array of toxic compounds, many of which exhibit structural similarities to known carcinogens, highlights the importance of further investigating the safety and health risks associated with microbial SM production in agricultural and environmental contexts.

4.5 Specificity and complexity of microbial interaction dynamics in inducing cytotoxic SMs

Our knowledge on the synthesis of SM toxins during microbial confrontations and the associated transcriptome and metabolome changes remains sparse. Moreover, the toxicity of SMs produced under microbial confrontations must be addressed in approval processes for antagonistic MBCAs due to their potential adverse effects on human health. It is evident that the toxicity of products of an enormous number of SMBGCs remain to be explored, particularly in the context of microbial confrontations brought about in agricultural environments. As previously mentioned, the deregulation of SMBGCs is highly specific to each type of microbial confrontation. For instance, in our study, the number of SMBGCs deregulated in *C. graminicola* when confronted by *B. amyloliquefaciens* or *A. nidulans* was significantly different, with 29 and 36 clusters affected respectively, resulting in distinct sets of 1456 and 1185 metabolite features, with only 282 features overlapping between both confrontations. This specificity shows that different microbial confrontations can lead to vastly discrete transcriptome and metabolome responses.

In general, the intricate dynamics of microbial interactions often drive the induction of cytotoxic SMs, as organisms engage in biochemical warfare to outcompete one another. These complex interactions can lead to the formation of distinct inhibition patterns and the production of toxic compounds. In our study, the dual-culture assays involving the ubiquitous fungus *A. nidulans* demonstrated diverse inhibition patterns when challenged by various MBCAs and plant pathogens. Previous research from Bertrand and co-workers have highlighted multiple patterns of inhibition, particularly in co-cultures where induction of toxic metabolites plays a significant role (Bertrand et al., 2014). Chemical inhibition is impressively shown in confrontations between the fungus *A. niger* and the bacterium *Collimonas fungivorans*¸ resulting in distance inhibition (Mela et al., 2011). Distance inhibition has also been observed in my study between *A. nidulans* and various biocontrol *Bacillus* species used in plant protection. These inhibitions are indicative of secreted chemistries produced during confrontations as described in various studies (Fernando Devasahayam et al., 2024; Murakami et al., 2020; Sun et al., 2021). In terms of secreted chemistries, specific regulation of SMs under microbial competitions has previously been reported in fungal vs. bacterial and fungal vs. fungal interactions. Intriguingly, an intimate cross-kingdom interplay between *S. rapamycinicus* and *A. fumigatus* resulted in the epigenetic deregulation of the *PKS* based SMBGC required for synthesis of C-prenylated fumicycline by the bacterium (König

et al., 2013). In addition, microbial toxins were also reported to be specifically produced in several other co-cultivation experiments. In *F. culmorum*, increased production of mycotoxins such as DON and ZEA was observed in the competition led to with two *Alternaria tenuissima* isolates (Müller et al., 2012), and in the cross-kingdom interaction between the bacterium *Burkholderia glumae* and *F. graminearum*, higher levels of DON were produced in *F. graminearum*, presumably as a defense response to a toxic bacterial metabolite toxoflavin (Jung et al., 2018). The SMs produced may not be toxic *per se*, but can also be modulated by certain microbial species, including *Trichoderma*. For instance, by means of direct competition and employing biochemical modification, *T. atroviride* mitigated *Fusarium* mycotoxins such as trichothecenes and fusaric acid as reported by Tian and co-workers (Tian et al., 2020).

To increase the complexity, toxins also act as crucial weapons in microbial rivalry. A notable confrontation involves the potato wilt-causing bacterium *Ralstonia solanacearum* and the foolish seedling disease caused by the plant pathogen *F. fujikuroi.* The bacterium produces the lipopeptide ralsolamycin, a compound inducing formation of fungal chlamydospores, which are then colonized by the bacterium. In turn, in order to prevent or counteract bacterial colonization, *F. fujikuroi* increases the localized production of bikaverin and beauvericin (BEA), which exhibit antibacterial effects, demonstrating a sophisticated chemical counterattack (Spraker et al., 2016). In addition, an unique set of chemistries have been described in a comparative metabolome study between sponge holobionts associated with microbial cells. Within this interaction, the shared compounds include 2-methylbutyryl-carnitine, scyllo-inositol, and mannitol, while unique compounds include loliolide, fucoxanthin, and defensive metabolites such as 1-monolinoleoyl-rac-glycerol, and methyl vaccinate (Zhang et al., 2022). This suggests that the holobiont tailors its metabolic responses to different microbial adversaries, resulting in the production of unique suites of SMs. These findings illustrate the complexity of chemical interactions that occur during microbial confrontations, where each organism tailors its secondary metabolism profile to outcompete, inhibit, or tolerate its opponent. The dynamic interplay between microorganisms through the production and modulation of (toxic) SMs defines their competitive strategies.

Of the secreted chemistries in our study, it is reasonable to assume the presence of compounds with cytotoxic properties against mammalian cells. Multiple reports emphasize the cell toxicity of mycotoxins from various fungi (Coulet et al., 2024; Gutleb et al., 2002; Wen et al., 2016). In a

study conducted by Ruiz and co-workers (Ruiz et al., 2011), the toxicity of toxins such as BEA, DON, and T-2 were evaluated in hamster ovarian cells (CHO-K1), which yielded IC_{50} values ranging between 17 and 52 nM for T-2, 0.53 to 2.30 µM for DON, and 2.77 to 17.22 µM for BEA. In the experiment we conducted with confrontations between *A. nidulans* and two distinct biocontrol bacteria and a biocontrol fungus, we demonstrate that some metabolites synthesized in confrontations result in complete loss of viability of human cells. The IC_{50} values for these metabolites ranged between 52 - 250 µg/mL for HEK-293 cells, and 80 - 214 µg/mL for HCT-116 cells, demonstrating a significant level of toxicity. Fungal toxins may cause disruption of mitochondrial functions, leading to the generation of ROS and, in turn, result in DNA damage, apoptosis, lipid peroxidation, cell cycle arrest, and immunosuppression. Moreover, mycotoxins such as T-2 toxin, and DON disrupt protein synthesis by inducing a ribotoxic stress response (RSR), further impairing cellular functions such as cell growth, survival, inflammatory responses and blood-brain barrier functions (Wu et al., 2014).

The fact than a large number of so far unidentified and putatively toxic compounds are produced in microbial confrontations underlines the importance of identifying and functionally characterizing these chemistries (Demain & Fang, 2000; Keller, 2019). The lack of comprehensive data on these metabolites hampers the ability to fully assess their potential impacts on human health and the environment. Recent advances in metabolomics and high-resolution mass spectrometry have highlighted the vast chemical diversity of microbial SMs produced under different conditions, suggesting that many potentially toxic compounds are still undiscovered (Patti et al., 2012; Wolfender et al., 2019). Furthermore, the complexity of microbial interactions and their confrontation in natural environments may frequently lead to synthesis of novel SMs that do not occur in standard laboratory conditions (Scherlach & Hertweck, 2009). Studies have shown that microbial co-cultivation can trigger the production of unique SMs, driven by interspecies chemical signaling or even interspecies physical contact not occurring in solo culture (Netzker et al., 2015). The complexity of existing data suggests that there is a growing need for more sophisticated screening and characterization approaches to detect compounds with potential risks for consumers, especially when they are produced in contexts like biocontrol or agricultural applications (Bottalico & Perrone, 2002; Munkvold & Desjardins, 1997).

4.6 Implications of microbial confrontations for biocontrol and agricultural applications

It is not surprising that a large number of acute toxic and carcinogenic chemistries were detected in confrontations in the present research study, which were not synthesized in solo cultures of antagonists and, plausibly, would therefore not be evaluated in legislation efforts for antagonists to be used as biological plant protection agents. In contrast, in the EU, chemistries to be used in plant protection are known compounds and must be intensively evaluated and peer-reviewed by the member states and the European Food Safety Authority before a decision on approval can be made. Approval criteria defined in **Regulation (EC) No 1107/2009** (https://eur-lex.europa.eu/eli/reg/2009/1107/oj) exclude carcinogenic or otherwise adverse chemistries. For known chemical compounds, it is necessary to provide comprehensive safety data, including toxicological risk assessments, to demonstrate that the compounds do not pose any risks to humans, animals, or the environment. One may argue that fungicides, though neither toxic nor carcinogenic, may induce SMBGCs in fungi when applied at sublethal concentrations. Interestingly, in *F. graminearum* the application of 5 parts per million (ppm) of the azole fungicide Tebuconazole to a SNP mutant of the TF *AZR1* as well as to the Δ*azr1* deletion strain was used to investigate the transcriptional response to sublethal fungicide stress (Eisermann, 2023). In both experiments, the WT strain served as control and allowed assessing the response of SMBGC genes to a challenge by a synthetic fungicide. Even at a low threshold of log2FC ≥ 1, the WT strain showed only 14 and four de-regulated SM genes in these two experiments (Iris Eisermann, personal communication). For comparison, in my study, 82 and 116 SMBGC genes were de-regulated in *C. graminicola* in confrontations with *B. amyloliquefaciens* and *A. nidulans*, respectively. The great variety in newly synthesized metabolites supports the idea that synthesis of putatively toxic SMs is significantly more dramatic in microbial confrontations than fungicide challenges .

Collectively, combinations of transcriptome and metabolome analyses of multiple fungus vs. fungus and fungus vs. bacterium confrontations have revealed dramatic reprogramming in microbial secondary metabolism and synthesis of chemistries representing enormous putative consumers' health risks. Moreover, this research supports the idea that microbial confrontations are decided based on the ability of the interacting partners to synthesize toxic SMs. The fact that a large array of novel and, in part, toxic and carcinogenic chemistries are formed in confrontations between approved biocontrol bacterium and a plant pathogenic fungus questions the hypothesis

that biological disease control promotes consumer safety and strongly demands more rigorous analyses of microbial SMs before microorganisms are approved for plant protection.

5 Conclusion and outlook

The study of microbial SMs and their toxicological impacts has long been a critical area of research, given the significant threats they pose to human health, agriculture, and livestock. Our research study explored the intricate dynamics of microbial interactions, particularly focusing on the confrontations between the maize pathogen *C. graminicola* and the biocontrol bacterium *B. amyloliquefaciens* as well as the ubiquitous model fungus *A. nidulans*. In another part of this study, multiple confrontations were made between *A. nidulans* and various biocontrol bacteria and phytopathogens. Through a combination of transcriptome, metabolome (performed by Dr. Henriette Uthe, iDiv and IPB; and Dr. Yvonne Poeschl, iDiv, and MLU) and cytotoxicity studies (conducted by Dr. Robert Rennert, IPB), this study uncovered the substantial reprogramming of microbial secondary metabolism and the synthesis of a vast array of novel, potentially toxic and even carcinogenic chemistries.

One of the most striking findings is the sheer complexity and diversity of SMs produced during microbial confrontations. The interactions between *C. graminicola* and its microbial antagonists resulted in the synthesis of numerous novel compounds, many of which exhibit structural similarities to known fungicidal and toxic chemistries. This discovery underscores the significant role of microbial confrontations in driving chemical diversity and the production of chemical compounds. The fact that these interactions can induce the production of toxic and carcinogenic SMs, which are not synthesized under solo culture conditions, highlights the potential health risks associated with the use of MBCAs in agriculture. The findings presented in this research challenge the prevailing assumption that biological disease control methods are inherently safer than chemical pesticides. While MBCA such as *B. amyloliquefaciens* are often considered environmentally friendly alternatives, this study demonstrates that their interactions with pathogenic fungi can lead to the production of toxic SMs. The detection of toxic compounds, including those with carcinogenic potential, in microbial confrontations necessitates a re-evaluation of the safety protocols for biocontrol agents (Figure 26).

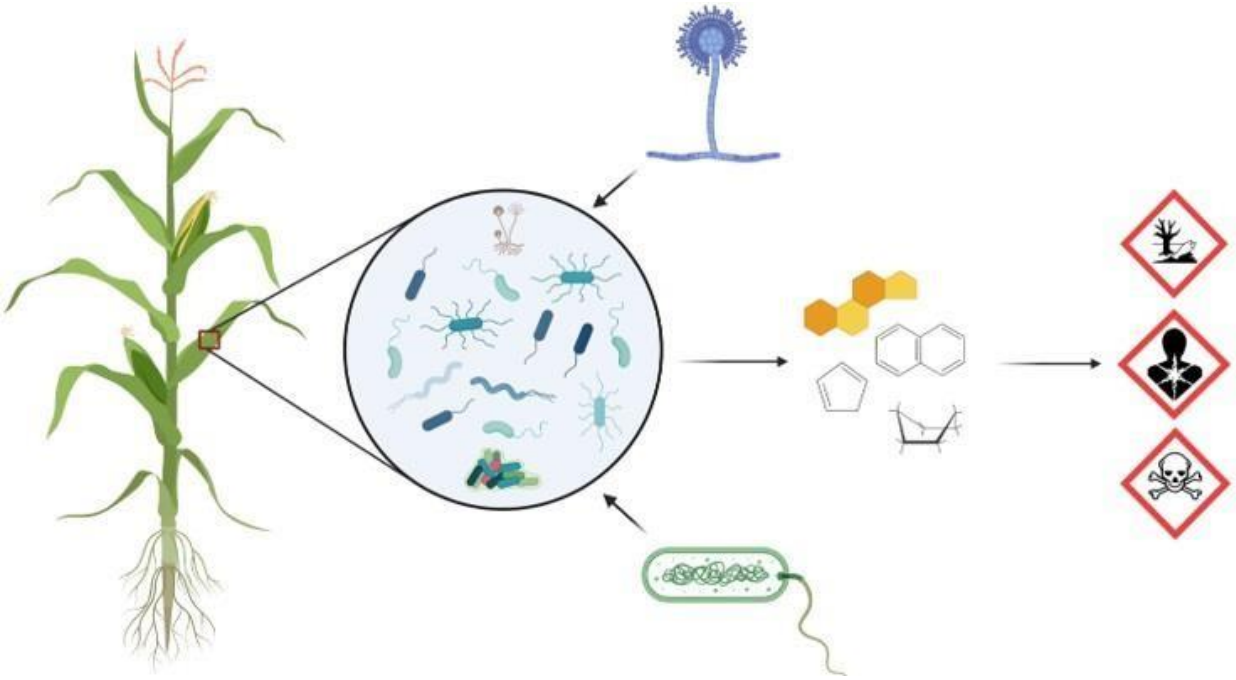

Figure 26. Graphical illustration of microbial confrontations on maize leaf.

The unaltered microbiome on the maize leaf surface undergoes significant disruption upon the introduction of external MBCAs, including bacterial and fungal species. This disturbance in the native microbial community by antagonists triggers the production of (novel) SMs, many of which are toxic. These SMs can be taken up and further modified by other organisms, resulting in a complex "cocktail" of chemistries.

Given these insights, it is imperative to implement more stringent regulatory frameworks for the approval and use of MBCAs. Current safety assessments may not fully account for the complex and dynamic nature of microbial interactions that occur in natural and agricultural environments. Therefore, comprehensive evaluations that include detailed metabolome and transcriptome analyses should be mandatory before approval of biocontrol agents. Such target assessments would help ensure that potentially toxic or carcinogenic metabolites are thoroughly evaluated before approving biological control agents. Furthermore, this research highlights the need for advanced monitoring and risk assessment strategies in agricultural practices. The potential for MBCAs to synthesize toxic chemistries when confronted with pathogenic fungi calls for vigilant oversight and management. To ensure a comprehensive evaluation of toxic SMs produced under microbial confrontations, specific experimental setups can be designed to mimic relevant agricultural and environmental conditions. For example, potential biocontrol agents could be co-cultivated with a range of bacterial and fungal microbes to identify the spectrum of SMs produced under various

interactions. This targeted approach would help capture the specific metabolites generated in realistic scenarios, allowing for a thorough assessment of their toxicity and safety before the approval of these agents for use.

To sum up, this research underscores the critical importance of re-thinking the use of MBCAs in agricultural practices. While they offer promising alternatives to chemical pesticides, their potential to produce SMs putatively toxic to humans poses significant health risks. Rigorous regulatory measures and comprehensive safety assessments are essential to ensure that biocontrol methods do not inadvertently give rise to new hazards. By advancing our understanding of microbial secondary metabolism and enhancing safety protocols, we can better harness the benefits of MBCAs while safeguarding public health and environmental sustainability.

6. Bibliography

Afendi, F. M., Okada, T., Yamazaki, M., Hirai-Morita, A., Nakamura, Y., Nakamura, K., Ikeda, S., Takahashi, H., Altaf-Ul-Amin, M., Darusman, L. K., Saito, K., & Kanaya, S. (2012). KNApSAcK family databases: integrated metabolite-plant species databases for multifaceted plant research. *Plant Cell Physiol 53*, e1. https://doi.org/10.1093/pcp/pcr165

Aliyeva-Schnorr, L., Schuster, C., & Deising, H. B. (2023). Natural Urease Inhibitors Reduce the Severity of Disease Symptoms, Dependent on the Lifestyle of the Pathogens. *J Fungi 9*, Accession Number: 37504697. https://doi.org/10.3390/jof9070708

Allard, P. M., Péresse, T., Bisson, J., Gindro, K., Marcourt, L., Pham, V. C., Roussi, F., Litaudon, M., & Wolfender, J. L. (2016). Integration of Molecular Networking and In-Silico MS/MS Fragmentation for Natural Products Dereplication. *Anal Chem 88*, 3317-3323. https://doi.org/10.1021/acs.analchem.5b04804

Alshannaq, A., & Yu, J. H. (2017). Occurrence, Toxicity, and Analysis of Major Mycotoxins in Food. *Int J Environ Res Public Health 14*, Accession Number: 28608841. https://doi.org/10.3390/ijerph14060632

Altschul, S. F., Madden, T. L., Schäffer, A. A., Zhang, J., Zhang, Z., Miller, W., & Lipman, D. J. (1997). Gapped BLAST and PSI-BLAST: a new generation of protein database search programs. *Nucleic Acids Res 25*, 3389-3402. https://doi.org/10.1093/nar/25.17.3389

Arguelles-Arias, A., Ongena, M., Halimi, B., Lara, Y., Brans, A., Joris, B., & Fickers, P. (2009). *Bacillus amyloliquefaciens* GA1 as a source of potent antibiotics and other secondary metabolites for biocontrol of plant pathogens. *Microb Cell Fact 8*, 63. https://doi.org/10.1186/1475-2859-8-63

Azziz-Baumgartner, E., Lindblade, K., Gieseker, K., Rogers, H. S., Kieszak, S., Njapau, H., Schleicher, R., McCoy, L. F., Misore, A., DeCock, K., Rubin, C., & Slutsker, L. (2005). Case-control study of an acute aflatoxicosis outbreak, Kenya, 2004. *Environ Health Perspect 113*, 1779-1783. https://doi.org/10.1289/ehp.8384

Banerjee, P., Kemmler, E., Dunkel, M., & Preissner, R. (2024). ProTox 3.0: a webserver for the prediction of toxicity of chemicals. *Nucleic Acids Res 52*, W513-W520. https://doi.org/10.1093/nar/gkae303

Baral, B., Akhgari, A., & Metsä-Ketelä, M. (2018). Activation of microbial secondary metabolic pathways: Avenues and challenges. *Synth Syst Biotechnol 3*, 163-178. https://doi.org/10.1016/j.synbio.2018.09.001

Barbe, V., Cruveiller, S., Kunst, F., Lenoble, P., Meurice, G., Sekowska, A., Vallenet, D., Wang, T., Moszer, I., Médigue, C., & Danchin, A. (2009). From a consortium sequence to a unified sequence: the *Bacillus subtilis* 168 reference genome a decade later. *Microbiology 155*, 1758-1775. https://doi.org/10.1099/mic.0.027839-0

Batut, B., Hiltemann, S., Bagnacani, A., Baker, D., Bhardwaj, V., Blank, C., Bretaudeau, A., Brillet-Guéguen, L., Čech, M., Chilton, J., Clements, D., Doppelt-Azeroual, O., Erxleben, A., Freeberg, M. A., Gladman, S., Hoogstrate, Y., Hotz, H.-R., Houwaart, T., Jagtap, P., Lariviere, D., Corguille, G. L., Manke, T., Mareuil, F., Ramirez, F., Ryan, D., Sigloch, F. C., Soranzo, N., Wolff, J., Videm, P., Wolfien, M., Wubuli, A., Yusuf, D., Taylor, J., Backofen, R., Nekrutenko, A., Grüning, B. (2018). Community-Driven Data Analysis Training for Biology. *Cell Syst 6*, 752-758.e751. https://doi.org/10.1016/j.cels.2018.05.012

Bauer, A. W., Perry, D. M., & Kirby, W. M. (1959). Single-disk antibiotic-sensitivity testing of *staphylococci*; an analysis of technique and results. *AMA Arch Intern Med 104*, 208-216. https://doi.org/10.1001/archinte.1959.00270080034004

Bayram, O., Krappmann, S., Ni, M., Bok, J. W., Helmstaedt, K., Valerius, O., Braus-Stromeyer, S., Kwon, N. J., Keller, N. P., Yu, J. H., & Braus, G. H. (2008). VelB/VeA/LaeA complex coordinates light signal with fungal development and secondary metabolism. *Science 320*, 1504-1506. https://doi.org/10.1126/science.1155888

Bechinger, C., Giebel, K. F., Schnell, M., Leiderer, P., Deising, H. B., & Bastmeyer, M. (1999). Optical measurements of invasive forces exerted by appressoria of a plant pathogenic fungus. *Science 285*, 1896-1899. https://doi.org/10.1126/science.285.5435.1896

Beckerman, J., Palmer, C., Tedford, E., & Ypema, H. (2023). Fifty Years of Fungicide Development, Deployment, and Future Use. *Phytopathology 113*, 694-706. https://doi.org/10.1094/phyto-10-22-0399-ia

Benkerroum. (2020a). Aflatoxins: Producing-Molds, Structure, Health Issues and Incidence in Southeast Asian and Sub-Saharan African Countries. *Int J Environ Res Public Health 17*, Accession Number: 32070028. https://doi.org/10. 3390/ijerph17041215

Benkerroum. (2020b). Chronic and Acute Toxicities of Aflatoxins: Mechanisms of Action. *Int J Environ Res Public Health 17*, 423. https://www.mdpi.com/1660-4601/17/2/423

Bergstrom, G. C., & Nicholson, R. L. (1999). The Biology of Corn Anthracnose: Knowledge to Exploit for Improved Management. *Plant Dis 83*, 596-608. https://doi.org/10.1094/PDIS.1999.83.7.596

Bertrand, S., Bohni, N., Schnee, S., Schumpp, O., Gindro, K., & Wolfender, J. L. (2014). Metabolite induction via microorganism co-culture: a potential way to enhance chemical diversity for drug discovery. *Biotechnol Adv 32*, 1180-1204. https://doi.org/10.1016/j.biotechadv.2014.03.001

Bertrand, S., Schumpp, O., Bohni, N., Monod, M., Gindro, K., & Wolfender, J.-L. (2013). De Novo Production of Metabolites by Fungal Co-culture of *Trichophyton rubrum* and *Bionectria ochroleuca*. *J Nat Prod 76*, 1157-1165. https://doi.org/10.1021/np400258f

Blin, K., Shaw, S., Augustijn, H. E., Reitz, Z. L., Biermann, F., Alanjary, M., Fetter, A., Terlouw, B. R., Metcalf, W. W., Helfrich, E. J. N., van Wezel, G. P., Medema, M. H., & Weber, T. (2023). antiSMASH 7.0: new and improved predictions for detection, regulation, chemical structures and visualisation. *Nucleic Acids Res 51*, W46-W50. https://doi.org/10.1093/nar/gkad344

Bottalico, A., & Perrone, G. (2002). Toxigenic *Fusarium* species and Mycotoxins Associated with Head Blight in Small-Grain Cereals in Europe. *Eur J Plant Pathol 108*, 611-624. https://doi.org/10.1023/A:1020635214971

Böttcher, C., Westphal, L., Schmotz, C., Prade, E., Scheel, D., & Glawischnig, E. (2009). The multifunctional enzyme CYP71B15 (PHYTOALEXIN DEFICIENT3) converts cysteine-indole-3-acetonitrile to camalexin in the indole-3-acetonitrile metabolic network of *Arabidopsis thaliana*. *Plant Cell 21*, 1830-1845. https://doi.org/10.1105/tpc.109.066670

Bouhired, S., Weber, M., Kempf-Sontag, A., Keller, N. P., & Hoffmeister, D. (2007). Accurate prediction of the *Aspergillus nidulans* terrequinone gene cluster boundaries using the transcriptional regulator LaeA. *Fungal Genet Biol 44*, 1134-1145. https://doi.org/10.1016/j.fgb.2006.12.010

Brakhage, A. A. (2013). Regulation of fungal secondary metabolism. *Nat Rev Microbiol 11*, 21-32. https://doi.org/10.1038/nrmicro2916

Brakhage, A. A., & Schroeckh, V. (2011). Fungal secondary metabolites - strategies to activate silent gene clusters. *Fungal Genet Biol 48*, 15-22. https://doi.org/10.1016/j.fgb.2010.04.004

Brauer, V. S., Rezende, C. P., Pessoni, A. M., De Paula, R. G., Rangappa, K. S., Nayaka, S. C., Gupta, V. K., & Almeida, F. (2019). Antifungal Agents in Agriculture: Friends and Foes of Public Health. *Biomolecules 9*, 521. https://doi.org/10.3390%2Fbiom9100521

Brown, D. W., Yu, J. H., Kelkar, H. S., Fernandes, M., Nesbitt, T. C., Keller, N. P., Adams, T. H., & Leonard, T. J. (1996). Twenty-five coregulated transcripts define a sterigmatocystin gene cluster in *Aspergillus nidulans*. *Proc Natl Acad Sci USA 93*, 1418-1422. https://doi.org/10.1073/pnas.93.4.1418

Brown, R., Priest, E., Naglik, J. R., & Richardson, J. P. (2021). Fungal Toxins and Host Immune Responses. *Front Microbiol 12*, 643639. https://doi.org/10.3389/fmicb.2021.643639

Brunson, J. C., & Read, Q. D. (2019). "ggalluvial: Alluvial Plots in ggplot2". J Open Source Softw 5, 1-6. https://doi.org/10.21105/joss.02017

Bullock, W. O. (1987). XL1-Blue: a high efficiency plasmid transforming recA *Escherichia coli* strain with beta-galactosidase selection. *Biotechniques 5*, 376-379. (No DOI available)

Burandt, Q. C., Deising, H. B., & von Tiedemann, A. (2024). Further Limitations of Synthetic Fungicide Use and Expansion of Organic Agriculture in Europe Will Increase the Environmental and Health Risks of Chemical Crop Protection Caused by Copper-Containing Fungicides. *Environ Toxicol Chem 43*, 19-30. https://doi.org/10.1002/etc.5766

Butler, W. H. (1964). Acute Toxicity of Aflatoxin B1 in Rats. *Br J Cancer 18*, 756-762. https://doi.org/10.1038/bjc.1964.87

Caceres, I., Al Khoury, A., El Khoury, R., Lorber, S., P. Oswald, I., El Khoury, A., Atoui, A., Puel, O., & Bailly, J.-D. (2020). Aflatoxin Biosynthesis and Genetic Regulation: A Review. *Toxins 12*, 150. https://www.mdpi.com/2072-6651/12/3/150

Caesar, L. K., Kelleher, N. L., & Keller, N. P. (2020). In the fungus where it happens: History and future propelling Aspergillus nidulans as the archetype of natural products research. *Fungal Genet Biol 144*, 103477. https://doi.org/10.1016/j.fgb.2020.103477

Cane, D. E., Walsh, C. T., & Khosla, C. (1998). Harnessing the biosynthetic code: combinations, permutations, and mutations. *Science 282*, 63-68. https://doi.org/10.1126/science.282.5386.63

Cannon, P. F., Damm, U., Johnston, P. R., & Weir, B. S. (2012). *Colletotrichum* - current status and future directions. *Stud Mycol 73*, 181-213. https://doi.org/10.3114/sim0014

Carpane, P. D., Peper, A. M., & Kohn, F. (2020). Management of Northern Corn Leaf Blight using Nativo (Trifloxistrobin + Tebuconazole) Fungicide Applications. *Crop Prot 127*, 104982. https://doi.org/10.1016/j.cropro.2019.104982

Chavas, J.-P., Shi, G., Nehring, R., & Stiegert, K. (2018). The Effects of Biotechnology on Productivity and Input Demands in U.S. Agriculture. *J Agric Appl Econ 50*, 387-407. https://doi.org/10.1017/aae.2018.6

Chemudupati, M., Johns, M., & Osmani, S. A. (2019). The mode of mitosis is dramatically modified by deletion of a single nuclear pore complex gene in *Aspergillus nidulans*. *Fungal Genet Biol 130*, 72-81. https://doi.org/10.1016/j.fgb.2019.04.010

Chevrette, M. G., Thomas, C. S., Hurley, A., Rosario-Meléndez, N., Sankaran, K., Tu, Y., Hall, A., Magesh, S., & Handelsman, J. (2022). Microbiome composition modulates secondary metabolism in a multispecies bacterial community. *Proc Natl Acad Sci USA 119*, e2212930119. https://doi.org/doi:10.1073/pnas.2212930119

Chiang, Y.-M., Szewczyk, E., Nayak, T., Davidson, A. D., Sanchez, J. F., Lo, H.-C., Ho, W.-Y., Simityan, H., Kuo, E., Praseuth, A., Watanabe, K., Oakley, B. R., & Wang, C. C. C. (2008). Molecular Genetic Mining of the *Aspergillus* Secondary Metabolome: Discovery of the Emericellamide Biosynthetic Pathway. *Chem Biol 15*, 527-532. https://doi.org/10.1016/j.chembiol.2008.05.010

Chiang, Y. M., Szewczyk, E., Davidson, A. D., Keller, N., Oakley, B. R., & Wang, C. C. (2009). A gene cluster containing two fungal polyketide synthases encodes the biosynthetic pathway for a polyketide, asperfuranone, in *Aspergillus nidulans. J Am Chem Soc 131*, 2965-2970. https://doi.org/10.1021/ja8088185

Chung, C. T., Niemela, S. L., & Miller, R. H. (1989). One-step preparation of competent *Escherichia coli*: transformation and storage of bacterial cells in the same solution. *Proc Natl Acad Sci USA 86*, 2172-2175. https://doi.org/10.1073/pnas.86.7.2172

Cichewicz, R. H. (2010). Epigenome manipulation as a pathway to new natural product scaffolds and their congeners. *Nat Prod Rep 27*, 11-22. https://doi.org/10.1039/B920860G

Collado, I. G., Sánchez, A. J. M., & Hanson, J. R. (2007). Fungal terpene metabolites: biosynthetic relationships and the control of the phytopathogenic fungus *Botrytis cinerea*: *Nat Prod Rep 24*, 674-686. https://doi.org/10.1039/B603085H

Collemare, J., & Seidl, M. F. (2019). Chromatin-dependent regulation of secondary metabolite biosynthesis in fungi: is the picture complete? *FEMS Microbiol Rev 43*, 591-607. https://doi.org/10.1093/femsre/fuz018

Coulet, F., Coton, M., Iperi, C., Belinger Podevin, M., Coton, E., & Hymery, N. (2024). Cytotoxic Effects of Major and Emerging Mycotoxins on HepaRG Cells and Transcriptomic Response after Exposure of Spheroids to Enniatins B and B1. *Toxins 16*, 54. https://www.mdpi.com/2072-6651/16/1/54

Crofton, K. M. (1996). A structure-activity relationship for the neurotoxicity of triazole fungicides. *Toxicol Lett 84*, 155-159. https://doi.org/10.1016/0378-4274(95)03618-0

Cui, J., Wang, J., Huang, S., Jiang, X., Li, Y., Wu, W., & Zhang, X. (2017). Sterigmatocystin induced apoptosis in human pulmonary cells in vitro. *Exp Toxicol Pathol 69*, 695-699. https://doi.org/10.1016/j.etp.2017.07.002

Daoubi, M., Pinedo-Rivilla, C., Rubio, M. B., Hermosa, R., Monte, E., Aleu, J., & Collado, I. G. (2009). Hemisynthesis and absolute configuration of novel 6-pentyl-2H-pyran-2-one derivatives from *Trichoderma* spp. *Tetrahedron 65*, 4834-4840. https://doi.org/10.1016/j.tet.2009.04.051

de Oliveira Silva, A., Fernando Devasahayam, B. R., Aliyeva-Schnorr, L., Glienke, C., & Deising, H. B. (2024). The serine-threonine protein kinase Snf1 orchestrates the expression of plant cell wall-degrading enzymes and is required for full virulence of the maize pathogen *Colletotrichum graminicola*. *Fungal Genet Biol 171*, 103876. https://doi.org/10.1016/j.fgb.2024.103876

Degenkolb, T., Heinze, S., Schlegel, B., Strobel, G., & Gräfe, U. (2002). Formation of new lipoaminopeptides, acremostatins A, B, and C, by co-cultivation of *Acremonium* sp. Tbp-5 and *Mycogone rosea* DSM 12973. *Biosci Biotechnol Biochem 66*, 883-886. https://doi.org/10.1271/bbb.66.883

Deising, H. B., Gase, I., & Kubo, Y. (2017). The unpredictable risk imposed by microbial secondary metabolites: how safe is biological control of plant diseases? *J Plant Dis Prot 124*, 413-419. https://doi.org/10.1007/s41348-017-0109-5

Deising, H. B., Werner, S., & Wernitz, M. (2000). The role of fungal appressoriain plant infection. *Microbes Infect 2*, 1631-1641. https://doi.org/10.1016/S1286-4579(00)01319-8

Dejea, C. M., Fathi, P., Craig, J. M., Boleij, A., Taddese, R., Geis, A. L., Wu, X., DeStefano Shields, C. E., Hechenbleikner, E. M., Huso, D. L., Anders, R. A., Giardiello, F. M., Wick, E. C., Wang, H., Wu, S., Pardoll, D. M., Housseau, F., & Sears, C. L. (2018). Patients with familial adenomatous polyposis harbor colonic biofilms containing tumorigenic bacteria. *Science 359*, 592-597. https://doi.org/10.1126/science.aah3648

Demain, A. L., & Fang, A. (2000). The Natural Functions of Secondary Metabolites. In A. Fiechter (Ed.), *History of Modern Biotechnology I*, 1-39. Springer Berlin Heidelberg. https://doi.org/10.1007/3-540-44964-7_1

Demain, A. L., & Sanchez, S. (2009). Microbial drug discovery: 80 years of progress. *J Antibiot 62*, 5-16. https://doi.org/10.1038/ja.2008.16

Díaz Nieto, C. H., Granero, A. M., Zon, M. A., & Fernández, H. (2018). Sterigmatocystin: A mycotoxin to be seriously considered. *Food chem toxicol 118*, 460-470. https://doi.org/10.1016/j.fct.2018.05.057

Didelot, X., Barker, M., Falush, D., & Priest, F. G. (2009). Evolution of pathogenicity in the *Bacillus cereus* group. *Syst Appl Microbiol 32*, 81-90. https://doi.org/10.1016/j.syapm.2009.01.001

Djoumbou Feunang, Y., Eisner, R., Knox, C., Chepelev, L., Hastings, J., Owen, G., Fahy, E., Steinbeck, C., Subramanian, S., Bolton, E., Greiner, R., & Wishart, D. S. (2016). ClassyFire: automated chemical classification with a comprehensive, computable taxonomy. *J Cheminform 8*, 61. https://doi.org/10.1186/s13321-016-0174-y

Döbbeling, U. (2000). Simultaneous RNA and DNA Extraction from Biopsy Material, Culture Cells, Plants, and Bacteria. In R. Rapley (Ed.), *The Nucleic Acid Protocols Handbook*, 53-56. Humana Press. https://doi.org/10.1385/1-59259-038-1:53

Doble, M., & Kumar, A. (2005). Chapter 8 - Biodegradation of Pesticides. In M. Doble & A. Kumar (Eds.), *Biotreatment of Industrial Effluents*, 89-100. Butterworth-Heinemann. https://doi.org/10.1016/B978-075067838-4/50009-9

Dührkop, K., Fleischauer, M., Ludwig, M., Aksenov, A. A., Melnik, A. V., Meusel, M., Dorrestein, P. C., Rousu, J., & Böcker, S. (2019). SIRIUS 4: a rapid tool for turning tandem mass spectra into metabolite structure information. *Nat Methods 16*, 299-302. https://doi.org/10.1038/s41592-019-0344-8

Dührkop, K., Nothias, L. F., Fleischauer, M., Reher, R., Ludwig, M., Hoffmann, M. A., Petras, D., Gerwick, W. H., Rousu, J., Dorrestein, P. C., & Böcker, S. (2021). Systematic classification of unknown metabolites using high-resolution fragmentation mass spectra. *Nat Biotechnol 39*, 462-471. https://doi.org/10.1038/s41587-020-0740-8

Dührkop, K., Shen, H., Meusel, M., Rousu, J., & Böcker, S. (2015). Searching molecular structure databases with tandem mass spectra using CSI:FingerID. *Proc Natl Acad Sci USA 112*, 12580-12585. https://doi.org/10.1073/pnas.1509788112

EFSA. (2013). Scientific Opinion on the risk for public and animal health related to the presence of sterigmatocystin in food and feed. *EFSA J 11*, 3254. https://doi.org/10.2903/j.efsa.2013.3254

Ehrlich, K. C., Montalbano, B. G., & Cary, J. W. (1999). Binding of the C6-zinc cluster protein, AFLR, to the promoters of aflatoxin pathway biosynthesis genes in *Aspergillus parasiticus*. *Gene 230*, 249-257. https://doi.org/10.1016/s0378-1119(99)00075-x

Eisermann. (2023). A single amino acid exchange in a novel transcription factor leads to dramatically increased azole resistance in *Fusarium graminearum*. Martin Luther University Halle-Wittenberg. https://opendata.uni-halle.de//handle/1981185920/114563

Ekwomadu, T. I., & Mwanza, M. (2023). *Fusarium* Fungi Pathogens, Identification, Adverse Effects, Disease Management, and Global Food Security: A Review of the Latest Research. *Agriculture 13*, 1810. https://www.mdpi.com/2077-0472/13/9/1810

Enomoto, M., Hatanaka, J., Igarashi, S., Uwanuma, Y., Ito, H., Asaoka, S., Iyatomi, A., Kuyama, S., Harada, T., & Hamasaki, T. (1982). High incidence of angiosarcomas in brown-fat tissue and livers of mice fed sterigmatocystin. *Food Chem Toxicol 20*, 547-556. https://doi.org/10.1016/S0278-6915(82)80063-X

Epstein, L., & Nicholson, R. (2016). Adhesion and Adhesives of Fungi and Oomycetes. In A. M. Smith (Ed.), *Biological Adhesives*, 41-62. Springer. https://doi.org/10.1007/978-3-319-46082-6_2

Erenstein, O., Jaleta, M., Sonder, K., Mottaleb, K., & Prasanna, B. M. (2022). Global maize production, consumption and trade: trends and R&D implications. *Food Secur 14*, 1295-1319. https://doi.org/10.1007/s12571-022-01288-7

Essigmann, J. M., Barker, L. J., Fowler, K. W., Francisco, M. A., Reinhold, V. N., & Wogan, G. N. (1979). Sterigmatocystin-DNA interactions: identification of a major adduct formed after metabolic activation in vitro. *Proc Natl Acad Sci USA 76*, 179-183. https://doi.org/10.1073/pnas.76.1.179

Fernández-Ortuño, D., Torés, J. A., de Vicente, A., & Pérez-García, A. (2008). Mechanisms of resistance to QoI fungicides in phytopathogenic fungi. *Int Microbiol 11*, 1-9. https://pubmed.ncbi.nlm.nih.gov/18683626/

Fernando Devasahayam, B. R., Barrera Adame, D. A., Uthe, H., Pöschl-Grau, Y., Niedermeyer, T. H. J., & Deising, H. B. (2024). Metabolic re-programming in confrontations of *Colletotrichum graminicola* and *Aspergillus nidulans* with *Bacillus* biocontrol agents. *J Plant Dis Prot 131*, 1271-1277. https://doi.org/10.1007/s41348-024-00905-1

Fritze, D., & Pukall, R. (2001). Reclassification of bioindicator strains *Bacillus subtilis* DSM 675 and *Bacillus subtilis* DSM 2277 as *Bacillus atrophaeus*. *Int J Syst Evol Microbiol 51*, 35-37. https://doi.org/10.1099/00207713-51-1-35

Gao, L., Song, Y., Cao, J., Wang, S., Wei, H., Jiang, H., & Lu, L. (2011). Osmotic stabilizer-coupled suppression of NDR defects is dependent on the calcium–calcineurin signaling cascade in *Aspergillus nidulans*. *Cell Signal 23*, 1750-1757. https://doi.org/10.1016/j.cellsig.2011.06.009

Gao, W., Jiang, L., Ge, L., Chen, M., Geng, C., Yang, G., Li, Q., Ji, F., Yan, Q., Zou, Y., Zhong, L., & Liu, X. (2015). Sterigmatocystin-induced oxidative DNA damage in human liver-derived cell line through lysosomal damage. *Toxicol In Vitro 29*, 1-7. https://doi.org/10.1016/j.tiv.2014.08.007

Ge, S. X., Jung, D., & Yao, R. (2019). ShinyGO: a graphical gene-set enrichment tool for animals and plants. *Bioinformatics 36*, 2628-2629. https://doi.org/10.1093/bioinformatics/btz931

Ghorbanpour, M., Omidvari, M., Abbaszadeh-Dahaji, P., Omidvar, R., & Kariman, K. (2018). Mechanisms underlying the protective effects of beneficial fungi against plant diseases. *Biol Control 117*, 147-157. https://doi.org/10.1016/j.biocontrol.2017.11.006

Gilbert, G. S., Parke, J. L., Clayton, M. K., & Handelsman, J. (1993). Effects of an Introduced Bacterium on Bacterial Communities on Roots. *Ecology 74*, 840-854. https://doi.org/10.2307/1940810

Gong, A.-D., Li, H.-P., Yuan, Q.-S., Song, X.-S., Yao, W., He, W.-J., Zhang, J.-B., & Liao, Y.-C. (2015). Antagonistic Mechanism of Iturin A and Plipastatin A from *Bacillus amyloliquefaciens* S76-3 from Wheat Spikes against *Fusarium graminearum*. *PLoS One 10*, e0116871. https://doi.org/10.1371/journal.pone.0116871

Gosálvez, M. (1983). Carcinogenesis with the insecticide rotenone. *Life Sci 32*, 809-816. https://doi.org/10.1016/0024-3205(83)90216-3

Gu, Q., Qiao, J., Wang, R., Lu, J., Wang, Z., Li, P., Zhang, L., Ali, Q., Khan, A. R., Gao, X., & Wu, H. (2022). The Role of Pyoluteorin from *Pseudomonas protegens* Pf-5 in Suppressing the Growth and Pathogenicity of *Pantoea ananatis* on Maize. *Int J Mol Sci 23*, 6341. https://doi.org/10.3390/ijms23126431

Gullino, M. L., Tinivella, F., Garibaldi, A., Kemmitt, G. M., Bacci, L., & Sheppard, B. (2010). Mancozeb: Past, Present, and Future. *Plant Dis 94*, 1076-1087. https://doi.org/10.1094/pdis-94-9-1076

Gutleb, A. C., Morrison, E., & Murk, A. J. (2002). Cytotoxicity assays for mycotoxins produced by *Fusarium* strains: a review. *Environ Toxicol Pharmacol 11*, 309-320. https://doi.org/10.1016/S1382-6689(02)00020-0

Haarmann, T., Rolke, Y., Giesbert, S., & Tudzynski, P. (2009). Ergot: from witchcraft to biotechnology. *Mol Plant Pathol 10*, 563-577. https://doi.org/10.1111/j.1364-3703.2009.00548.x

Haas, D., & Défago, G. (2005). Biological control of soil-borne pathogens by fluorescent pseudomonads. *Nat Rev Microbiol 3*, 307-319. https://doi.org/10.1038/nrmicro1129

Han, K. H. (2009). Molecular Genetics of *Emericella nidulans* Sexual Development. *Mycobiology 37*, 171-182. https://doi.org/10.4489/myco.2009.37.3.171

Hass, H., Taylor, T. N., & Remy, W. (1994). Fungi from the Lower Devonian Rhynie chert: My Coparasitism. *Am J Bot 81*, 29-37. https://doi.org/10.1002/j.1537-2197.1994.tb15405.x

Heussner, A. H., & Bingle, L. E. (2015). Comparative Ochratoxin Toxicity: A Review of the Available Data. *Toxins 7*, 4253-4282. https://doi.org/10.3390/toxins7104253

Hiltemann, S., Rasche, H., Gladman, S., Hotz, H.-R., Larivière, D., Blankenberg, D., Jagtap, P. D., Wollmann, T., Bretaudeau, A., Goué, N., Griffin, T. J., Royaux, C., Le Bras, Y., Mehta, S., Syme, A., Coppens, F., Droesbeke, B., Soranzo, N., Bacon, W., Psomopoulos, F., Gallardo-Alba, C., Davis, J., Föll, M. C., Fahrner, M., Doyle, M. A., Serrano-Solano, B., Fouilloux, A. C., Heusden, P. V., Maier, W., Clements, D., Heyl, F., Grüning, B., Batut, B. (2023). Galaxy Training: A powerful framework for teaching! *PLoS Computat Biol 19*, e1010752. https://doi.org/10.1371/journal.pcbi.1010752

Horio, T., Szewczyk, E., Oakley, C. E., Osmani, A. H., Osmani, S. A., & Oakley, B. R. (2019). SUMOlock reveals a more complete *Aspergillus nidulans* SUMOylome. *Fungal Genet Biol 127*, 50-59. https://doi.org/10.1016/j.fgb.2019.03.002

Howlett, B. J. (2006). Secondary metabolite toxins and nutrition of plant pathogenic fungi. *Curr Opin Plant Biol 9*, 371-375. https://doi.org/10.1016/j.pbi.2006.05.004

Huang, Y., Deverall, B. J., Tang, W. H., Wang, W., & Wu, F. W. (2000). Foliar Application of Acibenzolar-S-Methyl and Protection of Postharvest Rock Melons and Hami Melons from Disease. *European J Plant Pathol 106*, 651-656. https://doi.org/10.1023/A:1008767719691

Huelsenbeck, J. P., & Ronquist, F. (2001). MRBAYES: Bayesian inference of phylogenetic trees. *Bioinformatics 17*, 754-755. https://doi.org/10.1093/bioinformatics/17.8.754

Hulsen, T., de Vlieg, J., & Alkema, W. (2008). BioVenn - a web application for the comparison and visualization of biological lists using area-proportional Venn diagrams. *BMC Genomics 9*, 488. https://doi.org/10.1186/1471-2164-9-488

Hutchison, K. A., Green, J. R., Wharton, P. S., & O'Connell, R. J. (2002). Identification and localisation of glycoproteins in the extracellular matrices around germ-tubes and appressoria of *Colletotrichum* species. *Mycol Res 106*, 729-736. https://doi.org/10.1017/S095375620200597X

Hwang, S., Lee, N., Cho, S., Palsson, B., & Cho, B. K. (2020). Repurposing Modular Polyketide Synthases and Non-ribosomal Peptide Synthetases for Novel Chemical Biosynthesis. *Front Mol Biosci 7*, 87. https://doi.org/10.3389/fmolb.2020.00087

Inglis, D. O., Binkley, J., Skrzypek, M. S., Arnaud, M. B., Cerqueira, G. C., Shah, P., Wymore, F., Wortman, J. R., & Sherlock, G. (2013). Comprehensive annotation of secondary metabolite biosynthetic genes and gene clusters of *Aspergillus nidulans*, *A. fumigatus*, *A. niger* and *A. oryzae*. *BMC Microbiol 13*, 91. https://doi.org/10.1186/1471-2180-13-91

Jeffreys, M. D. W. (1955). Columbus and the Introduction of Maize into Spain. *Anthropos 50*, 427-432. http://www.jstor.org/stable/40451037

Jung, B., Park, J., Kim, N., Li, T., Kim, S., Bartley, L. E., Kim, J., Kim, I., Kang, Y., Yun, K., Choi, Y., Lee, H. H., Ji, S., Lee, K. S., Kim, B. Y., Shon, J. C., Kim, W. C., Liu, K. H., Yoon, D., Kim, S., Seo, Y-S., Lee, J. (2018). Cooperative interactions between seed-borne bacterial and air-borne fungal pathogens on rice. *Nat Commun 9*, 31. https://doi.org/10.1038/s41467-017-02430-2

Karahoda, B., Pardeshi, L., Ulas, M., Dong, Z., Shirgaonkar, N., Guo, S., Wang, F., Tan, K., Sarikaya-Bayram, Ö., Bauer, I., Dowling, P., Fleming, A. B., Pfannenstiel, Brandon T., Luciano-Rosario, D., Berger, H., Graessle, S., Alhussain, M. M., Strauss, J., Keller, N. P., Wong, K. H., Bayram, Ö. (2022). The KdmB-EcoA-RpdA-SntB chromatin complex binds regulatory genes and coordinates fungal development with mycotoxin synthesis. *Nucleic Acids Res 50*, 9797-9813. https://doi.org/10.1093/nar/gkac744

Karnatam, K. S., Mythri, B., Un Nisa, W., Sharma, H., Meena, T. K., Rana, P., Vikal, Y., Gowda, M., Dhillon, B. S., & Sandhu, S. (2023). Silage maize as a potent candidate for sustainable animal husbandry development-perspectives and strategies for genetic enhancement. *Front Genet 14*, 1150132. https://doi.org/10.3389/fgene.2023.1150132

Kashyap, S., Kumar, R., Ram, H., Kumar, A., Basak, N., Sheoran, P., Bhatacharjee, S., Biswal, B., Ali, G., Kumar, B., Bhakuni, K., Hindoriya, P. S., Birbal, & Min, D. (2023). Quantitative and Qualitative Response of Fodder Maize to Use of Bulk and Nano-fertilizers in North Western Plains of India. *Agronomy 13*, 1889. https://doi.org/10.3390/agronomy13071889

Ke, R., Haynes, K., & Stark, J. (2013). Modelling the activation of alkaline pH response transcription factor PacC in *Aspergillus nidulans*: Involvement of a negative feedback loop. *J Theor Biol 326*, 11-20. https://doi.org/10.1016/j.jtbi.2013.02.006

Keller, N. P. (2019). Fungal secondary metabolism: regulation, function and drug discovery. *Nat Rev Microbiol 17*, 167-180. https://doi.org/10.1038/s41579-018-0121-1

Kerr, J. R., Taylor, G. W., Rutman, A., Høiby, N., Cole, P. J., & Wilson, R. (1999). *Pseudomonas aeruginosa* pyocyanin and 1-hydroxyphenazine inhibit fungal growth. *J Clin Pathol 52*, 385-387. https://doi.org/10.1136/jcp.52.5.385

Khosla, C., Tang, Y., Chen, A. Y., Schnarr, N. A., & Cane, D. E. (2007). Structure and mechanism of the 6-deoxyerythronolide B synthase. *Annu Rev Biochem 76*, 195-221. https://doi.org/10.1146/annurev.biochem.76.053105.093515

Knutsen, H. K., Alexander, J., Barregård, L., Bignami, M., Brüschweiler, B., Ceccatelli, S., Cottrill, B., Dinovi, M., Grasl-Kraupp, B., Hogstrand, C., Hoogenboom, L. R., Nebbia, C. S., Oswald, I. P., Petersen, A., Rose, M., Roudot, A. C., Schwerdtle, T., Vleminckx, C., Vollmer, G., Wallace, H., Bodlin, L., Cravedi, J-P., Halldorsson, T. I., Haug, L. S., Johansson, N., Loveren, H. V., Gergelova, P., Mackay, K., Levorato, S., Manen, M. V., & Edler, L. (2017). Risks to human and animal health related to the presence of deoxynivalenol and its acetylated and modified forms in food and feed. *Efsa J 15*, e04718. https://doi.org/10.2903/j.efsa.2017.4718

König, C. C., Scherlach, K., Schroeckh, V., Horn, F., Nietzsche, S., Brakhage, A. A., & Hertweck, C. (2013). Bacterium induces cryptic meroterpenoid pathway in the pathogenic fungus *Aspergillus fumigatus*. *Chembiochem 14*, 938-942. https://doi.org/10.1002/cbic.201300070

Krespach, M. K. C., Stroe, M. C., Netzker, T., Rosin, M., Zehner, L. M., Komor, A. J., Beilmann, J. M., Krüger, T., Scherlach, K., Kniemeyer, O., Schroeckh, V., Hertweck, C., & Brakhage, A. A. (2023). *Streptomyces* polyketides mediate bacteria–fungi interactions across soil environments. *Nat Microbiol 8*, 1348-1361. https://doi.org/10.1038/s41564-023-01382-2

Krijger, J. J., Horbach, R., Behr, M., Schweizer, P., Deising, H. B., & Wirsel, S. G. (2008). The yeast signal sequence trap identifies secreted proteins of the hemibiotrophic corn pathogen *Colletotrichum graminicola*. *Mol Plant Microbe Interact 21*, 1325-1336. https://doi.org/10.1094/mpmi-21-10-1325

Kubo, Y., Takano, Y., Endo, N., Yasuda, N., Tajima, S., & Furusawa, I. (1996). Cloning and structural analysis of the melanin biosynthesis gene *SCD1* encoding scytalone dehydratase in *Colletotrichum lagenarium*. *Appl Environ Microbiol 62*, 4340-4344. https://doi.org/10.1128/aem.62.12.4340-4344.1996

Kufka, R., Rennert, R., Kaluđerović, G. N., Weber, L., Richter, W., & Wessjohann, L. A. (2019). Synthesis of a tubugi-1-toxin conjugate by a modulizable disulfide linker system with a neuropeptide Y analogue showing selectivity for hY1R-overexpressing tumor cells. *Beilstein J Org Chem 15*, 96-105. https://doi.org/10.3762/bjoc.15.11

Kumar, B., Choudhary, M., Kumar, K., Kumar, P., Kumar, S., Bagaria, P. K., Sharma, M., Lahkar, C., Singh, B. K., Pradhan, H., Jha, A. K., Kumar, S., & Rakshit, S. (2022). Maydis leaf blight of maize: Update on status, sustainable management and genetic architecture of its resistance. *Physiol Mol Plant Pathol 121*, 101889. https://doi.org/10.1016/j.pmpp.2022.101889

Kunzler, M. (2018). How fungi defend themselves against microbial competitors and animal predators. *PLoS Pathog 14*, e1007184. https://doi.org/10.1371/journal.ppat.1007184

Lai, Y. R., Lin, P. Y., Chen, C. Y., & Huang, C. J. (2016). Feasible Management of Southern Corn Leaf Blight via Induction of Systemic Resistance by *Bacillus cereus* C1L in Combination with Reduced Use of Dithiocarbamate Fungicides. *Plant Pathol J 32*, 481-488. https://doi.org/10.5423/ppj.Oa.02.2016.0044

Lam, Y. T. H., Hoppe, J., Dang, Q. N., Porzel, A., Soboleva, A., Brandt, W., Rennert, R., Hussain, H., Davari, M. D., Wessjohann, L., & Arnold, N. (2023). Purpurascenines A-C, Azepino-Indole Alkaloids from *Cortinarius purpurascens*: Isolation, Biosynthesis, and Activity Studies on the 5-HT(2A) Receptor. *J Nat Prod 86*, 1373-1384. https://doi.org/10.1021/acs.jnatprod.2c00716

Larsson, J. (2018). eulerr: area-proportional Euler diagrams with ellipses. https://cran.r-project.org/package=eulerr

Lee, B. N., & Adams, T. H. (1994). Overexpression of flbA, an early regulator of *Aspergillus* asexual sporulation, leads to activation of brlA and premature initiation of development. *Mol Microbiol 14*, 323-334. https://doi.org/10.1111/j.1365-2958.1994.tb01293.x

Lee, M. R. (2009). The history of ergot of rye (*Claviceps purpurea*) I: from antiquity to 1900. *J R Coll Physicians Edinb 39*, 179-184. https://doi: 10.4997/JRCPE.2009.416

Li, S., He, P., Fan, H., Liu, L., Yin, K., Yang, B., Li, Y., Huang, S. M., Li, X., & Zheng, S. J. (2021). A Real-Time Fluorescent Reverse Transcription Quantitative PCR Assay for Rapid Detection of Genetic Markers' Expression Associated with *Fusarium* Wilt of Banana Biocontrol Activities in *Bacillus*. *J Fungi 7*, Accession Number: 33946404. https://doi.org/10.3390/jof7050353

Lim, Hou, Y., Chen, Y., Oh, J. H., Lee, I., Bugni, T. S., & Keller, N. P. (2012). Genome-based cluster deletion reveals an endocrocin biosynthetic pathway in *Aspergillus fumigatus*. *Appl Environ Microbiol 78*, 4117-4125. https://doi.org/10.1128/aem.07710-11

Lindow, S. E., & Brandl, M. T. (2003). Microbiology of the phyllosphere. *Appl Environ Microbiol 69*, 1875-1883. https://doi.org/10.1128/aem.69.4.1875-1883.2003

Liu, Y., Du, M., & Zhang, G. (2014). Proapoptotic activity of aflatoxin B(1) and sterigmatocystin in HepG2 cells. *Toxicol Rep 1*, 1076-1086. https://doi.org/10.1016/j.toxrep.2014.10.016

Liu, Y., Štefanič, P., Miao, Y., Xue, Y., Xun, W., Zhang, N., Shen, Q., Zhang, R., Xu, Z., & Mandic-Mulec, I. (2022). Housekeeping gene *gyrA*, a potential molecular marker for *Bacillus* ecology study. *AMB Express 12*, 133. https://doi.org/10.1186/s13568-022-01477-9

Livak, K. J., & Schmittgen, T. D. (2001). Analysis of relative gene expression data using real-time quantitative PCR and the 2(-Delta Delta C(T)) Method. *Methods 25*, 402-408. https://doi.org/10.1006/meth.2001.1262

Loehrer, M., Botterweck, J., Jahnke, J., Mahlmann, D. M., Gaetgens, J., Oldiges, M., Horbach, R., Deising, H., & Schaffrath, U. (2014). In vivo assessment by Mach-Zehnder double-beam interferometry of the invasive force exerted by the Asian soybean rust fungus (*Phakopsora pachyrhizi*). *New Phytol 203*, 620-631. https://doi.org/10.1111/nph.12784

Lozano, G. L., Park, H. B., Bravo, J. I., Armstrong, E. A., Denu, J. M., Stabb, E. V., Broderick, N. A., Crawford, J. M., & Handelsman, J. (2019). Bacterial Analogs of Plant Tetrahydropyridine Alkaloids Mediate Microbial Interactions in a Rhizosphere Model System. *Appl Environ Microbiol 85*, Accession Number: 30877115. https://doi.org/10.1128/aem.03058-18

Ludwig, N., Löhrer, M., Hempel, M., Mathea, S., Schliebner, I., Menzel, M., Kiesow, A., Schaffrath, U., Deising, H. B., & Horbach, R. (2014). Melanin is not required for turgor generation but enhances cell-wall rigidity in appressoria of the corn pathogen *Colletotrichum graminicola*. *Mol Plant Microbe Interact 27*, 315-327. https://doi.org/10.1094/mpmi-09-13-0267-r

Luo, A., Qiao, H., Zhang, Y., Shi, W., Ho, S. Y., Xu, W., Zhang, A., & Zhu, C. (2010). Performance of criteria for selecting evolutionary models in phylogenetics: a comprehensive study based on simulated datasets. *BMC Evol Biol 10*, 242. https://doi.org/10.1186/1471-2148-10-242

Macheleidt, J., Mattern, D. J., Fischer, J., Netzker, T., Weber, J., Schroeckh, V., Valiante, V., & Brakhage, A. A. (2016). Regulation and Role of Fungal Secondary Metabolites. *Annu Rev Genet 50*, 371-392. https://doi.org/10.1146/annurev-genet-120215-035203

Madariaga-Mazón, A., Hernández-Alvarado, R. B., Noriega-Colima, K. O., Osnaya-Hernández, A., & Martinez-Mayorga, K. (2019). Toxicity of secondary metabolites. *Phys Sci Rev 4*, 1-11. https://doi.org/doi:10.1515/psr-2018-0116

Maksimov, I. V., Blagova, D. K., Veselova, S. V., Sorokan, A. V., Burkhanova, G. F., Cherepanova, E. A., Sarvarova, E. R., Rumyantsev, S. D., Alekseev, V. Y., & Khayrullin, R. M. (2020). Recombinant *Bacillus subtilis* 26DCryChS line with gene *Btcry1Ia* encoding Cry1Ia toxin from *Bacillus thuringiensis* promotes integrated wheat defense against pathogen *Stagonospora nodorum* Berk. and greenbug *Schizaphis graminum* Rond. *Biol Control 144*, 104242. https://doi.org/10.1016/j.biocontrol.2020.104242

Mansouri, A., Cregut, M., Abbes, C., Durand, M. J., Landoulsi, A., & Thouand, G. (2017). The Environmental Issues of DDT Pollution and Bioremediation: a Multidisciplinary Review. *Appl Biochem Biotechnol 181*, 309-339. https://doi.org/10.1007/s12010-016-2214-5

Maqbool, M. A., Beshir Issa, A., Khokhar, E. S., & Tuberosa, R. (2021). Quality protein maize (QPM): Importance, genetics, timeline of different events, breeding strategies and varietal adoption. *Plant Breed 140*, 375-399. https://doi.org/10.1111/pbr.12923

Marx-Stoelting, P., Knebel, C., & Braeuning, A. (2020). The Connection of Azole Fungicides with Xeno-Sensing Nuclear Receptors, Drug Metabolism and Hepatotoxicity. *Cells 9*, Accession Number: 32403288. https://doi.org/10.3390/cells9051192

Mattupalli, C., Spraker, J. E., Berthier, E., Charkowski, A. O., Keller, N. P., & Shepherd, R. W. (2014). A microfluidic assay for identifying differential responses of plant and human fungal pathogens to tobacco phylloplanins. *Plant Health Prog 15*, 130-134. https://doi.org/10.1094/PHP-RS-14-0009

McCallan, S. E. A. (1949). The nature of the fungicidal action of copper and sulfur. *Bot Rev 15*, 629-643. https://doi.org/10.1007/BF02861716

Medema, M. H., Blin, K., Cimermancic, P., de Jager, V., Zakrzewski, P., Fischbach, M. A., Weber, T., Takano, E., & Breitling, R. (2011). antiSMASH: rapid identification, annotation and analysis of secondary metabolite biosynthesis gene clusters in bacterial and fungal genome sequences. *Nucleic Acids Res 39*, W339-W346. https://doi.org/10.1093/nar/gkr466

Meena, S., & Nirupma, S. (2021). The Impact of Climate Change on Changing Pattern of Maize Diseases in Indian Subcontinent: A Review. In E.-E. Mohamed Ahmed (Ed.), *Maize Genetic Resources*. IntechOpen. https://doi.org/10.5772/intechopen.101053

Mela, F., Fritsche, K., de Boer, W., van Veen, J. A., de Graaff, L. H., van den Berg, M., & Leveau, J. H. J. (2011). Dual transcriptional profiling of a bacterial/fungal confrontation: *Collimonas fungivorans* versus *Aspergillus niger*. *ISME J 5*, 1494-1504. https://doi.org/10.1038/ismej.2011.29

Miedaner, T., & Juroszek, P. (2021). Global warming and increasing maize cultivation demand comprehensive efforts in disease and insect resistance breeding in north-western Europe. *Plant Pathol 70*, 1032-1046. https://doi.org/10.1111/ppa.13365

Monheit, J. E., Cowan, D. F., & Moore, D. G. (1984). Rapid detection of fungi in tissues using calcofluor white and fluorescence microscopy. *Arch Pathol Lab Med 108*, 616-618. (No DOI available)

Moree, W. J., Phelan, V. V., Wu, C. H., Bandeira, N., Cornett, D. S., Duggan, B. M., & Dorrestein, P. C. (2012). Interkingdom metabolic transformations captured by microbial imaging mass spectrometry. *Proc Natl Acad Sci USA 109*, 13811-13816. https://doi.org/10.1073/pnas.1206855109

Müller, M. E., Steier, I., Köppen, R., Siegel, D., Proske, M., Korn, U., & Koch, M. (2012). Cocultivation of phytopathogenic *Fusarium* and *Alternaria* strains affects fungal growth and mycotoxin production. *J Appl Microbiol 113*, 874-887. https://doi.org/10.1111/j.1365-2672.2012.05388.x

Munkvold, G. P., & Desjardins, A. E. (1997). Fumonisins in Maize: Can We Reduce Their Occurrence? *Plant Dis 81*, 556-565. https://doi.org/10.1094/pdis.1997.81.6.556

Murakami, S., Hayashi, N., Inomata, T., Kato, H., Hitora, Y., & Tsukamoto, S. (2020). Induction of secondary metabolite production by fungal co-culture of *Talaromyces pinophilus* and *Paraphaeosphaeria* sp. *J Nat Med 74*, 545-549. https://doi.org/10.1007/s11418-020-01400-1

National Toxicology Program. (2011). *Toxicology and carcinogenesis studies of tetralin* (*CAS No. 119-64-2*) *in F344/N rats and B6C3F1 mice and a toxicology study of tetralin in male NBR rats* (*Inhalation studies*). U.S. Department of Health and Human Services, Public Health Service, National Institutes of Health. https://ntp.niehs.nih.gov/ntp/htdocs/lt_rpts/tr582.pdf

Németh, Z., Kulcsár, L., Flipphi, M., Orosz, A., Aguilar-Pontes, M. V., de Vries, R. P., Karaffa, L., & Fekete, E. (2019). l-Arabinose induces d-galactose catabolism via the Leloir pathway in *Aspergillus nidulans*. *Fungal Genet Biol 123*, 53-59. https://doi.org/10.1016/j.fgb.2018.11.004

Netzker, T., Fischer, J., Weber, J., Mattern, D. J., König, C. C., Valiante, V., Schroeckh, V., & Brakhage, A. A. (2015). Microbial communication leading to the activation of silent fungal secondary metabolite gene clusters. *Front Microbiol 6*, 299. https://doi.org/10.3389/fmicb.2015.00299

Nicholson, R. L., & Moraes, W. B. (1980). Survival of *Colletotrichum graminicola*: importance of the spore matrix. *Phytopathology 70*, 255-261. https://doi.org/10.1094/Phyto-70-255

Nicholson, W. L., Munakata, N., Horneck, G., Melosh, H. J., & Setlow, P. (2000). Resistance of *Bacillus* endospores to extreme terrestrial and extraterrestrial environments. *Microbiol Mol Biol Rev 64*, 548-572. https://doi.org/10.1128/mmbr.64.3.548-572.2000

Noble, L. M., & Andrianopoulos, A. (2013). Reproductive competence: a recurrent logic module in eukaryotic development. *Proc R Soc B 280*, 20130819. https://doi.org/doi:10.1098/rspb.2013.0819

O'Connell, Thon, M. R., Hacquard, S., Amyotte, S. G., Kleemann, J., Torres, M. F., Damm, U., Buiate, E. A., Epstein, L., Alkan, N., Altmüller, J., Alvarado-Balderrama, L., Bauser, C. A., Becker, C., Birren, B. W., Chen, Z., Choi, J., Crouch, J. A., Duvick, J. P., Farman, Mark A., Gan, P., Heiman, D., Henrissat, B., Howard, R. J., Kabbage, M., Koch, C., Kracher, B., Kubo, Y., Law, A. D., Lebrun, M-H., Lee, Y-H., Miyara, I., Moore, N., Neumann, U., Nordström, K., Panaccione, D. G., Panstruga, R., Place, M., Proctor, R. H., Prusky, D., Rech, G., Reinhardt, R., Rollins, J. A., Rounsley, S., Schardl, C. L., Schwartz, D. C., Shenoy, N., Shirasu, K., Sikhakolli, U. R., Stüber, K., Sukno, S. A., Sweigard, J. A., Takano, Y., Takahara, H., Trail, F., van der Does, H. C., Voll, L. M., Will, I., Young, S., Zeng, Q., Zhang, J., Zhou, S., Dickman, M. B., Schulze-Lefert, P., Ver Loren van Themaat, E., Ma, L-J., Vaillancourt, L. J. (2012). Lifestyle transitions in plant pathogenic *Colletotrichum* fungi deciphered by genome and transcriptome analyses. *Nat Genet 44*, 1060-1065. https://doi.org/10.1038/ng.2372

O'Connell, R. J. (1991). Cytochemical analysis of infection structures of *Colletotrichum lindemuthianum* using fluorochrome-labelled lectins. *Physiol Mol Plant Pathol 39*, 189-200. https://doi.org/10.1016/0885-5765(91)90003-Z

Obadi, M., Qi, Y., & Xu, B. (2023). High-amylose maize starch: Structure, properties, modifications and industrial applications. *Carbohydr Polym 299*, 120185. https://doi.org/10.1016/j.carbpol.2022.120185

Oliveira-Garcia, E., & Deising, H. B. (2013). Infection structure-specific expression of β-1,3-glucan synthase is essential for pathogenicity of *Colletotrichum graminicola* and evasion of β-glucan-triggered immunity in maize. *Plant Cell 25*, 2356-2378. https://doi.org/10.1105/tpc.112.103499

Ongena, & Jacques. (2008). *Bacillus* lipopeptides: versatile weapons for plant disease biocontrol. *Trends Microbiol 16*, 115-125. https://doi.org/10.1016/j.tim.2007.12.009

Osbourn, A. (2010). Secondary metabolic gene clusters: evolutionary toolkits for chemical innovation. *Trends Genet 26*, 449-457. https://doi.org/10.1016/j.tig.2010.07.001

Pain, N. A., Green, J. R., Jones, G. L., & O'Connell, R. J. (1996). Composition and organisation of extracellular matrices around germ tubes and appressoria of *Colletotrichum lindemuthianum*. *Protoplasma 190*, 119-130. https://doi.org/10.1007/BF01281311

Partida-Martinez, L. P., & Hertweck, C. (2005). Pathogenic fungus harbours endosymbiotic bacteria for toxin production. *Nature 437*, 884-888. https://doi.org/10.1038/nature03997

Patti, G. J., Yanes, O., & Siuzdak, G. (2012). Innovation: Metabolomics: the apogee of the omics trilogy. *Nat Rev Mol Cell Biol 13*, 263-269. https://doi.org/10.1038/nrm3314

Perfect, S. E., O'Connell, R. J., Green, E. F., Doering-Saad, C., & Green, J. R. (1998). Expression cloning of a fungal proline-rich glycoprotein specific to the biotrophic interface formed in the *Colletotrichum*-bean interaction. *Plant J 15*, 273-279. https://doi.org/10.1046/j.1365-313x.1998.00196.x

Perpetua, N. S., Kubo, Y., Yasuda, N., Takano, Y., & Furusawa, I. (1996). Cloning and characterization of a melanin biosynthetic *THR1* reductase gene essential for appressorial penetration of *Colletotrichum lagenarium*. *Mol Plant Microbe Interact 9*, 323-329. https://doi.org/10.1094/mpmi-9-0323

Petit, A. N., Fontaine, F., Vatsa, P., Clément, C., & Vaillant-Gaveau, N. (2012). Fungicide impacts on photosynthesis in crop plants. *Photosynth Res 111*, 315-326. https://doi.org/10.1007/s11120-012-9719-8

Pfeiffer, E., Fleck, S. C., & Metzler, M. (2014). Catechol formation: a novel pathway in the metabolism of sterigmatocystin and 11-methoxysterigmatocystin. *Chem Res Toxicol 27*, 2093-2099. https://doi.org/10.1021/tx500308k

Pfeiffer, T., von Galen, A., Zink, P., Hübner, S., Linkies, A., Felgentreu, D., Drechsel, J., Birr, T., Röder, O., Kotte, M., Dietel, K., Junge, H., Schwarz, E., & Koch, E. (2021). Selection of bacteria and fungi for control of soilborne seedling diseases of maize. *J Plant Dis Prot 128*, 1227-1241. https://doi.org/10.1007/s41348-021-00498-z

Pickova, D., Ostry, V., Toman, J., & Malir, F. (2021). Aflatoxins: History, Significant Milestones, Recent Data on Their Toxicity and Ways to Mitigation. *Toxins 13*, Accession Number: 34205163. https://doi.org/10.3390/toxins13060399

Pinar, M., Arias-Palomo, E., de Los Ríos, V., Arst, H. N., Jr., & Peñalva, M. A. (2019). Characterization of *Aspergillus nidulans* TRAPPs uncovers unprecedented similarities between fungi and metazoans and reveals the modular assembly of TRAPPII. *PLoS Genet 15*, e1008557. https://doi.org/10.1371/journal.pgen.1008557

Poeschl, Y., Grosse, I., & Gogol-Döring, A. (2014). Explaining gene responses by linear modeling. *German Conference on Bioinformatics* P-235, 27-35. https://dl.gi.de/items/22b35a8c-f8f6-407d-9026-9d2669e2ee9f

Pontecorvo, G., Roper, J. A., Hemmons, L. M., Macdonald, K. D., & Bufton, A. W. (1953). The genetics of *Aspergillus nidulans*. *Adv Genet 5*, 141-238. https://doi.org/10.1016/s0065-2660(08)60408-3

Probst, C., Njapau, H., & Cotty, P. J. (2007). Outbreak of an acute aflatoxicosis in Kenya in 2004: identification of the causal agent. *Appl Environ Microbiol 73*, 2762-2764. https://doi.org/10.1128/aem.02370-06

Punt, P. J., Oliver, R. P., Dingemanse, M. A., Pouwels, P. H., & van den Hondel, C. A. (1987). Transformation of *Aspergillus* based on the hygromycin B resistance marker from *Escherichia coli*. *Gene 56*, 117-124. https://doi.org/10.1016/0378-1119(87)90164-8

Rachid, R. (2010). Introduction and Toxicology of Fungicides. In C. Odile (Ed.), *Fungicides*, 364-382. IntechOpen. https://doi.org/10.5772/12967

Ráduly, Z., Szabó, L., Madar, A., Pócsi, I., & Csernoch, L. (2020). Toxicological and Medical Aspects of *Aspergillus*-Derived Mycotoxins Entering the Feed and Food Chain. *Front Microbiol 10*, Accession Number: 31998250. https://doi.org/10.3389/fmicb.2019.02908

Rambaut, A. (2010). FigTree v1. 3.1. Institute of Evolutionary Biology, University of Edinburgh. http://tree.bio.ed.ac.uk/software/figtree/ (COMPUTER SOFTWARE)

Raudvere, U., Kolberg, L., Kuzmin, I., Arak, T., Adler, P., Peterson, H., & Vilo, J. (2019). g:Profiler: a web server for functional enrichment analysis and conversions of gene lists. *Nucleic Acids Res 47*, W191-W198. https://doi.org/10.1093/nar/gkz369

RCoreTeam. (2022). *R: A Language and Environment for Statistical Computing*. R Foundation for Statistical Computing. https://www.r-project.org/ (COMPUTER SOFTWARE)

Reino, J. L., Guerrero, R. F., Hernández-Galán, R., & Collado, I. G. (2008). Secondary metabolites from species of the biocontrol agent *Trichoderma*. *Phytochem Rev 7*, 89-123. https://doi.org/10.1007/s11101-006-9032-2

Robey, M. T., Caesar, L. K., Drott, M. T., Keller, N. P., & Kelleher, N. L. (2021). An interpreted atlas of biosynthetic gene clusters from 1,000 fungal genomes. *Proc Natl Acad Sci USA 118*, e2020230118. https://doi.org/doi:10.1073/pnas.2020230118

Rogerio, F., Taati, A., Garcia-Rodriguez, P., Baroncelli, R., Thon, M. R., Santiago, R., Revilla, P., & Sukno, S. A. (2023). First Report of *Colletotrichum graminicola* Causing Maize Anthracnose in Galicia, Northwestern Spain. *Plant Dis 107*, Accession Number: 37208822. https://doi.org/10.1094/PDIS-04-23-0729-PDN

Ruiz-García, C., Béjar, V., Martínez-Checa, F., Llamas, I., & Quesada, E. (2005). *Bacillus velezensis* sp. nov., a surfactant-producing bacterium isolated from the river Vélez in Málaga, southern Spain. *Int J Syst Evol Microbiol 55*, 191-195. https://doi.org/10.1099/ijs.0.63310-0

Ruiz, M. J., Franzova, P., Juan-García, A., & Font, G. (2011). Toxicological interactions between the mycotoxins beauvericin, deoxynivalenol and T-2 toxin in CHO-K1 cells in vitro. *Toxicon 58*, 315-326. https://doi.org/10.1016/j.toxicon.2011.07.015

Russell, P. E. (2005). A century of fungicide evolution. *J Agric Sci 143*, 11-25. https://doi.org/10.1017/S0021859605004971

Rutledge, R. G. (2004). Sigmoidal curve-fitting redefines quantitative real-time PCR with the prospective of developing automated high-throughput applications. *Nucleic Acids Res 32*, e178. https://doi.org/10.1093/nar/gnh177

Sawada, Y., Nakabayashi, R., Yamada, Y., Suzuki, M., Sato, M., Sakata, A., Akiyama, K., Sakurai, T., Matsuda, F., Aoki, T., Hirai, M. Y., & Saito, K. (2012). RIKEN tandem mass spectral database (ReSpect) for phytochemicals: A plant-specific MS/MS-based data resource and database. *Phytochemistry 82*, 38-45. https://doi.org/10.1016/j.phytochem.2012.07.007

Scariot, F. J., Jahn, L. M., Maianti, J. P., Delamare, A. P., & Echeverrigaray, S. (2016). The fungicide Mancozeb induces metacaspase-dependent apoptotic cell death in *Saccharomyces cerevisiae* BY4741. *Apoptosis 21*, 866-872. https://doi.org/10.1007/s10495-016-1251-4

Schaechter, M. (2009). *Encyclopedia of microbiology*. In M. Schaechter (Ed.), Academic Press. https://books.google.de/books/about/Encyclopedia_of_Microbiology.html?id=rLhdW5YzuO4C&redir_esc=y

Schaeffer, A. B., & Fulton, M. D. (1933). A Simplified Method of Staining Endospores. *Science 77*, 194. https://doi.org/doi:10.1126/science.77.1990.194

Scherlach, K., & Hertweck, C. (2009). Triggering cryptic natural product biosynthesis in microorganisms. *Org Biomol Chem 7*, 1753-1760. https://doi.org/10.1039/B821578B

Schiewe, A., & Mendgen, K. (1992). Identification of Antagonists for Biological Control of the Post-Harvest Pathogens *Pezicula malicorticis* and *Nectria galligena* on Apples. *J Phytopat 134*, 229-237. https://doi.org/10.1111/j.1439-0434.1992.tb01231.x

Schönig, B., Brown, D. W., Oeser, B., & Tudzynski, B. (2008). Cross-Species Hybridization with *Fusarium verticillioides* Microarrays Reveals New Insights into *Fusarium fujikuroi* Nitrogen Regulation and the Role of AreA and NMR. *Eukaryotic Cell 7*, 1831-1846. https://doi.org/doi:10.1128/ec.00130-08

Schroeckh, V., Scherlach, K., Nützmann, H.-W., Shelest, E., Schmidt-Heck, W., Schuemann, J., Martin, K., Hertweck, C., & Brakhage, A. A. (2009). Intimate bacterial-fungal interaction triggers biosynthesis of archetypal polyketides in *Aspergillus nidulans*. *Proc Natl Acad Sci USA 106*, 14558-14563. https://doi.org/doi:10.1073/pnas.0901870106

Sella, S. R. B. R., Vandenberghe, L. P. S., & Soccol, C. R. (2014). Life cycle and spore resistance of spore-forming *Bacillus atrophaeus*. *Microbiol Res 169*, 931-939. https://doi.org/10.1016/j.micres.2014.05.001

Serrão, C. P., Ortega, J. C. G., Rodrigues, P. C., & de Souza, C. R. B. (2024). *Bacillus* species as tools for biocontrol of plant diseases: A meta-analysis of twenty-two years of research, 2000–2021. *World J Microbiol Biotechnol 40*, 110. https://doi.org/10.1007/s11274-024-03935-x

Shahaf, N., Rogachev, I., Heinig, U., Meir, S., Malitsky, S., Battat, M., Wyner, H., Zheng, S., Wehrens, R., & Aharoni, A. (2016). The WEIZMASS spectral library for high-confidence metabolite identification. *Nat Commun 7*, 12423. https://doi.org/10.1038/ncomms12423

Shen, B. (2003). Polyketide biosynthesis beyond the type I, II and III polyketide synthase paradigms. *Curr Opin Chem Biol 7*, 285-295. https://doi.org/10.1016/s1367-5931(03)00020-6

Shen, H., Dührkop, K., Böcker, S., & Rousu, J. (2014). Metabolite identification through multiple kernel learning on fragmentation trees. *Bioinformatics 30*, i157-164. https://doi.org/10.1093/bioinformatics/btu275

Siddiqui, F. A., & Bussey, H. (1981). Radioimmunoassay for yeast killer toxin from *Saccharomyces cerevisiae*. *Can J Microbiol 27*, 847-849. https://doi.org/10.1139/m81-132

Sievert, C. (2020). *Interactive web-based data visualization with R, plotly, and shiny*. CRC Press. https://doi.org/10.1201/9780429447273

Silva, T. S., da Fonseca, L. F., Yamada, J. K., & Pontes, N. d. C. (2021). Flutriafol and azoxystrobin: An efficient combination to control fungal leaf diseases in corn crops. *Crop Prot 140*, Accession Number: 105394. https://doi.org/10.1016/j.cropro.2020.105394

Singh, V. K., Singh, R., Kumar, A., & Bhadouria, R. (2021). Chapter 2 - Current status of plant diseases and food security. In A. Kumar & S. Droby (Eds.), *Food Security and Plant Disease Management*, 19-35. Woodhead Publishing. https://doi.org/10.1016/B978-0-12-821843-3.00019-2

Skidmore, A. M., & Dickinson, C. H. (1976). Colony interactions and hyphal interference between *Septoria nodorum* and phylloplane fungi. *Trans Br Mycol Soc 66*, 57-64. https://doi.org/10.1016/S0007-1536(76)80092-7

Sluyter, A., & Dominguez, G. (2006). Early maize (*Zea mays* L.) cultivation in Mexico: Dating sedimentary pollen records and its implications. *Proc Natl Acad Sci 103*, 1147-1151. https://doi.org/doi:10.1073/pnas.0510473103

Smart, N. A. (2003). Fungicides. In B. Caballero (Ed.), *Encyclopedia of Food Sciences and Nutrition*, 2832-2842. Academic Press. https://doi.org/10.1016/B0-12-227055-X/00543-5

Soares, M. V., Viçozzi, G. P., Kuhn, E. C., Weishaupt, A.-K., Kubens, L., Bornhorst, J., & Avila, D. S. (2023). Chapter Five - Neurotoxicology of organic environmental toxicants using *Caenorhabditis elegans* as a model. In J. Batista Rocha, M. Aschner, & L. G. Costa (Eds.), *Advances in Neurotoxicology*, 149-180. Academic Press. https://doi.org/10.1016/bs.ant.2023.03.003

Son, Y. E., Yu, J. H., & Park, H. S. (2023). Regulators of the Asexual Life Cycle of *Aspergillus nidulans*. *Cells 12*, 1544. https://doi.org/10.3390/cells12111544

Soukup, A. A., Chiang, Y. M., Bok, J. W., Reyes-Dominguez, Y., Oakley, B. R., Wang, C. C., Strauss, J., & Keller, N. P. (2012). Overexpression of the *Aspergillus nidulans* histone 4 acetyltransferase EsaA increases activation of secondary metabolite production. *Mol Microbiol 86*, 314-330. https://doi.org/10.1111/j.1365-2958.2012.08195.x

Spraker, J. E., Sanchez, L. M., Lowe, T. M., Dorrestein, P. C., & Keller, N. P. (2016). *Ralstonia solanacearum* lipopeptide induces chlamydospore development in fungi and facilitates bacterial entry into fungal tissues. *ISME J 10*, 2317-2330. https://doi.org/10.1038/ismej.2016.32

Stein, T. (2005). *Bacillus subtilis* antibiotics: structures, syntheses and specific functions. *Mol Microbiol 56*, 845-857. https://doi.org/10.1111/j.1365-2958.2005.04587.x

Stringer, M. A., Dean, R. A., Sewall, T. C., & Timberlake, W. E. (1991). Rodletless, a new *Aspergillus* developmental mutant induced by directed gene inactivation. *Genes Dev 5*, 1161-1171. https://doi.org/10.1101/gad.5.7.1161

Sukno, S. A., Garcia, V. M., Shaw, B. D., & Thon, M. R. (2008). Root infection and systemic colonization of maize by *Colletotrichum graminicola*. *Appl Environ Microbiol 74*, 823-832. https://doi.org/10.1128/AEM.01165-07

Sun, L., Li, R., Tai, B., Hussain, S., Wang, G., Liu, X., & Xing, F. (2023). Current Status of Major Mycotoxins Contamination in Food and Feed in Asia - A Review. *ACS Food Sci Technol 3*, 231-244. https://doi.org/10.1021/acsfoodscitech.2c00331

Sun, Y., Liu, W.-C., Shi, X., Zheng, H.-Z., Zheng, Z.-H., Lu, X.-H., Xing, Y., Ji, K., Liu, M., & Dong, Y.-S. (2021). Inducing secondary metabolite production of *Aspergillus sydowii* through microbial co-culture with *Bacillus subtilis*. *Microb Cell Fact 20*, 42. https://doi.org/10.1186/s12934-021-015270

Takeda, T., Suzuki, M., Kano, H., Matsumoto, M., & Umeda, Y. (2023). Clear evidence of the carcinogenic potential of anthracene: A 2-year feeding study in rats and mice. *Environ Toxicol 38*, 709-726. https://doi.org/10.1002/tox.23722

Tamm, L., Thuerig, B., Apostolov, S., Blogg, H., Borgo, E., Corneo, P. E., Fittje, S., de Palma, M., Donko, A., Experton, C., Alcázar Marín, É., Morell Pérez, Á., Pertot, I., Rasmussen, A., Steinshamn, H., Vetemaa, A., Willer, H., & Herforth-Rahmé, J. (2022). Use of Copper-Based Fungicides in Organic Agriculture in Twelve European Countries. *Agronomy 12*, 673. https://doi.org/10.3390/agronomy12030673

Tamura, K., Stecher, G., & Kumar, S. (2021). MEGA11: Molecular Evolutionary Genetics Analysis Version 11. *Mol Biol Evol 38*, 3022-3027. https://doi.org/10.1093/molbev/msab120

Tang, D., Chen, M., Huang, X., Zhang, G., Zeng, L., Zhang, G., Wu, S., & Wang, Y. (2023). SRplot: A free online platform for data visualization and graphing. *PLoS One 18*, e0294236. https://doi.org/10.1371/journal.pone.0294236

Tannous, J., Kumar, D., Sela, N., Sionov, E., Prusky, D., & Keller, N. P. (2018). Fungal attack and host defence pathways unveiled in near-avirulent interactions of *Penicillium expansum creA* mutants on apples. *Mol Plant Pathol 19*, 2635-2650. https://doi.org/10.1111/mpp.12734

Theumer, M. G., Henneb, Y., Khoury, L., Snini, S. P., Tadrist, S., Canlet, C., Puel, O., Oswald, I. P., & Audebert, M. (2018). Genotoxicity of aflatoxins and their precursors in human cells. *Toxicol Lett 287*, 100-107. https://doi.org/10.1016/j.toxlet.2018.02.007

Tian, Y., Yu, D., Liu, N., Tang, Y., Yan, Z., & Wu, A. (2020). Confrontation assays and mycotoxin treatment reveal antagonistic activities of *Trichoderma* and the fate of *Fusarium* mycotoxins in microbial interaction. *Environ Pollut 267*, 115559. https://doi.org/10.1016/j.envpol.2020.115559

Tong, P. Z., Zhang, G. J., Zhang, X. H., Yan, X., & Wang, J. L. (2013). Effects of sterigmatocystin on esophageal epithelium and experimental reflux esophagitis in rats. *Mol Med Rep 8*, 1043-1048. https://doi.org/10.3892/mmr.2013.1631

Trenner, J., Poeschl, Y., Grau, J., Gogol-Döring, A., Quint, M., & Delker, C. (2016). Auxin-induced expression divergence between *Arabidopsis* species may originate within the TIR1/AFB–AUX/IAA–ARF module. *J Exp Bot 68*, 539-552. https://doi.org/10.1093/jxb/erw457

Trösken, E. R., Fischer, K., Völkel, W., & Lutz, W. K. (2006). Inhibition of human CYP19 by azoles used as antifungal agents and aromatase inhibitors, using a new LC–MS/MS method for the analysis of estradiol product formation. *Toxicology 219*, 33-40. https://doi.org/10.1016/j.tox.2005.10.020

Turnbull, P. C. B. (1996). *Bacillus*. In S. Baron (Ed.), *Medical Microbiology*. University of Texas Medical Branch at Galveston. https://www.ncbi.nlm.nih.gov/books/NBK7627/

Tyndall, J. D. A., Sabherwal, M., Sagatova, A. A., Keniya, M. V., Negroni, J., Wilson, R. K., Woods, M. A., Tietjen, K., & Monk, B. C. (2016). Structural and Functional Elucidation of Yeast Lanosterol 14α-Demethylase in Complex with Agrochemical Antifungals. *PLoS One 11*, e0167485. https://doi.org/10.1371/journal.pone.0167485

Ushimaru, T., Terada, H., Tsuboi, K., Kogou, Y., Sakaguchi, A., Tsuji, G., & Kubo, Y. (2010). Development of an efficient gene targeting system in *Colletotrichum higginsianum* using a non-homologous end-joining mutant and *Agrobacterium tumefaciens*-mediated gene transfer. *Mol Genet Genomics 284*, 357-371. https://doi.org/10.1007/s00438-010-0572-1

Vida, T. A., & Emr, S. D. (1995). A new vital stain for visualizing vacuolar membrane dynamics and endocytosis in yeast. *J Cell Biol 128*, 779-792. https://doi.org/10.1083/jcb.128.5.779

Villa-Rodríguez, E., Ibarra-Gámez, C., & de los Santos-Villalobos, S. (2018). Extraction of high-quality RNA from *Bacillus subtilis* with a lysozyme pre-treatment followed by the Trizol method. *J Microbiol Methods 147*, 14-16. https://doi.org/10.1016/j.mimet.2018.02.011

Vorholt, J. A. (2012). Microbial life in the phyllosphere. *Nat Rev Microbiol 10*, 828-840. https://doi.org/10.1038/nrmicro2910

Voss, K. A., & Riley, R. T. (2013). Fumonisin Toxicity and Mechanism of Action: Overview and Current Perspectives. *Food Saf 1*, 2013006-2013006. https://doi.org/10.14252/foodsafetyfscj.2013006

Walsh, C. T. (2004). Polyketide and nonribosomal peptide antibiotics: modularity and versatility. *Science 303*, 1805-1810. https://doi.org/10.1126/science.1094318

Wang, J. S., Shen, X., He, X., Zhu, Y. R., Zhang, B. C., Wang, J. B., Qian, G. S., Kuang, S. Y., Zarba, A., Egner, P. A., Jacobson, L. P., Muñoz, A., Helzlsouer, K. J., Groopman, J. D., & Kensler, T. W. (1999). Protective alterations in phase 1 and 2 metabolism of aflatoxin B1 by oltipraz in residents of Qidong, People's Republic of China. *J Natl Cancer Inst 91*, 347-354. https://doi.org/10.1093/jnci/91.4.347

Wang, M., Carver, J. J., Phelan, V. V., Sanchez, L. M., Garg, N., Peng, Y., Nguyen, D. D., Watrous, J., Kapono, C. A., Luzzatto-Knaan, T., Porto, C., Bouslimani, A., Melnik, A. V., Meehan, M. J., Liu, W.-T., Crüsemann, M., Boudreau, P. D., Esquenazi, E., Sandoval-Calderón, M., Kersten, R. D., Pace, L. A., Quinn, R. A., Duncan, K. R., Hsu, C-C., Floros, D. J., Gavilan, R. G., Kleigrewe, K., Northen, T., Dutton, R. J., Parrot, D., Carlson, E. E., Aigle, B., Michelsen, C. F., Jelsbak, L., Sohlenkamp, C., Pevzner, P., Edlund, A., McLean, J., Piel, J. Murphy, B. T., Gerwick, L., Liaw, C-C., Yang, Y-L., Humpf, H-U., Maansson, M., Keyzers, R. A., Sims, A. C., Johnson, A. R., Sidebottom, A. M., Sedio, B. E., Klitgaard, A., Larson, C. B., Boya P, C. A., Torres-Mendoza, D., Gonzalez, D. J., Silva, D. B., Marques, L. M., Demarque, D. P., Pociute, E., O'Neill, E. C., Briand, E., Helfrich, E. J. N., Granatosky, E. A., Glukhov, E., Ryffel, F., Houson, H., Mohimani, H., Kharbush, J. J., Zeng, Y., Vorholt, J. A., Kurita, K. L., Charusanti, P., McPhail, K. L., Nielsen, K. F., Vuong, L., Elfeki, M., Traxler, M. F., Engene, N., Koyama, N., Vining, O. B., Baric, R., Silva, R. R., Mascuch, S. J., Tomasi, S., Jenkins, S., Macherla, V., Hoffman, T., Agarwal, V., Williams, P. G., Dai, J., Neupane, R., Gurr, J., Rodríguez, A. M. C., Lamsa, A., Zhang, C., Dorrestein, K., Duggan, B. M., Almaliti, J., Allard, P-M., Phapale, P., Nothias, L-F., Alexandrov, T., Litaudon, M., Wolfender, J-L., Kyle, J. E., Metz, T. O., Peryea, T., Nguyen, D-T., VanLeer, D., Shinn, P., Jadhav, A., Müller, R., Waters, K. M., Shi, W., Liu, X., Zhang, L., Knight, R., Jensen, P. R., Palsson, B. Ø., Pogliano, K., Linington, R. G., Gutiérrez, M., Lopes, N. P., Gerwick, W. H., Moore, B. S., Dorrestein, P. C., Bandeira, N. (2016). Sharing and community curation of mass spectrometry data with Global Natural Products Social Molecular Networking. *Nat Biotechnol 34*, 828-837. https://doi.org/10.1038/nbt.3597

Wang, Y., Zhang, C., Liang, J., Wu, L., Gao, W., & Jiang, J. (2020). Iturin A Extracted From *Bacillus subtilis* WL-2 Affects Phytophthora infestans via Cell Structure Disruption, Oxidative Stress, and Energy Supply Dysfunction. *Front Microbiol 11*, Accession Number: 33013776. https://doi.org/10.3389/fmicb.2020.536083

Wen, J., Mu, P., & Deng, Y. (2016). Mycotoxins: cytotoxicity and biotransformation in animal cells. *Toxicol Res 5*, 377-387. https://doi.org/10.1039/c5tx00293a

Werner, S., Sugui, J. A., Steinberg, G., & Deising, H. B. (2007). A chitin synthase with a myosin-like motor domain is essential for hyphal growth, appressorium differentiation, and pathogenicity of the maize anthracnose fungus *Colletotrichum graminicola*. *Mol Plant Microbe Interact 20*, 1555-1567. https://doi.org/10.1094/mpmi-20-12-1555

Wickham, H. (2016). *ggplot2: Elegant graphics for data analysis*. Springer. https://doi.org/10.1007/978-3-319-24277-4

Wolf, S., Schmidt, S., Müller-Hannemann, M., & Neumann, S. (2010). In silico fragmentation for computer assisted identification of metabolite mass spectra. *BMC Bioinformatics 11*, 148. https://doi.org/10.1186/1471-2105-11-148

Wolfender, J. L., Nuzillard, J. M., van der Hooft, J. J. J., Renault, J. H., & Bertrand, S. (2019). Accelerating Metabolite Identification in Natural Product Research: Toward an Ideal Combination of Liquid Chromatography-High-Resolution Tandem Mass Spectrometry and NMR Profiling, in Silico Databases, and Chemometrics. *Anal Chem 91*, 704-742. https://doi.org/10.1021/acs.analchem.8b05112

Wright, M. H., Adelskov, J., & Greene, A. C. (2017). Bacterial DNA Extraction Using Individual Enzymes and Phenol/Chloroform Separation. *J Microbiol Biol Educ 18*, Accession Number: 28861145. https://doi.org/10.1128/jmbe.v18i2.1348

Wu, F. (2014). Perspective: Time to face the fungal threat. *Nature 516*, S7. https://doi.org/10.1038/516S7a

Wu, Q.-H., Wang, X., Yang, W., Nüssler, A. K., Xiong, L.-Y., Kuča, K., Dohnal, V., Zhang, X.-J., & Yuan, Z.-H. (2014). Oxidative stress-mediated cytotoxicity and metabolism of T-2 toxin and deoxynivalenol in animals and humans: an update. *Arch Toxicol 88*, 1309-1326. https://doi.org/10.1007/s00204-014-1280-0

Xu, H., Wang, L., Sun, J., Wang, L., Guo, H., Ye, Y., & Sun, X. (2022). Microbial detoxification of mycotoxins in food and feed. *Crit Rev Food Sci Nutr 62*, 4951-4969. https://doi.org/10.1080/10408398.2021.1879730

Yin, W.-B., Amaike, S., Wohlbach, D. J., Gasch, A. P., Chiang, Y.-M., Wang, C. C. C., Bok, J. W., Rohlfs, M., & Keller, N. P. (2012). An *Aspergillus nidulans* bZIP response pathway hardwired for defensive secondary metabolism operates through *aflR*. *Mol Microbiol 83*, 1024-1034. https://doi.org/10.1111/j.1365-2958.2012.07986.x

Yin, W., & Keller, N. P. (2011). Transcriptional regulatory elements in fungal secondary metabolism. *J Microbiol 49*, 329-339. https://doi.org/10.1007/s12275-011-1009-1

Yu, J. H., Hamari, Z., Han, K. H., Seo, J. A., Reyes-Domínguez, Y., & Scazzocchio, C. (2004). Double-joint PCR: a PCR-based molecular tool for gene manipulations in filamentous fungi. *Fungal Genet Biol 41*, 973-981. https://doi.org/10.1016/j.fgb.2004.08.001

Zhang, Song, W., Nothias, L.-F., Couvillion, S. P., Webster, N., & Thomas, T. (2022). Comparative metabolomic analysis reveals shared and unique chemical interactions in sponge holobionts. *Microbiome 10*, 22. https://doi.org/10.1186/s40168-021-01220-9

Zhang, D., Qiang, R., Zhou, Z., Pan, Y., Yu, S., Yuan, W., Cheng, J., Wang, J., Zhao, D., Zhu, J., & Yang, Z. (2022). Biocontrol and Action Mechanism of *Bacillus subtilis* Lipopeptides' Fengycins Against

Alternaria solani in Potato as Assessed by a Transcriptome Analysis. *Front Microbiol 13*, 861113. https://doi.org/10.3389/fmicb.2022.861113

Zhgun, A. A. (2023). Fungal BGCs for Production of Secondary Metabolites: Main Types, Central Roles in Strain Improvement, and Regulation According to the Piano Principle. *Int J Mol Sci 24*, 11184. https://www.mdpi.com/1422-0067/24/13/11184

Zhu, F., Chen, G., Chen, X., Huang, M., & Wan, X. (2011). Aspergicin, a new antibacterial alkaloid produced by mixed fermentation of two marine-derived mangrove epiphytic fungi. *Chem Nat Compd 47*, 767-769. https://doi.org/10.1007/s10600-011-0053-8

Zhu, M., Duan, X., Cai, P., Zhang, W., Liu, Y., Cui, J., Li, Z., & Qiu, Z. (2022). Biocontrol action of *Trichothecium roseum* against the wheat powdery mildew fungus *Blumeria graminis* f. sp. *tritici*. *Front Sustain Food Syst 6*, 998830. https://doi.org/10.3389/fsufs.2022.998830

Zhu, Z., Peng, Q., Man, Y., Li, Z., Zhou, X., Bai, L., & Peng, D. (2020). Analysis of the Antifungal Properties of *Bacillus velezensis* B-4 Through a Bioassay and Complete-Genome Sequencing. *Front Genet 11*, Accession Number: 32765583. https://doi.org/10.3389/fgene.2020.00703

Zingales, V., Taroncher, M., Martino, P. A., Ruiz, M.-J., & Caloni, F. (2022). Climate Change and Effects on Molds and Mycotoxins. *Toxins 14*, 445. https://www.mdpi.com/2072-6651/14/7/445

7 Appendix

7.1 Supporting Figures

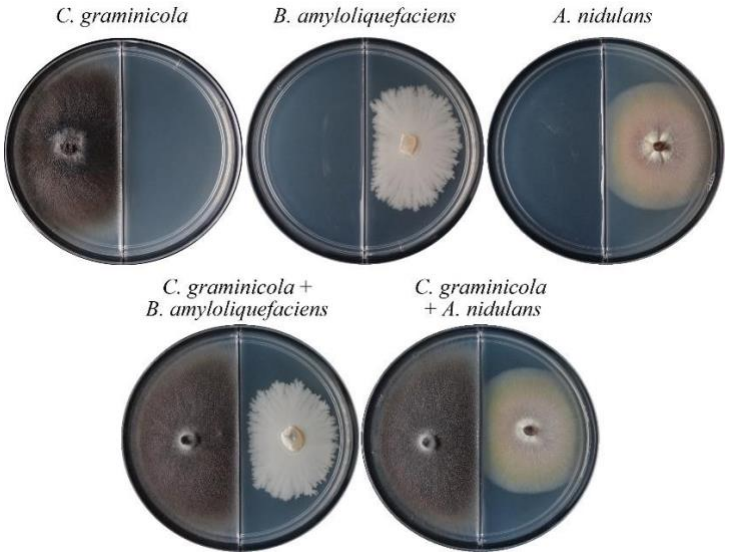

Supporting Figure S1. Split plate assays indicate that volatile organic compounds (VOCs) do not contribute to distance inhibition.

Note that colonies growing in monocultures in different compartments show comparable distances to the split as neighboring colonies separated the split.

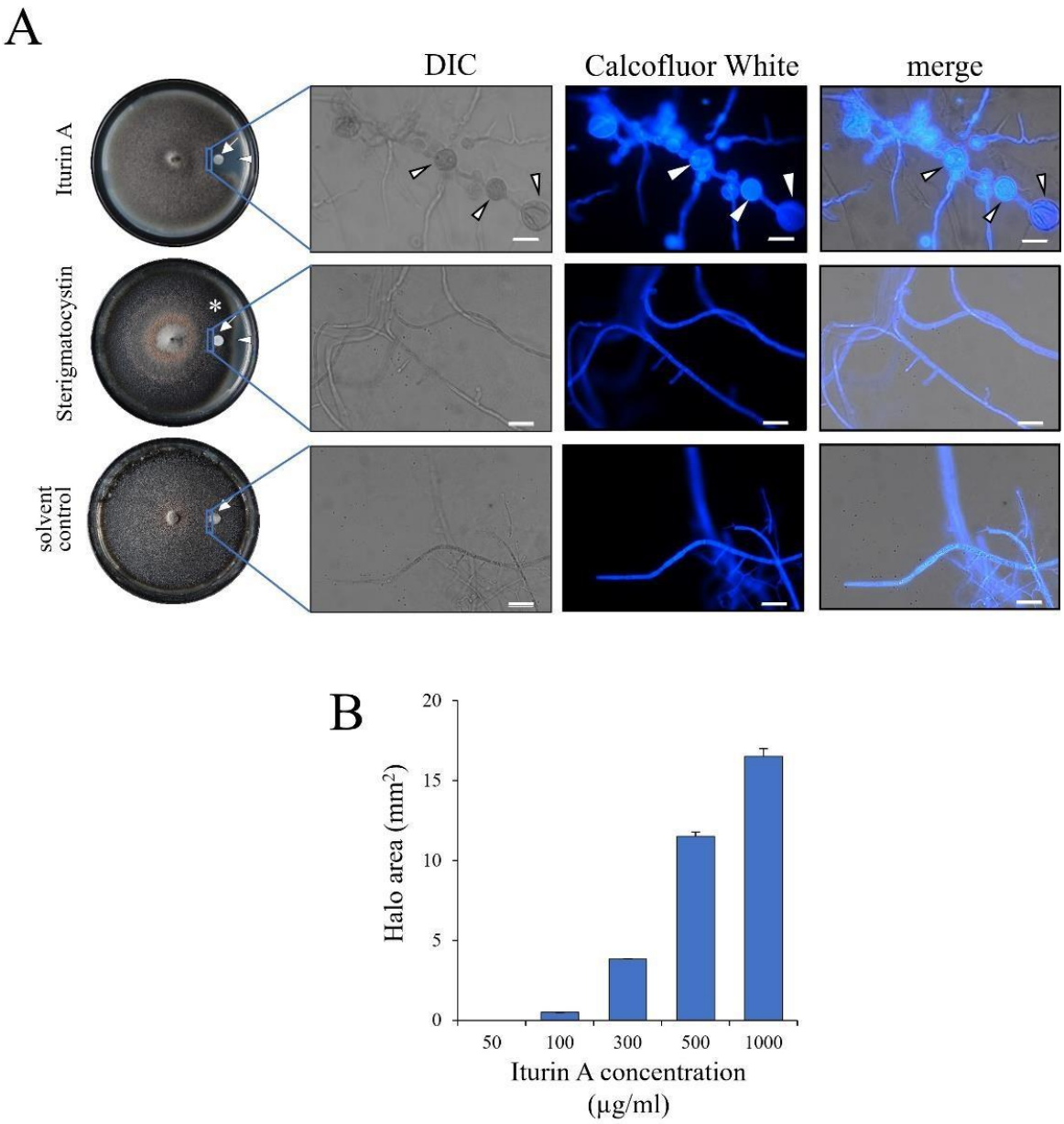

Supporting Figure S2. Growth inhibition of *C. graminicola* by Iturin A and Sterigmatocystin measured by Kirby-Bauer disc diffusion assays.

(A) Left panel Petri dishes with colonies of *C. graminicola* and a filter disc (arrow) containing Iturin A or Sterigmatocystin (1mg/mL). Ethanol and/or methanol acts as a solvent control. Arrowheads indicate inhibition zones. The asterisk indicates areas of reduced conidiation. Photographs were taken at 12 dpi. From the area marked by the rectangle, samples were taken for microscopy. Arrowheads in DIC, Calcofluor White and in merged micrographs indicate hyphal swellings. Scale bar corresponds to 50 µm. **(B)** Halo area indicative of hyphal growth inhibition increased with increasing Iturin A concentrations. Data is means of three independent biological replicates. Error bars are + SDs. CFW, Calcofluor White; DIC, Differential Interference Contrast.

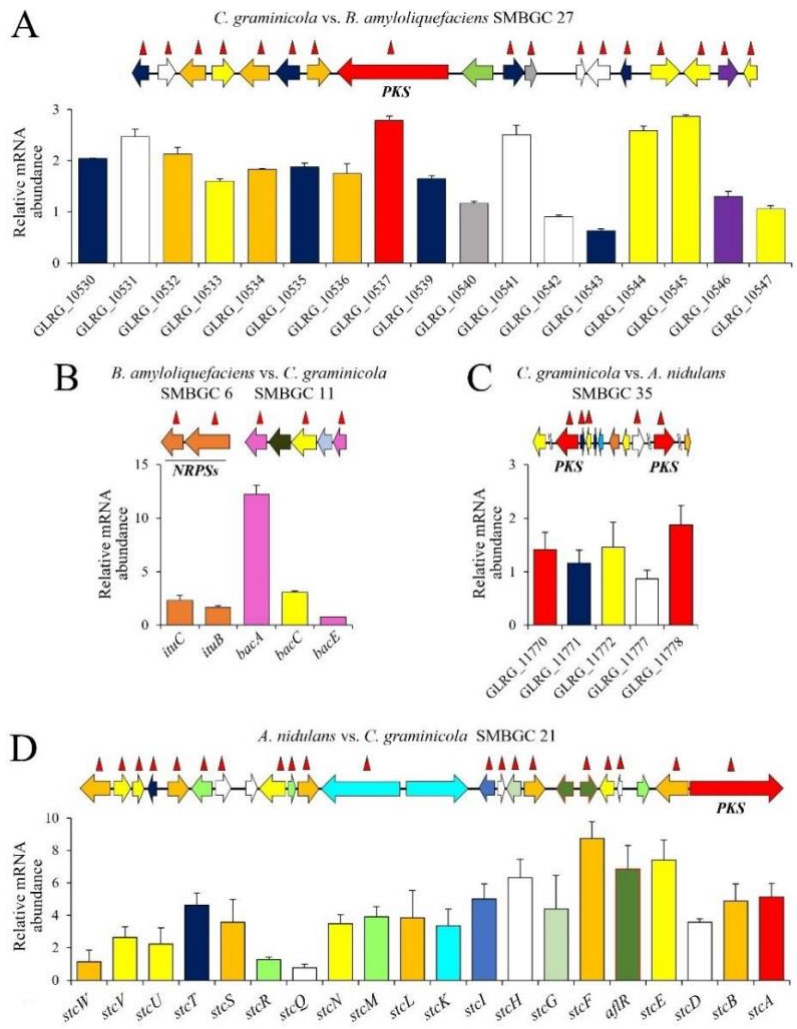

Supporting Figure S3. Validation of RNA-Seq data by RT-qPCR as an independent method.

(A) Seventeen genes of SMBGC 27 from *C. graminicola* showing increased transcript abundances in confrontation with *B. amyloliquefaciens* were validated by RT-qPCR. **(B)** As in RNA-Seq analyses, two iturin and three bacilysin genes of SMBGCs 6 and 11 in *B. amyloliquefaciens* showed increased transcript abundances in confrontation with *C. graminicola*. **(C)** Confirmation of increased transcript abundances of the five genes of SMBGC 35 of *C. graminicola* confronting *A. nidulans*. **(D)** Twenty out of 24 genes of the STC SMBGC 21 of *A. nidulans* exhibited increased transcript abundances also when analyzed by RT-qPCR. **(A, B, C, D** and **E)** The physical maps of the corresponding SMBGCs and genes with increased transcript abundances, as analyzed by RNA-Seq studies, are given above the respective bar plot. The constitutively expressed actin biosynthesis genes of *C. graminicola* and *A. nidulans*, as well as the *gyrA* of *B. amyloliquefaciens* served as standards. Data shown is mean of three independent biological replicates and three technical replicates. Error bars are + SDs. *ituc* and *ituB*, iturin genes; *bacA*, *bacC* and *bacE*, bacilysin genes; *stc*, sterigmatocystin; SMBGC, Secondary Metabolite Biosynthetic Gene Cluster, *PKS*, Polyketide Synthase; *NRPS*, Non-ribosomal Peptide Synthetase; mRNA, messenger RNA;

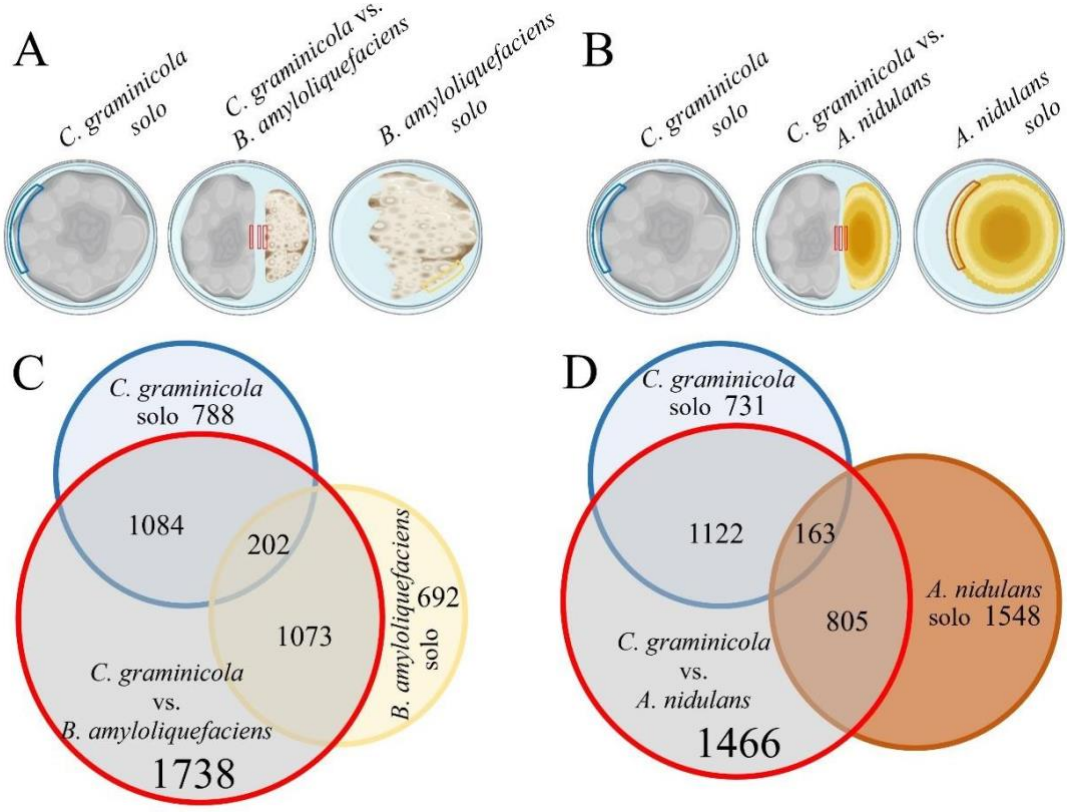

Supporting Figure S4. Sample collection for metabolome analyses and Venn diagram showing numbers of chemistries newly synthesized in distinct confrontations.

(A and **B)** Samples collected from 5 mm of the confronting culture margins and from the area between cultures lacking fungal or bacterial cells (red rectangles). Samples from margins of monocultures (blue, yellow and brown marked areas) served as controls. Blue and yellow areas denote the sample isolation spots in solo cultures, and red area in co-culture denotes the sample isolation from confrontation partners and inhibition zone. **(C** and **D)** Venn diagram showing 1,738 chemistries specifically synthesized in the confrontation between *C. graminicola* and *B. amyloliquefaciens*, and 1,466 in the *C. graminicola* vs. *A. nidulans* confrontation.

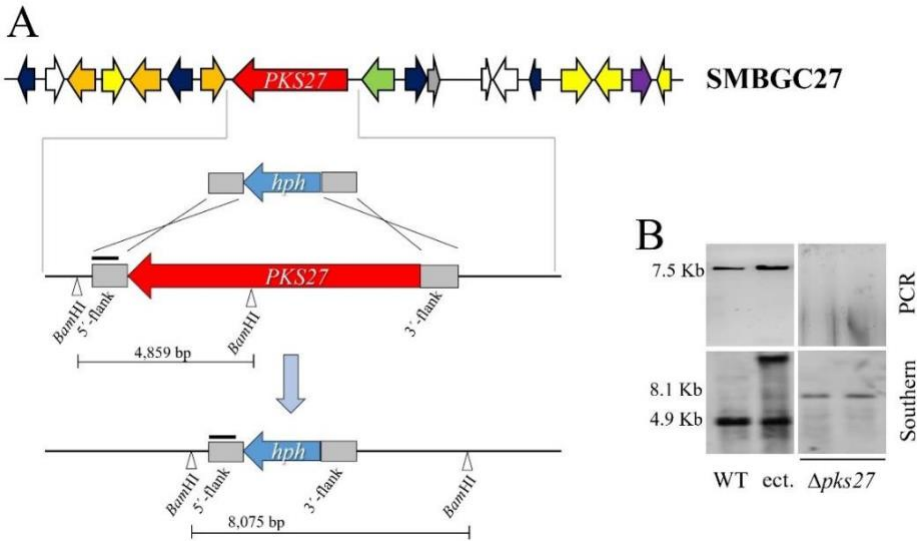

Supporting Figure S5. Targeted deletion of the core *PKS* gene of SMBGC 27 of *C. graminicola*.

The 5'- and 3'- flanks of *PKS27* and the hygromycin B resistance gene (*hph*) of *Escherichia coli* were PCR-amplified, ligated by DJ-PCR, and transformed into protoplasts of *C. graminicola*. Homologous recombination **(A)** resulted in replacement of *PKS27* by *hph* in two independent mutants, as confirmed by PCR and Southern blot analyses of *Bam*HI-digested DNA of WT, ect. and Δ*pks27* strains **(B)**. *PKS27*, Polyketide Synthase from SMBGC 27; *hph*, Hygromycin B phosphotransferase gene; WT, Wild type; ect., Ectopic; Δ*pks27*, Deletion mutants; SMBGC, Secondary Metabolite Biosynthetic Gene Cluster; PCR, Polymerase Chain Reaction; Southern, Southern blot;

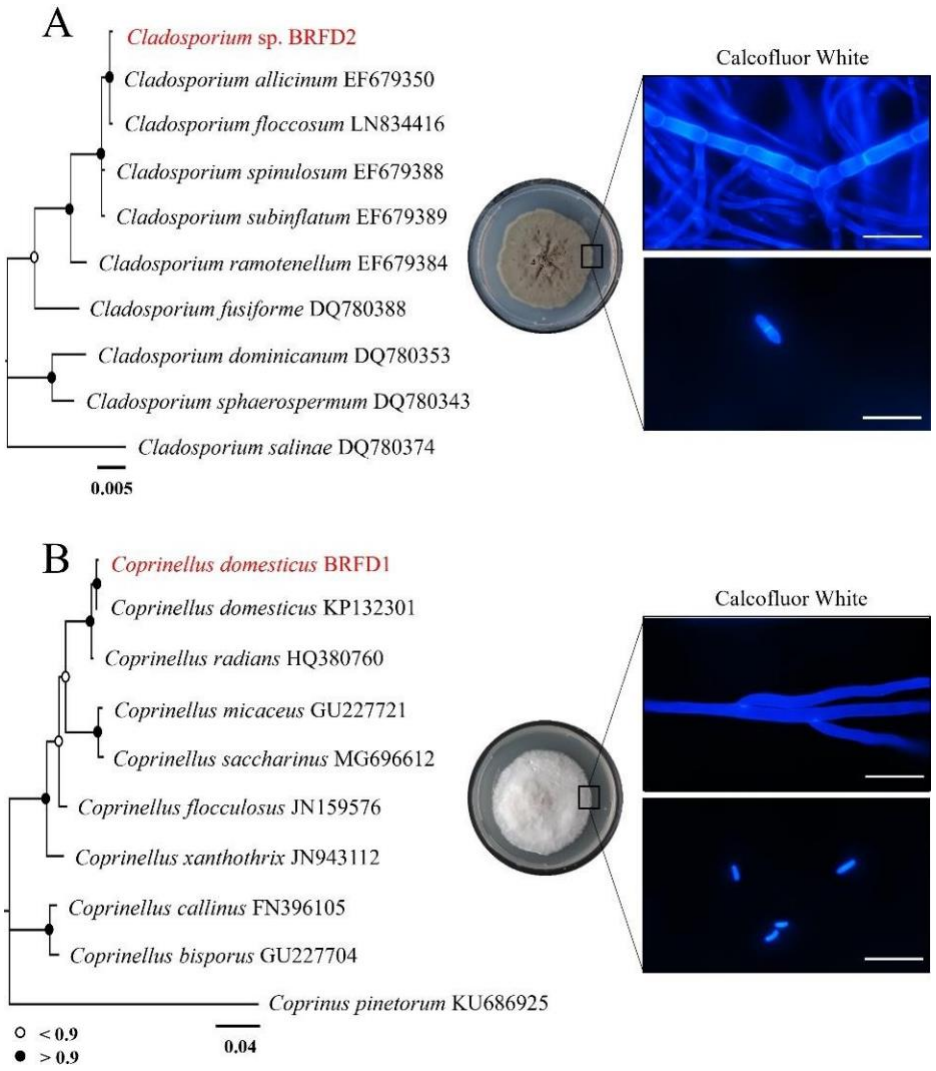

Supporting Figure S6. Phylogenetic analysis and morphological characterization of fungal isolates obtained from maize leaves.

(A) Phylogenetic tree of the *Cladosporium* sp. BRFD2 isolate based on the analysis of ITS sequences. The isolate clusters closely with *Cladosporium allicinum* EF679350 and *Cladosporium floccosum* LN834416, suggesting a close relationship with these species. *Cladosporium salinae* DQ780374 was used as an outgroup. Scale indicates 0.005 substitutions per site. **(B)** Phylogenetic tree of the *Coprinellus domesticus* BRFD1 isolate based on ITS sequence analysis. The isolate is closely related to *Coprinellus domesticus* KP132301, as indicated by the bootstrap values. *Coprinus pinetorum* KU686925 was used as an outgroup. Scale indicates 0.04 substitutions per site. **(A** and **B)** Filled and open circles in the phylogenetic trees indicate bootstrap values higher or lower than 90. *Cladosporium* sp. BRFD2 forms a dense colony with a greenish-gray and fluffy appearance, while *Coprinellus domesticus* BRFD1 forms a white, cottony, and velvet appearance in PDA 7dpi. Plates were photographed 7 dpi. The adjacent fluorescence microscopy images show Calcofluor white staining of hyphae (upper panels) and spores (lower panels), revealing the structural details of the fungal cell walls. Scale bars represent 50 µm.

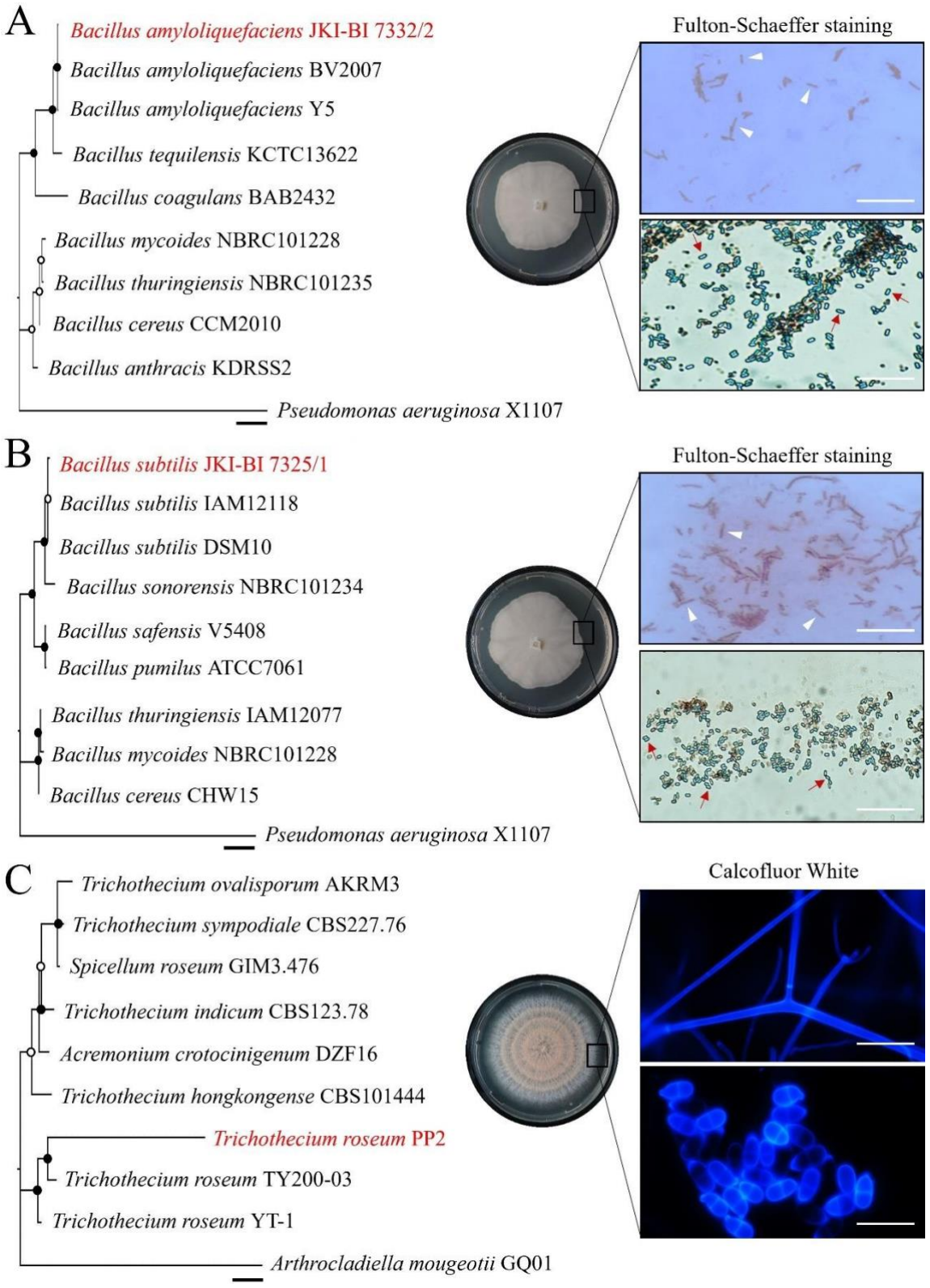

Supporting Figure S7. Phylogeny and morphological characterization of biocontrol bacterial and fungal strains employed in transcriptome assays.

(A and **B)** shows the phylogenetic trees based on 16S rRNA gene sequences of *B. amyloliquefaciens* JKI-BI 7332/2 and *B.subtilis* JKI-BI 7325/1, showing its close relationship to other *Bacillus* species. The outgroup was assigned to *P. aeruginosa*. **(A** and **B)** shows the morphological characterization of *B. amyloliquefaciens* and *B. subtilis* indicating the colony morphology on PDA 4dpi, while the microscopy panel shows a Schaeffer Fulton stain of the bacterial cells, highlighting the presence of vegetative cells (red stained; indicated by white arrowheads) and endospores (green stained; indicated by red arrows). Scale bars represent 50 µm. **(C)** Phylogenetic tree based on ITS region sequences of *T. roseum* ATCC 13412, showing its relationship with other *Trichothecium* species. *A. mougeotii* GQ01 is assigned as an outgroup. Morphological characterization of *T. roseum* with colony morphology shown on petri dish with PDA 7 dpi. The microscopy panel shows the calcofluor white staining of hyphae (upper) and spores (lower), highlighting the chitin-rich cell walls. Scale bars represent 50 µm. The Bootstrap values in **(A, B,** and **C)** are indicated by circles, with filled circles representing higher (< 0.9) and open circles representing lower support (< 0.9). Scale bar of phylogenetic tree represents 0.04 substitutions per site.

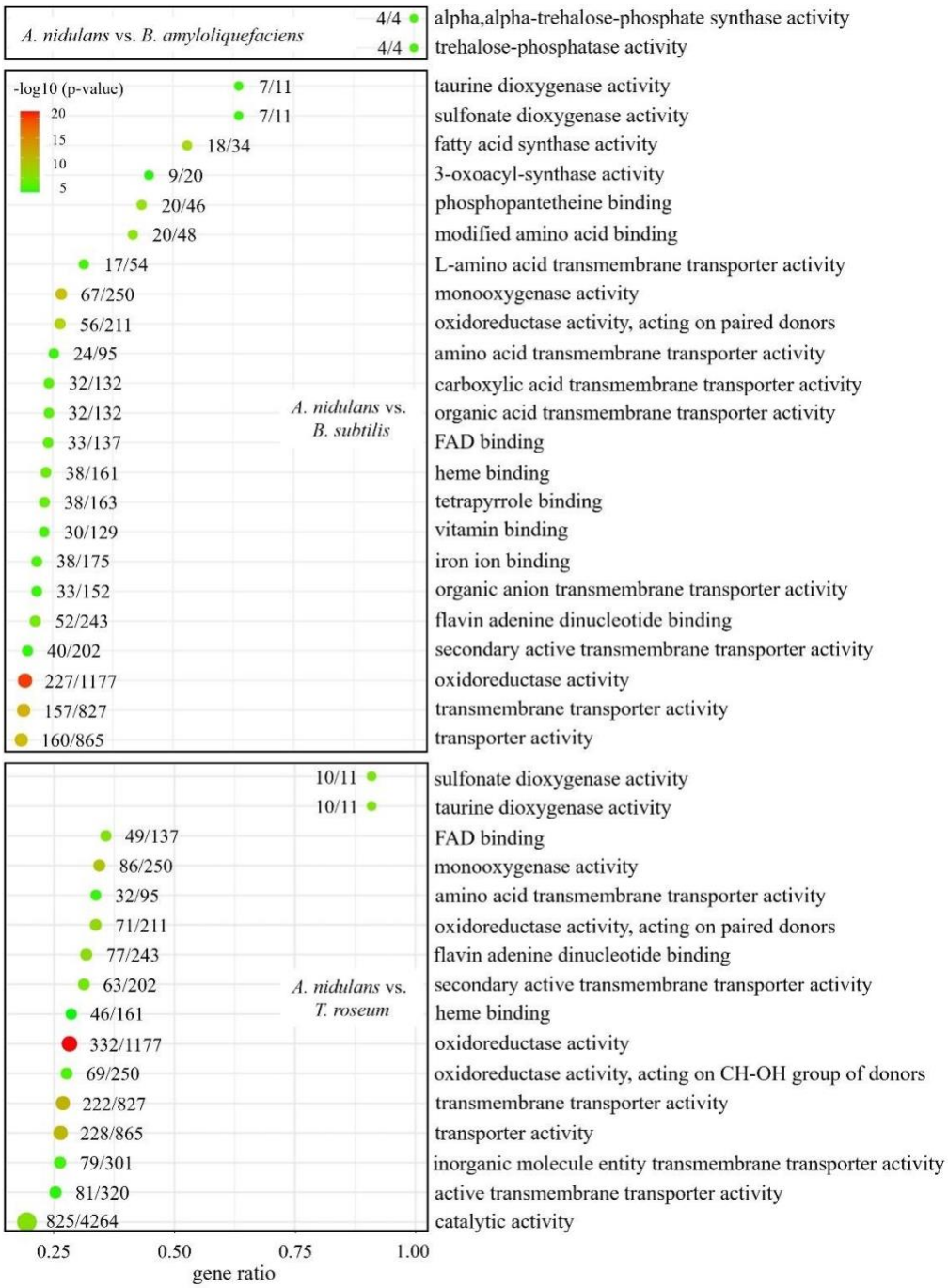

Supporting Figure S8. Functional enrichment analysis by GO of DEGs in *A. nidulans* against *B. amyloliquefaciens*, *B. subtilis*, and *T. roseum*.

Bubble plot depicting the GO terms for molecular function (MF) ranked by color codes based on the fold enrichment (adjusted $p < 0.05$). The X-axis indicates the gene ratio i.e. the ratio of DEGs to the total number of genes associated with a specific term. The size of each bubble indicates the number of DEGs corresponding to each GO term, while the color gradient reflects the significant level (-log 10 of the adjusted p-value). GO, Gene Ontology.

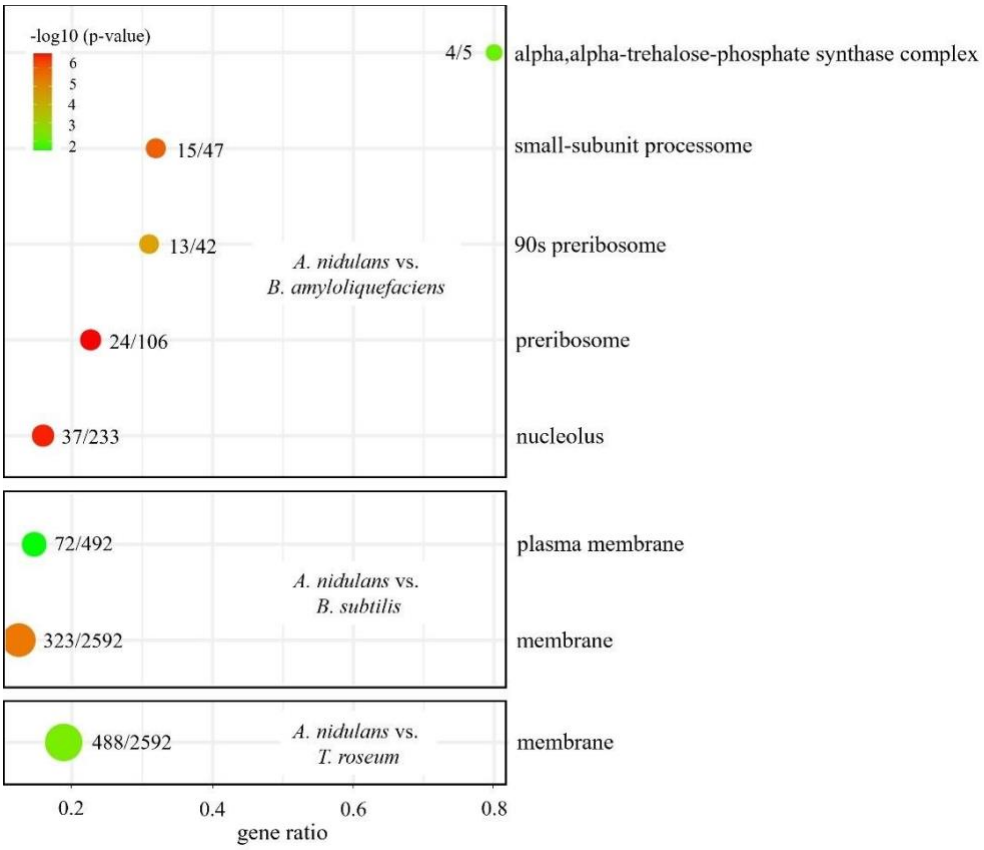

Supporting Figure S9. Functional enrichment analysis by GO of DEGs in *A. nidulans* against *B. amyloliquefaciens*, *B. subtilis*, and *T. roseum*.

Bubble plot depicting the GO terms for cellular component (CC) ranked by color codes based on the fold enrichment (adjusted $p < 0.05$). The X-axis indicates the gene ratio i.e. the ratio of DEGs to the total number of genes associated with a specific term. The size of each bubble indicates the number of DEGs corresponding to each GO term, while the color gradient reflects the significant level (-log 10 of the adjusted p-value). GO, Gene Ontology.

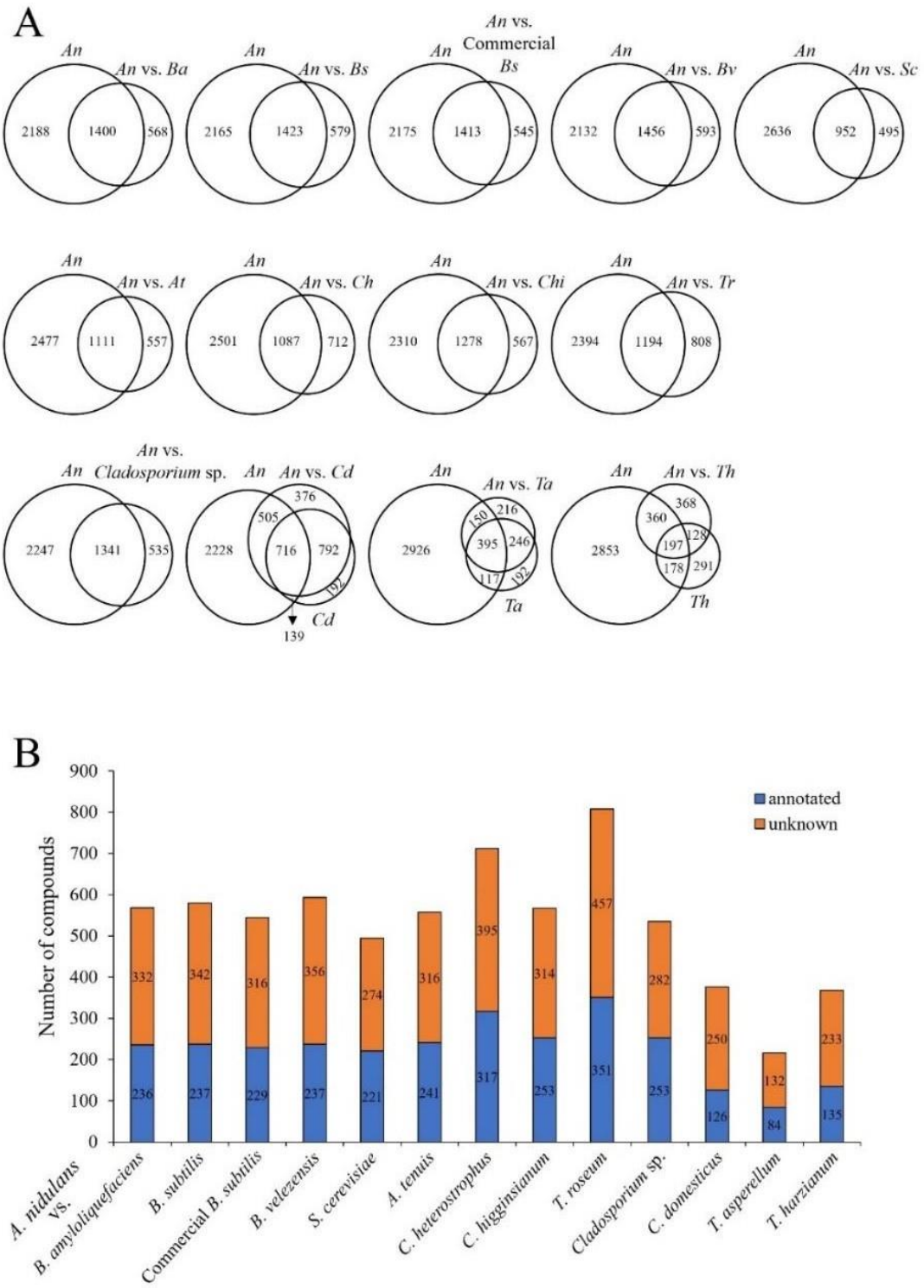

Supporting Figure S10. Metabolome analysis of shared and specific SMs in *A. nidulans* expressed under confrontations.

(A) Venn diagram showing the number of compounds produced specifically during confrontations and those that are shared with solely grown *A. nidulans*. Confrontations involving *A. nidulans* against *C. domesticus*, *T. asperellum*, and *T. harzianum* had overgrowth contact. To account for this condition, the solo cultures of *C. domesticus*, *T. asperellum*, and *T. harzianum* were included and shown in the respective venn plots. **(B)** Bar plot demonstrating the proportion of annotated versus unannotated features, highlighting that the majority of the newly synthesized chemistries remain unannotated. This underscores the unique SM production in *A. nidulans* driven by specific microbial confrontations, with a significant portion of these metabolites remaining novel. *An, A. nidulans*; *An* vs. *Ba*, *A. nidulans* vs. *B. amyloliquefaciens*; *An* vs. *Bs, A. nidulans* vs. *B. subtilis*; *An* vs. Commercial *Bs, A. nidulans* vs. Commercial *B. subtilis*; *An* vs. *Bv, A. nidulans* vs. *B. velezensis*; *An* vs. *Sc, A. nidulans* vs. *S. cerevisiae*; *An* vs. *At, A. nidulans* vs. *A. tenuis*; *An* vs. *Ch, A. nidulans* vs. *C. heterostrophus*; *An* vs. *Chi, A. nidulans* vs. *C. higginsianum*; *An* vs. *Tr, A. nidulans* vs. *T. roseum*; *An* vs. *Cladosporium* sp., *A. nidulans* vs. *Cladosporium* sp.; *An* vs. *Cd, A. nidulans* vs. *C. domesticus*; *An* vs. *Ta, A. nidulans* vs. *T. asperellum*; *An* vs. *Th, A. nidulans* vs. *T. harzianum*; *Cd, C. domesticus*; *Ta, T. asperellum*, *Th, T. harzianum*.

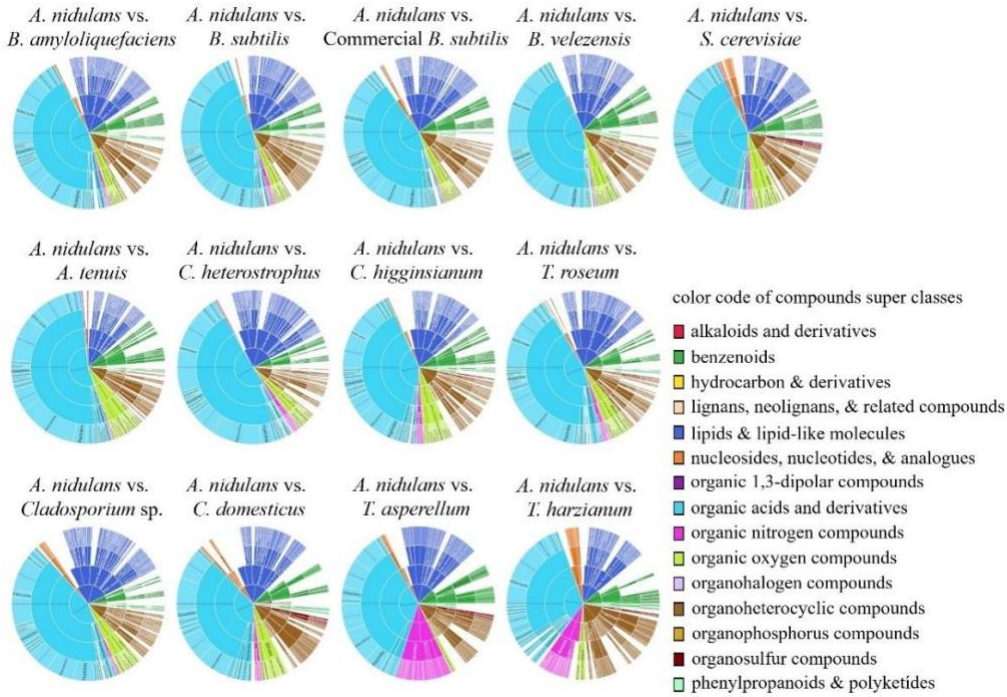

Supporting Figure S11. Visualization of annotated compound classes in *A. nidulans* under microbial confrontations.

Sunburst plots illustrate the hierarchical classification of annotated compounds produced by *A. nidulans* under specific microbial confrontation. The plots depict four levels of compound specificity viz., super classes, classes, sub-classes, and the most specific classes (inside to outside). The color code indicates compound super classes. The fractions of annotated compound classes vary depending on the type of confrontation.

7.2 Media, buffers, and solutions

7.2.1 Media

Unless otherwise indicated, all media were sterilized by autoclaving at 121 ºC for 20 min. Heat sensitive ingredients were added after cooling the medium to 45 ºC.

- **Complete medium (CM)**

10 mL	Solution A (see stock solution A; Appendix 7.2.3)
10 mL	Solution B (see stock solution B; Appendix 7.2.3)
10 g	Glucose
1 g	Yeast extract
1 g	Casein hydrolysate
1 L	dH_2O

- **Glucose Yeast Malt (GYM) medium**

4 g	Yeast extract
10 g	Malt extract
10 g	Glucose
15 g	Agar (for solid medium only)
1 L	dH_2O

- **Lysogeny Broth (LB) medium**

10 g	Bacto tryptone
5 g	Yeast extract
10 g	NaCl
15 g	Agar (for solid medium only)
1 L	dH_2O

- **Minimal medium (MM)**

20 g	Glucose
0.01 g	Yeast extract
10 mL	Solution A (see stock solution A; Appendix 7.2.3)
10 mL	Solution B (see stock solution B; Appendix 7.2.3)
15 g	Agar (for solid medium only)

1	L	dH_2O

- **Oat Meal Agar (OMA) medium**

40 g	Oat flakes
15 g	Agar (for solid medium only)
1 L	dH_2O

- **Potato Dextrose Agar (PDA) medium**

24 g	PDB
15 g	Agar (for solid medium only)
1 L	dH_2O

- **Regeneration medium (RM)**

137.2	g	Sucrose (1M)
0.4	g	Yeast extract (0.1%)
0.4	g	Casein hydrolysate (0.1%)
400	mL	dH_2O

Mix well and divide into two fractions:

100	mL	add 0.6 g (0.6%) agar
300	mL	add 4.5 g (4.5%) agar

- **Yeast Extract Sucrose (YES) medium**

24 g	PDB
15 g	Agar (for solid medium only)
1 L	dH_2O

7.2.2 Buffers

All buffers, unless otherwise stated, were autoclaved at 121 ºC for 20 min at 2 bar pressure. Heat sensitive solutions were filter sterilized using 0.2 µm pore CA membrane filter (Heinemann Labortechnik, Duderstadt, Germany)

- **2x / 0.5x / 0.25x / 0.1x wash buffer I**

2x or 0.5x or 0.25x or 0.1x	SSC
0.1% (w/v)	SDS

- **20x SSC (stock)**

3 M	NaCl
0.3 M	Sodium citrate
pH 7.5	

- **50x TAE buffer (stock)**

242 g	Tris base
57.1 mL	Acetic acid
50 mM	EDTA
pH 8.5	

- **6x Loading buffer**

30% (v/v)	Glycerin
60% 10x	TAE-buffer
0.25% (w/v)	Bromophenol blue

To 1mL of the above-mentioned solution, 10µl of 10000x GelRed Nucleic acid stain was added and used as loading dye.

- **Blocking buffer**

2 mL	10% (w/v) blocking reagent (Roche, Mannheim, Germany)
18 mL	Maleic acid buffer

- **Detection buffer**

100	mM	NaCl
100	mM	Tris-HCl
pH	9.5	

- **DNA extraction buffer I**

7	M	Urea
2%	(w/v)	SDS
5	mM	EDTA
50	mM	Tris-HCl
pH	8.0	

- **DNA extraction buffer II**

150	mM	NaCl
5	mM	EDTA
50	mM	Tris-HCl
pH	8.0	

- **GeneRuler mix**

1	mL	GeneRuler DNA Ladder Mix
6	µl	GelRed Nucleic acid stain (Merck, Darmstadt, Germany)

- **Hybridization buffer (20mL)**

5	mL	SSC (5x)
200	µl	N-Lauroylsarcosine (0.1% w/v)
200	µl	SDS (0.02% w/v)
2	mL	Blocking reagent (1% w/v) dissolved in 0.1 M Maleic acid
12.78	mL	dH_2O

- **STC buffer**

18.217	g	Sorbitol (1M)
0.5549	g	$CaCl_2$ (50mM)
1	mL	Tris-HCl pH 8.0 (1M)
100	mL	$dH_2O´$

- **TE buffer**

10	mM	Tris-HCl
1	mM	EDTA
pH	8.0	

- **TSS buffer (50 mL)**

5	g	PEG 8000
0.3	g	$MgCl_2 . 6H_2O$
2.5	mL	DMSO
50	mL	LB medium

- **Wash buffer M**

150	mM	NaCl
0.3%	(v/v)	Tween 20
100	mM	Maleic acid-NaOH
pH	7.5	

7.2.3 Solutions

All solutions (except microscopic dyes), unless otherwise stated, were autoclaved at 121 ºC for 20 min at 2 bar pressure. Heat sensitive solutions were filter sterilized using 0.2 µm pore CA membrane filter (Heinemann Labortechnik, Duderstadt, Germany).

- **Ampicillin stock solution**

  100 µg/mL Ampicillin (Roth, Karlsruhe, Germany) in ddH_2O, filter sterilized, and stored at -20 ºC.

- **Tetracycline stock solution**

  50 µg/mL Tetracycline (Roth, Karlsruhe, Germany) in ddH_2O, filter sterilized, and stored at -20 ºC.

- **Calcofluor white solution (CFW)**

  A working solution of 1mL of Calcofluor White-M2R (Fluka analytical, Sigma-Aldrich, Steinheim, Germany) was dissolved in 1mL of 10% KOH.

- **Diethylpyrocarbonate (DEPC)-H_2O**

  0.1% DEPC in H_2O
  Shake vigorously, let stand overnight and autoclave

- **FM lipophilic styryl dye (FM4-64)**

  A working solution of 1 µg/mL of FM4-64 (Thermo Fisher Scientific, Schwerte, Germany) was dissolved in HBSS without phenol, Ca^{2+}, Mg^{2+}.

- **PEG solution**

  40% (w/v) Polyethylene glycol 4000
  0.6 M KCl
  50 mM $CaCl_2$
  50 mM Tris-HCl
  pH 8.0

- **Protoplastization solution (10 mL)**

10 mL	NaCl (0.7 M)
Autoclaved	
10 mg/mL	Kitalase (Fujifilm Wako, Osaka, Japan)
10 µl	Ampicillin (100 mg/mL)

- **Stock solution A**

50 g	$Ca(NO_3)_2$
500 mL	dH_2O
Autoclaved	

- **Stock solution B**

10 g	KH_2PO_3
12.5 g	$MgSO_4 . 7H_2O$
2.7 g	NaCl
500 mL	dH_2O
Autoclaved	

7.3 Primers

Primers used in this study are listed below.

Table 1. RT-qPCR primers for *C. graminicola* under confrontation with *B. amyloliquefaciens*

Primer name	Sequence (5´ - 3´)
GLRG_10530_F	CTCGAGCTGGTTTGATCTTG
GLRG_10530_R	CAGAGAGGCATTTGCCGTAG
GLRG_10531_F	CTGATGGCAACGACGTCAAG
GLRG_10531_R	AAATCGACCGCAATGGACAC
GLRG_10532_F	CAGCTGAGGGAGAGCAAAAG
GLRG_10532_R	TATCCATTCCGGCGAATACG
GLRG_10533_F	CTAGCGCTTTGAAAGAATCG
GLRG_10533_R	CGTGGTCGATAGGAACGATG
GLRG_10534_F	GAGAAGGTCCGAGACATTAG
GLRG_10534_R	AAAGATTGCTGACGTGAGCG
GLRG_10535_F	CAAGCTCGACTTGGAGAAGA
GLRG_10535_R	TACTTGGAGAGGCCTGCTAC
GLRG_10536_F	ACAAGAGCGCCTTTCAAGTC
GLRG_10536_R	CTCAGGAATGTCATGCCGTC
GLRG_10537_F	GTCTAATGAAGGCGGTCCTC
GLRG_10537_R	TTGACAGAGGCTCTCCGTAG
GLRG_10539_F	ACGTCAAGATATGCACGACC
GLRG_10539_R	ACGCAGACAAGGAGCAAATC
GLRG_10540_F	ATCTCAAAGAGCGGCAGAAC
GLRG_10540_R	CCGGAGAAGACTCGGAGATG
GLRG_10541_F	CTCCCATGGTGCTCAGATTC
GLRG_10541_R	CGATATGTAACGGCGTCTTC
GLRG_10542_F	TCTCATCGCTCTGTTCTACC
GLRG_10542_R	CCCAGCTTCCGTTCACAATG
GLRG_10543_F	GAAGGCATTGTCCAATACGC
GLRG_10543_R	GCTTGAGAAGTAGTTCCAGG
GLRG_10544_F	TACCGCACCTGTCATCTTTG
GLRG_10544_R	AAGGCAGAAGCGTACAATGG
GLRG_10545_F	TTATCGAGGGTGCAGGTGTC
GLRG_10545_R	TCCGAGGATGTTGCAAAGTG

GLRG_10546_F	CGTAAAGTCTGGTGCCAGAA
GLRG_10546_R	ACGTATTTCGCCATACGAGC
GLRG_10547_F	CCATTCTGCGGATGGAAGTC
GLRG_10547_R	TCTTGCCTCAAGATCGGTTC
*α-actin*_F	TCCTACGAGCTTCCTGACGG
*α-actin*_R	CCGCTCTCAAGACCAAGGAC

Table 2. RT-qPCR primers for *B. amyloliquefaciens* under confrontation with *C. graminicola*

Primer name	Sequence (5´ - 3´)
*ituA*_F	CGAAAGGTGCAGCAATTGAG
*ituA*_R	CAGACGTTACCGTCAGATCA
*ituB*_F	CTGCCATTTGACGTACAGAG
*ituB*_R	GAACGATCAGCCAGAATAGC
*bacA*_F	AGGGACTAGCAGTGAGTAAG
*bacA*_R	GCTTAATACCGTCATACGCG
*bacC*_F	GGTTCAGGCGTTTCTGAATC
*bacC*_R	AACTTGTCAACCGCTGACAG
*bacE*_F	CGCTTTCGTTTATGGGAGAC
*bacE*_R	ACATCCGTCCACAGCATGATT
*gyrA*_F	AGTCAGGAAATGCGGACATC
*gyrA*_R	GGGTGGTACTTACCGATAAC

Table 3. RT-qPCR primers for *C. graminicola* under confrontation with *A. nidulans*

Primer name	Sequence (5´ - 3´)
GLRG_11770_F	CGTCATCGACCTCCTGATAG
GLRG_11770_R	CCATGTCCTCGTCATTCATG
GLRG_11771_F	CAGAGGACCTGTTCAACAAG
GLRG_11771_R	AAGATCCGGGTAGGAGATGG
GLRG_11772_F	CGGCTAATGTGCTTCCTCAG
GLRG_11772_R	TCGGTTATCTCCTGCATGAC
GLRG_11777_F	CCTGCCAAGGACTTTGAGAG
GLRG_11777_R	GTCGGAAGAGTTGGAGATGG
GLRG_11778_F	TGGCAACACATCTGTCAAGG
GLRG_11778_R	TAAAGAAGCGGGCGTCAAAG

Table 4. RT-qPCR primers for *A. nidulans* under confrontation with *C. graminicola*

Primer name	Sequence (5´ - 3´)
*stcW*_F	TCATCAAAGCCTGCTGGAAC
*stcW*_R	CTGGATGGAAGAAGCACCAG
*stcV*_F	TTTCTCTACGAGCGTCGAAG
*stcV*_R	CTCAAAGTCGCGGTAGGAAC
*stcU*_F	TCTAACGCGGGAATTGTCTC
*stcU*_R	GCTGTGTTGGAACTTGTGAG
*stcT*_F	GGCTACGTATTGACGGAATC
*stcT*_R	CTAACGCTGGGAGGATTTCG
*stcS*_F	CACTCTGAGGTTGACAGTTG
*stcS*_R	GGCGGTTATTGTACCACATC
*stcR*_F	TGCCTGATGTCATCAACGAG
*stcR*_R	CTGCGAGTGCTTCTGCTATG
*stcQ*_F	TCAAACCCCGCTCTCATTTC
*stcQ*_R	CCACATCCCAATCCGAATAG
*stcN*_F	ACAACGGCCATGTCAAGAAC
*stcN*_R	GCCAATTGTCCCAAGTGTAG
*stcM*_F	GCGCTATCACCATTAGCATG
*stcM*_R	GATTGACCAGCCTCATTTCC
*stcL*_F	CCGTCATCGACGAAACCTTG
*stcL*_R	GTTGTATGGCGCGTAGTAAG
*stcK*_F	TGGAGGTGGTCAACTACAAC
*stcK*_R	GCAAAGGGCTTCCCTGTTAC
*stcI*_F	CGTATCCCGTGCAATCAATC
*stcI*_R	TGTATACTCTCCTCGGTCTC
*stcH*_F	CCTCAGTATGCCGGTATATC
*stcH*_R	CCAGCTTGCAGATCCAGTAG
*stcG*_F	GAGTCGATATGGCCAAGGTA
*stcG*_R	CATCCGTCCTCCAAATCATC
*stcF*_F	ATATCCTGCAGTGCCAATGC
*stcF*_R	CACCGCTCGGGAATAAACTC
*aflR*_F	GTCTGCCTTGCGAGTATATG
*aflR*_R	CGCCGTAGTAATGACAGGTG
*stcE*_F	CCCACGACGATAGAGGAAAG

*stcE*_R	GCACATGGTAGCCAAGTAAC
*stcD*_F	CGCTCATCGCCATTGGATTC
*stcD*_R	AGAACGAAAAGCCCCAGAAG
*stcB*_F	GTTATGTCGGCAGCTTCTTC
*stcB*_R	GCTATGGACGTAGTGGATTC
*stcA*_F	ATGGCGATACCATTGTGCTG
*stcA*_R	TTGACGGCTTGTTGATTCCC
*actA*_F	AATGGTTCGGGTATGTGC
*actA*_R	ACGCTTGGACTGTGCCTC

Table 5. *PKS27* gene deletion primers. Lowercase letters are overhangs of DJ-PCR primers

Primer name	Sequence (5´ - 3´)
PKSCgF5	CGGTCAACCGATACCTGTAC
PKSCgR5	gtgcaactgacagtcgtacaGGGCAAAGATAGGAGGATAG
PKSCgF3	gtctggagtctcactagcttAGTGAATGGTACGGACAGAC
PKSCgR3	TGGGGAATGGGGTGGTATAG
UniHygTF	tgtacgactgtcagttgcacTGACCGGTGCCTGGATCTTC
UniHygTR	aagctagtgagactccagacGGTCGGCATCTACTCTATTCC
PKS10537F	CTATCCTCCTATCTTTGCCC
PKS10537R	GTCTGTCCGTACCATTCACT
PKSCgProbeF	GGTCAACCGATACCTGTACG
PKSCgProbeR	TCAATTTCTGCAGTCCTCCG

Table 6. ITS and 16s universal primers employed in this study

Primer name	Sequence (5´ - 3´)
ITS1	TCCGTAGGTGAACCTGCGG
ITS4	TCCTCCGCTTATTGATATGC
27F	AGAGTTTGATCCTGGCTCAG
1492R	CGGTTACCTTGTTACGACTT

8 Research output and author contributions

8.1 Publications

Bennet Rohan Fernando Devasahayam, Diana Astrid Barrera Adame, Henriette Uthe, Yvonne Poeschl-Grau, Timo H. J. Niedermeyer and Holger B. Deising (2024). Metabolic re-programming in confrontations of *Colletotrichum graminicola* and *Aspergillus nidulans* with *Bacillus* biocontrol agents. *Journal of Plant Diseases and Protection*. https://doi.org/10.1007/s41348-024-00905-1.

Alan de Oliveira Silva, Bennet Rohan Fernando Devasahayam, Chirlei Glienke, and Holger B. Deising (2024). The serine-threonine protein kinase snf1 orchestrates expression of plant cell wall-degrading enzymes and is required for full virulence of the maize pathogen *Colletotrichum graminicola*. *Fungal Genetics and Biology*. https://doi.org/10.1016/j.fgb.2024.103876.

Bennet Rohan Fernando Devasahayam, Henriette Uthe, Yvonne Poeschl, and Holger B. Deising. Microbial confrontations trigger broad array synthesis of putatively human-toxic secondary metabolites. **(IN PREPARATION)**

Bennet Rohan Fernando Devasahayam, Lena Hartmann, Henriette Uthe, Yvonne Poeschl, Robert Rennert and Holger B. Deising. The ubiquitous fungus *Aspergillus nidulans* exhibits differential secondary metabolism responses in confrontations with distinct biocontrol bacteria, yeast and filamentous fungi. **(IN PREPARATION)**

Lala Aliyeva-Schnorr, Bennet Rohan Fernando Devasahayam, Christoph Goldbach, Rene Csuk and Holger B. Deising. *NPS2*, encoding a non-ribosomal peptide synthetase is a virulence factor of the maize anthracnose fungus *Colletotrichum graminicola*. **(IN PREPARATION)**

8.2 Conference talks

Title: Are Microbial Biological Control agents (MBCAs) Consumers' friends or foes?

- Metabolomic symposium, 7th March 2023, iDiv, Leipzig, Germany.
- International Reinhardsbrunn Symposium, 27th April 2023, Friedrichroda, Germany.
- Mycology Conference, 17th March 2023, TUM, Freising, Germany.

8.3 Courses and events

- Introduction to R, 12th April 2021, iDiv, Leipzig, Germany.
- Introduction to Ecometabolomics for Ecologists, 26th to 30th April 2021, iDiv, Leipzig, Germany.
- Introduction to Integrative Biodiversity Science, 28th June to 2nd July 2021, iDiv, Leipzig, Germany.
- Data Analysis with R, 13th, 15th, 18th and 19th October 2021, iDiv, Leipzig, Germany.
- Goodbye academia? Hello industry, 11th November 2021, iDiv, Leipzig, Germany.
- Good Scientific Practice, 16th to 17th December 2021, iDiv, Leipzig, Germany.
- Designing Scientific Poster, 17th and 18th March 2022, iDiv, Leipzig, Germany.
- Dealing with fake news, 8th April 2022, iDiv, Leipzig, Germany.
- Scientific writing, 10th May 2022, iDiv, Leipzig, Germany.
- Chemical compound annotation using Sirius and MEtIgel, 26th June and 5th July 2023, iDiv, Leipzig, Germany.
- Teaching in Higher education, 14th and 15th May 2024, iDiv, Leipzig, Germany.
- Laboratory animal science, 12th to 14th June 2024, Berlin mouse clinic, Germany.

8.4 Author contributions

This PhD research was conducted in collaboration with several esteemed colleagues who made significant contributions in their respective areas of expertise. The metabolome analysis by liquid chromatography-mass spectrometry (LC-MS/MS) was performed by Dr. Henriette Uthe at the Institute of Plant Biochemistry (IPB) in Halle (Saale), providing crucial data for the identification of SMs produced during microbial confrontations. Dr. Yvonne Poeschl from the Biometrics and Agricultural Informatics Department at Martin Luther University Halle-Wittenberg (MLU) was responsible for the meticulous processing and analysis of the metabolome data, ensuring high-quality and reliable results. Additionally, Dr. Robert Rennert, also from the Institute of Plant Biochemistry (IPB) in Halle, contributed significantly to the cytotoxicity studies, enabling the evaluation of the potential human toxicity of the identified compounds. Their collaborative efforts were invaluable to the successful completion of this research.

9 Curriculum Vitae

Education

April 2021 - December 2024

Doctoral researcher in Phytopathology, Institute of Agricultural and Nutritional Sciences, Martin-Luther-University Halle-Wittenberg, Germany

October 2018 - August 2020

Master’s in Plant Sciences, Rheinische Friedrich-Wilhelms University, Bonn, Germany

August 2013 - April 2017

Bachelor’s in Biotechnology, Sathyabama University, Chennai, India

10 Acknowledgements

First and foremost, I would like to express my deepest gratitude to God for His unwavering guidance, strength, and blessings throughout this journey.

A special thank you goes to Prof. Dr. Holger B. Deising for granting me the opportunity to pursue my doctorate in his Phytopathology and Plant Protection working group. I am deeply appreciative of his support in writing my dissertation and for his invaluable advice throughout this research.

I am grateful to my collaboration partners Dr. Henriette Uthe, Dr. Yvonne Poeschl, and Dr. Robert Rennert for their contributions to this research. I am also thankful to Prof. Timo Niedermeyer and Diana Astrid Barrera Adame for their assistance with the metabolome analyses. For the insightful discussions, I am thankful to Prof. Dr. Gary Sawers, Dr. Dörte Falke, Prof. Dr. Eckhart Thines, and Dr. Larissa Heck. My thanks also extend to Dr. Ada Linkies, Dr. Vito Valiante, and Dr. Stefan Wirsel for providing the microbial strains used in this study.

My heartfelt gratitude goes to Dr. Lala Aliyeva Schnorr for her constant support, guidance, and valuable tips that greatly contributed to the success of this research study. My appreciation extends to Diana Gottschling, Otto Naumann, and Thomas Korbica for their skilled technical support, and to Elke Vollmer for the professional cultivation and care of the plants. Additionally, I would like to thank Dr. Steffanie Döll and Jennifer Gabriel for their technical support with metabolome analyses.

On a personal note, I would like to extend my deepest gratitude to my parents, Marcelin and Devasahayam Fernando, and my sister Betteena for their unwavering love and support. A special mention goes to my little nephew Claren, who brings immense joy to my life. I am also deeply indebted to my aunts Esther and Mary, and Uncles Johnsons and Jim, for their incredible support and affection. I would like to thank my friends for their unwavering support and warmth, which have been a constant source of encouragement throughout this journey.

Last but not least, I am profoundly grateful to the German Centre for Integrative Biodiversity Research (iDiv) Halle-Jena-Leipzig for their generous support and funding this project.

11 Declaration under Oath

Eidesstattliche Erklärung / Declaration under Oath*

Ich erkläre an Eides statt, dass ich die Arbeit selbstständig und ohne fremde Hilfe verfasst, keine anderen als die von mir angegebenen Quellen und Hilfsmittel benutzt und die den benutzten Werken wörtlich oder inhaltlich entnommenen Stellen als solche kenntlich gemacht habe.

I declare under penalty of perjury that this thesis is my own work entirely and has been written without any help from other people. I used only the sources mentioned and included all the citations correctly both in word or content.

Datum / Date	Unterschrift des Antragstellers / Signature of the applicant